This thesis was supervised by :

Prof. dr. ir. A. Holeyman,	Université catholique de Louvain (Belgium)

Members of the Jury :

Prof. dr. ir. J.-D. Legat, President	Université catholique de Louvain (Belgium)
ir. F. De Cock, co-advisor	Geo.be (Belgium)
Prof. dr. ir. R. Frank; co-advisor	CERMES Laboratoire Central des Ponts & Chaussées (France)
Prof. dr. ir. J.-F. Thimus	Université catholique de Louvain (Belgium)
ir. D. Vié	C.E.B.T.P. (France)

Loading rate effects on pile load-displacement behaviour derived from back-analysis of two load testing procedures

Thesis presented for the degree of Doctor in Applied Sciences

by

Nicolas CHARUE

October 2004

Acknowledgements

This research, during the last four years, would not have been possible without the help, encouragements and support of many people. I would like to thank them with my sincere gratitude.

Special thanks go to my adviser, Professor Alain Holeyman (UCL), who initiated and supported this research. He gave me the opportunity and trust to perform this research in the institution of UCL. His encouragements, comments, numerous ideas and permanent optimism helped me all through my work. He transmitted me the need to completely understand what I was looking for and found out, and the freedom to organize my work around my centres of interest in an accurate, creative and autonomous way. His numerous comments about the present document were an essential guide to this final version.

Profuse thanks go equally to ir. Flor De Cock(GEO.BE, Belgium) and to Professor Roger Frank (CERMES, France) for their involvement in my thesis steering committee. I had the opportunity to share my research process with a very active committee, internationally recognized for its competence in the deep foundation arena. Moreover, one or two meetings per year framed my research with long and interesting discussions. These meetings brought every time a lot of comments and new ideas that pushed the research forward. They also spend their precious time to comment the submitted text and help me to organize the writing process.

I would also like to warmly thank Professor Jean-Francois Thimus (UCL) and ir. Dominique Vié (C.E.B.T.P., France) for their participation to the jury of this thesis. The time needed to read, comment the text and their participations to the defences were highly appreciated.

I would like to extend my gratitude to the Dean of the faculty of Applied Sciences (UCL), Professor Jean-Didier Legat, for honouring my jury by presiding it.

A special thank goes to the Belgian Building Research Institute (BBRI) allowing us to use data of two national projects focused on the design methods and the installation influence of screwed pile in two types of soil encountered in Belgium. The extraordinary amount of data including a huge geotechnical survey and the load tests results was the foundation of this research. A particular thank is given to ir Noël Huybrechts for his help, comments and availability at any moment and to Rosario Bonsangue and Christian Verbeke for their technical support during the data measurements.

The environment where this research was achieved has to be highlighted. The Université catholique de Louvain and particularly the Civil and Environmental Engineering Department is a remarkable and

comfortable place where every scientist could find the adequate conditions to perform his job. This is due to the quality and the comfort of the installation but also and especially to the human being quality of the people who are working there. The friendly atmosphere of work and the team spirit existing between all the members of the Laboratory of Civil Engineering and the Civil and Environmental Engineering Department was an appreciated environment and a precious help contributing to the accomplishment of the present research. Each of them must be thanked for that. I would like to specially express my gratitude for the "Measurement" section of the laboratory composed of Alex Bertholet and André Renard, and to Eric Dupuis who responded with patience to many practical and stupid questions during all my work. I would like also to express my thanks to our secretaries, Marie-Rose Bodart-Decelle and Viviane Misson-Delmarcelle for their permanent help and support. Finally, Jean-Francois Vanden Berghe who preceded me in the PhD experience was a great guide and a very good officemate in the first year of this research. Thanks to him.

I am indebted to the University of Western Ontario (London-Canada) that hosted me for 5 months and made available the exchange with researchers from other institutions. I want to thank first Professor Hesham El Naggar who accepted me and helped me scientifically and practically during my stay. Besides, I would like to extend my gratitude to the staff of the Geotechnical Centre and especially to Mohamed Sakr who guides and helped me everyday.

All my gratitude is also going to Nicolas Bronchart, a very good friend, who reviewed all the text in order to correct my mistakes. His precious contribution was more than just correcting errors. His review increased significantly the quality of the text. In the same way, I would like to extend my gratitude to all the persons who helped me by reviewing the text of the thesis: in particular Flor De Cock, Roger Frank, Alain Holeyman and Céline Paulus. The final result is also richly illustrated by pictures and pictograms drawn by the "artist" of the department : José Flemal. I would thank him for his availability and pleasure to work with.

I gladly acknowledge the different funds that helped me to work without having to worry about material concerns. During the first year, the research was funded by the Fonds special de recherche (FSR) of UCL. The next three years were supported by BBRI and the Belgian Federal Ministry of Economic Affairs through two national research programs : Screw piles in sand (Biennale 2000-2002) and Harmonization of pile design method (Biennale 2002-2004). In that regard, the support provided by ir Christian Legrand, Head of the Infrastructure Division of the BBRI, is fully acknowledged. The stay at the Canadian University was supported by the “bourse of excellence” of the Belgian French Community.

I would like to give special thanks to the Laboratory of Civil Engineering, and particularly to its director, ir Albert Mertens de Wilmars to allow me to finish this work calmly and serenely.

And last but not least, I would like to thank my parents whose presence and support were never missing during the last 30 years. I am extremely grateful to them and indebted for all they did.

To all my friends and parents who never stopped to support me in my research, sincerely thanks to them.

Finally, extremely warm thanks go to Céline without whom the end of this thesis would have been much more difficult or simply impossible. I thank her for her daily encouragements and supports, for her patience, for her presence in the difficult periods and for her confidence in my abilities. Thanks to be there.

Abstract

Soils, like several other materials, exhibit strong time-dependent behaviour which can be evidenced in terms of creep or strain-rate effects. The degree of this rheological behaviour varies with the type of soil, its structure, and with the stress history. This effect is exacerbated in pile load testing where the procedure duration tends to be shortened under increasing time pressures. The modelling needed to interpret the results therefore becomes more and more complex, including soil viscosity, wave radiation into the soil and other significant phenomena. Within this framework, it would be interesting to study the influence of the loading rate on the load-displacement behaviour of the pile through the results of two testing procedures loading piles with variable duration (Static Loading Test (SLT) used as reference and Dynamic Load Test (DLT)). Based on these data issued from two national research programs organised by the Belgian Building Research Institute (BBRI), the objective of the research reported herein is to refine the rheological parameters characterizing the influence of the loading rate within the framework of a relevant pile/soil interaction model fed with dynamic measurements acquired during pile Dynamic Load Tests. The final goal is to predict and simulate the quasi-static pile load settlement curve.

After an overview of the loading rate effects in the literature through the experimental and modelling aspects, the dynamic data measured on field are analysed. It has been observed that some relationships exist between maximum quantities such as: energy transmitted to the pile, pile head velocity and force and the settlements (maximum and permanent) measured after a sequence of blows during a DLT event. These relationships are similar for the sandy and clayey sites and repeatable in time. It has been found that there are some critical quantities (correlated with the hammer drop height) from which a significant settlement of the pile is possible while the pile does not settle if these quantities are not exceeded.

The pile/soil interaction system is described by a non-linear mass/spring/dashpot system supposed to represent the pile and the soil, with constitutive relationships existing within and between them. These relationships account for the static and the dynamic or rheologic behaviour. A back-analysis process based on a matching procedure between measured and computed curves (force and velocity) allows one to describe the pile/soil interaction in terms of constitutive and rheologic parameters based on the

dynamic measurements. After optimisation of the matching procedure, the parameters obtained are used to simulate the “static” load-settlement curve. The matching procedure is based on an automatic multi dimensional parameter perturbation analysis. Since the parameters influence the system response with a relative weight, they are sorted in order to optimise all the parameters by successively retrieving the most influential ones and working on the remaining ones.

The back-analysis performed on dynamic measurements of both sites of Sint-Katelijne Waver (B) and Limelette (B) are generally successful but the obtained pile/soil system description appears to be unrealistic for some of the parameters. Consequently, the pile/soil model has been readjusted in order to account for the slippage between pile and adjacent soil along the pile shaft. This refinement increases the number of degrees of freedom needed to describe the pile/soil system but brings deeper insight into the behaviour of an interfacing zone of limited thickness surrounding the pile shaft.

Résumé

Le sol, comme bon nombre de matériaux, est fortement influencé par le facteur temps. Cette influence s'exprime par des propriétés de fluage et de relaxation ainsi que par une dépendance vis-à-vis de la vitesse de déformation. Ce comportement rhéologique varie en fonction du type de sol, de sa structure et de son histoire de chargement. Ce caractère est fortement marqué dans les résultats d'essais de mise en charge de pieux effectués à différents vitesses de chargement.

Si la durée de mise en charge tend à être raccourcie pour des raisons de rendement, le travail de modélisation nécessaire pour interpréter les résultats devient de plus en plus complexe du fait des facteurs mis en jeu tels que la viscosité du sol ou le rayonnement des ondes dans le sol. C'est dans ce contexte que s'inscrit cette recherche dont l'objet réside dans l'analyse de l'influence de la vitesse de mise en charge d'un pieu sur sa courbe de chargement. Des données issues de deux campagnes nationales d'essais organisées par le Centre Scientifique et Technique de la Construction (CSTC) et provenant de deux procédures de mises en charge à vitesses différentes (mises charge statique et dynamique) sont utilisées. L'objectif est de quantifier et de caractériser les paramètres rhéologiques définissant l'influence de la vitesse de mise en charge dans un modèle pieu/sol cohérent et, sur base des mesures de chargement dynamique, de simuler la courbe quasi-statique de charge-enfoncement du pieu étudié.

Premièrement, une étude de la littérature traitant du sujet tant sur les aspects expérimentaux que modélisatoires est proposé. Ensuite, une analyse des données dynamiques mesurées est effectuée et des relations particulières entre grandeurs physiques maximum sont mises en lumière. Ces grandeurs sont soit la vitesse particulaire de la tête du pieu, soit l'onde de force la traversant ou soit l'énergie transmise au pieu. Elles sont liées aux enfoncements maximum et permanent du pieu suite au coup donné. Ces relations montrent qu'il existe des seuils, appelés valeurs critiques, au dessus desquelles l'enfoncement permanent devient significatif alors que pour des valeurs inférieures, aucun enfoncement permanent n'est observable.

Le modèle d'interaction pieu/sol est décrit par un système de masses/ressorts/amortisseurs non linéaires modélisant le pieu, le sol et les relations constitutives les liant. Ces relations rendent compte des comportements statique et dynamique. Un processus d'analyse inverse basé sur l'ajustement de signaux mesurés (signaux dynamique et cinématique en tête de pieu) et calculés permet de décrire l'interaction sol/structure au moyen des paramètres constitutifs et rhéologiques du sol. Ainsi

l’optimisation de cet ajustement de courbes implique que la description du modèle pieu/sol y résultant est satisfaisante. La courbe de mise en charge statique correspondante peut être simulée et comparée à celle mesurée lors de l’essai de mise en charge statique.

La phase d’ajustement est basée sur une analyse stochastique des paramètres décrivant le système pieu/sol. Comme chaque paramètre a une influence relative sur la réponse du système, une classification est opérée de manière à optimiser tous les paramètres et à retirer successivement les plus influents pour pouvoir optimiser les paramètres restant. L’analyse inverse effectuée sur les enregistrements des deux sites (Sint-Katelijne-Waver (B) et Limelette (B)) donne de bons résultats en terme d’ajustement mais ne permet pas de caractériser correctement et physiquement le modèle pieu/soil utilisé. Ce modèle a donc dû être modifié pour tenir compte du glissement à l’interface pieu/sol le long du pieu. Cette amélioration du modèle n’est pas sans conséquence sur le nombre de degrés de liberté et donc sur la complexité du modèle et permet d’étudier en détail le comportement du sol dans une zone d’épaisseur limitée entourant latéralement le pieu.

Table of Contents

Chapter 2: Loading Rate Effect and Literature

Chapter 3: Pile/Soil Interaction Model & Dynamic Signal Analysis

Chapter 4: Back-analysis and optimisation

Chapter 5: The Slippage Event

Chapter 6: Conclusions and Perspectives

References

List of Symbol

CHAPTER 0
Introduction

Pile design is an activity where the theory, the experience and the experiment still have a similar weight. The designer can have the best knowledge of the used material and of the applied load (in magnitude and history), a potential uncertainty remains because the main structure interacts with a highly variable and evolving material: the soil. Due to this variability, and in order to be able to design this kind of structure, the method generally followed in the pile design is a semi-empirical method based on a rational approach and based on the experiment and experience. The soil fundamental properties and their implication in the pile/soil interaction are generally mixed with the result of field or model testing. However, these methods are dependent of the pile type, the pile installation, the pile material, the type of soil and, last but not least, the type of testing.

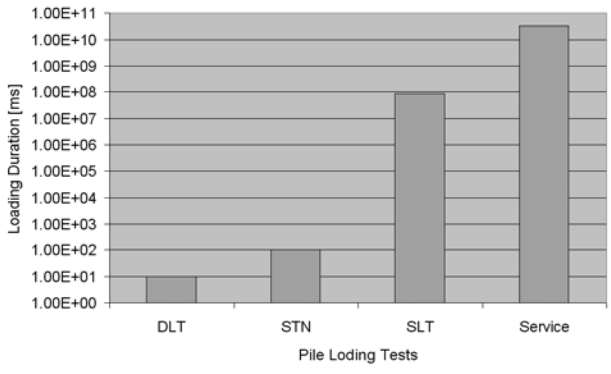

Figure 1 : Durations of the loading procedures

The methods of testing aims to match as best as possible with the real load history applicable during the foundation life. International codes and specifications exist and inform of the correct procedure to apply in order to perform a reliable and sound pile testing. However, the economical and practical aspects generally counter this objective. It is not possible to carry out a test in the same conditions than the real load history.

Different testing procedures have been developed. Most of them want to evaluate the working loads and simulate the load-settlement curve defining the pile/soil response to a given load history. These methods can be characterized, inter alia, by the rate of implementing: slow procedures (like the static load test – SLT) can be carried out during a long period (up to 3 days) and rapid methods (like the

dynamic load test – DLT) lasts barely a fraction of a second. But this rate of loading have a strong influence on the measurements and, consequently, on the complexity of the underlying post-treatment and interpretation. Indeed, the soil, in addition to its high level of variability is subject to time-dependent behaviour. This can be translated in terms of creep, relaxation or strain rate effect. This rheological behaviour varies with the type of soil, the stress history and the type of loading. The faster the pile test, the more developed the loading rate effect in the pile/soil reaction. Many authors focused their research on a specific and narrow aspect of this influence either on a laboratory or a rational aspect or from field test point of view. This specific intersection of the rheologic behaviour of soil under dynamic conditions and its influence on the result of a pile test performed at a certain velocity is the framework within this research has been undertaken.

In the last 5 years, since 1998, two ambitious national researches have been organised by the Belgian Building Research Institute in order to execute an experimental test campaign able to lead a proposal of semi empirical design methods of axially loaded piles using installation coefficients. This program is organised equally in two typical types of soil met in Belgium: the tertiary overconsolidated Boom clay in Sint Katelijne Waver (Belgium) and the sandy bearing stratum of Bruxellian sand in Limelette (Belgium). The program included the intensive geotechnical investigation of both sites and the installation of 30 piles to be loaded statically, dynamically and by the statnamic[1] procedure. The 30 piles are composed of 5 types of cast in place soil displacement screw piles plus a prefabricated driven pile as reference.

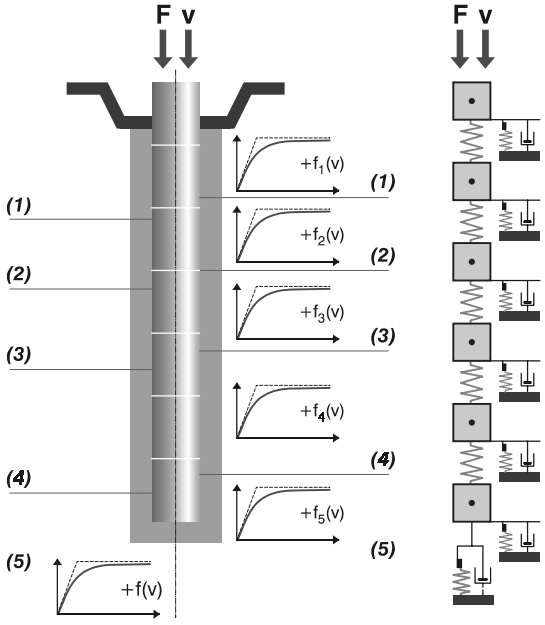

Figure 2 : Pile soil model representation (schematic and modelled)

With the courtesy of the BBRI, it is possible to use this wide amount of data generated by these two research programs as raw material of a precise research focused on the loading rate effect. Indeed, the testing procedures are ranged on a wide spectrum of loading duration or loading rate (Figure 1) and the comparison of their results in a comparable environment could result in a better comprehension of the loading rate effect on the range of high and low velocities.

This research aimed to analyse the influence of the loading rate by modelling the pile/soil interaction system in a mass/spring/dashpot system supposed to represent the pile, the soil and the constitutive relationships existing between them. These relationships account for the static and the so-called dynamic behaviour (Figure 2).

The dynamic measurements are introduced as input in the system and the pile/soil interaction system parameters are obtained from a back-analysis process where the matching between a measured and a

[1] A load controlled testing procedure of which the loading rate is intermediate between the SLT and the DLT.

calculated curves issued from the pile/soil response is used as quality control. This optimisation process allows to identify the “static” and the “rheologic” parameters from dynamic measurements. When the “static” parameters are obtained, a simulation of the equivalent static load-settlement curve is obtained and compared with the real one measured on field. There is a large amount of parameters to be optimised. A rational technique is required to perform this analysis but this process must be guided in a geotechnical way. The parameters have to be sorted and managed in function of their relative weight and reliability. An automatic technique has been developed based on the systematic study of the vicinity of the combination of parameters in order to find a better combination or to know the evolution of the matching criterion with a slight variation of the parameters.

Chapter 1 describes the three load testing procedures (measurements, procedure and methods of interpretations) and their main methods of interpretation. An overview of the wave equation applied to pile dynamic analysis is also given.

Chapter 2 is dedicated to the load rate effects through literature. An overview of the specific results focused on this behaviour is given allowing to make a first synthesis of the trend observed between the measured soil reaction and the rate of loading applied. The Smith aspect (1960) is also investigated and the link between the rheologic parameters (J, quake) and the soil type is summarized. Finally, the main lumped models describing the loading rate effects are listed and compared.

Chapter 3 is focused on the description of the pile/soil interaction model. Both pile and soil models are detailed and the main algorithms used for the dynamic analysis and the simulation of the static load-settlement are described. After, the dynamic data from the dynamic load tests on prefabricated piles are analysed: different aspects are investigated, namely the relationships existing between the maximum quantities and the quality of the signals in the post-treatment or during the acquisition.

Chapter 4 is dedicated to the back-analysis procedure and the automatic optimisation process. The description of the method and the main algorithms used are given. A short analysis of the uniqueness of the solution and a large analysis of the sensitivity of the matching result to a parameter perturbation are proposed. Afterwards, This technique is used to perform a complete set of analysis (6 blows) on the measurements of the pile A7 (prefabricated one) in Sint-Katelijne Waver, and on 6 blows of the pile B8 (prefabricated) in Limelette. Conclusions about the reliability of the pile/soil model and the need of the slippage between the pile and the soil taken into account are drawn.

Chapter 5 is a consequence of chapter 5. The simple SDOF model describing the pile/soil interaction behaviour defined in chapter 4 is replaced by two other propositions of modelling where the soil adjacent to the pile is defined with its own motion system of reference. this allows to introduce the slippage at the interface between pile and soil. These models are either the 1-D radial approach with concentric cylinders of soil surrounding the pile or a DDOF (Double Degree Of Freedom) system similar to the classical one but where pile and soil have their motion dissociated during the slippage. Description, comparison and a special attention to the slippage event are proposed for both approaches.

CHAPTER 1
Load Testing Procedures: Description and Methods of Interpretation

1. Introduction

Design analysis of pile is required to assess whether the foundation is resistant enough to fulfil its function. This function could be either to carry a particular load, or to settle less than an allowable maximum deformation. The analysis involves generally the calculation of bearing capacity (sometimes split into shaft and base bearing capacities) and the estimation of the possible deformations under working loads. Both points are summarized in the drawing of the load-settlement curve.

Design analysis could also be performed in order to assess the installation feasibility in terms of driving, machine and field aspects. The design methods can be divided in two main groups: the methods based on the fundamental soil properties and the empirical approaches. Most of the pile design methods use a mix of these two main branches. However, the calibration of all these methods remains dependent of the pile type, the pile installation, the pile material, the type of soil and geotechnical conditions.

In order to assess the adequacy of the chosen design method with field conditions, some pile load tests are carried out on specific and representative piles. The first and main preoccupation during these tests is to match as closely as possible the real load history applicable during the foundation life. But this progressive and slow gradation to reach the maximum load level is not convenient with respect to the economical and practical aspects. Several testing methods have been designed to respond to both antagonist requirements: a pile test as close as possible to the actual situation to confirm the design but that can be performed as quickly as possible in order to be efficient and useful.

Two of them, the Static Load Test (SLT) and the Dynamic Load Test (DLT) are involved in this research through the results of two majors test campaigns organised in Belgium during the last 4 years. Since the results of these pile load tests are the reference data of the current research, an explanation of their procedures is required like the main techniques used for their analysis. In this chapter, each proposed testing method is described with a particular attention on the methodology, the measured quantities, the general and main theoretical assessments allowing these tests and the advantages and disadvantages of each.

2. Static Loading Tests

Static pile load testing is the most commonly adopted method of checking the performance of a pile and is often used as reference for the calibration of others pile testing methods.

2.1. Definitions and characteristics

Amongst the procedures developed in this testing category, the maintained load test is commonly used in the general practice. It is characterized by a set of stages where a constant load is applied on the pile head during a given duration. The load is monotonically increased (ΔQ) until reaching a determined load Q_{max} [1] (see Figure I-1). When the maximum test load is reached, the applied load is progressively unloaded to zero with potential different time duration and decrement loads.

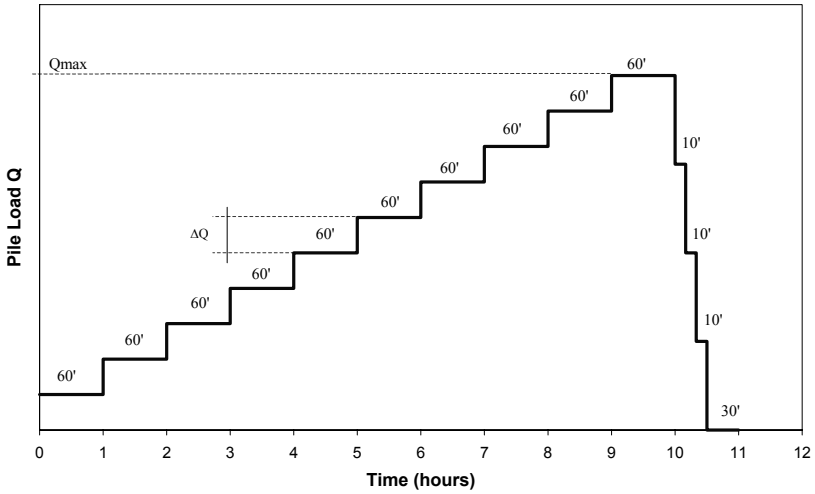

Figure I-1 : Test procedure adopted for the static pile load tests (after Maertens et al., 2001)

If the applied load reaches a value close to the estimated ultimate pile capacity, the load increment can be reduced to avoid a quick failure.

The load is applied by hydraulic jack(s) and kentledge[2], adjacent tension piles or soil anchors are used to provide the reaction for the load applied on the pile (Figure I-2 and Figure I-3).

[1] Either a multiple of the design working load or the predicted ultimate resistance, or another limit imposed by the test schedule

[2] A mass of heavy material placed on a platform constructed on the head of the pile.

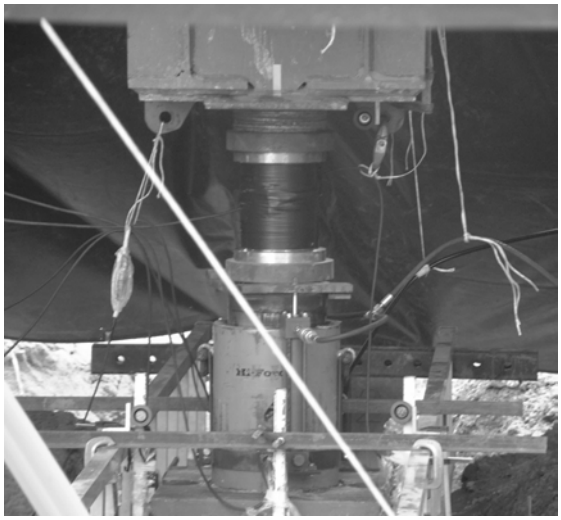

Figure I-2 : Detail of the loading device

Figure I-3 : Steel kentledge

The maintained load test is ruled by official specifications and procedures: the ASTM Test Designation D-1143, the ICP Piling Model Procedure and Specifications (1988 & 1996) or the BS-8004 1986. They give the specification required for the maintained load test including the loading increment schedule and periods of load application.

The ERTC3 (European Regional Technical Committee-Piles, ISSMGE Subcommittee) proposes a document (De Cock et al., 2003) gathering the recommendations for the execution of Axial Static Pile Load Tests (ASPLT). This document contains advice about the preparation, execution, reporting and evaluation of the ASPLT for compression and tension piles. In particular, the paper describes three quality levels in relation with the purpose of the pile load test (from high requirement level (research or design test) to basic requirement (control or acceptance test)). For each category, a summary of the relevant test specifications is given and detailed.

2.2. Measurements

The basic measurements include the pile head displacement and the applied load in function of time. These quantities allow the determination of the pile's performance.

The displacement devices (dial gauges) are fixed on a reference frame and the pile head displacement is generally the average of several distinct values. The measurement can be reinforced and checked with an optical measurement apparatus. The load measurement can be obtained from a load cell or from the pressure of the jack system (De Cock et al. 2003).

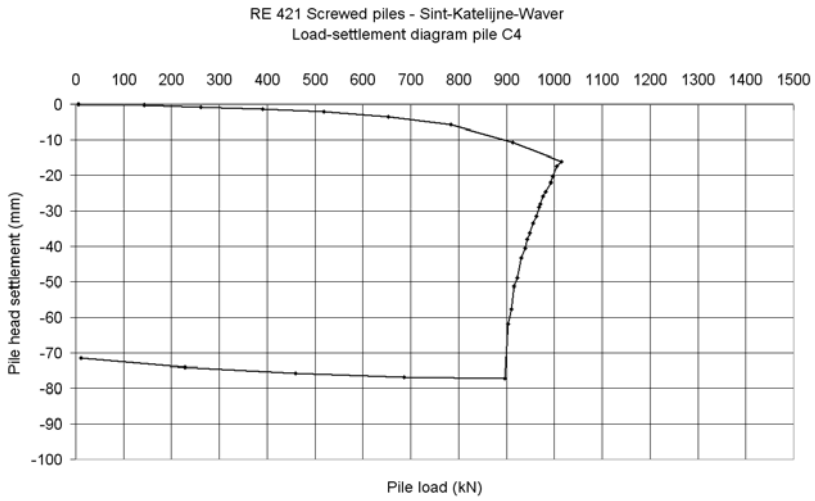

Figure I-4 : Load-settlement curve of a static pile load test (after Huybrechts, 2000)

Figure I-4 shows the pile head displacement measured and averaged vs. the pile head load measurement. This representation is the most used and called the pile load settlement curve.

2.3. Interpretations of the results

According to the amount of measured data and according to the main purposes of the test, the interpretation of the results could be simple, sophisticated, direct or involving considerable post-treatment. All of them concern the analysis of the measurements: displacement and load. Measurement can be analysed separately (vs. time with linear or logarithmic scales allowing the estimation of the creep Resistance Q_c which is deduced by analytical or graphical means as the point of maximum curvature on the creep curve (Figure I-5)) or together (Figure I-4). If the pile is instrumented, (Q_b,s_o) and (Q_s,s_o) plot respectively the base and shaft capacities in function of the pile head displacement.

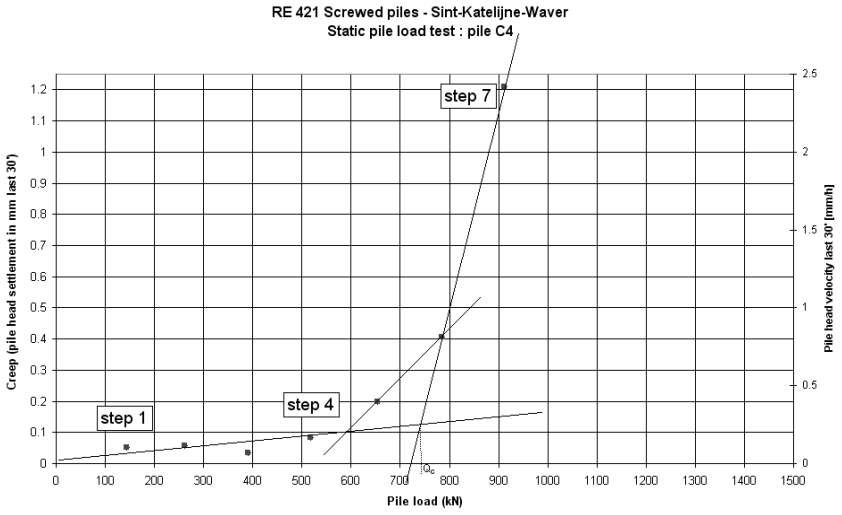

Figure I-5 : Creep curve (load vs. Δso, last 30 min) (after Huybrechts, 2000)

The interpretations of all these curves and figures give a better understanding of the pile/soil interactions and load transfers during the test.

An important operation still remains after drawing and analysing the rough figures: the estimation of the ultimate load, required for the estimation of the working and design loads. There are several approaches, all of them being based on the load settlement diagram:

- The *Chin method* that assumes a hyperbolic relation between the pile head settlement and the mobilized soil resistance expressed by the applied load.

- The *Van der Veen method* that proposes an exponential relation between the base settlement and resistance.

- The *Brinch-Hansen's 80% criteria* that defines the ultimate load as the load for which the pile head settlement is four times the settlement corresponding to 80% of this load. In this configuration, the load settlement diagram becomes a parabola.

Three commonly and simple criteria can be used without an explicit reference to the ultimate resistance but preferably called "conventional rupture load" :

- The load corresponding to a progression of the settlement with no variation of load;
- The Davisson criteria that determines the load as the intersection of the load settlement curve with the straight line of slope $\frac{L}{EA}$ and starting a the settlement s_0 (L: pile length, E: Elastic modulus of the pile material, A: pile section):

$s_o = 3.81\ 10^{-3} + \frac{Diam_{Pile}}{120}$ [SI units];

$$s\left(Q_{rupt}\right) = 3.8110^{-3} + \frac{\phi}{120} + \frac{Q \cdot L}{EA} \qquad \textbf{Equ. I-1}$$

- The load corresponding to a settlement of 10% of the pile base diameter ($Q_{10\%Db}$).

These last conditions consider that the base capacity is fully mobilized for this settlement (the shaft settlement is obviously mobilized for a long time). It happens probably in clay, but not with certainty in sands.

3. The Dynamic Loading Test

3.1. General presentation

Dynamic load testing consists in predicting pile capacity and pile/soil interaction from hammer blows during driving and/or restrike of an instrumented pile. This testing method has been developed owing to the driving analysis improvement emerging during the last 50 years. The computer use and its more and more efficient working capacity, plus the transducers progresses were also pertinent parameters helping the driving analysis development.

The dynamic load testing consists of letting a mass (e.g. 4 tons) fall from a set height upon the pile head (Figure I-6). Transducers (strain gauges and accelerometers) are placed along pile shaft next to the pile head (Figure I-9). A pile/soil model is then used to interpret the dynamic event in terms of an equivalent static load-settlement curve.

The main advantages of this load test are obviously the economical and accurate way to evaluate the hammer-pile-soil system based on force and velocity measurements and to check the integrity and performance of the foundation.

Figure I-6 : Dynamic loading test (crane + mass + pile)

The pile dynamic testing procedure is also accepted and standardized in numerous specifications such as ASTM D4945-89, AASHTO T298, the recommendations for static and dynamic pile tests of the DGGT in Germany (1997) or specifications from many countries (Bein et al., 2000).

The models used in the dynamic pile testing procedure take into account further elements assuming to be representative of the static part, the viscous part, the radiation term of soil reaction and the hysteretic loss of energy through the soil. It is possible to estimate the ultimate resistance of the soil

under static conditions but often the soil mobilization during a test does not allow one to have sufficient information to fulfil this requirement. Nevertheless, a good estimation can be done and a conservative value can be given and interpreted as a lower bound. A considerable experience is however required especially to quantify the damping factor often used to take all the mentioned terms (except the static term) into account.

3.2. Definitions and characteristics of the Dynamic Load Test

Different purposes guide the use of dynamic testing, some of them concern the pile driving procedure, others insists on the integrity and the quality of the pile installation and finally, the main goal is guided by the bearing capacity evaluation.

Nowadays, one of the main purposes to use dynamic loading test is the pile bearing capacity evaluation. This is due to the improvements in the pile/soil interaction modelling, due to the computer progress allowing a shorter process and a higher complexity. This is also due to the experience and the numerous comparisons available between static tests and dynamic tests on the same soil and pile configuration. Therefore, the timing of the test becomes a very important parameter, absolutely essential to be integrated. Increase (set-up) or decrease (relaxation) of the pile capacity with time occurs almost always after driving depending of the type of soil and driving. Hence, dynamic testing gives the capacity of the pile at the time of testing. It seems to be appropriate to wait for a few hours (sand) to several weeks (clay) to try and evaluate the long-term capacity through a dynamic test. Using the short-term capacity could result in over- or under-estimate the long term one and it can have dangerous consequences.

It has to be noted that the dynamic testing capacity estimates the mobilized pile capacity at the time of testing and for the dynamic test soil mobilization because the base resistance is rarely fully activated during a single hammer blow. The more energetic the blow (or higher the ram drop), the closer the bearing capacity estimation to the ultimate resistance.

3.2.1 Test procedure

The basic testing procedure is defined as the drop a of mass on the head of the tested pile where transducers are attached in order to measure the transient signals generated by the impact. The system is composed of a the falling mass, a guide for the correct alignment of the mass and the pile head cushion, a device controlling the energy transfer between the mass and the pile (Figure I-7). A rule of thumb assesses that the ram weight should be 1.5% of the estimated capacity of the tested pile (Goble & Likins, 1996). The ram used for the tests performed at Sint-Katelijne-Waver and Limelette is 4 tons. The scheme of the mass and guide is shown on Figure I-7 and Figure I-8.

The cushion is needed to control the energy coming from the mass to the pile in order to mechanically limit the intensity of the peak stress and lengthen its duration. The material has to be elastic (the cushion can be modelled by a spring and a dashpot in parallel) but should consume as little energy as possible. The goal is to transform the input force signal in a longer and smoother form.

The positioning screwes are used to place the guide of the mass as vertically as possible in the pile axis, so that the pile can be loaded with a purely axially load and not decentralized due to the

possible bending and tension stress generated in the section. This device allows also maintaining the guide on the pile when the crane lifts the mass before dropping it.

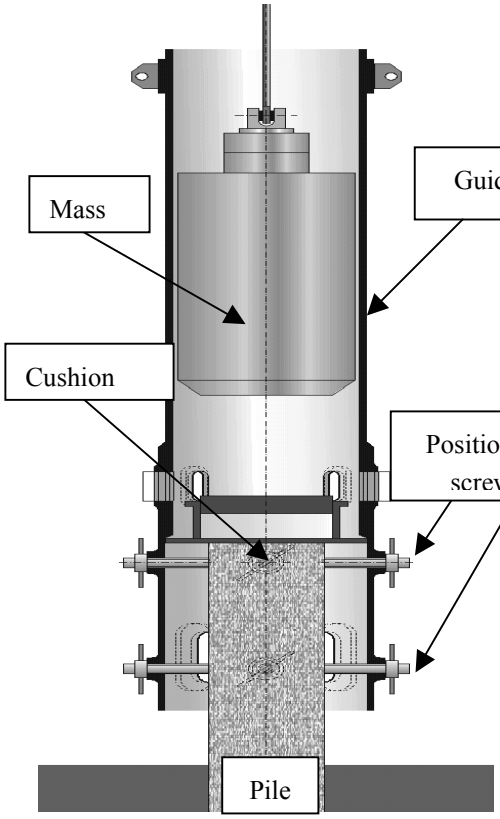

Figure I-7 : Schematic view of the dropping mass and mass guide (after Holeyman, 1992)

Figure I-8 : Dropping mass and mass guide

The guide is a metallic tube allowing the mass to drop from a height of about 2 meters vertically on the head pile even if the mass is not exactly upright with the pile.

Before the test, and in function of the goal of the testing session, the transducers are placed on the head pile. Some recommendations express a minimum distance from the pile head and from any change in the pile section dimensions. The minimum distance is generally fixed to 1.5 pile diameter (Goble & Likins, 1996). This distance aims to avoid measurement of local stresses surrounding discontinuities such as corners, angles or section variations.

Two conditions are needed to evaluate correctly the long term capacity:

- The test must be performed on a restrike and during the early blows of the restrike;
- The set per blow must be large enough to ensure significant soil failure during the test.

3.2.2 Data acquisition

The transducers are generally twofold: accelerometers to measure the pile head vertical acceleration and strain gauges to measure the vertical strain in the local section due to the force transmitted by the falling mass.

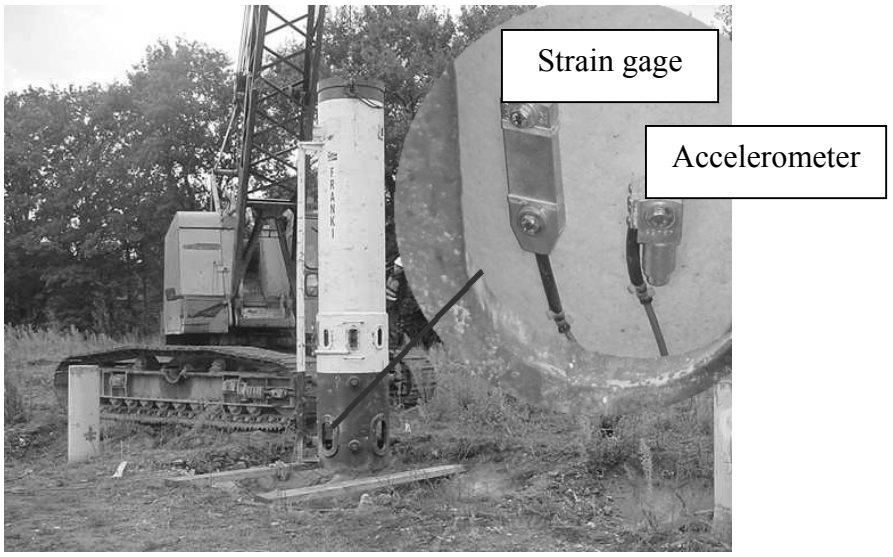

Figure I-9 : Detail of transducers placed on the pile shaft

Figure I-9 blown-up exhibits the detail of the transducers placed on the pile shaft during a dynamic loading test. The figure shows only two sensors, but in reality, the transducers are placed diametrically opposed on the pile section in order to mitigate the influence of bending on the acceleration signal and particularly on the strain measurements. The used data are the average value of both measurements.

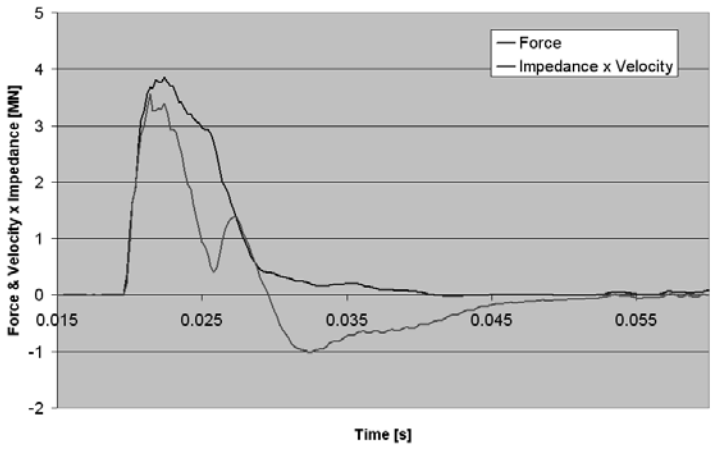

Figure I-10 : Proportionality of the velocity and force signals

Both measured signals can give others very important information after mathematical treatment:

Strain → Stress → Force in the section.

Acceleration → Velocity → pile head displacement.

A next section (chapter 3) will develop the potential errors emerging from this treatment by assessing the values of the elastic modulus E, the section,

…

3.2.3 Data interpretation & data analysis techniques

Due to the viscous effect added to the static soil reaction and due to the wave equation phenomenon occurring during a dynamic test event, post treatment and assessments are needed to get the required results. Numerous methods of interpretation have been developed in order to overcome this difficulty. Here after is a short description of some of them.

3.2.3.1 Visual inspection

The visual inspection includes the first inspection of all signals in order to validate their quality. This is not really an interpretation method but an essential step in the interpretation process. The signals must correspond to what is expected: duration, noise, amplitude, final zero value for velocity and force. It is also possible to interpret these defaults or defects as a particular cause. The method remains highly subjective.

3.2.3.2 Driving formulae or energy approach

The main principle of the driving formulae links the called pile dynamic capacity to the measured permanent displacement of the pile (set) at each blow. These formulae are based on the energy balance of the hammer input energy (energy given to the pile) and the work spent by the pile to settle down permanently. The result represents a capacity between the static and dynamic ones since no differentiation is made between the static ultimate resistance of the pile and the dynamic driving resistance.

The mass falls from a determined height, equivalent to a potential energy, to the pile head. The potential energy turns into kinetic energy. This energy is transferred to the pile during impact. The pile translates immediately this kinetic energy into a deformation energy and a pile kinetic energy and turns it out in a penetration work of the pile into the soil.

The penetration work allowing the driving of the pile can be divided into plastic and elastic terms and is limited by the soil reaction mobilization. The energy balance between these elements is given by Holeyman, 1984:

$$\eta_i \eta_c M_m g h = Q_d \left(\frac{s_{el}}{2} + s\right) \qquad \textbf{Equ. I-2}$$

Where:

- η_i : impact efficiency [-];
- η_c : falling efficiency [-];
- M_m : ram mass [kg];
- g : gravity acceleration [9,81 m/s²];
- h : dropping height [m];
- Q_d : dynamic soil reaction [N];
- s_{el} : elastic deformation or “quake” [m];
- s : permanent deformation or “set” [m].

The left part of Equ. I-2 corresponds to the transmitted energy (potential energy and efficiency effects) and the right part represents the penetration work based on the modelled displacement/resistance model (Figure I-11).

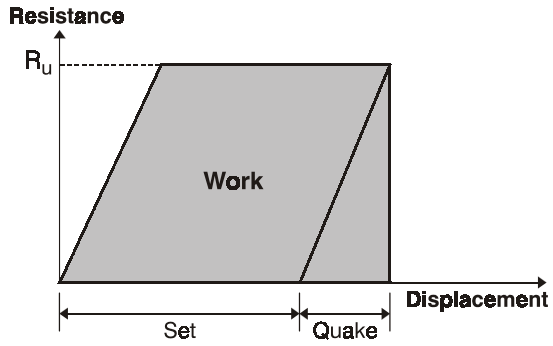

Figure I-11 : Displacement-soil reaction relationship

From Equ. I-2, the static pile bearing capacity is evaluated:

$$Q_{adm} = \frac{Q_s}{SF} \cong \frac{Q_d}{SF} \qquad \textbf{Equ. I-3}$$

Where "SF" is a safety factor imposed to the driving formula result. During the driving, the estimated pile capacity can be checked out. If this capacity is assessed, the blow count can be investigated by extracting the permanent set of the driving formulae.

Paikowski and Chernauskas (1992) merge the energy approach with the use of the dynamic signals to evaluate an estimation of the pile resistance. The main principle link the energy transferred to the pile (Enthru) to the work done by the resisting forces along the pile.

The energy transferred to the pile is calculated from the measured dynamic signals instead of the potential energy and the efficiency effects.

$$Enthru = \int_0^{t_\infty} V(t) \cdot F(t) \cdot dt \qquad \textbf{Equ. I-4}$$

Where:

- V(t) is the pile particle velocity [m/s];
- F(t) is the force measured close to the pile head [N].

This equation consider only the elasto-plastic energy losses of the pile-soil system and can be regarded as a upper bound of the pile resistance.

3.2.3.3 Signal processing

The signal processing methods work with the measured signals (strain or force, and acceleration or velocity at pile head) by simple operations in order to result in the evaluation of the shaft, base and total resistances. They are all based on the application of the stress-wave theory. The main assessment states that the signal generated by the mass hitting the pile head goes down into the pile towards the pile base. This compression wave travels down the shaft, reaches the base and is reflected back in the direction of the pile head. The time needed for the travelling back and forth is function of the pile length and the wave propagation velocity.

$$T_{\updownarrow} = \frac{2L}{c}$$ **Equ. I-5**

Where:

- T is the time it takes the wave to reach the pile and come back [s];
- L is the pile length (from the transducers position to the pile base) [m];
- c is the wave propagation velocity [m/s].

The form of the reflected wave depends on the base reaction encountered. If the base is free from reaction, the pile is free to deform itself and the force wave that returns back is a tension wave. When the base reaction is infinitely rigid, the force wave is entirely reflected and the upward wave is a compression one identical to the downward wave. The same process generates also particles velocity of opposed sign.

When the pile is considered with the surrounding soil, each soil layer reacts like the base. The incident wave is divided in an upward compression wave (proportional to the soil restraint) and the complementary downward part of the initial wave. Since the main and initial wave is going through the pile to the base, its reflection is expected to arrive at the pile head after a time equal to 2L/c. During this time, all the upward information is only resulting from the shaft soil reaction. Consequently, the shaft reaction can be evaluated by taking the upward wave into account during the instants following the blow; and since all the waves travel at the same propagation velocity (for a homogeneous pile), the arrival time can be used as a indicator of the pile depth.

It seems possible to evaluate the shaft soil reaction during a dynamic load test through the analysis of the upward and downward waves. Moreover, these waves can be extracted from the data measured (force and velocity) at the pile head. The upwards velocity and force waves are function of the pile/soil system, as developed here after.

The Wave Equation

The wave equation theory applied on the pile dynamic test analysis idealizes the pile as a prismatic elastic rod where a wave propagates with a constant velocity depending on the material properties. This wave expresses the travel of a longitudinal strain initiated by a shock on one of its extremities. The main principle expresses that all material does not feel the shock effect immediately but gradually as the wave advances in the rod, like a wave in a cable. The wave is a compressive one if the shock applies a compression on the rod. The motion of each pile particle depends on its position in the rod and regarding the wave position and the time. The wave is considered as one-dimensional because of the large dimension of the length of the pile compared to the diameter. The general referential is Z pointed downwards as shown on figure I-12. The pile is considered as elastic, homogeneous and of constant section A.

Wave Equation Form

Figure I-12 exhibits the section A, positioned at the distance z. Its displacement u_z due to the compression is defined by

$$u_z = u_z(z,t)$$ **Equ. I-6**

In function of time and of the main dimension z.

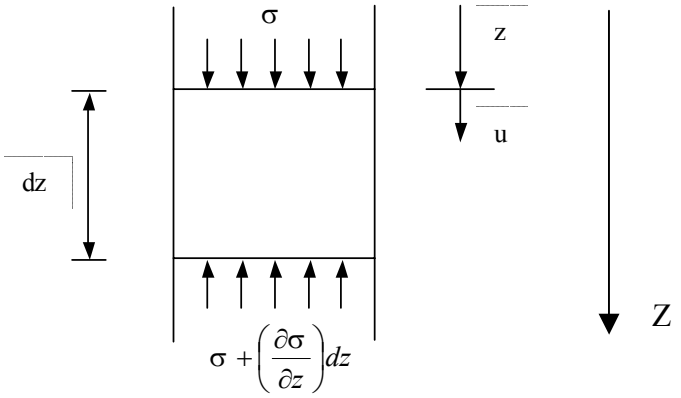

Figure I-12 : Infinitesimal volume of a pile section

Due to the balance of forces applying on an infinitesimal volume plus the inertial effects (Figure I-12) and due to the joint application of Hooke's and Newton's laws, the following equation is obtained:

$$A_p \sigma - A_p \left[\sigma + \left(\frac{\partial \sigma}{\partial z} \right) dz \right] = \rho_p A_p dz \frac{\partial^2 u}{\partial t^2}$$ **Equ. I-7**

$$\left(\frac{\partial u}{\partial z} + \left(\frac{\partial^2 u}{\partial z^2} \right) dz \right) A_p E_p - A E_p \frac{\partial u}{\partial z} = \rho_p A_p dz \frac{\partial^2 u}{\partial t^2}$$

Where :

- A_p is the pile section [m²];
- ρ_p is the volumetric mass of the pile material [kg/m³];
- σ is the axial stress [MPa] and the compression is positive;
- E_p is the elastic modulus of the pile material [MPa];
- dz is an infinitesimal thickness of pile [m];
- $\frac{\partial^2 u}{\partial t^2}$ is the acceleration of the considered section [m/s²].

Simplification of Equ. I-7 gives:

$$\frac{\partial^2 u}{\partial z^2} = \frac{\rho_p}{E_p} \frac{\partial^2 u}{\partial t^2}$$ **Equ. I-8**

And by defining the wave propagation velocity c as :

$$c = \sqrt{\frac{E_p}{\rho_p}} \text{ [m/s]} \qquad \textbf{Equ. I-9}$$

Equ. I-8 becomes the fundamental wave equation of the propagation of an elastic compression wave in an elastic media:

$$\frac{\partial^2 u}{\partial z^2} = \frac{1}{c^2}\frac{\partial^2 u}{\partial t^2} \qquad \textbf{Equ. I-10}$$

The solution of Equ. I-10 is obtained after substitution. Two fundamental forms compose it:

$$f(z,t) = f_1\,(z - ct) + f_2\,(z + ct) \qquad \textbf{Equ. I-11}$$

Where $f_1\,(z-ct)$ and $f_2\,(z+ct)$ are progressive waves propagating in the rod (the pile) without modification with the constant velocity +c (downward wave ↓) and –c (upward wave ↑) , respectively.

The velocity is determined by the material mechanical properties, and the form of the waves (f_1 and f_2) are determined by the initial and boundary conditions.

The functions f_1 and f_2 can be used to describe any behaviour propagating in the pile respecting the elastic propagation assumptions (i.e. force & pile particle velocity). Superposition of both forms respects the general wave equation (Equ. I-10).

It is possible to express the forms of the force waves and the pile particle velocity waves in function of the pile particle displacement:

$$F(z,t) = F^{\downarrow}(z,t) + F^{\uparrow}(z,t) = -\,E_p\,A_p\,\frac{\partial u}{\partial z} \qquad \textbf{Equ. I-12}$$

$$\rightarrow \quad F(z,t) = -E_p A_p \frac{\partial u}{\partial z} = -E_p A_p \left(\frac{\partial u^{\downarrow}}{\partial (z-ct)} + \frac{\partial u^{\uparrow}}{\partial (z+ct)} \right)$$

$$v(z,t) = v^{\downarrow}(z,t) + v^{\uparrow}(z,t) = \frac{\partial u}{\partial t} \qquad \textbf{Equ. I-13}$$

$$\rightarrow \quad v(z,t) = \frac{\partial u}{\partial t} = -c\frac{\partial u^{\downarrow}}{\partial (z-ct)} + c\frac{\partial u^{\uparrow}}{\partial (z+ct)}$$

If the geometric conditions impose to work only with one of the two forms, either the downwards waves (semi infinite pile with $z \geq 0$) or the upwards waves (semi infinite pile with $z \leq 0$), Equ. I-12 and Equ. I-13 allow to write:

$$F^{\downarrow}(z,t) = -\frac{E_p A_p}{c} v^{\downarrow}(z,t) \text{ or } F^{\downarrow}(z,t) = I \cdot v^{\downarrow}(z,t) \qquad \textbf{Equ. I-14}$$

$$F^{\uparrow}(z,t) = -\frac{E_p A_p}{c} v^{\uparrow}(z,t) \text{ or } F^{\uparrow}(z,t) = -I \cdot v^{\uparrow}(z,t) \quad \textbf{Equ. I-15}$$

Where:

$$I = \frac{E_p A_p}{c} = A_p \sqrt{E_p \rho_p} \ [\text{N/ms}^{-1}] \quad \textbf{Equ. I-16}$$

I is defined as the nominal impedance of the pile, or the damping factor of the dashpot modelling the behaviour of the semi-infinite pile subjected to a force. The force transmitted through a pile section and the pile particle velocity are proportional, if the pile is supposed free of any other forces of solicitations.

Equ. I-14 and Equ. I-15 express that the force and the particle velocity have the same sign when the force is a compression, and have opposite signs when the force is in traction.

It is possible to express $F^{\uparrow}(z,t)$ and $F^{\downarrow}(z,t)$ as functions of F(z,t) and v(z,t):

$$F^{\downarrow}(z,t) = \frac{1}{2}\left(F(z,t) + I \cdot v(z,t)\right) \quad \textbf{Equ. I-17}$$

$$F^{\uparrow}(z,t) = \frac{1}{2}\left(F(z,t) - I \cdot v(z,t)\right) \quad \textbf{Equ. I-18}$$

If initial conditions are imposed to the extremity of the semi-infinite pile (initial force F_0 and initial velocity v_0), each quantity must respect the following statements:

$$v(z,t) = v_0 + v^{\uparrow} + v^{\downarrow} \quad \textbf{Equ. I-19}$$

$$F(z,t) = F_0 + F^{\uparrow} + F^{\downarrow} \quad \textbf{Equ. I-20}$$

Hypothesis of the method of interpretation

As already explained, the force and velocity are proportional to each other by a term known as the pile impedance, but this relationship is only true when there are no soil reactions along and beneath the pile. If soil is present and acts against the pile, corresponding upward and downward force and velocity waves are influenced. The difference of behaviours is not a net measurement of the soil reaction but a consequence of it. It is the result of all the interactions between generated waves along the pile.

By analysing the formulae of $F^{\uparrow}$ and $F^{\downarrow}$ (see Equ. I-17 and Equ. I-18), in case of no soil interaction and in the real situation, the difference represents the soil reaction.

The distribution of the resistance along the pile shaft can be interpreted from the time development of the upward reflected wave up to 2L/c. After this time, all the waves received and considered as upward waves are indeed a mixing resulting of the interaction of several waves. These waves are generally difficult to interpret because they integrate the effects of several depth-and time-dependent variables (Holeyman, 1992).

The shaft friction can be determined if a constant resistance is assumed to be activated during a certain time. Fortunately, the shaft friction is quickly mobilized and even a dynamic load test can

fully activate the shaft resistance along the pile. So the rigid-plastic behaviour can be assumed for the modelling of this soil reaction part.

The same assessment cannot be done for the base resistance evaluation because the assumption of reaching the ultimate level of soil resistance cannot be met during a dynamic load test. Consequently, the evaluation of the base resistance term from a dynamic load test using the signal processing analysis is dependent on the assumed hypothesis.

The CASE method (Goble et al., 1975) is based on the signal processing approach. Other methods try to differentiate the base and shaft resistances (Liang, 2003) but all of them assume that all terms use a rigid-plastic behaviour.

CASE method

The CASE method (Goble et al. 1975) is derived from the signal processing theory and results in a single pile capacity either "dynamic", namely taking all the loading rate effects into account, or static, with a the use of an empirical dimensionless factor J_c.

The CASE method uses several severe hypothesis to build up the model allowing the calculation of the total soil reaction from the measured dynamic and kinetic signals: the pile is homogenous, elastic and uniform; the permanent pile displacement is sufficient to fully mobilize the pile shaft and base resistances; the damping (J_c) is only considered to be representative on the pile base; the pile must be short enough in order to ensure that the wave travelling during the 2L/c does not perturb the mobilization of the shaft resistance layers.

The downward and upward travelling waves $F^{\downarrow}$ and $F^{\uparrow}$ are determined from the force and the velocity signals at the section of control marqued with x_1 in Figure I-13 (Equ. I-17 & Equ. I-18).

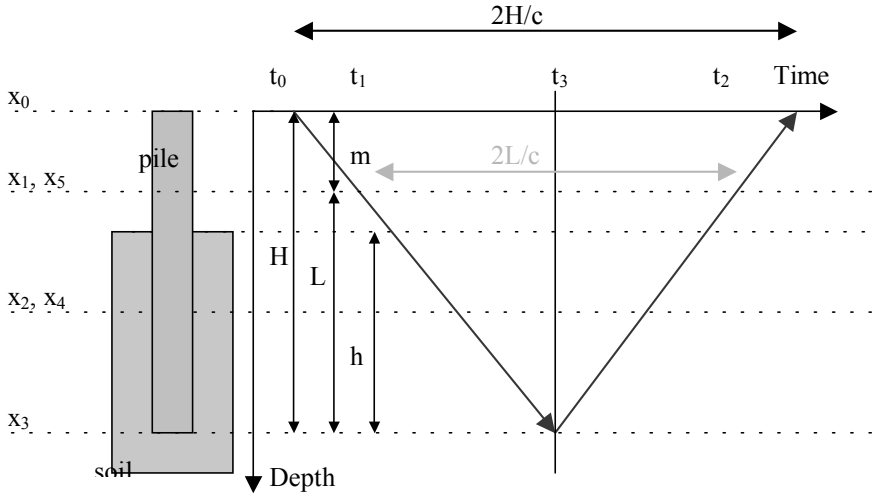

Figure I-13: Description of the propagation wave into the pile (after TNOWAVE manual, 2000)

The driving resistance is calculated from an input/output relation. A wave is introduced to the pile top (input), identified at a time $t_{max} = t_1$ (maximum F_{down}). After one travel, $t = t_{max} + 2L/c = t_5$, part of the wave (F_{up}) returns to the pile top (output). The modification of the wave during this duration is interpreted as the Driving Resistance:

$$R_{tot} = F^{\downarrow}(t_{\max}) + F^{\uparrow}(t_{\max} + \frac{2L}{c}) \qquad \textbf{Equ. I-21}$$

The total driving resistance R_{tot} is defined as the sum of the downward travelling force wave at a time t_{max} and the upward travelling force wave at a time t_{max} + 2L/c.

To determine the static term from the total estimated resistance, the CASE method assumes that the driving resistance is entirely at the toe and the dynamic driving resistance is assumed to be proportional to the pile toe velocity, calculated from the measured pile head force and velocity. The factor of proportionality is J_c called the "CASE damping constant", and determined by correlation with static load test or from signal matching.

$$F^{\downarrow}(t_{\max}) = F_{t1}^{\downarrow} \text{ and } F^{\uparrow}(t_{\max} + \frac{2L}{c}) = F_{t2}^{\uparrow} \qquad \textbf{Equ. I-22}$$

$$R_{tot} = F_{t1}^{\downarrow} + F_{t2}^{\uparrow} = R_{stat} + R_{dyn}$$

$$R_{dyn} = J_c \cdot I \cdot v_{base} \qquad \textbf{Equ. I-23}$$

Where I is the pile nominal impedance.

Since

$$v_{base} = \frac{F_{t1}^{\downarrow} - F_{t2}^{\uparrow}}{I} \qquad \textbf{Equ. I-24}$$

$$R_{stat} = F_{t1}^{\downarrow}\left(1 - J_c\right) + F_{t2}^{\uparrow}\left(1 + J_c\right) \qquad \textbf{Equ. I-25}$$

$$R_{stat} = \frac{\left(F\left(t_1\right) + I \cdot v(t_1)\right)}{2} \cdot \left(1 - J_c\right) + \frac{\left(F\left(t_2\right) - I \cdot v(t_2)\right)}{2}\left(1 + J_c\right) \qquad \textbf{Equ. I-26}$$

Equ. I-21 can be transformed into:

$$\frac{\left(F\left(t_{\max}\right) + F\left(t_{\max} + \frac{2L}{c}\right)\right)}{2} + M \cdot \frac{\left(v(t_{\max}) - v(t_{\max} + \frac{2L}{c})\right)}{\frac{2L}{c}} = R_{tot} \qquad \textbf{Equ. I-27}$$

This last result interpreted as the driving resistance is the sum of the average forces applied to the pile head at the times t and (t+2L/c) and the inertial effect of the pile during the period 2L/c considering the average deceleration. (Holeyman, 1984).

Some typical values for the CASE damping constant J_c are given in chapter 2.

The time t_1 can be chosen at any time, but, practically, it must be chosen in order to ensure that the corresponding second time (t_1 + 2L/c) does not correspond to a time where some reaction along the shaft have been inverted. This situation should underestimate the total pile resistance.

3.2.3.4 Numerical models

The numerical models approach the pile/soil interaction by a computer simulation of the event measured during the test. A model is needed to describe the different terms of the soil reaction mobilized: the shaft friction reaction, the base reaction, the viscous and radiation terms of the soil mobilization. The main goal of the technique is to adjust the parameters characterizing the pile/soil model chosen in order to fulfil a criterion based on the measured data issued from the dynamic test. When the criterion is achieved, the model is considered as describing the pile/soil system and the purpose of the test or the design is satisfied.

The criterion commonly used by numerous procedures uses the force and the velocity at the head of the pile in function of time as input and control data of the matching procedure. When the model is processed, both signals (or a combination of both signals) can be calculated if the model is excited with an input corresponding to a dynamic event. The procedure follows the following steps:

Either the force or the velocity[3] is imposed as a stimulus at a boundary of the model;

The model uses this stimulus and calculates the pile/soil response according to the requirements of the operator. Either the velocity (if the force is used as stimulus) or the force (if the velocity is used as stimulus) is calculated in function of the pile/soil model parameters;

The computed signal and the measured signal (non used as a stimulus) are compared and a quality criterion determines the degree of agreement between both signals.

If the matching is sufficient, the procedure is finished and the chosen parameters are considered to describe the pile/soil model for the dynamic test used in the configuration of the chosen model;

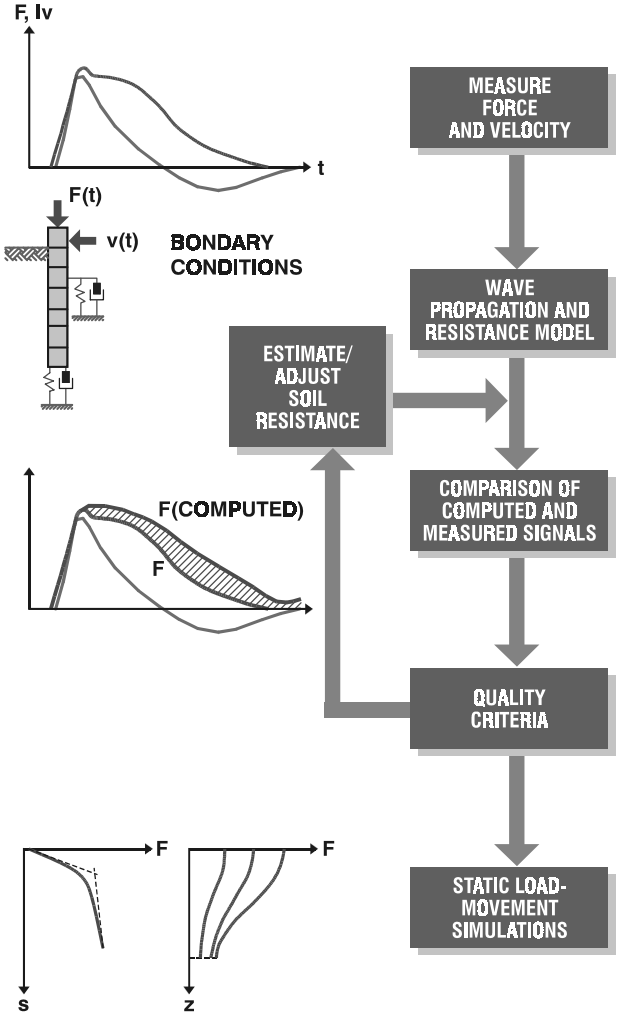

Figure I-14 : NUSUMS procedure (Holeyman, 1992)

If the quality criterion does not fulfil the requirements of agreement, the model parameters are re-estimated and a new loop is launched in order to improve the matching agreement.

[3] Or a combination of signals like the downwards force wave

The described procedure is summarized in Figure I-14. All these procedures can be referred to as NUSUMS for NUmerical Simulations Using Measured Signals (according to Holeyman, 1992). Several methods related to this methodology have been developed, CAPWAP® (Rausche et al., 1972) TNOWAVE® (Middendorp, 1987), KWAVE® (Matsumoto et al. 1991), SIMBAT® (Paquet, 1988), the method developed inside the Civil an Environmental Department of the Université catholique de Louvain and called NUMSUM-UCL and a lot of methods without a specific brand names and often corresponding to a scientific research without commercial or wide utilization.

All the methods use the algorithm aiming at minimizing the gap between a measured and a computed signal in order to achieve the matching procedure. But there are some essential differences either in the model describing the pile, the soil or the propagation of the waves in the soil, or the model describing the resolution of the pile/soil interaction:

- The previous methods use either a finite element or a finite difference method in a lumped model or a continuous model based on the differential equation characteristics or still a full continuous description.

- The pile/soil system can be modelled with a classical 1-D longitudinal approach (Smith, 1960; Holeyman, 1984), a construction allowing for the soil behaviour in a near and far field (Deeks and Randolph, 1992, El Naggar, 1992 & 1994), a development of the soil motion in a 1-D radial approach (Holeyman, 1985, 1994, 1996) or a model working with a complete 3-D representation (Chow, 1981).

- The soil interaction is described by many authors (either for shaft or base reaction): Smith (1960) – Holeyman (1984, 1985, 1988) – Randolph and Simons (1985), Randolph and Deeks (1992) – Paquet (1988) – El Naggar & Novak (1992, 1994) – …

- And different loading rate effects on the pile capacity: the viscous term – the radiation term - …

- Each method uses a quality criterion that can be purely mathematical, oriented with statistical data and/or geotechnical guide or purely visual.

- The input and the reference signal can be the raw measured signals (Acceleration and Strain), the same signals after a first treatment (Velocity and Force) or a combination of them (Up and Downward waves).

Examples

TNOWAVE®

TNOWAVE® is based on the method of characteristics, firstly introduced by Voitus van Hamme (1974) and derived from the stress wave theory.

The pile is divided in continuous elements (Figure I-15). Each segment has an uniform section and is modelled with elastic and homogeneous material. The length is equal to the travelling distance of the wave during an incremental time step.

As derived from the wave equation theory and shown by Figure I-15, every soil reaction (base or shaft friction) or impedance sudden change (section, volumetric change) implies the creation of a reflected wave to the incident one. Consequently, at each Δt, the calculations of the propagation of all waves (upward and downward) is done and results in the creation of all reflected waves in function of the soil and pile modelling. The superposition of all waves, the equilibrium and continuity conditions at the boundaries of the segments allow the calculation of the dynamic and kinetic states of each pile segment: forces, velocities, accelerations and displacements are known.

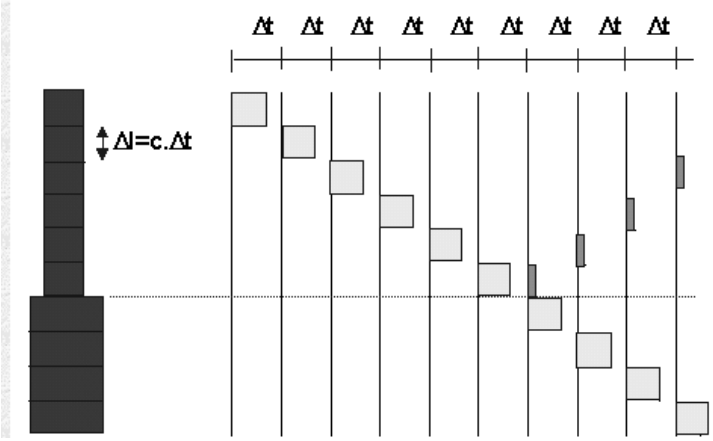

Figure I-15 : propagation of a wave into the TNOWAVE pile discretization (with differentiation) (after TNOWAVE manual, 2000)

The TNOWAVE soil model follows either the approach of Smith 1960, with an elasto-plastic static term and a dynamic term linearly dependent to the velocity, or a more complicated soil model (Randolph and Simons, 1986 and Randolph and Deeks, 1992) allowing for radiation of energy into the soil.

The model allows for loading, and unloading with a possible stiffer unloading. A yield factor allowing the use of an ultimate soil resistance different for the tension and compression domains is also available in the program. The program allows for the analysis of tubular piles and the differentiation of the inside and outside friction. The soil fatigue can also be taken into account. (TNOWAVE help manual, 2000).

CAPWAP®

The CAPWAP® program (CASE Pile Wave Analysis Program) developed by Rausche (1970) is a method allowing to determine soil resistance forces (dynamic and static) and their distribution along the shaft and at the base based on the method of characteristics (like TNOWAVE). This analysis can also determine the soil quake, damping parameter and simulated load –settlement curve for the base and head behaviours.

In each pile element, the superposition of both upward and downward waves yields forces and velocities at the upper and/or lower boundaries of segments. The velocity is integrated into displacement for each pile segment. The pile motion and force states are solved for the chosen description of pile/soil interaction for all the pile elements.

The displacement and velocity of each pile segment are chosen relative to the soil. The static term of the soil reaction is modelled by an elasto-plastic spring and a linear dashpot describes the

viscous part of the resistance. The model allows to use either pile head velocity, pile head force or a combination of both measured signals for the signal matching procedure. The model allows for unloading and reloading, stiffer shaft unloading than loading, toe model working with plug and gap between pile and soil (Figure I-16).

A radiation damping can be also added to the basic Smith model in order to account for the energy radiated away from the pile into the soil when the soil reaction is low. The radiation term is function of the pile velocity. A mass and a dashpot are used to replace the rigid soil support of the Smith model. The masses are present in order to express the relative displacement and velocity quantities of the soil adjacent to the pile.

The program models splices and cracks. Internal damping is also modelled by reducing the magnitude of waves travelling into the pile. Finally, a module allows one to take the residual stresses of previous blows into account.

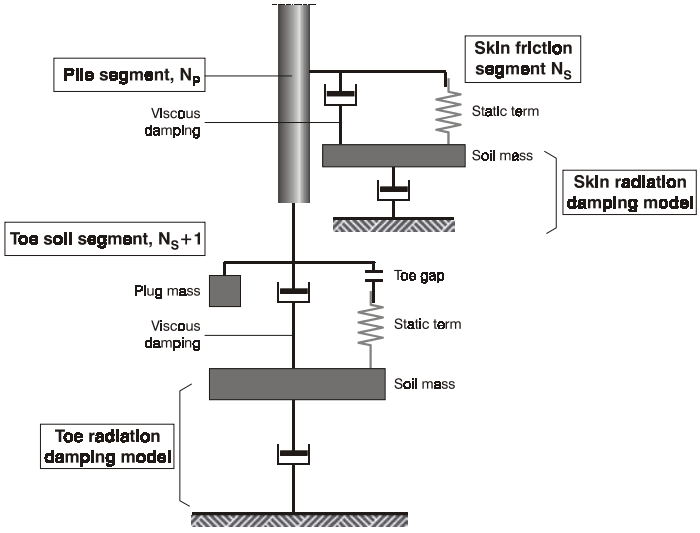

Figure I-16 : CAPWAP extended soil resistance model (after CAPWAP manual, 2000)

SIMBAT®

The SIMBAT® method (Paquet, 1988; Dali & Heritier, 1992; Stain, 1992) is a global procedure used to determine the equivalent static load-settlement curve using a complete sequence of blows of a dynamic load test. In the classical methods, only one blow is used to study the dynamic behaviour and evaluate the static resistance from a dynamic test. SIMBAT uses a sequence of blows in order to transmit different levels of energy.

The SIMBAT philosophy is based on the fact that at high strain rates the ratio "Dynamic" Resistance / "Static" Resistance is higher than at low strain rates. In this way of thinking, a sequence of blows is arranged so that a wide range of strain rate is explored with the aim to project the dynamic resistance versus the penetration per blow for different strain rates (Figure I-17). Where the zero strain rate is reached, the dynamic resistance is supposed to be the static one.

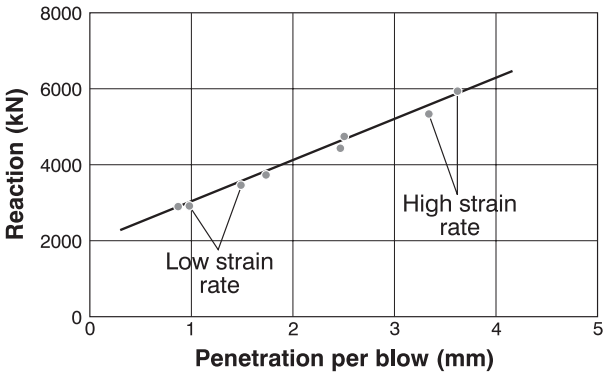

Figure I-17 : Dynamic testing at varying strain rates

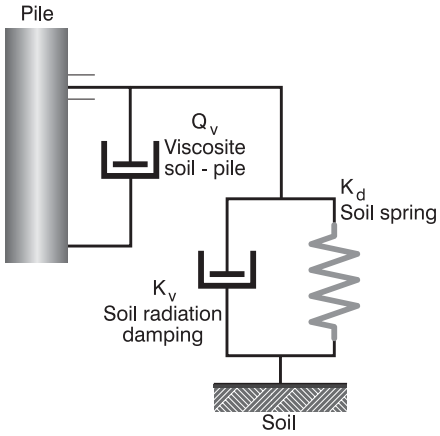

Figure I-18 : SIMBAT shaft model (after Dali & Heritier, 1992)

The dynamic resistance, R_d, is calculated by the classical wave equation theory by using the CASE formula (Equ. I-26) (Goble et al. , 1975). After calculation, a simulation programme can be used to check if rupture has occurred at each point during the return of the wave. If this condition is fulfilled (if the total dynamic resistance calculated from the model corresponds to the CASE one), the failure is assumed everywhere in the pile/soil interface and the model of the pile/soil interaction is validated. If not, the model does not correspond and the soil probably does not reach the ultimate resistance everywhere around the pile. A new simulation with the program must be performed to recalculate R_d and describe the pile/soil model.

The pile soil model adopted for SIMBAT differentiates the interface behaviour than the soil behaviour. The three media (pile, interface, soil) have their own motion and the associated reaction is linked to this motion.

The main methodology is the following:

- Signal acquisition & corrections (several blows);
- Separation of forces (upwards and downwards);
- Measurement of dynamic soil reaction R_{dyn};
- Regression analysis amongst all the blows to deduce the pile/soil system parameters;
- Extracting of the static resistance from the dynamic resistance;
- Take the elastic shortening of the pile into account and plot the load-settlement curve;
- Confirm with a computer simulation using the model explained below to check the hypothesis, and to calculate the distribution of soil resistance. An hyperbolic curve could also represent the total load-settlement computed curve.

KWAVE®

KWAVE®, developed in Japan (Matsumoto & Takei, 1991 takes into account the wave propagation in the soil inside a pipe pile and the influence of the internal shaft resistance on the

wave propagation. The pile soil model follows a lumped model (Figure I-19). The soil models for shaft and base follow the models of Deeks and Randolph (1992) and Simons & Randolph (1985).

The values of the spring constants, the radiation damping constants, the dashpot and the soil mass parameters for both shaft and base models are determined from soil test data such as the shear modulus, Poisson's ratio and the soil density (Matsumoto et al, 2000). The process of matching uses the downward stress wave as input for the back analysis resolution.

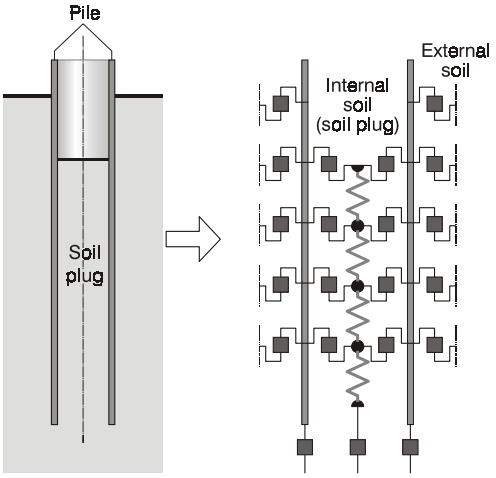

Figure I-19 : KWAVE® pile/soil system for pipe pile (after Matsumoto et al. 2000)

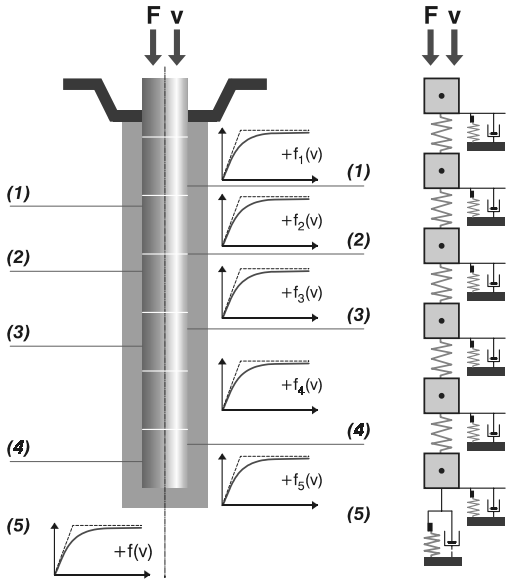

Figure I-20 : Description of the model used in NUSUM-UCL

NUSUM-UCL

The pile and its environment are described with a lumped model such as described in Figure I-20. This model allows a description of the kinetic and dynamic fields either of the pile or the soil in the direct vicinity of the pile during a transient solicitation. Force or velocity can be imposed at the pile head and the relative state of all parts of the model (stresses, forces, displacements, velocities, accelerations, …) is calculated at each time step in an explicit algorithm based on the finite difference scheme. The pile/soil model takes the loading rate effect into account with respect to the radiation damping and the viscous effect. It can consider also a hyperbolic or elasto-plastic static stress-strain relationship either for the base or the shaft modelling. The base and soil models follow the Holeyman approach (Holeyman, 1984) for the of the soil reaction's modelling. The model is allowed to take into account of the slippage between the pile and the soil. The process of the dynamic signal solving is based on an automatic signal matching technique using an algorithm working on the sensitivity of parameters to change towards the best solution.

This model is detailed in chapters 3, 4 and 5 of this thesis, either for the pile/soil model or the optimisation procedure. Slippage is also described in detail. The application of this treatment on the Sint-Kateline Waver and Limelette loading tests will be also proposed in order to point out the loading rate effect.

4. Advantages and disadvantages

There is no test available which can provide unequivocal information on all the design aspects required. A load test, either SLT or DLT, is influenced by many factors (installation, pile type, soil conditions, load history and test, …) but its goal remains the evaluation of the behaviour of the infrastructure in term of safety and settlement during the pile service. None of the tests can be considered as an accurate method but rather as an insight in combination with the test limitations. So, as conclusions to this chapter, it is interesting to gather the advantages and disadvantages of each method in a non-exhaustive list.

4.1. Static Loading Test

4.1.1 Advantages

The static test is considered as the reference test because it is the one that corresponds the most with the way that the load is applied in reality (duration, loading rate and type of loading). Moreover, the static test is generally regarded as the definitive test the one against which other types of tests are compared. These elements are obviously the best advantages of this kind of test.

Another point is that the data obtained are directly interpretable because they are linked to the acceptance criteria (maximum settlement and authorised stiffness and/or design load) and because the main interpretations were created with respect to this kind of test. Consequently, all the other methods tried to predict a response comparable to the load settlement produced by the Static Load Test.

The measurements are generally independent of the pile material properties even if this independence can be called into question (see the disadvantages).

4.1.2 Disadvantages

Because of the similarity of the test to the reality, the time needed to carry it out is necessarily long, and this duration is costly in term of money and contract planning. Moreover, the slow loading rate imposes that the load applied is high enough to get closer to the real load to be applied to the foundation. So the mobilization of this load and of this associated reaction is strongly expensive regarding to the obtained result (one pile tested). Consequently, the higher disadvantages of this loading test motivate the engineers to create other loading tests reliable, rapid, economic, and generating a comparable result.

The reaction supplied for the applied loading (kentledge, reaction piles, ground anchors) generates some associated effects or interaction with pile that perturb the interpretation of the results. These stresses will increase the shaft friction and the base capacity and the pile settlement is reduced and the pile head stiffness is also overestimated. Those interactions can perturb the beam of reference used to measure the settlement.

It should also be noted that there are many procedures for static pile load testing. From Maintained Load Test to Constant Rate of Penetration Test, a broad set of test regimes and procedures are possible. Due to the different loading paths, any pile subjected to the various tests will exhibit a

different load-settlement response influencing the conclusions because the results are influenced by loading history (steps and duration).

4.2. Dynamic Loading Test

4.2.1 Advantages

The dynamic test was created with the aim to improve the productivity in term of quality control and design confirmation. These objectives seem to be achieved because the test is accepted as a routine procedure and also used for the estimation of the static load-settlement behaviour to be compared to the corresponding static one.

Since the test need a short time to be organised, performed and analysed, since the used device weighs about 1.5 to 2 % of the mobilized pile capacity, the test can be performed on more piles on site (till 10% of the installed piles) during the same period generating a huge cost saving.

The test is often used to integrity testing giving a method of inspection of the pile profile and of the pile homogeneity. This a direct consequence of the underlying wave equation theory.

The tests can also be performed on very large in diameter and capacity piles that can be tested statically with difficulty. The test can also be applied on piles offshore without difficulty.

4.2.2 Disadvantages

The potential limitations of DLT tests include the fact that the load-settlement behaviour is estimated and not unique (corresponding to a best fit estimation with respects to assumptions made about the pile/soil interaction model). The acceptance criterion is consequently dependent of the assumptions made in term of pile stiffness and soil ultimate resistance.

The high technicality of the test causes a sophisticated phase of interpretation. Without well trained personnel, it is impossible to achieve a correct and proper dynamic test.

As the load is applied very quickly, the time-dependent settlement behaviour are not developed during the test. Besides, the dynamic effect of loading rate generates strongly non linear adding soil resistance that needs an interpretation significantly sensitive to assumptions.

Under impact, a pile is subjected to a complex combination of compressive, tensile and bending forces that may produce much higher stresses than under service conditions. If not accounted for, these stresses can exceed material strength and cause structural damage.

The measurement accuracy is also dependent of either the pile material properties (concrete or steel volumetric mass, wave propagation velocity or dynamic modulus), or the mathematical process needed to evaluate the pile particle velocity and displacement from the measured acceleration. Due to the fact that the pile is struck by a falling mass, the soil is rarely completely mobilized. The dynamic tests can often mobilize the shaft friction but rarely the base reaction. So the prediction of a complete load-settlement curve until large settlements is highly unlikely or must be considered with regards to the assumptions.

Finally, the set-up or relaxation effects and the evolution of the pile bearing capacity with time impose to the test to be performed at a certain time after driving.

5. Conclusions

This chapter aimed to describe the procedures of loading studied in this research, their definitions, their main characteristics and methods of interpretations. It was shown that the pile testing is performed with a wide variety of methods of which the complexity is generally proportional to the rate of the applied loading. the faster is the loading, the more complex is the interpretation and the data management. This complexity is due to the viscous and inertial additive terms that must be withdrawn in order to obtain the equivalent static pile/soil behaviour.

The so-called" dynamic procedures of loading (DLT) are "young" processes and present a large quantity of interpretation methods. Each of them are based on a typical characteristic of the loading procedure: either the propagation of the wave (CAPWAP, …), or the wave equation theory (CASE method). The complexity of the method is often linked to the precision and the diversity of the result (the static pile bearing capacity, the static load settlement curve or the soil reaction distribution along the pile). A general overview of these methods is proposed and each one is described with respects to their main characteristics.

Finally a short critic of the two loading procedures is given and a specific attention is put on their differences, advantages and disadvantages.

CHAPTER 2
Loading Rate Effect and Literature

1. Introduction

Soils like many other materials, exhibit strong time-dependent behaviour, which can be translated in term of creep, relaxation or strain-rate effect. The degree of this rheological behaviour varies with the type of soil (sand and the opposite, clay), the type of structure, the soil stress history (Mitchell, 1976).

It is widely recognized that cohesive soils behaviour is very sensitive to the rate of loading, i.e. there is a general agreement that an increase in rate of deformation results in an increase of the undrained shear strength (Richardson and Whitman, 1963; Berre and Bjerrum, 1973). Generally, an increase of 10 … 20% of strength is measured per logarithm cycle of strain rate (10 times). Loading rate effects can be considered sometimes as minor for sands, sometimes not. And for problems involving dynamic loading, the influence can be significant.

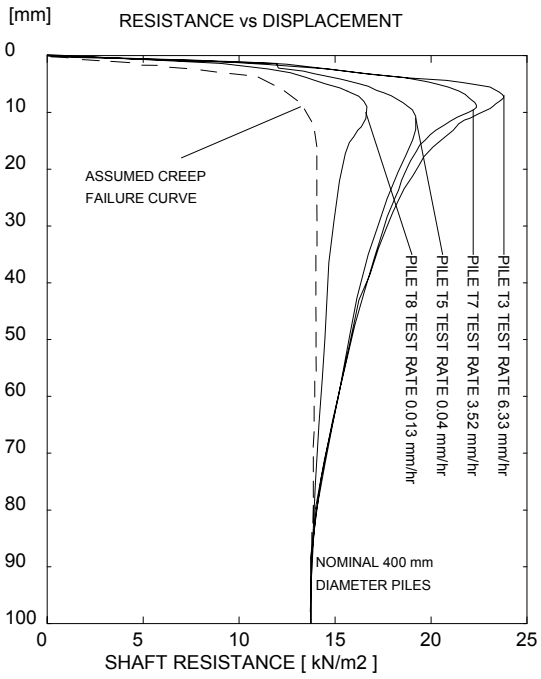

Figure II-1 : Shaft friction deduced from different CRP tests (after Lyndon et al., 1994)

Loading rates have also affected the axial capacity of piles. Kraft et al. (1981) reported that the ultimate bearing capacity of piles embedded in clay increases by about 40% to 75% when the loading rate is increased by about three orders of magnitude. The development of the Constant Rate of Penetration Test (Whitaker, 1963) has shown that the rate of penetration enhances pile shaft resistance in clay soils (Whitaker and Cooke (1966), Burland et al (1988), etc…). Indeed, a gradual loading rate increase for

many CRP tests in clay exhibits a variation of peak resistance as illustrated in Figure II-1. It is therefore concluded that the peak resistance is induced by the testing regime employed, and is therefore a function of the rate of load application.

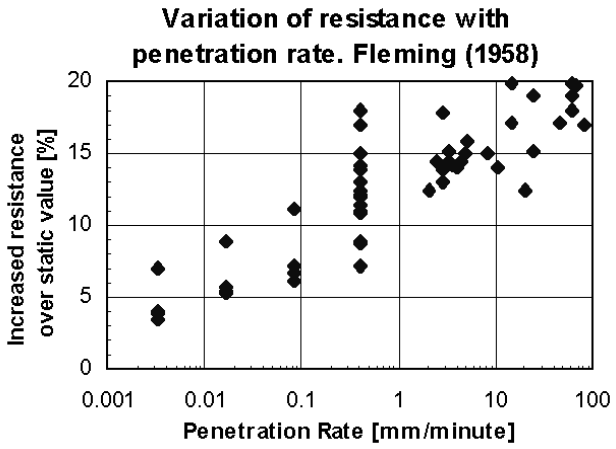

Figure II-2 : Model pile resistance vs penetration rate (after Fleming, 1958)

For cohesionless materials, the increased skin friction due to rate is also apparent: a series of experimental results from model piles in sands are illustrated in Figure II-2 (Fleming, 1958).

Pile driving and dynamic pile testing are situations where the effect of the loading rate are exacerbated because of the high impact velocity of the hammer on the pile head. Smith (1960), has observed numerous driving processes on many piles in many soil configurations. He developed the first practical model of hammer-pile-soil system used for numerical analysis of pile driving to foresee the drivability and the bearing capacity of driven piles. He introduced a simple parameter, called the Smith damping factor, linearly dependent upon pile velocity to describe the additional resistance of the soil due to the dynamic solicitation.

This first attempt of modelling of the loading rate effect led the way followed by scientists and contractors to differentiate the static term from the measured resistance. This parameter has been evaluated after correlations with Static Load Tests. More elaborated models have been built based on the simplicity of the Smith approach or including a sophisticated description of the loading rate effect.

This chapter presents these developments including the tests carried out to highlight the phenomenon, the general approach based on a global parameter and the analytical models developed in terms of fundamental soil parameters with the aim to describe more precisely the loading rate effect.

2. Definitions

The Smith's empirical parameter includes many aspects of pile-soil behaviour occurring during the loading, either along the pile shaft or at the base, or either in the direct interface or into the close vicinity in the surrounding soil. These parameters can be summarized as:

- The inertia of the soil and the level of coupling between the soil and the foundation;
- The excess pore pressure generated in the soil due to driving;
- The undrained behaviour of the pile/soil interaction during dynamic loading;
- The failure mechanisms different during static and dynamic loading events;
- The losses of energy due to the viscous intrinsic behaviour of soils;

- The hysteretic losses of energy of the loading-unloading soil behaviour.

All these effects are commonly taken into account by a simple viscous parameter because of the analogy with the mechanical models where a loss of energy can be modelled by a dashpot. It is also due to the ease and the simplification in the solving process to use only one parameter. This section is focused on the succinct definition of the underlying behaviours introduced by some of the authors of the analytical models.

2.1. The hysteretic term

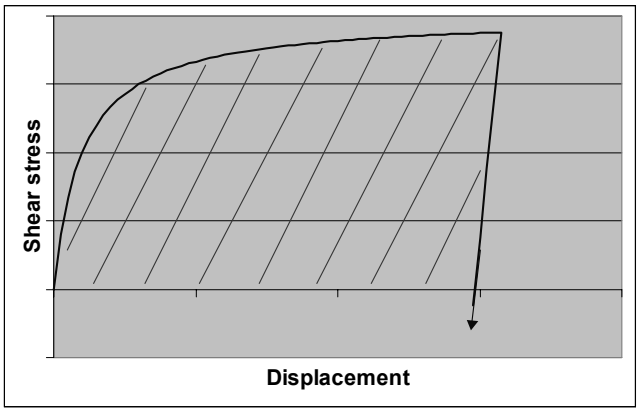

Figure II-3 : Representation of the hysteretic damping

The pile/soil interaction is governed by a stress-strain or stress-displacement relationship. The form of this function portrays not only the intrinsic behaviour of the soil during the loading (elastic, elasto-plastic, hyperbolic, rigid-plastic,…) but also during the unloading. Often, the soil does not follow the same stress path for loading and unloading processes, generating a permanent settlement and a loss of energy used to settle permanently (Figure II-3). This behaviour is sometimes governed by the initial tangent modulus. It is due to the nature of the intrinsic behaviour of the soil. The hysteretic behaviour leads to damping of a free system governed by this law, and is called hysteretic damping. It is not related to the rate of loading and is solely defined by the pile/soil interaction law. It is not a velocity dependent term even if Svinkin et Abe (1992), describe a correlation between the hysteretic damping and the CASE damping factor.

2.2. The viscous term

The viscous term is related to the intrinsic behaviour of soil material. It is similar to the notion of damping introduced by Smith and follows the next formulation for a normal stress:

$$\sigma = \varepsilon \cdot E + E' \cdot \frac{\partial \varepsilon}{\partial t} \qquad \textbf{Equ. II-1}$$

- σ is the stress generated [Pa];
- E is the elastic modulus [Pa];
- ε is the strain generating this stress [-];
- E' is the modulus of viscosity [$Pa.s^{-1}$].

(after Holeyman, 1988)

This visco-elastic behaviour is dependent of the loading and unloading rates. It is also relevant to the soil behaviour and is related to the dissipative behaviour of the soil. The typical viscous term is often neglected due to its small contribution to the total loss of energy. Some authors do not neglect it, such as Nguyen et al. (1988) or El Naggar et al. (1994). The viscous term is also often combined with the

increase of ultimate resistance observed when the loading rate is stepped up. This observation is made after the soil sample or the soil reaches failure, so the observation concerns the ultimate resistance and can be interpreted as the sum of all above mentioned behaviours. But the term used for the present definition is not the same and does not have the same amplitude than the global term (even if both parameters have the same denomination in literature). The effect of internal viscous damping on the strength of concrete is shown on Figure II-4 in a similar behaviour than expected for soil.

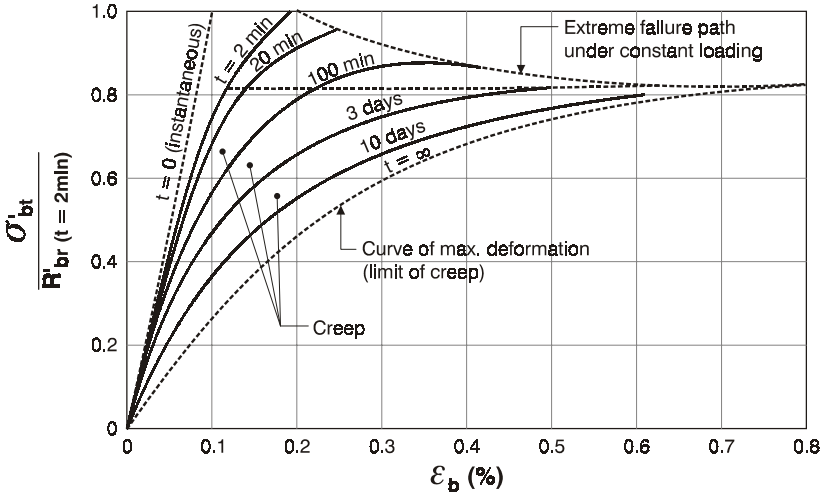

Figure II-4 : Effect of loading rate on concrete strength

2.3. The radiation term

The radiation term is one of the most important factor responsible of the loss of energy during the dynamic loading, more for the pile shaft than the pile base behaviour (Holeyman, 1992). This term can lead the pile to failure by itself (Heritier and Paquet, 1984).

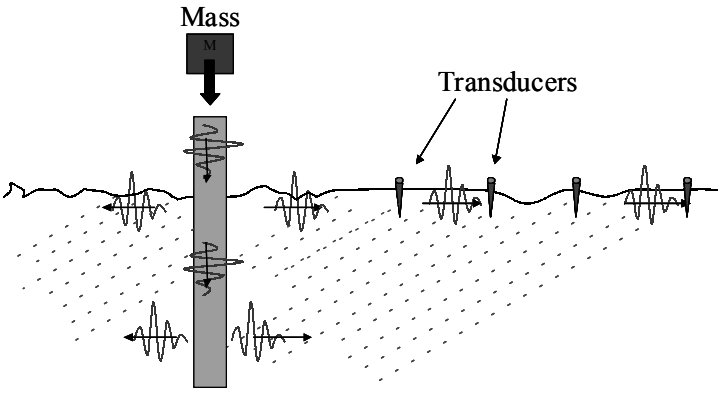

Figure II-5 : Energy radiation in the surrounding soil

The pile forces due to impact generate downward pile motion and soil forces react against the pile penetration. The energy dissipation associated with the soil resistance occurs in the interface between the pile and the soil but also in the surrounding soil by creation of the soil motion (linked to its inertia). This behaviour can be highlighted by transducers placed on the soil surface in the vicinity of the pile (Figure II-5). Several factors such as soil type, pile shape and pile volume, pile shaft smoothness or soil stiffness and volumetric mass modify this motion. Moreover, the level of soil mobilization is inversely related to the transmitted wave. The closer the soil is to failure, the less radiation energy is transmitted. The slip layer created with the failure between the pile and the soil acts like a barrier that no wave can pass through.

Several authors tried to take this term into account out of the general viscous damping: Novak et al., 1978; Holeyman, 1985 & 1988; Randolph and Simon, 1986; Corte and Lepert, 1986; Mitwally and Novak, 1988; Paquet, 1988; Randolph and Deeks, 1992, Likins et al., 1992, and many others.

2.4. The excess pore pressure generated by the dynamic loading

Generally the pore pressure is getting higher during a dynamic pile loading test or driving. This behaviour causes an instant decrease of the effective stresses and an underestimation of the bearing capacity. It is the main reason explaining the set-up effect, and motivating restrike tests a few hours, days or weeks after driving (depending on the soil type) in order to check the bearing capacity. With this delay, the excess pore pressure has sufficient time to be gradually dissipated. Moreover, the analysis must be performed on the first blows of the restrike to avoid new excess pore pressure to be generated. A lot a authors have written on this subject in the last 30 years (Randolph et al., 1979; Skov & Denver, 1988; Svinkin et al, 1995; Svinkin, 1996, 1997 & 2000; Paikowsky et al. 1996; Axelsson, 1999, Chow et al. 2000, Seidel & Kalinowsky, 2000) but it is not specifically a loading rate effect. Nevertheless, some authors, working on the driving of pile models in clay and sand in calibration chambers (Brown et al. 2002; Eiksund & Nordal, 1996) observe that the pore pressure response in the region below the pile is a function of the stress distribution. Some negative pore pressure can occur increasing the dynamic resistance due to the instant blow.

2.5. The static and rheologic denominations

The term generally used to describe the loading rate effect is called the "viscous" damping factor determining the so-called "dynamic" resistance. In order to be clear with each term used or not within each reviewed theory, the following denominations are used to describe each parameters:

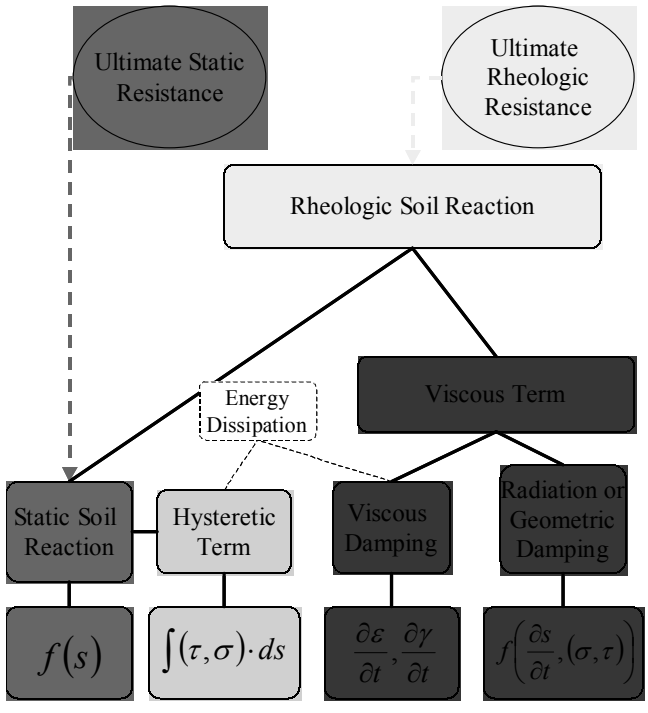

Figure II-6 : Overview of loading rate effects

The **radiation damping** or geometric damping reflects the transfer of energy into the soil surrounding the pile by moving it. This term is directly linked to the loading rate and to the level of mobilization;

The **hysteretic and viscous dampings** are intrinsic parts of the soil behaviour. Both are energy dissipating, it is the reasons why they are both called "damping". One is velocity dependent, the other is function of the strain path and the soil motion. Both are linked to the soil reaction and they are associated in a term called the dissipative term;

The sum of the viscous and the radiation terms is introduced as a **viscous term** added to the static soil reaction.

It is defined as directly linked to the

velocity of the moving element (pile, soil or interface) and is dependent to the loading rate;

The sum of the static soil reaction and the viscous term defined here above is called the **rheologic soil reaction** by analogy with the rheology (science of the deformation and flow of materials);

The ultimate and maximum reaction of the soil is called the **static ultimate resistance** and the sum of the static and viscous ultimate resistances is called the **rheologic ultimate resistance**.

Figure II-6 summarizes each terms and their associations. Both circles also express the ultimate resistances available.

3. The global damping parameter J

This section is focused on the mainly used velocity dependent relationship in the pile driving and dynamic loading test domains. First based on the approach of Smith (1960), followed by Coyle & Gibson (1968) and the theoretical approaches of Goble et al. (1975) and Rausche et al.(1985), the first attempt to describe the added soil resistance during driving was a velocity dependent approach. This section aims to describe these attempts in the framework of the driving and dynamic load testing with a particular attention made on correlations with static pile tests and typical parameters (soil type, transmitted energy, …).

3.1. The Smith approach

Smith (1960) developed a method to obtain the ultimate load versus set by using a finite difference method in which the wave equation theory is implemented. The pile/soil system is idealized by appropriate springs, dashpots and masses (with respect to the mechanical properties of the pile material) (Figure II-7). The model used to describe the pile/soil interaction is the elasto-plastic relationship allowing for loading and unloading (oabcdef on Figure II-8) for the shaft friction and only the compression mode (oabcf on Figure II-8) for the base reaction.

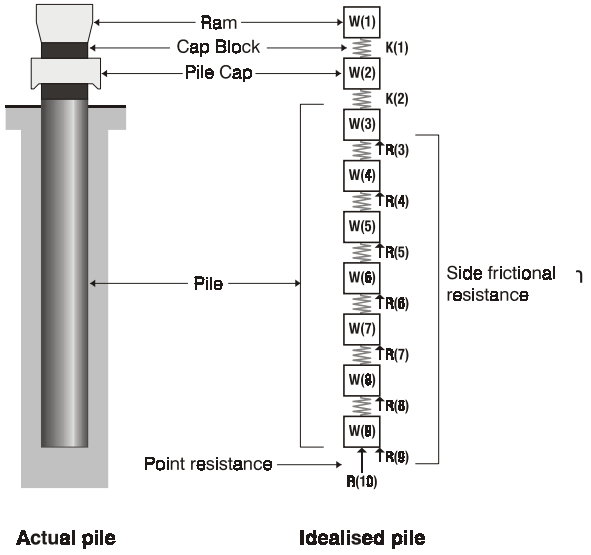

Figure II-7 : Idealization of pile Smith (1960)

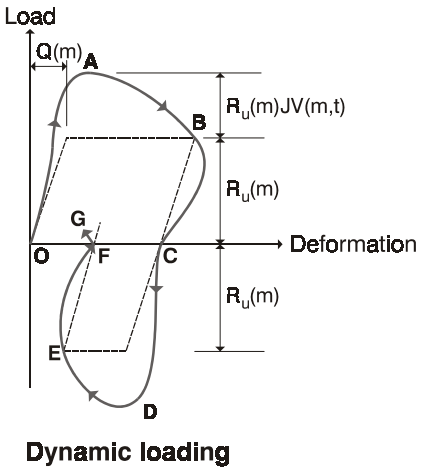

Figure II-8 : Static and dynamic load-deformation curves for the Smith model

Smith decomposed the observed soil reaction in a static term (dashed line) and in a so-called dynamic term (called "viscous" in this research). The static behaviour is pile displacement dependent and defined by the quantities Q and R_u where Q is the quake or the maximum soil deformation that may occur elastically and R_u is the ultimate static soil resistance (Equ. II-2). The static behaviour can be replaced by a spring in an equivalent rheological model where the spring stiffness can be deduced from Q and R_u:

$$K = \frac{R_u}{Q} \qquad \textbf{Equ. II-2}$$

The viscous term is added as a linearly pile velocity dependent term of which the main factor is J_s, called the Smith damping factor [s/m]. The viscous reaction is also proportional to the static soil reaction. Smith considers that the fast driving of the pile causes the flow of the soil around the base. According to that, he considers that the soil reaction must be proportional to the rate of the mobilization.

$$R_{rheol} = R_s + \left|R_s\right| \cdot J_S \cdot v \qquad \textbf{Equ. II-3}$$

R_{rheol} is the rheologic soil reaction [N];

R_s is the mobilized static soil reaction [N];

v is the pile velocity, soil is motionless [m/s];

J_s is the Smith standard damping [s/m].

The value of R_s in absolute value is related to the velocity sign.

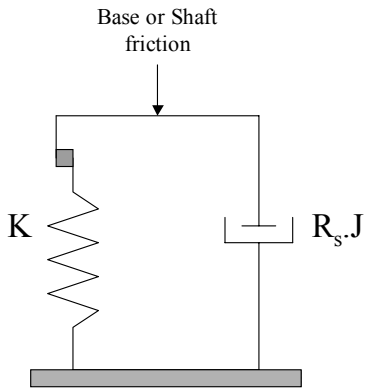

Figure II-9 : Equivalent rheological soil model

The addition of both terms models the rheologic soil reaction and is described by the load-deformation curve of Figure II-8 and the equivalent rheological model on Figure II-9. This model is used either for the base or the shaft reaction. The soil beyond the slip layer is considered fixed. So all the energy lost in transmission in the surrounding soil is included in the rheologic parameters of the equivalent soil model. The observations made by Smith concerned the ultimate resistances but this form is used for the intermediate steps during the numerical processing in many programs.

3.2. The J values and the evolution of the relationship

Initially, the quake Q is shown equal for base and shaft, (0.1 inch ~ 2.5 mm) and J_s is found to be less for the shaft than the base :

$$Q = 0.1\,\text{inch} \sim 2.5\,\text{mm} \text{ (base and shaft)} \qquad \textbf{Equ. II-4}$$

$$J_S(shaft) = \frac{1}{3} J_S(base) = 0.05 \text{ s/ft} = 0.16 \text{ s/m}$$

Forehand and Reese (1964) suggested empirical values for Q and J_S(base) as seen on Table II-1.

Soil	Q [in.]	J_S(base) [s/feet]
Coarse Sand	0.1	0.15
Sand gravel mixed	0.1	0.15
Fine sand	0.15	0.15
Sand and clay or loam (50% of pile in sand)	0.2	0.2
Silt and fine sand underlain by hard strata	0.2	0.2
Sand and gravel underlain by hard strata	0.15	0.15

Table II-1 : Empirical values of Q, J_s - Smith approach (after Forehand and Reese, 1964)

Q values can be derived from pile-settlement theory in the elastic theory or the soil-resistance curves. According to this theory, the value of Q must be greater with depth and larger at the pile base than at the pile shaft. Coyle and Gibson (1970) relate the value of J_S(base) to the internal friction angle ϕ' for sands and to the liquidity index (LI) for clays.

GRLWEAP recommends using the following values for damping and quake:

	Soil Type	**Pile Type**	**Q [inch/mm]**
Shaft quake	All soil types	All types	0.1/2.5
Toe quake	All soil types, Soft Rock	Open ended pipes	0.1/2.5
	Dry soils or very danse or hard soils	Displacement piles of ϕ D	D/120
	Submerged soils or loose or soft soils	Displacement piles of ϕ D	D/60
	Hard rock	All types	0.4/10
			Damping Factor J_S [s/ft]/[s/m]
Shaft damping	Non cohesive soils		0.05/0.16
	Cohesive soils		0.2/0.65
Toe damping	In all soil types		0.15/0.5

Table II-2 : Recommended values for quake and damping factor (after GRLWEAP manual, 2000)

Coyle and Gibson (1970) and Wu et al (1989) found that Smith's original damping parameters vary with pile velocity (decreasing as velocity increase). Consequently, the basic formulation evolved. A non-linear relationship between the viscous resistance and the loading velocity was highlighted and the simple model of Smith was modified according to the works of **Coyle and Gibson (1968, 1970)**, Litkouhi and Poskitt (1980) and Heerema (1979).

$$R_{rheol} = R_s \cdot \left(1 + J_N \cdot v^N\right) \qquad \textbf{Equ. II-5}$$

studies give generally the value of N and J_N for some kind of soils: N = 0.18 (clay); 0.2 (sand) and J_N different from J_S. (Coyle and Gibson, 1970) - N = 0.2 for sand and clay (Heerema, 1979) - N = 0.2 for clays (Litkouhi and Poskitt, 1980). Coyle et al. (1972) determined for various soil from model pile tests in a range of 0.3-1.8 m/s that the Smith's approach is acceptable for the base resistance (N=1) and they modified only the shaft damping parameters: N = 0.35 and J_N = 1.98 s/m^{-N} (Coyle et al. 1972). Finally, data of published damping constant were compiled in "The Interim Report" (GRL, Inc. 1992):

Soil Type	Damping constant N=1		Soil Type	Damping constant N≠1			
	Shaft [s/m]	Base [s/m]		Shaft		Base	
Clay	0 – 2.4	0.009 – 0.87		$(s/m)^N$	N	$(s/m)^N$	N
Sand	0.17 – 0.5	0.33 – 0.5	Clay	1.339 – 4.106	0.17 – 0.57	0.683 – 1.99	0.17 – 0.37
Silt	0.33 – 0.34	0.3 – 0.5	Sand	1.015 – 1.649	0.2	1.015 – 2.536	0.2

Table II-3 : Range of damping factors J (after Interim Report, GRL and Associates, Inc, 1992)

Rausche et al. (1992) suggest the following equation to bypass the difficulties encountered by the numerical instabilities around 0 of Equ. II-5:

$$R_{rheol} = R_s \cdot \left(1 + J_R \cdot v_x^N \cdot \frac{v}{v_x} \cdot \frac{R_a}{R_s}\right) \qquad \textbf{Equ. II-6}$$

- J_R is the Rausche damping factor [s/m^N];
- v_x is the maximum velocity achieved up prior the time under consideration [m/s];
- v is the classical variable, the velocity of the moving body [m/s];
- R_a is the maximum static resistance mobilized prior the time under consideration [N];
- R_s is the static soil mobilization at the time of consideration [N];
- R_{rheol} is the rheologic soil reaction equal to the sum of the static and viscous term [N].

This modification respects the non linearity of the velocity dependent relationship and makes the result free of numerical disturbances but the coefficient J_R is dependent of the level of maximum mobilization of the blow (determined by the couple (v_x, R_a)).

Finally the main results remain simple: the ultimate viscous soil resistance is velocity dependent and its dependency is not linear for shaft and possibly for the base. This non-linearity is expressed by an exponent = 0.2 either for sand and clay.

The CASE method (Goble et al. (1975); Rausche et al. (1985), introduced in chapter 1 (Equ I-26), uses also a velocity dependent relationship to take into account of the load rate effect but with no links to the static soil reaction in the viscous term. The dimensionless parameter J_c can be associated to the Smith and the Coyle and Gibson ones.

3.3. Attempt of classification of J

Many researchers have tried to correlate the results of dynamic loading tests with static loading tests performed on same or similar pile in the same conditions in order to differentiate the base and shaft friction behaviours and the parameters of the static and viscous terms. One of the purposes of these researchers was to find a relationship between the soil damping factors and a type of soil.

Paikowsky et al. (1994) presented a large study of dynamic load tests analysis (372 cases) and summarized the values of Smith damping coefficients needed to obtain the best match between measured and calculated force or velocity signals (by using CAPWAP analysis). The damping factor J_s were sorted according to soil type for base and shaft. The authors conclude from this large statistical study that there is no specific correlation between the type of soil and the damping parameters used. The spreading of J_s is too wide. Other authors tried to correlate data form pile driving to damping parameters using the wave equation analysis (CAPWAP).

Likins et al. (1996) performed a systematic correlation study on 82 piles loaded dynamically and statically (from the GRL Database). The authors estimate that no clear trend can be established even if the average Smith damping constants slightly decreases for both skin and base when the soil grain size increases. The shaft quake seems to be constant (0.1 inch), as expected. The same type of correlations was also carried out on data coming from the GRL Database (**Thendean et al. 1996)** and one more time, the Smith damping factors vary strongly foe each soil type and no correlation can be extracted from these analysis.

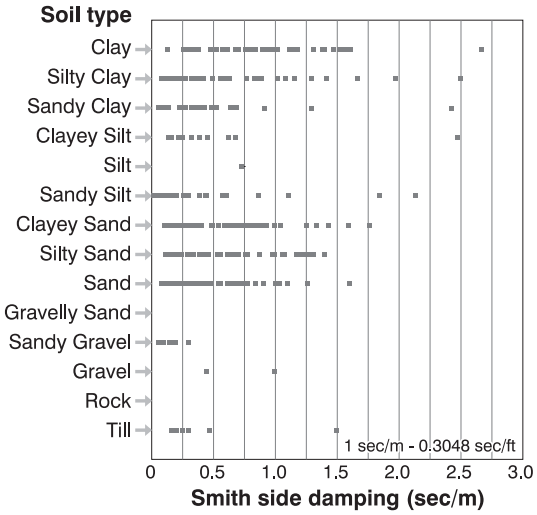

Figure II-10: classification of Smith damping factor vs. soil type (after Paikowsky et al. 1994)

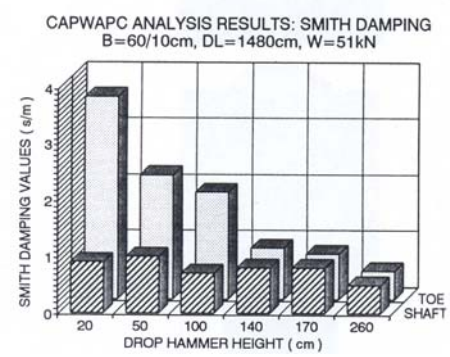

Figure II-11 : Estimated damping parameters (after Aoki et al. 1992)

Besides the classification of the damping factors with soil types, **Svinkin (1995, 1996)** proposes to consider the rheologic resistance with the damping factor as a function of time in order to take account for the set-up effect either for the static pile bearing capacity or the viscous soil reaction. Svinkin shows the evolution of the pile –soil response with elapsed time after end of driving, the pile-soil stiffness increases with time. Svinkin proposes to get the damping factor variable with respect to time or to another parameter characterizing the soil consolidation around the pile (like the shear modulus or the frequency of the fundamental mode of the pile system).

Aoki et al. (1992) describes the results of a systematic study performed on dynamic data coming from a restrike test on a concrete tube pile driven in dense sand. The blows (given by a free falling mass) were characterised by successive increasingly heights (from 0.2 to 2.6m). It can be observed that:

- The resistance mobilized at the base and along the pile shaft evolves with the transmitted energy and are not synchronised (transfer of resistance);

- The quake (for base and shaft friction) is not a constant value but evolves with the energy transmitted. Moreover, the ratio of base resistance on the quake value gives an almost constant value, similar to a spring stiffness.

- The associated values of the damping factor exhibit an evolution of constant reduction of the base damping factor with the increasingly height of drop. Figure II-11.

Many authors tried to use the Standard Penetration Test to estimate the Smith rheological parameters (the damping factor and the quake). **Goble et al. (1992)** and **Abou-Matar et al.(1996)** determines them from SPT measurements (acceleration and force on SPT-rod head). The method uses an unconstrained minimization routine to match the base soil reaction.

Liang (2000) proposes a method to correlate the Smith damping coefficient with SPT blow count. The method uses GRLWEAP to simulate the SPT results. Assumptions are made for the quakes (shaft and base) and the evaluation of the damping factor is achieved through an iterative process and a parametric optimisation where the matched unknown is the N value and the variable are the damping factors (comparisons are made with the real SPT-N values).

Concerning the CASE damping parameter, the same approach to correlate the value of J_c with soil type was also investigated and resulted in such a poor conclusions similarly to the previous analysis for the Smith viscous parameters. The authors of the method (**Goble et al. 1975**) estimate the value of J_c based on the comparison and analysis of driving data with respect to a corresponding static load test (the static resistance being evaluated with the Davisson criterion). Figure II-12 shows a plot of the J_c range within 20% of the statically observed capacity. The values of J_c have been sorted by soil types (as for the Smith damping factor) and the results are also scattered for each soil type. The negative values of J_c have been removed because of their "non-logical " meaning.

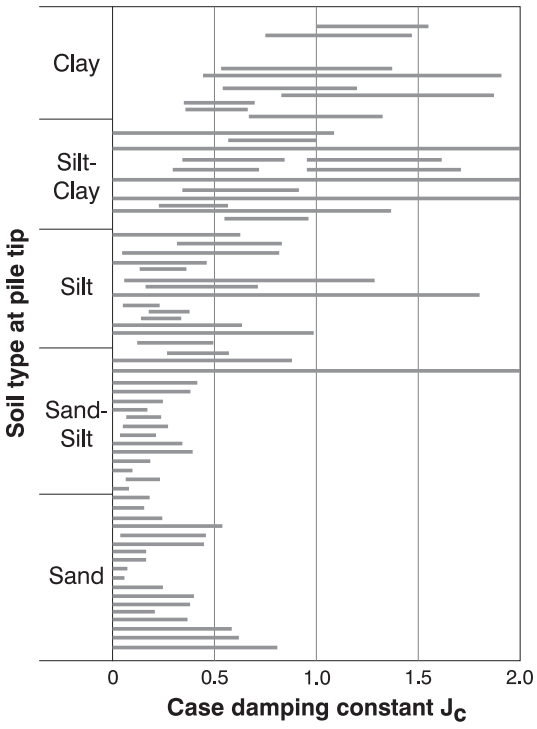

Figure II-12 : Dimensionless damping factor J_c vs. soil type (after Goble et al. 1975)

Other researchers have tried to link this parameter to the soil type. **Paikowsky et al. (1994)** have performed a large study of dynamic load tests analysis by using CAPWAP analysis in order to back-calculate the value of J_c needed to obtain the best match between measured and calculated force or velocity signals. The scattering is too wide to conclude something relevant. Some typical values for the CASE damping factor J_c are given by:

Soil Type	Suggested range of Jc	Best value of Jc
Sand	0.05-0.2	0.05
Silty sand or sandy silt	0.15-0.3	0.15
Silt	0.2-0.45	0.3
Silty clay or clayed silt	0.4-0.7	0.55
Clay	0.6-1.1	1.1

Table II-4 : suggested value for the Case damping factor J_c (after Rausche et al. 1985)

3.4. Conclusions

After a wide review of the empirical methods used to determine some influence of the Smith based damping factor with soil or driving method related parameters, it is not possible to conclude to some particular trend. It is rather the opposite.

All the authors try to find a correlation between a determined parameter and a given soil oriented parameter. The results tend to highlight the impossibility to classify the global damping parameter.

The reasons are simple as following: The damping parameter described by these relationships includes some behaviours that are not correlated with the same soil parameters, all these behaviours identified in Section 2 do not have the same magnitude at the same instant because of their origin and particular links to stress or strain evolution; second, the levels of mobilization for both dynamic and static tests are not of the same order; finally, each author concentrates his works on one parameter whereas a global study should be more appropriate.

The model described by Smith was a first attempt requiring more development with further scientifically improvements. Moreover, the Smith (or Coyle-Gibson) law is representative of the ultimate behaviour of the soil. It is only a viscous soil response corresponding to the failure state produced at a certain velocity. The trend observed, even if it is well established, can therefore only describe this situation. There is a need to study the low strain field with large range of applied velocity in order to develop the knowledge of the intermediate velocity dependent relationships. It seems to be possible to correlate the value of J with more and more parameters from the pile, soil or driving system description. But its global and artificial role prevents any general trend to be found. All the contradictions observed in the literature show the inadequacy of the use of this all-inclusive parameter J and the necessity of a more developed model including other viscous or so-called “dynamic” influences like the radiation and the dissipative damping. This is the subject of the next section.

4. Analytically based models

In parallel with the empirical refinements of the Smith model, analytically-based alternative models have been proposed by many authors. This aim is to differentiate the terms included in the global and empirical damping factor J and to derive their parameters from standard geotechnical soil properties. The models are generally separated in shaft and base responses. The shaft main theoretical studies are primarily based on the work of Novak et al. (1978) and the base main approaches are generally based on the work of Lysmer and Richart (1966). For these reasons, a short presentation of these theories is firstly covered, followed by a brief description of some models separated in shaft friction and base terms. The models related to Novak are firstly described, followed by others models chronologically. The model related to the base are described according to the same sequence than the friction ones.

All these models are generally characterised by a main term, displacement dependent, often defined as the static term and modelled by a spring (linear or not). Another important parameter of these models is the velocity dependent term (pile, soil or interface velocity) representative of the radiation damping in the soil what is a major difference compared to the Smith based models already presented. Besides these two constants, each model describes the dynamic pile/soil interaction with some differences that are explained hereafter.

The models are firstly described according to the shaft modelling. The firsts models describe the

4.1. Shaft friction models

4.1.1. Novak et al. (1978)

Novak et al. (1978) developed the plane strain soil reactions under dynamic loading, based on the work of Baranov (1968): for harmonically vertical vibrations[1], the plane strain solution of soil displacement for an infinitely long massless and rigid cylinder vibrating in an infinite elastic, homogeneous and isotropic medium is given by a complex formulation:

$$w(a_0, r) = f(a_0, r, G, \beta, P_v, i) \qquad \textbf{Equ. II-7}$$

Where:

- $w(a_0, r)$ is the vertical displacement amplitude corresponding to a distance r from the centre of the cylinder and to the dimensionless frequency a_0;
- $a_0 = \frac{\omega r_0}{V_s}$ is the dimensionless frequency of the cyclic motion;
- r_0 is the pile radius;
- ω is the circular frequency;
- V_s is the shear wave velocity of the soil = $\sqrt{\frac{G}{\rho_s}}$;
- P_v is the vertical exciting force;
- G is the initial shear modulus of the soil;
- β is the soil material damping ratio (= 0.05 or 0 in function of the soil).

Equ. II-7 can be developed into a complex stiffness:

$$K = G(S_{v1} + iS_{v2}) \qquad \textbf{Equ. II-8}$$

Figure II-12 shows the variation of the real and imaginary parts S_{v1} and S_{v2}. The real part S_{v1} is almost constant for $a_0 > 0.3$ and S_{V2} increases monotonously, almost linearly, with the frequency. Within that frequency domain, the soil reaction can be modelled by a spring and a dashpot whose constants are frequency independent and defined by:

[1] The main assumptions of this model are : -1- soil medium infinite, homogeneous, isotropic, visco-elastic with an internal damping frequency independent. -2- The cylinder is rigid, infinite and massless -3- no separation between soil and pile, -4- small displacements. -5- harmonic vibrations.

The spring relates to the elastic and static displacement dependent behaviour of soil and the dashpot relates to the energy lost in radiation in the soil (inertia of soil, vertical motion initiated by the imposed cylinder motion). The units of K and c are related to the unit of length of the pile.

$$K = G \cdot S_{v1} \text{ [N/m/m]} \qquad \textbf{Equ. II-9}$$

$$c = \frac{G_s r_0}{V_s} S_{v2}(a_0 = 1) \text{ [N.s/m/m]} \qquad \textbf{Equ. II-10}$$

This approach is followed by many researchers to describe the pile shaft soil resistance under dynamic loading. Generally, they consider a horizontally homogeneous soil medium but this leads to over-predictions of the radiation damping because the Novak's theory has been established for small strain where the shear modulus can be considered as non degraded. However pile dynamic testing generates large displacements, large stresses and plastic deformation. Consequently, the shear modulus undergoes a reduction that must be accounted for the radiation damping evaluation. Some of the authors developed models allowing a radial non-homogeneity in the soil accounting for the soil shear modulus degradation.

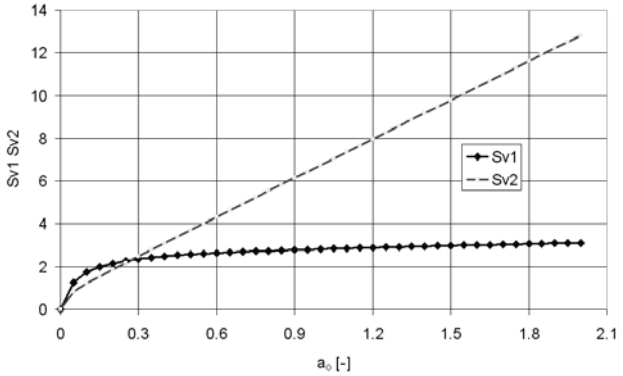

Figure II-13: Parameters S_{v1} and S_{v2} for homogeneous elastic soil medium under plane strain conditions

4.1.2. Other models

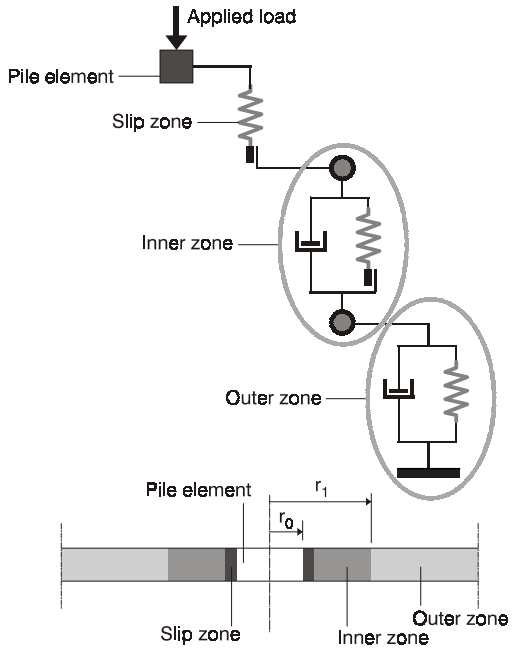

Figure II-14 : Mitwally & Novak and El Naggar & Novak soil model (after El Naggar et al, 1994)

Mitwally and Novak (1988) propose a reduced shear modulus G_m in a massless inner zone (Figure II-14). The radial and non-homogeneous zone is characterized by an internal boundary of radius r_1. This zone limits the modelled place where the high stress and deformations are presents: "the inner zone". This zone is surrounded by two particular media: the slip zone where the slippage occurs when the pile displacement yields an exceeding stress in the adjacent soil; and the outer zone extending to infinity where the stress and strain are assumed to remain in the elastic domain already described by Novak et al. (1978). In the inner zone, the soil stiffness is modified and becomes lower at low frequencies and larger at high frequencies. The damping factor becomes lower for all frequencies and the reduction is much greater for higher frequencies.

This model follows the classical elasto-plastic

formulation respecting the value of the stiffness and limited by the ultimate soil resistance determined by the quake value (set to 0.1 inch). The soil and pile motions are independent but both motions are equal until the slippage occurs and the soil stress exceeds the ultimate value. The radiation damping continues to occur during plastic deformation and the static soil resistance is constant during slip.

El Naggar and Novak (1992, 1994) propose the same construction model with substantial modifications: extension to rate dependent parameters - addition of inner masses into the main algorithm - modification of the inner zone particularity: the reduction of the shear modulus is obtained by a stress-strain relationship. The inner field is still representing the nonlinear response of the soil when the pile is strongly excited. But the difference in the modelling comes from the fundamental law used to describe this behaviour. Instead of the reduced shear modulus incorporated in an elasto-plastic relationship, a hyperbolic stress-strain relationship (Kondner, 1963) is chosen. This relationship smoothly indicates the transition between linear and nonlinear behaviours and respects the elastic behaviour in case of small strains and the plastic deformation in case of large strains. Moreover, the instant shear modulus is degraded according to the mobilization level.

For the plane strain assumptions, the displacement at the pile surface is obtained directly after integration of the angular distortion from the radius of the inner field r_1 to the pile radius r_0:

$$w_0 = \int_{r_0}^{r_1} \gamma \cdot dr = \frac{\tau_0 r_0}{G_i} \ln \left(\frac{\frac{r_1}{r_0} - \eta_0}{1 - \eta_0} \right) \qquad \textbf{Equ. II-11}$$

- τ_0, w_0 is the pile shaft stress-displacement state;
- η_0 is the mobilization ratio at pile shaft $= \frac{\tau_0}{\tau_{ult}}$.

Similarly to the shear modulus, the stiffness associated to the inner field is function of the stress state. A hysteretic behaviour is also assumed by the introduction of a completely elastic unloading phase. There is a possible material damping in the inner field: a dashpot is set in parallel of the non-linear spring described above of which the constant c_m must be suitably chosen.

To account for the loading rate effects, the ultimate soil resistance in the slippage layer is modified to be similar to the velocity dependent Coyle-Gibson approach (Equ. II-5):

$$R_{ult,rheol} = R_{ult,stat} \left(1 + J \cdot V^N \right) \qquad \textbf{Equ. II-12}$$

- $R_{ult,rheol}$ is the ultimate rheologic soil resistance accounting for the rate effects [N];
- $R_{ult,stat}$ is the ultimate static soil resistance [N];
- v is the interface velocity [m/s];
- J, N are the rheological parameters [s/m^{-N}; -].

This variable ultimate soil resistance is managed in the plastic slider representing the slip layer where the slippage between the pile and the adjacent soil is modelled. Either the soil resistance is under the limit and the pile and soil move together, or the limit is exceeded and the soil reaction is kept constant in function of the velocity. The inner field masses are introduced in the model in order to write properly the equations of motion (needed for resolution).

Holeyman (1984, 1985) proposes to describe the shaft friction stress-displacement relationship as a result of an integration of the angular distortion of the soil from a radius R_m to the pile. This distance is fixed according to Randolph and Wroth (1978) who determined that the influence of the pile motion at this distance on the soil vertical stress is insignificant. The reference τ–γ relationship (Equ. II-13) to be integrated on this cylinder is the hyperbolic law proposed by Kondner (1963). This relation allows to progressively introduce plasticity smoothly, indicates the transition between linear to nonlinear behaviours and respects the elastic behaviour in case of small strains and the plastic deformation in case of large strains. Equ. II-14 gives the integration between both limits.

$$\gamma = \gamma_r \frac{\eta}{1-\eta} \qquad \textbf{Equ. II-13}$$

$$u_s = \int_{R}^{R_{m1}} \gamma \cdot dr = \frac{\tau_s R}{G_i} \ln\left(\frac{\frac{R_m}{R} - \eta}{1-\eta}\right) \qquad \textbf{Equ. II-14}$$

γ is the angular distortion or shear strain [%];

γ_r is the reference shear strain: $\frac{\tau_{ult}}{G_i}$ [%];

η is the mobilization ratio: $\frac{\tau}{\tau_{ult}}$ [-];

G_i is the initial tangent shear modulus [Pa];

τ_{ult} is the ultimate shear stress [Pa].

τ_s, u_s is the pile shaft stress-displacement state;

η is the mobilization ratio at pile shaft;

R is the pile radius [m];

R_m is the radius of influence.

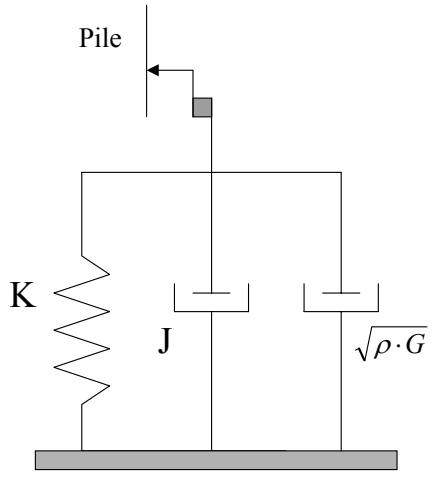

Figure II-15 : Holeyman shaft 1D-model

The associated stiffness is function of the stress state that can be illustrated by the degradation of the instant tangent shear modulus who decreases when η reaches 1. This approach allows the direct introduction of the hysteretic damping by the introduction of a completely elastic unloading phase.

This term is considered as the static term, displacement dependent, schematised by a non-linear spring of which the stiffness (K) is function of the stress state. The Holeyman's model is defined by only one degree of freedom, the pile motion, and consequently, the soil is considered as motionless. Hence, the soil reaction describes the soil directly adjacent to the pile.

The dynamic case is described by two terms according to the theory of Novak et al. (1978) already described and to account for the load rate effects by the introduction of a viscous term, non linearly function of the pile velocity, similarly to the results of

Coyle and Gibson (1968) (Equ. II-5). The radiation term is characterised by a damping parameter which is a simplification of the damping term of Novak. Since the model have only one degree of freedom, the radiation term must take the large strains and the plastic behaviour into account. However, this is in contrast to the Novak's assessments. In order to bypass this difficulty, Holeyman substitutes the shear modulus by the instant tangent shear modulus of the static hyperbolic relationship. When the soil is highly in plasticity, the value of G is become very small and the radiation damping is negligible, in agreement with the physics of the problem. Finally, a slider defined as the rheologic ultimate resistance limits the sum of all terms and the soil resistance. this term is also velocity dependent and function of the static ultimate resistance (Equ. II-12).

Randolph & Simons (1985,1986) propose a model also influenced by the works of Novak et al. (1978) for the description of the wave radiation generated in the soil around the pile.

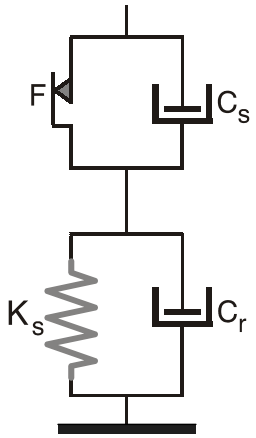

Figure II-16 : Shaft model (after Randolph & Simons, 1986)

The authors separates the soil in the vicinity of the pile in two zones, namely two degree of freedom. The closest is the perturbed zone where slippage, plasticity and large deformations occur. This zone is very narrow and the soil beyond behaves elastically. Consequently, Randolph & Simons describe the first and thin layer with a slider F (Equ. II-17) representing the ultimate shaft resistance under dynamic conditions according to the non linear velocity dependent relationship proposed by Coyle and Gibson (1968), and a dashpot Cs representing the internal viscous behaviour of the soil material, often set to 0. The outer zone is defined by a static (K_s) and radiation (C_r) terms similarly to the theory of Novak et al. The authors simplified the formulations of Equ. II-9 and Equ. II-10 to obtain Equ. II-15 and Equ. II-16.

$$K_s = \frac{G}{\phi_p} \qquad \textbf{Equ. II-15}$$

$$C_r = \sqrt{G\rho} \qquad \textbf{Equ. II-16}$$

$$\text{F} \rightarrow \tau_{rheol} = \tau_{stat} \cdot \left(k + \alpha \cdot \left(\frac{\Delta v}{v_0} \right)^{\beta} \right) \qquad \textbf{Equ. II-17}$$

Where Δv is the relative velocity between the pile and the soil, v_0 is the reference velocity (of the static test used as reference and α is the rheologic parameter). The soil stiffness is modified under static conditions in order to account for the Randolph and Wroth approach (1978).

Corte and Lepert (1986) and **Warrington (1988**) model the shaft friction with the SDOF system according to the works of Novak et al. (1978) following the simplification of Randolph and Simons (1985, 1986): Equ. II-15 and Equ. II-16. Corte and Lepert introduce a static stiffness equal to the 2/3 of the value of K_s and a limit value equal to the ultimate static resistance.

Chow et al. (1988) and **Lee et al. (1988)** based their works on a rigorous 3D finite element wave equation model for pile driving analysis (Smith & Chow (1982)). The soil resistance of this model is also represented by a spring and a dashpot in parallel. The spring is assumed to behave following an elasto-plastic relationship (Equ. II-15) and the dashpot represents the radiation damping effects (Equ. II-16). The parameters are still derived and simplified from the works of Novak et al. (1978).

The total soil resistance is represented by the sum of both terms. The rheologic ultimate soil resistance is approximated by the Coyle and Gibson approach (Equ. II-12). When the spring force exceeds this limit, the soil dashpot disconnects from the process and radiation damping ceases. It starts again when the spring force becomes inferior to the ultimate resistance. The significant difference with other models is the fact that the failure is only limited by the spring evolution and the damping effects vanishes at this instant. That means also that the rheologic soil resistance undergoes a sudden reduction and a sudden increase when the failure load is exceeded up or down respectively.

Nguyen et al. (1988) developed a model schematically described by Figure II-17.

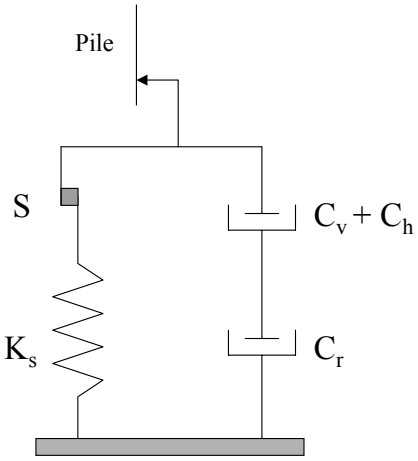

Figure II-17 : Nguyen et al. Model

Dashpots represent the effects of the radiation (C_r) and the material damping. The material damping regroups the intrinsic viscous damping (C_v) and the hysteretic damping (C_h). The spring represents the static soil stiffness (K_s); and the plastic slider (S) represents the ultimate static resistance of the soil. The model is only determined by the pile motion without taking the soil motion into account.

The static and the radiation terms are based on the simplified forms of the Novak's theory (similarly to Equ. II-15 and Equ. II-16). However, the value of G is function of the strain amplitude, what seems to be similar to the Holeyman's approach. The radiation term vanishes when the static term exceeds its ultimate resistance.

Paquet (1988) proposes a shaft model where the pile and the soil have distinct motions depending of the level of stress generated at their interface. This model is described in chapter 1 (SIMBAT model). The model could be described as the model proposed by Randolph and Simons with two degrees of freedom. The slippage limit is determined by the ultimate rheologic resistance of the soil, function of the interface velocity. The reaction of the soil is represented by a spring and a dashpot representing the soil stiffness and the radiation damping. Originally based on the expressions given by Briard (1970) and Novak (1974), the underlying theory is similar to other proposed models. Moreover, the limit value (R_l) of the interface resistance is function of the penetration velocity (Dali & Heritier, 1992).

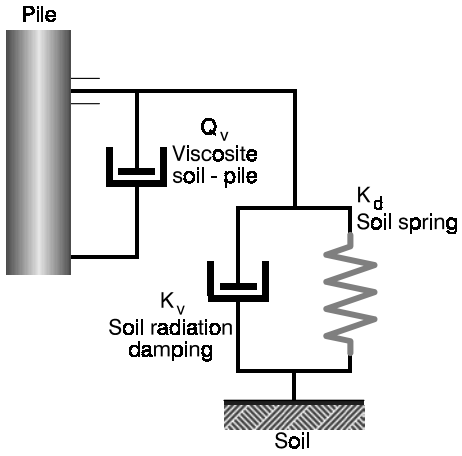

Figure II-18 : SIMBAT shaft model (after Dali & Heritier, 1992)

4.2. The base models

4.2.1. The Lysmer analogue

Similarly to the approach of Novak et al (1978), the Lysmer and Richart approach (1965) is used in most of the models describing the dynamic soil reaction at the pile base. Lysmer detailed the response[2] of an elastic half-space medium under vertical harmonic solicitations ($Q_o \cdot e^{i\omega t}$) applied on the centre of a circular and rigid footing resting on a plane soil surface (Figure II-19).

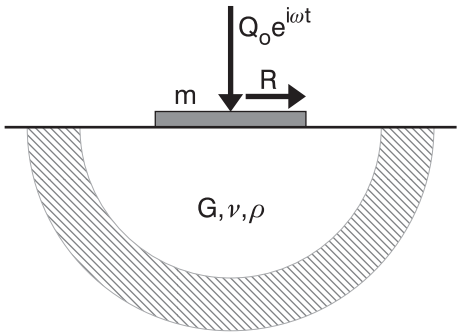

Figure II-19 : Lysmer & Richart model

The footing has a radius R, a mass m and the medium has an initial shear modulus G, a soil density ρ and a Poisson's ratio υ. The analogy with the pile base response is considered in the range of frequency undergone during a pile dynamic event and in the range of elastic stresses because of the assessments made by Lysmer and Richart. The Lysmer analogue is based on the works of Reissner (1936) who determined that the displacement in the centre of a flexible circular area under the same loading was function of a complex notation:

$$\overline{u} = \frac{Q_0 \cdot e^{i\omega t}}{GR}\left(f_1 + if_2\right) = \frac{Q_0 \cdot e^{i\omega t}}{GR} \cdot f \qquad \textbf{Equ. II-18}$$

Where f_1 and f_2 are functions of the dimensionless frequency $a_0 = \frac{\omega r_0}{V_s}$ and Poisson's ratio. If the frequency a_0 increases, the relative weight of the complex term in Equ. II-18 increases as well and for high frequencies, the half-space medium response looks like an impedance, and can be modelled with a dashpot velocity dependent.

$$C_Z = \frac{R^2}{a_0}\sqrt{G\rho} \cdot \left(\frac{-f_2}{f_1^2 + f_2^2}\right) \qquad \textbf{Equ. II-19}$$

And the associated reaction coefficient (displacement dependent term) is given by:

$$K_Z = GR \cdot \left(\frac{f_1}{f_1^2 + f_2^2}\right) \qquad \textbf{Equ. II-20}$$

However, f_1 and f_2 are still functions of the dimensionless frequency $a_0 = \frac{\omega r_0}{V_s}$ and of Poisson's ratio υ, and are difficult to be used in practice. Lysmer and Richart (1965) introduced new developments reducing the influence of the Poisson's ratio and observed that the new formulations of C_z and K_z were almost constant in the usual range of frequencies.

[2] The subsoil is perfectly elastic, isotropic, homogeneous where only normal stresses are transferred at the interface between footing and soil.

The corresponding spring stiffness and the damping factor are given by the well known Lysmer analogue values (Equ. II-21, Equ. II-22 and Figure II-20):

$$K_z = \frac{4G_i R}{(1-\upsilon)} \qquad \textbf{Equ. II-21}$$

$$C_z = \frac{3.4R\sqrt{G_i \rho}}{(1-\upsilon)} \qquad \textbf{Equ. II-22}$$

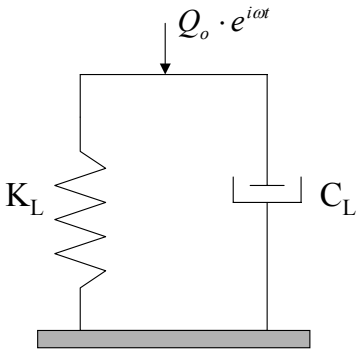

Figure II-20 : Lysmer analogue

The spring corresponds to the static response of the soil and the second term defines the geometrical or radiation damping of the soil assuming the energy losses in the soil by wave propagation. This model is only valid for homogeneous and elastic media.

4.2.2. Other models

For **Mitwally and Novak (1988)**, the base resistance is modelled by the reaction of an elastic half-space to a rigid massless circular disc undergoing harmonic vibration and can be written analogously to Equ. II-8 by:

$$R = G_b \cdot r_b \left(C_1 + iC_2\right) \qquad \textbf{Equ. II-23}$$

Where:

- C_i are the dimensionless parameters representing the soil stiffness and radiation damping and function of the Poisson's ratio and the dimensionless frequency a_0;
- G_b is the soil shear modulus beneath the pile base [MPa];
- r_b is the pile base radius [m].

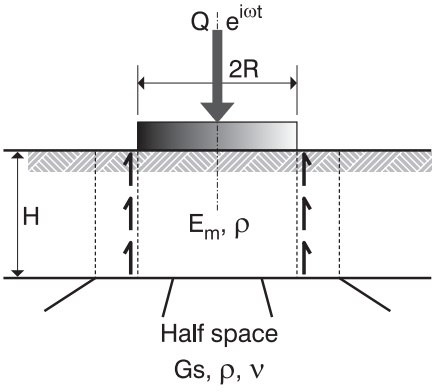

Figure II-21: El Naggar et al. base model

El Naggar and Novak (1992, 1994) improve the model of Mitwally and Novak: the homogeneous elastic half-space is replaced by the addition of two regions: a first layer accounts for heterogeneity and nonlinearity where a hyperbolic law is used. This media is built to allow for radial wave propagation and lateral confinement. This soil layer is underlain by a half-space where plane strain soil reactions are modelled by using the Lysmer and Richart analogue with linear dashpot and a spring in parallel (Equ. II-21 & Equ. II-22). The geometrical properties of the soil layer are evaluated such the static deflection and the dynamic behaviour at the interface with half space were satisfied (Figure II-21).

In the same way, **Holeyman (1984 & 1988)** modifies the half-space governing the approach of Lysmer and Richart by a two-part medium to account for non-homogeneous half-space and non-linear behaviour of the soil response. Figure II-22 represents an

equivalent axisymetric solid resting below the footing. It has finite lateral extent determined by the agreement of the response model under static and dynamic conditions (Holeyman, 1984). The model rests on the half-space medium governed by the analogue of Lysmer. The evolution of the cone radius r is function of the depth Z, the pile radius r_0 and the Poisson's ratio. Only the vertical mode of deformation is considered and the cone mass density is equal to the soil medium one.

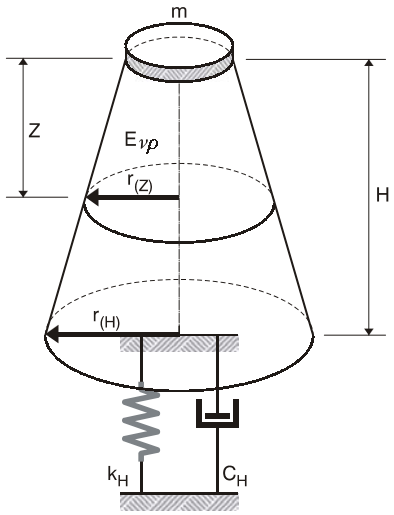

Figure II-22 : Concept of the equivalent solid (after Holeyman, 1988)

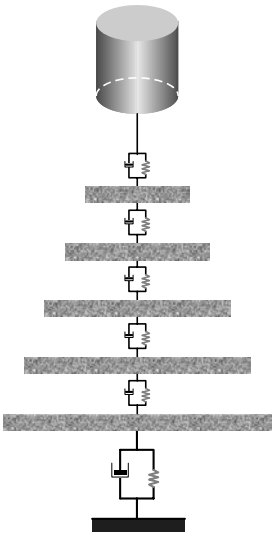

Figure II-23 : Holeyman base model

The model has the advantage to be easily discretized in lumped parameter accounting for the local properties (non-homogeneity) of each layers (Figure II-23). The non linear response of the soil, typical of large deformations, can be also integrated. As the shaft model, the hyperbolic law (Kondner, 1963) can reflect the smooth evolution from elasticity (small strains) to plasticity for the base soil reaction. This model is also characterized by an elastic unloading phase (related to the initial tangent modulus) defining the hysteretic damping of the pile movement. The viscosity effects can be incorporated related to the strain path and strain rate and the axial stress is limited by a value taking account of the loading rate effects (according to the Coyle and Gibson approach - Equ. II-12).

The radiation damping is accounted for by the geometry of the cone and the masses of the lumped elements. The behaviour at the base of the cone is assumed as low strain as sufficient in order to use the Lysmer analogue defined for an elastic behaviour.

The proposition of **Randolph & Deeks (1992)** is also based on a double degree of freedom system like the shaft model developed by Randolph and Simons. Contrary to many base models, this one is not based on the Lysmer analogue but based on the Wolf model (1988) who study the vibration of a circular rigid footing on the surface of a half-space (derived from the analogue of the dynamical spherical cavity expansion (Randolph & Pennington, 1988).

The model includes the slider Q_b that represents the ultimate base resistance under dynamic conditions; the dashpots C_b representing the radiation damping in the soil beneath the pile; the spring K_b representing the static deformation of the soil and the lumped mass M_b that takes into account the inertia of the soil moving under the base.

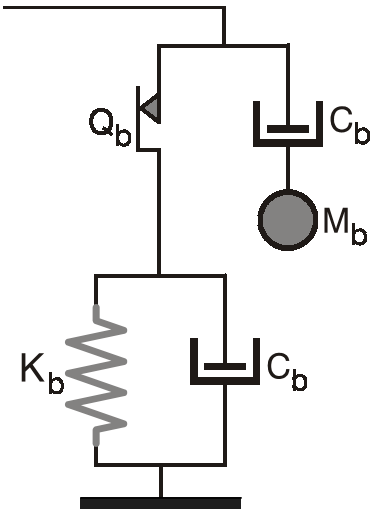

$$Q_b \rightarrow \sigma_{rheol} = \sigma_{stat} \cdot \left(k + \alpha \cdot \left(\frac{\Delta v}{v_0} \right)^{\beta} \right) \qquad \textbf{Equ. II-24}$$

$$K_b \rightarrow K_b = \frac{2G \cdot \phi_p}{1-\upsilon} \qquad \textbf{Equ. II-25}$$

$$C_b \rightarrow C_b = \frac{0.8\phi_p^2 \sqrt{G\rho}}{1-\upsilon} \qquad \textbf{Equ. II-26}$$

$$M_b \rightarrow M_b = 2 \cdot \phi_p^3 \rho \frac{0.1-\upsilon^4}{1-\upsilon} \qquad \textbf{Equ. II-27}$$

Figure II-24 : Base model (after Randolph & Deeks, 1992)

The ultimate limit of the based resistance is the general form of the non linear velocity dependent relationship proposed by Coyle and Gibson (1968). The authors specify it is possible to add a viscous dashpot in parallel of the plastic slider in case of a particularly dissipating soil (same effect than C_s for the shaft model). Generally this effect is neglected or integrated in the hysteretic energy losses.

Nguyen et al. (1988) present for the base a model similar to the model described for the shaft friction (Figure II-17). The static and radiation terms are based from the works of Lysmer and Richart (Equ. II-21 & Equ. II-22) and specific formulations account for the viscous and the hysteretic dampings.

The models of **Chow et al. (1988)** and **Warrington (1988)** also use strictly the analogue of Lysmer to describe the base soil reaction.

4.3. Conclusions

A major part of the models described herein uses either the Novak approach and the Lysmer analogue for the shaft and base modelling, respectively. However, both approaches are described for particular conditions including the elasticity and homogeneity of the soil and the elastic range of the strain induced. The high strains generated during a dynamic test or a pile driving cause pile/soil interactions not described by the aforementioned theories. To account for this important feature, some authors introduce elements more or less consequent to the initial model. Three types of upgrade can be observed for the shaft model:

- The modification of the stress-displacement relationships from a linear and elastic formulation to the hyperbolic one. The hyperbolic law (Kondner, 1963) can reflect the smooth evolution from elasticity (small strains) to plasticity and represents the non-linearity of the soil;
- To allow some parameters to evolve with the level of plasticity. The radiation damping is degraded or completely suppressed when the shear stress exceeds the ultimate shear resistance;
- To account for the large strains in a portion of soil surrounding the pile and differentiated from the soil located in the far field.

Generally the authors uses one, two or the three upgrades (Holeyman, El Naggar, Simons & Randolph, N'guyen, Paquet, Chow). The authors using the simple Novak approach to model the whole pile/soil interaction model an over-predicted radiation damping.

Concerning the base, a few number of authors modify the Lysmer analogue to account for the large strains and non linearity of the pile soil system. It is probably due to the fact that there is no failure occurrence similarly to the slippage along the pile shaft at the pile base and due to the fact that the radiation damping keeps acting also at large strain (authors like N'Guyen who makes the radiation term vanishing when the pile reaches plastic deformations at the pile base probably over-predicts the static term of the ultimate soil resistance). However the Lysmer analogue hypothesis does not agree with the applied range of loads and the soil response does not correspond. Construction of a typical model used as interface between the high level of solicitation in the vicinity of the pile base and the far field where the soil behaves elastically is a good way of bypassing this difficulty in keeping relevant with the theory and the Lysmer approach (equivalent solid of Holeyman, El Naggar).

On the other hand, for most of the authors, the only velocity dependent term is the radiation damping. The ultimate resistance takes also the loading rate into account but it is only the representation of the failure mode. A few authors introduce a viscous term, also described as velocity dependent by often neglected. This is a major difference with the observations of Smith where the "dynamic" resistance is directly linked to the static soil reaction (contrary to the radiation damping). However, the description of Smith only concerns the failure mode and not the complete description of the soil reaction. The lack of data in the low ranges of velocities and in the intermediate states of soil mobilization brings out this difference of interpretation between the modelling and the observation.

The loading rate effect is taking into account by the Coyle and Gibson formulation of the ultimate rheologic soil resistance: a power law relationship of the velocity multiplying the ultimate static resistance. Many authors use it as plastic slider in order to limit the evolution of the rheologic soil reaction and sometimes to get rid of the radiation term.

In conclusion, all these models are similar by the underlying theory used and by the necessity to describe the radiation behaviour for both base and shaft models. The models differentiate in the way of describing the soil non-linearity (especially in large strain) and the pile/soil motion system. it seems to be required to describe the radiation behaviour on a large range of strain and velocities. The close vicinity of the pile, either at the base or along the shaft must be investigated with a special attention put on the attenuation of the stresses and strains generated by the pile's motion.

5. The loading rate study through the literature

Besides the interest brought by Smith and its first model describing the static and viscous soil reactions, many researchers have performed specific studies in order to isolate the trend and the origin of the effects of an increase of loading rate on the bearing capacity of a pile. These studies have been carried out by observations during pile loading events or laboratory testing (use of models or standard lab procedures).

Generally, the analysis concerned the comparison of the static and the so-called "dynamic" soil reaction when the soil sample, the pile or the model reaches failure under a rapid load application. This empirical approach resulted in the development of many formulations describing the observations

measured. Each of them respects the trend of the respective experiments and was somehow linked to this experiment (assessments, testing procedures, …). However, it seems possible to classify these relationships modelling the loading rate effects in 4 categories following the mathematical approach or the reference quantity. All of them relate to the penetration velocity (with different units and orders of magnitude) or the time to reach failure (that can be considered as the inverse of the loading rate).

- Linear relationship with proportionality to the static soil reaction (mobilized);
- Linear relationship with relation to the pile properties;
- Power relationship with proportionality to the static soil reaction (mobilized);
- Logarithmic relationship with proportionality to the static soil reaction (mobilized).

This section is dedicated to a rapid overview of these categories with a description of the tests underlain and a list of the testing programs found in literature.

5.1. Linear velocity relationships

5.1.1. Proportionality to the static soil reaction & proportionality to the pile properties

Those two categories refer to basic formulations already introduced. The Smith's approach (section 3.1) was the first to attempt to quantify the loading rate effect based on the dynamic pile loading test results. The relationship is based on the observations of piles during their driving. The "dynamic" contribution to the soil resistance is linearly dependent upon pile velocity and also proportional to the static soil reaction. Equ II-3 resumes this formulation.

The second category refers to the CASE method introduced in chapter 1 and in section 3.3. The "dynamic" contribution to the pile capacity is pile velocity dependent but with no direct link to the static soil reaction (Equ I-26). Moreover, the pile properties (geometry, mechanical properties) influence the load rate effect with to the nominal impedance. This formulation is a mathematical result based on the Wave Equation Analysis applied to the pile driving resolution but looks like the empirical and global relationships described here with the use of the CASE damping parameter J_c and the velocity dependency.

5.2. Complex velocity relationships

5.2.1. Power relationship with proportionality to the static soil reaction

One of the major studies performed on the velocity dependent characteristic of soil resistance within the framework of the pile driving was carried out by **Coyle and Gibson (1968)**.They use a triaxial cell submitted to the falling of a dropping mass from varying heights generating varying impact velocities. Sands and clays of different types have been tested in a velocity range of 0.2 to 3.5 m/s.

A general trend of $\frac{Q_{rheol}}{Q_{stat}}$ is found to be similar for both types of soil at failure (Figure II-25).

The authors obtained a general formulation commonly used:

$$Q_{rheol} = Q_{stat} \cdot \left(1 + J_N \cdot V^N\right) \qquad \textbf{Equ. II-28}$$

Q_{rheol} is the soil resistance with all influences [N]; J_N is the damping factor [s/m^{-N}];

Q_{stat} is the static soil resistance [N]; N is the rheologic exponent [-].

According to the authors, N = 0.2 for sands and N = 0.18 for clays; J_N is correlated with the internal friction angle and the void ratio for sands, and with the liquidity index and the water content for clays.

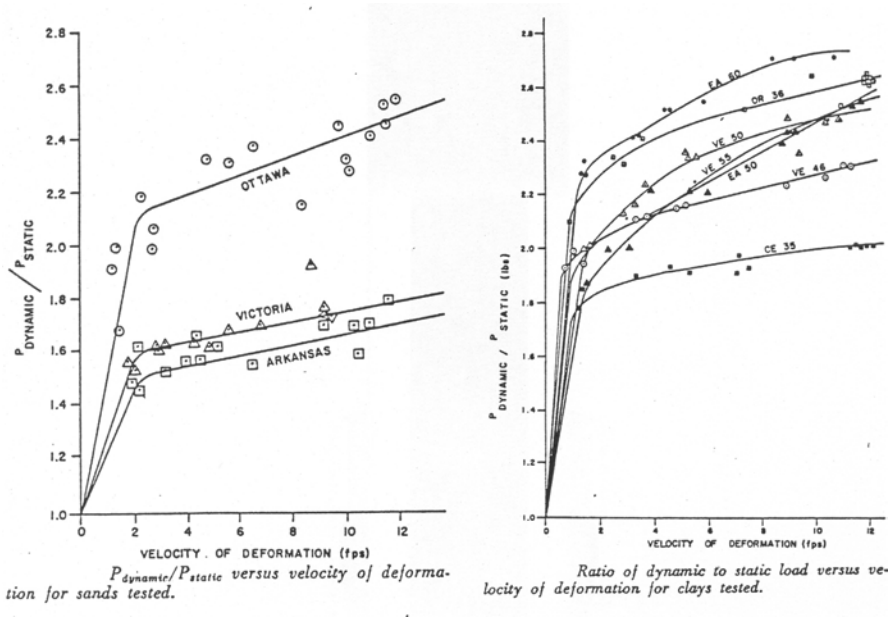

$P_{dynamic}/P_{static}$ versus velocity of deformation for sands tested.

Ratio of dynamic to static load versus velocity of deformation for clays tested.

Figure II-25 : Loading rate effect (by mass falling) in a triaxial cell (after Gibson and Coyle, 1968)

Heerema (1979) tested a range of clays and sands by shearing a steel plate under constant normal stress at different velocities. This test can be classified in a middle position between classical tests (simple shearing) and models tests. The velocities varied from 7 10^{-4} m/s to 0.6 m/s for sand and from 7.81 10^{-4} m/s to 1.04 m/s for clay. The tests performed on dry sands do not show any probative results on the failure friction but the tests performed on clays (stiff clay – Kontisch, Heather; soft clays – Claymore) exhibit a pronounced trend. The general form of the results is similar to the Coyle and Gibson modelling (Equ. II-28). Heerema suggests the value of 0.2 for N and gives a correlation for the J_N values with the undrained soil cohesion c_u.

Litkouhi & Poskitt (1980) carried out pile loading tests on models of diameter 10 mm driven with a constant rate of penetration in undisturbed and consolidated remoulded clay samples (London, Forties and Magnus clays). The rate of penetration varied from 0.0003 m/s (considered as static velocity) to 1.65 m/s. The authors performed tests with two different models to separate shaft and base behaviours. The velocity dependent trends observed in laboratory can be also modelled with a power law (Equ. II-28). N is fixed to 0.2 for the remoulded samples for base and shaft behaviours. N is found = 0.4 (base) and 0.6 (shaft) for the only undisturbed sample. J is in the range of [0.2; 0.3] s/m^{-N} for remoulded samples and 0.08 s/m^{-N} (base) and 0.06 s/m^{-N} (shaft) for the undisturbed samples. That confirms that both base and shaft frictions capacities have non-linear viscous behaviour.

Briaud and Garland (1985) use the results of lab tests and full-scale static and dynamic pile tests in order to predict the pile behaviour in cohesive soils subjected to axial load. Their study is focused on the analysis of the evolution of the undrained shear strength (S_u) with time to failure t_f.

After analysis of laboratory results focused on undrained shear strength, it was seen that a power law can link the values of S_u obtained for two different failure durations.

$$\frac{S_{U1}}{S_{U2}} = \left(\frac{t_2}{t_1}\right)^n \qquad \textbf{Equ. II-29}$$

- S_{u1} and S_{u2} are undrained shear strengths measured after time to failure $t_1$and t_2 respectively.
- n is the viscous exponent.

Statistically, the range of n values is limited to 0.02 for stiff and plastic clays and to 0.16 for soft clays. And the average value is 0.061. Correlations have been found with fundamental parameters of clays as the water content w, the plasticity index PI, the liquidity index LI or the overconsolidation ratio OCR. Afterwards, the authors applied the same equation (Equ. II-29) to 31 couples of load tests performed with two different loading rates on same or on similar piles. The scattering is larger but the range and the average value of n remains similar (average=0,068). Equ. II-29 becomes:

$$\frac{Q_{U1}}{Q_{U2}} = \left(\frac{t_2}{t_1}\right)^n \qquad \textbf{Equ. II-30}$$

Q_{ui} are the ultimate pile capacities reached during test at the time t_i.

The spreading of n is due to the scale and averaging effects between the sample in laboratory tests (10 cm high) and the pile shaft dimensions (several meters length). It is also due to the undrained behaviour maybe not encountered in the slow pile load tests. Site specific values of n can be obtained by performing pressuremeter or cone penetrometer tests at significantly rates of penetration (Briaud et al. 2000). Tests performed in 2000 in sand show that this approach is still valid in non-cohesive soil.

Brown et al. (2002) & **Anderson et al. (2003)** propose a similar approach to study the load rate effect in clay with a model pile in a calibration chamber. Clay (mix of Kaolin with sand and silt) is tested in an instrumented calibration chamber (pore pressure transducers and accelerometers in the soil). The partially embedded model pile has a diameter of 70 mm and more than 1 m length. It is instrumented in order to measure the pile tip and skin friction loads (load cells) to differentiate both rate of testing effects. The testing program includes Constant Rate of Penetration tests carried out at 0.01, 1, 10, 100 and 500 mm/s (Figure II-26) and load pulse similar to the Statnamic testing (pulses of 150 ms with target loads of increased value and corresponding increased settlement rate - Figure II-27).

It is shown that the magnitude of pore pressure increased with increasing rate of pile penetration, that the stiffness measured during the Statnamic pulses increases with the target loads.

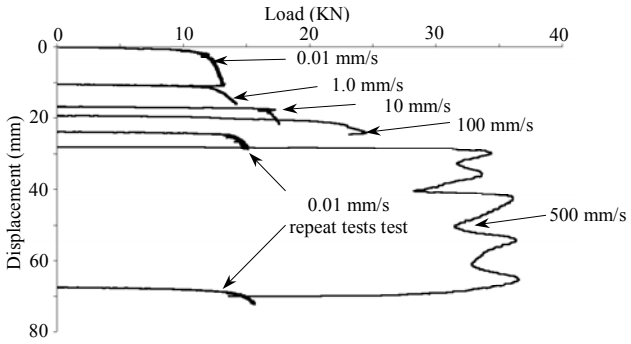

Figure II-26 : Pile load deflection response to CRP tests (after Brown et al., 2002)

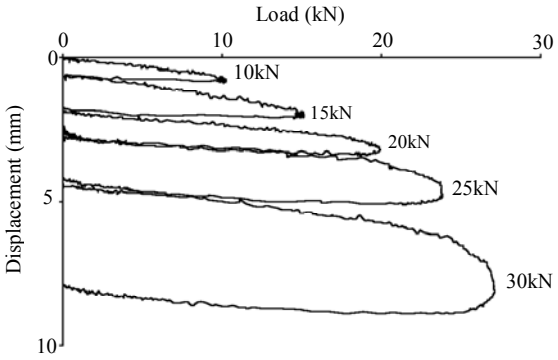

Figure II-27 : Pile load deflection response to statnamic load pulses (after Brown et al., 2002)

The load capacity of the pile is found to be particularly sensitive to the pile deformation rate with significant increase for the rates between 10 to 500 mm/s but this effect is more pronounced for the shaft than the base component of the pile capacity. The static reference pile capacity is chosen as the result of the CRP test performed at 0.01 mm/s. Figure II-28 shows the loading rate effects expressed through the ratio of maximum soil reaction during the CRP tests. The result from Figure II-28 can be modelled by a power law of the Coyle and Gibson type (Equ. II-35). The authors specify that more tests must be performed to differentiate correctly both trends corresponding to the base and shaft friction behaviours (rates between 10 to 100 mm/s and 100 to 500 mm/s).

$$\frac{R_r}{R_s} = 1 + \alpha \cdot \left(\frac{v}{v_0} \right)^{\beta}$$ **Equ. II-31**

- v is the pile penetration velocity [m/s];
- v_0 is a normalizing velocity [m/s];
- α and β are the rheologic parameters.

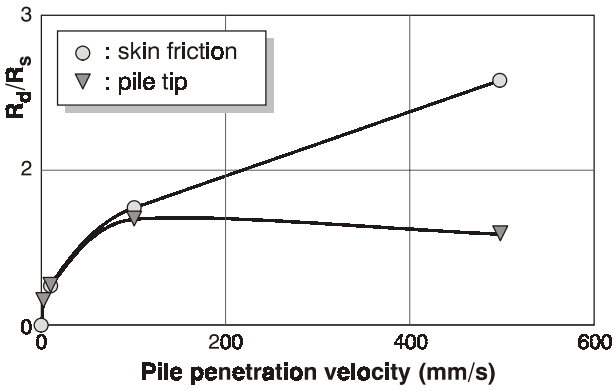

Figure II-28: Rate effects for the pile and base components (after Brown et al., 2002)

The normalizing velocity is taken as the velocity of the static reference test. Here, it is the velocity of the CRP test performed at 0.01 mm/s or 10^{-5} m/s. The values α and β based on the best fit curve possible are 1.22 and 0.32 respectively. A detailed study of the strength behaviour of the consolidated clay has been carried out by **Balderas-Meca (2003).** He carried out consolidated undrained (CU) triaxial tests at different rates of strain on 100 mm diameter specimens simulating the stress history followed in the calibration chamber. The deviator stress at 3% axial strain was taken as the failure stress. Secant elastic modulus values, E_{50}, were calculated using the strain at which 50% of the failure deviator stress

was reached. Values of the undrained strengths and moduli obtained at different strain rates increase significantly as the rate of testing increases. The values of the associated rheologic parameters α and β for those two quantities are 0.53 and 0.19 for the undrained shear strength and 1.85 and 0.15 for E_{50}. Brown (2003) suggests to modify the classical analysis method of the Statnamic tests to incorporate the non linear loading rate effect (power law).

5.2.2. Logarithmic relationship with proportionality to the static soil reaction

In parallel to the power relationship of the velocity, a second type of law has been developed by many authors especially based on laboratory testing (except for Bea): the logarithmic relationship of the velocity with the use of a reference velocity (corresponding to the reference static test).

Dayal & Allen (1974, 1975) work on cone penetration tests performed at high velocity. All the transducers of the classical device are available (cone resistance, unit shaft friction). CPT-E is used to penetrate the soil with a constant velocity. The velocities range from 0.0044 ft/s (0.0013 m/s) to 2.662 ft/s (0.812 m/s).The tested soils are dry sand and clayed silt. The cone resistance results show a variation of the dynamic resistance with the loading rate. The authors use the Peck law (1962) in order to analyse the results:

$$\frac{c_u^d - c_u}{c_u} = 0.1 \cdot \log\left(\frac{\dot{\varepsilon}^d}{\dot{\varepsilon}}\right) \qquad \textbf{Equ. II-32}$$

c^d_u and c_u are the undrained cohesion corresponding to the strain rates $\dot{\varepsilon}^d$ and $\dot{\varepsilon}$, respectively.

This formula is standardised for the cone approach:

$$\frac{q_c^d - q_c}{q_c} = K_l \cdot \log\left(\frac{v}{v_s}\right) \qquad \textbf{Equ. II-33}$$

Where:

- q_c is the cone resistance at the velocity v;
- q^d_c is the cone resistance at the reference velocity v_s;
- K_l is the coefficient of soil viscosity (dependent of the soil nature, the velocity range).

Equ. II-33 is similar to Equ. II-36:

$$\frac{q_c^d - q_c}{q_c} = K_l \cdot \log\left(\frac{v}{v_s}\right) = \frac{q_c^d}{q_c} - 1 \qquad \textbf{Equ. II-34}$$

$$\rightarrow \frac{q_c^d}{q_c} = 1 + K_l \cdot \log\left(\frac{v}{v_s}\right)$$

Bea (1982) analysed the results of pile load testing (0.355 m diameter tubular pile in plastic clay of the Gulf Coast) based on the works of Cox et al. (1979) (Figure II-29) and proposes the following law:

$$\beta = \frac{Q_{rheol}}{Q_{stat}} = F_1 + F_2 \log\left(\frac{\lambda}{\lambda_s}\right) \qquad \textbf{Equ. II-35}$$

Q_{rheol} is the rheologic soil reaction [kips]; λ_s is the reference loading rate [%Q_{ult}/h];

Q_{stat} is the static soil reaction [kips]; F_1 = 0.75 to 1 [-];

λ is the loading rate [%Q_{ult}/h]; F_2 = 0.10 to 0.20 [-].

An attempt is made to link F_2 to fundamental characteristics of clays: OCR, liquidity index LI,.

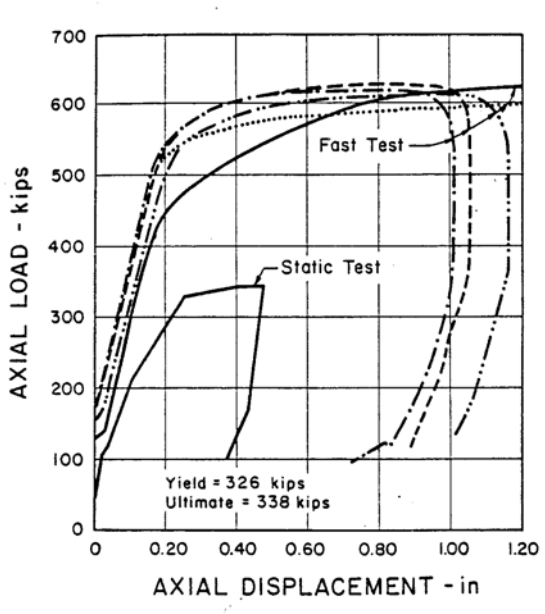

Figure II-29 : Loading rate effects from pile load tests (after Cox et al., 1979)

The majority of the research undertaken in laboratories was focused on the influence of an increase of strain rate on the undrained shear strength of clays S_u. The main results for tests in clay demonstrate that an increase of a factor 100 of the strain rate causes an increase of 25% of S_u (Vail et al., 1979); Graham et al (1983) show that triaxial compression tests increase by about 10…20% the value of S_u for a 10 times increase of the strain rate. Kulhawy & Mayne (1990) work on 26 different clays (normally and overconsolidated) and found an increase of about 10% per cycle of logarithm of strain rate. A tenuous influence of loading rate can be felt on fine sands (Seed and Lundgren, 1954; Whitman and Healy, 1962).

All these results can be modelled by using a dashpot in parallel with a soil spring (responsible of the static term of the soil reaction). The damping parameter is found by multiplying the relative pile velocity with respect to soil by an equivalent damping coefficient C_{eq}:

$$C_{eq} = \frac{\beta}{V}\log\left(\frac{V}{Vref}\right) \rightarrow\ Q_{rheol} = Q_{stat} \cdot \left(1 + \beta \cdot \log\left(\frac{V}{V_{ref}}\right)\right) \qquad \textbf{Equ. II-36}$$

- Q_{rheol} is the rheologic soil reaction [N];
- Q_{stat} is the static soil reaction [N];
- β is the rate of increase in shearing resistance per log cycle of increase in strain;
- V is the relative velocity of the pile with respect to the soil [m/s];
- V_{ref} is the reference (or static) velocity: 10^{-3} inch/s or $0.0254\ 10^{-3}$ m/s.

All the results can be used in numerical analysis by replacing the value of β by the found percentage of increase of shear resistance per log cycle of strain rate (after Chacko et al., 2002).

Matsumoto & Nishimura (1996) present the results of CU triaxial tests performed on diatomaceous mudstone (soft rock). Tests were performed with two different axial strain rates ($\dot{\varepsilon}$ = 0.1 and 0.01 %/min - Figure II-30). Both mudstone samples show a peak shear resistance and thereafter undergo a gradual reduction in shear resistance with increasing strain. The increase of undrained shear strength is similar to the previous results: 12% for a log cycle of strain rate. This deformation rate dependency of the shear resistance of the mudstone is also reporter in Sekiguchi et al. (1985) and Maekawa et al. (1991).

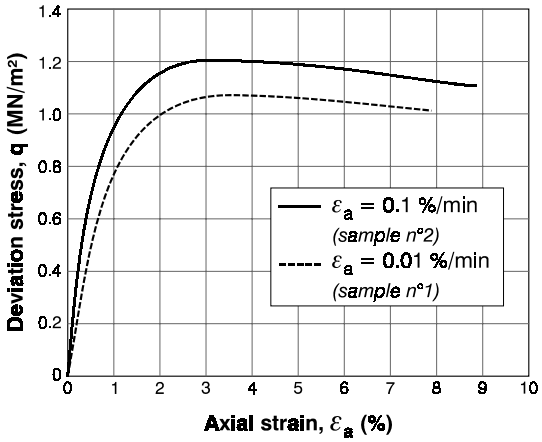

Figure II-30: Stress-strain curves under two shearing rates (after Matsumoto et al., 1996)

Eiksund and Nordal (1996) report on a model pile testing program in Ottawa sand where the dynamic soil resistance and the pore pressure response near the pile base is studied during driving. The model pile is a closed end steel tube of 107 cm long and 63.5 mm in diameter. The studied penetration velocities range from 0.8 to 1800 mm/s. The pile is instrumented with strain gages, accelerometers and LVDT and pore pressure transducers are installed in the soil. The observed increase in resistance is less than 10% for an increase of more than 1000 times in penetration velocity. The effect of the loading rate in sand is quasi non-existent.

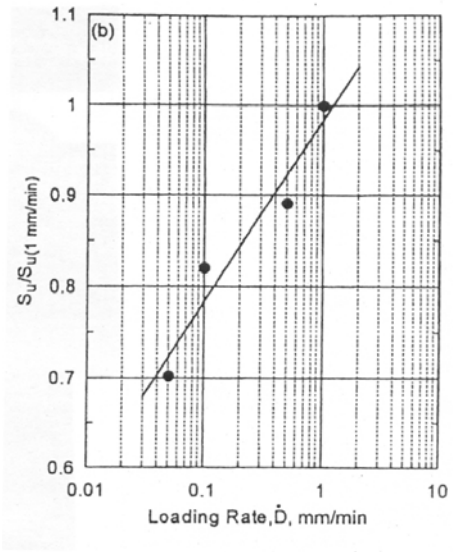

Figure II-31 : Undrained shear strength versus log loading rate (after Al-Shamrani, 2001)

Al-Shamrani (2001) carries out CU triaxial tests on clay samples by increasing the axial strain with a constant rate (0.05, 0.1, 0.5 and 1 mm/min) in order to determine the influence of loading rate on the undrained shear strength Figure II-31 shows a clear linear relationship in the semi-log plot for the S_u evolution which is similar to Equ. II-36. This linear relationship can be expressed by:

$$S_u\left(\dot{D}\right) = S_u\left(\dot{D}_{ref}\right)\left[1 + \beta \cdot \log\left(\frac{\dot{D}}{\dot{D}_{ref}}\right)\right] \qquad \textbf{Equ. II-37}$$

- $\dot{D}_{ref}$ and $\dot{D}$ are the reference and the analysed loading rate, respectively;
- $S_u\left(\dot{D}_{ref}\right)$ and $S_u\left(\dot{D}\right)$ are the undrained shear strength for $\dot{D}_{ref}$ and $\dot{D}$ respectively;
- β is the rate parameter defined as the slope of the straight line of the undrained shear strength vs the logarithm of the normalized loading rate.

The loading rate of reference ($\dot{D}_{ref}$) is set to 1 mm/min (0.0167 mm/s).The increase of S_u per log cycle of loading rate is found equal to 21.8 %, i.e. in general accordance with the above-mentioned results found in literature. Consequently, the value of β is fixed to be around 0.2. The author points out that the value of β and the shape of the modelled curve on the results are dependent of the range of studied loading range. Indeed, there is some authors that suggested a certain threshold limits the influence of the strain rate on the undrained shear strength for very slow loading rates. The author notes a stiffening effect and an increase of the initial tangent modulus with the strain rate (Al-Shamrani, 2001).

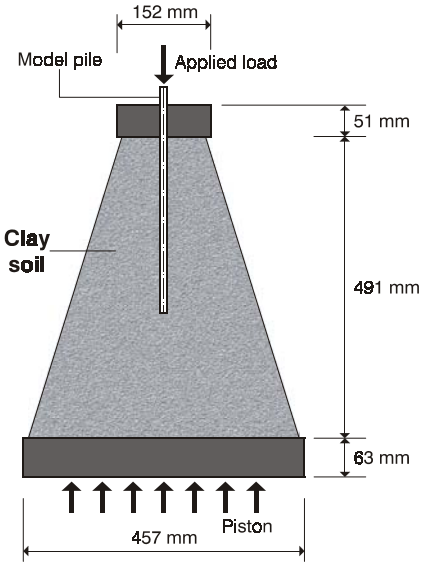

Figure II-32 : Cone-shaped soil chamber (after Horvath, 1995)

Horvath (1995) carried out a set of loading tests (CRP-QML-QCL)[3] on a model pile embedded in clay. The CRP results are used as reference. The duration of the QML tests is about 0.1 s and of the QCL tests 1.5 to 17 min. The CRP test is performed with a rate of 2 mm/min and the test duration is about 15 s. The maximum load applied on the pile is considered as the normative failure load ($Q_{CRP\text{-}f}$). The model pile is a closed-end steel pipe with a diameter of 12.7 mm and a length of 508 mm. The used soil is a low plasticity clay in an inverted steel cone confining chamber allowing a linearly increasing confining stress on the sample (0 at the top, maximum at the bottom) (see Figure II-32).The pile tests were loaded until failure occurs (when the pile is plunging). The failure load is taken as ultimate applied load. Figure II-33 indicates the influence of rate of loading on the capacity of the pile. The increase of failure load due to the loading rate effect can be plotted with a straight line in a semilog plot.

In order to find this straight line, the author interprets the results with the equilibrium point method (Midendorp et al., 1992; Horvath et al, 1993). This method is used to account for the rate effects in the statnamic tests interpretation. Horvath applies the method to the QCL and QML adjusted raw results (open square on Figure II-33) to find the adjusted failure loads (black triangles on Figure II-33). He concludes that the straight line is the real influence of the loading rate on the pile capacity without taking the soil damping (according to the author) into account. He concludes also that the soil damping is significant for QCL tests only and is negligible for the QML tests. ($Q_{CRP\text{-}f}$) is the CRP failure load.

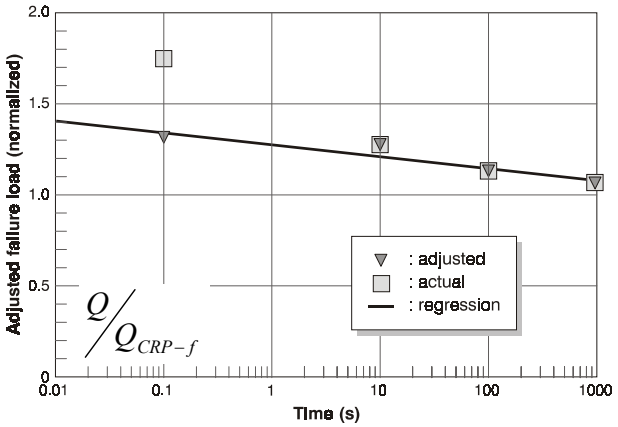

Figure II-33 : Adjusted failure load versus time (logarithm scale) (after Horvath, 1995)

[3] CRP means Constant Rate of Penetration Test, QML means Quick Maintained Loading test and QCL means Quick Continuous Loading test.

However, using the Briaud approach (Equ. II-30), and using the time to reach failure instead of the nominal loading durations in a log-log plot, Figure II-33 becomes Figure II-34. The raw points of the Horvath's paper follow a straight line that may be modelled by a power or a logarithmic law. The value of the viscous exponent related to the Briaud and Garland approach equal 0.058 which correspond to the expected range of value for a clay of type "low plasticity". Afterwards, with the adjustment made with respect to $Q_{CRP\text{-}f}$, Equ. II-38 can be written.

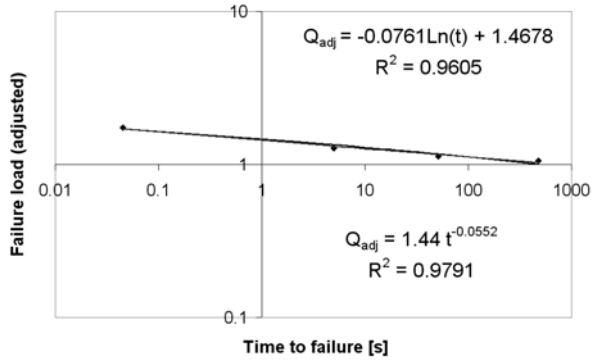

Figure II-34 : Application of the Briaud approach to the results of Horvath, 1995

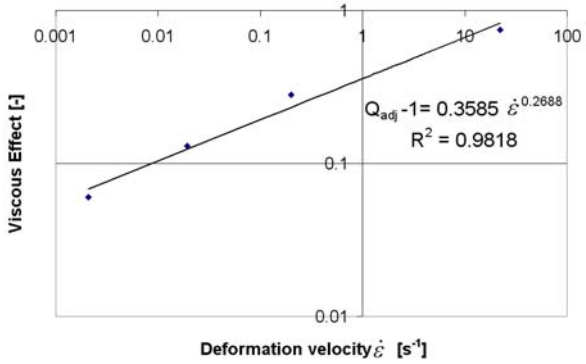

Figure II-35 : Viscous effect versus velocity of deformation

$$Q_{adj} = \frac{Q_{meas,dyn}}{Q_{ref}} = f(Q_{stat}, viscous\ effect)$$ **Equ. II-38**

If the general Smith approach is followed:

$$Q_{rheol} = Q_{stat} \cdot (1 + viscous\ effect)$$ **Equ. II-39**

$$Q_{meas,dyn} \equiv Q_{rheol} \quad \& \quad Q_{ref} \equiv Q_{stat}$$
$$Q_{adj} - 1 = Viscous\ effect$$

The velocity of deformation is defined as the inverted time to failure (Holeyman, 1984): $\dot{\varepsilon} = \frac{1}{t_f}$ and Figure II-34 becomes Figure II-35.

The exponent (0.2688) is close to the expected value of 0.2 from the Coyle and Gibson approach and

$$Q_{adj} = \frac{Q_{meas,dyn}}{Q_{ref,stat}} = 1 + J_{\_} \cdot \dot{\varepsilon}^{N_{\_}} = c \cdot \dot{\varepsilon}^{n}$$ **Equ. II-40**

- $J_{\_}$ is the damping parameter in a dimensionless formulation of the Coyle-Gibson model;
- $N_{\_}$ is the exponent in a dimensionless formulation of the Coyle-Gibson model;
- n is the viscous exponent of the Briaud model.

There is a relationship between the rheologic parameters of both models.

These developments show that all theories mentioned above are connected by mathematical approaches but finally describe the same behaviour with a similar trend, which is strongly non-linear.

5.3. Loading Rate Conclusions

Except for the Briaud and Garland form, all other power relationships can be written in a generic form:

$$\frac{Q_{rheol}}{Q_{stat}} = \left(1 + J_{LRE} \cdot V^{N}\right) \qquad \textbf{Equ. II-41}$$

J_{RLE} and N are the rheologic parameters accounting for the loading rate effects on the bearing capacity of the test performed at a velocity V compared to a test performed at a quasi null velocity.

All logarithmic relationships can be transformed in a generic formulation:

$$\frac{Q_{rheol}}{Q_{stat}} = \left(1 + Y_{LRE} \cdot \log\left(\frac{V}{V_{ref}}\right)\right) \qquad \textbf{Equ. II-42}$$

Y_{RLE} is the rheologic parameter accounting for the loading rate effect on the bearing capacity between a test performed at a velocity V_{ref} (the static test for example giving the capacity Q_{stat}) and the rapid test performed at the velocity V giving the capacity Q_{rheol}.

Except for the proposed law of Briaud and Garland, all proposed power laws work with the absolute velocity of the body considered (the pile, the soil or the in between interface). The reference test is considered with a null velocity. On the other hand, all logarithmic relationships consider a reference velocity, used in the denominator of the analysed velocity. This chosen reference has a great influence on the rheologic parameters (Holeyman, 1984; Al-Shamrani, 2001) like the units of the absolute velocity of the power law category.

The power laws family can be seen as a model type describing an absolute behaviour. The power law assumes that the effect of a increasing loading rate is always an addition of soil resistance. The logarithmic laws family describes a relative behaviour between two tests performed at different velocities. The evolution of the corresponding capacities is evaluated with the logarithmic relationship in function of the corresponding loading rates. Consequently, it is possible to compare two rapid tests, or a test performed with a slower loading rate than the reference one (with a ratio $\frac{Q_{rheol}}{Q_{stat}} < 1$).

All the tests performed concern tests conducted to failure. The tests results used for the models calibration are supposed to be the failure loads, corresponding to the ultimate resistances of soil under the submitted solicitations[4]. The conclusions can only concern a sort of envelope of the loading rate effect on the bearing capacity. It supposes the high strain state of the materials. Nevertheless, the

[4] Under the assumption that the failure under static and dynamic solicitation is comparable.

results of the tests performed in Sheffield (Anderson et al. 2003) have shown that the results ($S_{u,3\%\varepsilon}$-E_{50}) of undrained triaxial tests on clay-silt-sand samples were also influenced by the loading rate.

6. Conclusions

The testing programs and the evolution of the pile/soil models give the keys to delimit the knowledge existing about the loading rate effects. This section tries to resume the above mentioned results in terms of small and large strains, low and large velocities and types of soil.

6.1. Approach low and large strains

6.1.1. Low strains

The main effect due to the loading rate variation in the range of low strains is the radiation damping described by Novak et al. (1978) and used by many authors to totally or partially take the velocity dependent term into account. Unfortunately, too few tests have been performed focused on the loading rate effects on small levels of strain allowing the measurements of energy radiation in a large media. Most of the representative tests performed on a small level of deformation are laboratory tests which do not include the geometrical effect because of their characteristic size. However, there is a need to describe the evolution of the radiation damping because of the possible evolution of its parameter with the strain or stress level (the shear modulus) and because of its significant importance in the rheologic soil reaction especially for low strains.

The particular need to study the small strain range is motivated by the global understanding of the phenomena and also the need to correctly model the complete load history and its effect on the pile/soil interaction including the loading and unloading phases. Indeed, currently, the only thing sure is the validity of the general Coyle-Gibson relationship for ultimate loads and large strains. But these formulations are often used unconditionally on the all load-time history to quantify the loading rate effect.

Rausche et al. (1992) tried to take into account of a specific behaviour in function of the strain level and the loading path. Others researchers involved in the analytically based models tried to do the same approach (by introducing the viscous component) but without any real verifications of the behaviours involved.

6.1.2. Large strains

In the range of large strains, the main loading rate effects are based on dissipative and viscous dampings. Indeed, these two terms are theoretically significant because of the reduction of the radiation damping effect due to the degradation of the shear modulus and the entrance in plasticity. Since all the tests performed to investigate the loading rate effects are generally carried out until failure occurs, the relationship obtained and established as a power law function of the velocity could be interpreted as the sum of these terms. This is based on the fact the radiation damping theoretically vanishes when the soil enters in plasticity. But is this last assumption correct? Or is there still a radiative term for large strains despite the degradation of the shear modulus in the vicinity of the pile? For the base model, the assumptions generally express that the radiation continues to be generated when the plasticity increases. For the shaft, the assumptions assesses the opposite. The difference is

explained with the occurrence of slippage or not. There is a need to understand the radiation occurring at large strains in the close vicinity of the pile shaft.

Second, the high strain results are well known and usable for the characterization of the ultimate rheologic soil resistance depending on the velocity. There is a need to describe accurately the all different terms involved.

6.2. Approach low and large velocities

6.2.1. Low velocities

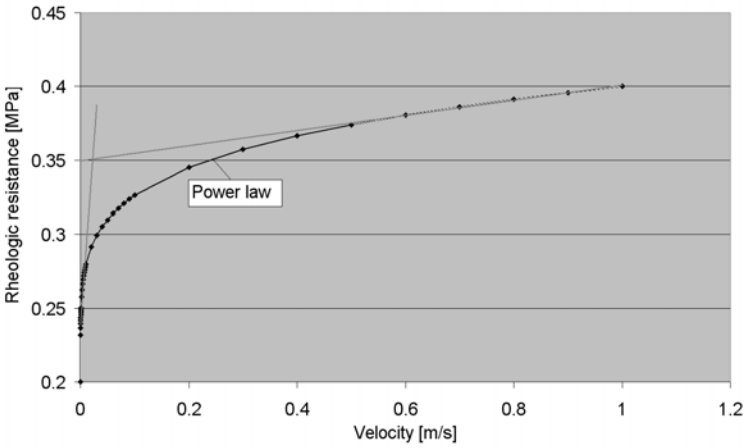

Figure II- 36 : Power law or juxtaposition of two different behaviours for the loading rate influence on the rheologic stress

The tests performed in laboratory and on footing models allow to assess a logarithmicrelationship in the range of small velocities that seems to be stiffer than the power-law relationship. Others testing programs investigate the large range of velocities correctly described by the power law, but the trend found is not wide enough to cover a large range of velocities. The problem resides in the connection between both velocity ranges (Figure II- 36): the static and the dynamic ranges of velocities or the stiffest part of the power-law. Is the power-law relationship representative of one sole behaviour or a juxtaposition of two behaviours of which the predominance is complementary? The domain of low velocities remains unexplored in terms of load rate effects and specific devices must be set-up in order to apply loading with small velocity.

6.2.2. Large velocities

A major part of the tests performed on model piles or on real piles in soil with the purpose to highlight the loading rate effect is carried out with a large velocity. The authors generally tried to vary the range of maximum velocities but the size and the devices used often impose to have a substantial velocity. Consequently, the tested velocities are still too high to analyse the first part of the theoretical power law curve that plunges suddenly to the value 1[5]. The consequences on the constitution of the models and on the further analysis are important because of the loading history where the velocity is not constant and maximum all the time, but evolves from zero to a maximum value and return back to zero. All the velocity and all the strain ranges must be investigated to have a general overview of the effect of the loading rate on the bearing capacity and on the load settlement curve. Currently, the major parts of the conclusions available concern large velocities.

[5] Where the rheologic resistance is equal to the static one for v=0

6.3. Clay and sand particularities

It is widely recognized that cohesive soils have a significant dependency to rate of loading. It comes from observations, experience and particular researches performed on the soil materials. On the other hand, even if this behaviour is assessed as similar for the sands, the amount of information available is much less larger. In the particular study of the loading rate effect, a major part o the tests performed concerns exclusively clay or soil containing a major part of clay. The results respect generally the same trend: a large, pronounced and non linear relationship between the rheologic soil resistance and the loading rate. Attempts were made to classify the rheologic parameters in function of the pile type, it was seen a large scattering of the results forbidding to have the smaller conclusion. The trend is there but not correlated to the soil type.

Sand has the poorest range of investigation and displays contradictory results (Svinkin, Eiksund, Paikowsky, Coyle & Gibson, Litkouhi & Poskitt). Sometimes a velocity trend exist, sometimes not. The explaination might come from the mix of the sand with one or several more "viscous" other materials. The sand can be saturated, mixed with a fine materials or a portion of clay or completely dry and pure. This last classification is almost insensitive to the loading rate where a mix of sand and clay shows a behaviour similar to the clayed one. These observations can support the assumption of a need of more tests, preferably in laboratory in order to evaluate the different components of the loading rate effects.

The following table summarizes the data available for each classification and highlights the necessity to increase the knowledge and to perform tests for sandy material and especially for small strains and velocities. The darker zone is the most characteristic and common tested range.

	Low strains		Large strains	
	Clay	*Sand*	*Clay*	*Sand*
Low Velocity	Cyclic lab tests	Cyclic lab tests	Model piles Lab tests	Models piles Lab tests
Large Velocity	Difficult to perfom	Difficult to perfom	Piles and models Lab tests	Piles and models Lab tests

Table II-5 : Summary of the data available in function of the strain, velocity level and of the sandy of clayey character of the soil

CHAPTER **3**

Pile/Soil Interaction Model & Dynamic Signal Analysis

1. Introduction

The main topic of this research is the analysis of dynamic data. As it was explained in chapter 1, this kind of analysis is not as simple as the static load test analysis. Since the measurements are influenced by the inertial efforts and obviously by the loading rate, and since the data are generally measured with transducers requiring a pre-treatment before exploitation, the method used to analyse these data is complex and requires to assess the pile/soil interaction system.

This chapter is focused on the presentation of this model and on the analysis of the dynamic data. The pile and soil are described in simple elements and defined by their mechanical or geomechanical parameters. The pile/soil model is described in term of fundamental relationships for both static and dynamic fields and for both base and shaft specific resistances. The algorithms used to perform the analysis of the dynamic signals and to simulate the static load-settlement curve are presented and the parameters required to describe this system are classified and sorted with respect to their reliability.

Since the model specificity is the possibility to account for the loading rate effect through the generation of viscous and radiation terms added to the static soil reaction, it is also helpful to define, to introduce and to illustrate each term involved in the process and to explain the way to evaluate the total rheologic stress. This fundamental approach is the practical continuation of the theoretical presentation of the loading rate effect in chapter 2.

After, a complete analysis of the dynamic data is proposed because their evolutions are typical of the loading rate. This analysis includes the study of the sole quantities measured (force, velocity, as well

as derived settlement and energy) and an overview of the signal quality with a special aspect to the post-treatment performed.

2. Presentation of the model

This section is focused on the description of the general pile/soil model. The main algorithm of resolution, the pile, the shaft and base reactions and the back-analysis program are described, commented and justified as needed.

2.1. Pile model description

The pile and its environment are modelled by a lumped mass model as described on Figure III-1. This system allows the discretization of the dynamic (force) and the kinetic (acceleration, velocity and displacement) fields for both pile and soil elements directly adjacent at the pile interface.

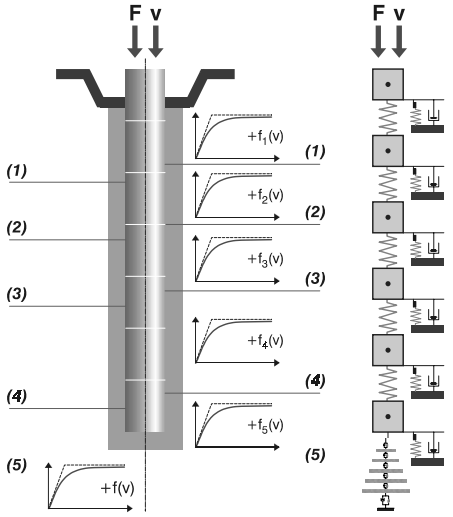

Figure III-1 : General description of the model NUMSUM-UCL

The system is defined by the stiffness, dampings, masses and dimensions of each component and some of them are either unknown or known. The model receives input data (force, velocity, displacement signals) and generates the pile/soil response (stress and deformation) in agreement with the pile/soil interaction definition. The number of unknowns is relatively large and function of the discretization. A good knowledge of the pile/soil environment (mechanical, geotechnical, geometrical) is required to reduce the number of unknowns to an acceptable and manageable amount. The pile/soil interaction is based on a modelling of the soil behaviour by two approaches: the shaft and base reactions. These models are developed by Holeyman (1984, 1985 & 1988) and described in chapter 2 and here below.

The pile is composed of lumped elements (springs and masses). The measured signals are imposed on the pile head. The integration scheme is explicit: the system state at time t is known and used to evaluate the system state at time $t + \Delta t$. The stability and the convergence of the system, in particular, depend on the relation between the mechanical characteristics of each element and the set time increment.

At each time step, for each node of the system, the balance of forces is evaluated (Equ. III- 1). These forces are the internal forces of the pile coming from the upper and lower node displacements (due to the input signal imposed in the pile head), and the external forces coming from the soil reaction (shaft friction for the nodes inside the pile and shaft friction and base resistance for the lower pile element). This force balance allows the evaluation of the acceleration of the concerned element (application of Newton's first law - Equ. III- 2), and by simple and double integration, its velocity and displacement respectively (Equ. III- 3 to Equ. III- 5). This motion description allows the calculation of the stress state for each element by means of the chosen stress-displacement and the defined velocity dependent

relationships. Consecutively, the balance of forces is re-evaluated and the cycle loops until the end of the calculation duration.

The nodes are located at the centre of the masses and a corresponding stiffness is evaluated from the pile material. This process is summarized on Figure III-2 and the following equations:

$$F_{result,i}(t) = \sum F_{\text{int},i}(t) + \sum F_{ext,i}(t) \qquad \textbf{Equ. III- 1}$$

$$acc_i(t) = \frac{F_{result,i}(t)}{mass_i} \qquad \textbf{Equ. III- 2}$$

$$vel_i(t + \Delta t) = vel_i(t) + acc_i(t) \cdot \Delta t \qquad \textbf{Equ. III- 3}$$

$$\Delta displ_i(t) = vel_i(t + \Delta t) \cdot \Delta t \qquad \textbf{Equ. III- 4}$$

$$displ_i(t + \Delta t) = displ_i(i,t) + \Delta displ_i(t) \qquad \textbf{Equ. III- 5}$$

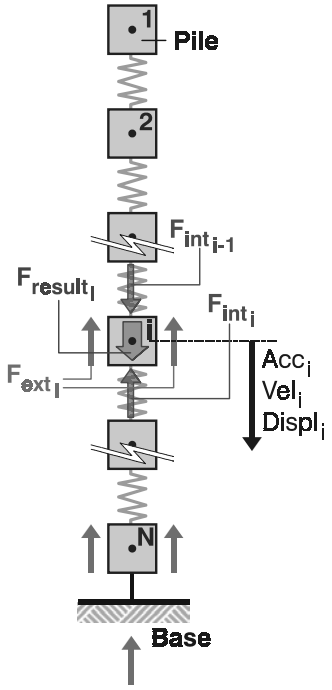

Figure III-2 : Model description

- $F_{result,\,i}(t)$ is the resulting force at the node i at the time t;

- $F_{int,\,i}(t)$ is one of the internal forces applied at the node i at the time t;

- $F_{ext,\,i}(t)$ is one of the external forces applied at the node i at the time t;

- $Mass_i$ is the mass of the element i;

- Acc_i, Vel_i, $\Delta displ_i$ and $displ_i(t)$ are the acceleration, the velocity, the increment of displacement and the displacement of the node i at time t, respectively;

– Δt is the time increment.

The system must be initiated with one field (force, acceleration, velocity or displacement) varying in time (a pulse, a dirac, a constant increase, or decrease,…). The system resolution also requires the calculation of the internal and external forces in function of the pile motion. This calculation is ruled by constitutive laws described hereafter.

In this model, only the pile is moving. The soil is supposed motionless and the reaction is located at the interface between the pile and the soil. The pile motion is consequently considered as the relative motion between pile and soil.

2.2. Pile/soil interaction model

2.2.1 Pile model

2.2.1.1 Stiffness

The pile is considered as an elastic material with an elastic modulus E_p and divided in N elements of equal lengths [1 to N]. Each element is limited in dimensions, so its mass and stiffness can be calculated.

$$mass_i = \rho_p \cdot A_i \cdot h_i \qquad \textbf{Equ. III- 6}$$

- ρ_p is the volumetric mass or mass density of the pile material [kg/m³];
- A_i is the normal section of the element i supposed to remain constant along the element and in time [m²];
- h_i is the height of the element, generally set to $\frac{H_p}{N}$ [m].

$$k_{el,i} = \frac{E_p.A_i}{h_i} \qquad \textbf{Equ. III- 7}$$

This is the elementary stiffness of the pile element. However, the spring used in the model is located in a mid position between two lumped masses (Figure III-2). The used equivalent stiffness is given by:

$$k_{calc,i} = \frac{1}{\frac{1}{\frac{k_{el,i-1}}{2}} + \frac{1}{\frac{k_{el,i}}{2}}} = 2 \cdot \frac{k_{el,i-1} \cdot .k_{el,i}}{k_{el,i-1} + k_{el,i}} \qquad \textbf{Equ. III- 8}$$

Where $k_{el,i}$ and $k_{el,i-1}$ are the elementary stiffness of two consecutive pile elements.

2.2.1.2 Internal forces

The internal forces are calculated taking into account the transmitted forces coming from the head pile or the base and the resulting shortenings of the pile elements. Spring forces are purely elastic:

$$F_{\text{int},i} = k_{calc,i} \cdot (displ_{i-1} - displ_i) \qquad \textbf{Equ. III- 9}$$

A small damping behaviour is introduced to account for all energy losses:

$$F_{\text{int},i} = k_{calc,i} \cdot (displ_{i-1} - displ_i) + C_p \cdot I \cdot (vel_{i-1} - vel_i) \qquad \textbf{Equ. III- 10}$$

- C_p is the damping factor (0.5) [-];
- I is the nominal impedance of the pile [MPa.s/m];

2.2.2 Shaft model

The lateral shaft friction is composed of a static and a dynamic term. Each component is described with its own relationships between soil resistance and either displacement or velocity. The shaft model does not take into account the potential interactions between the soil layers.

2.2.2.1 Elastic and plastic deformations in the static field

Stress-strain relationship (τ,γ)

The stress-strain relationships is described by elasto-plastic and hyperbolic laws (Figure III-3):

Elasto-plastic

$\tau = G_i \cdot \gamma \rightarrow \gamma \leq \gamma_r$ **Equ. III- 11**

$\tau = \tau_{ult} \rightarrow \gamma \geq \gamma_r$

- τ is the shear stress [Pa];
- G_i is the initial shear modulus [Pa];
- γ is the angular distortion [-].

Hyperbolic

$\gamma = \gamma_r \frac{\eta}{1-\eta}$ **Equ. III- 12**

- γ_r is the reference shear strain: $\frac{\tau_{ult}}{G_i}$ [-];
- η is the mobilization ratio: $\frac{\tau}{\tau_{ult}}$ [-];
- τ_{ult} is the ultimate shear stress [Pa].

The change from linear elasticity to a constant strength in plasticity does not reflect the reality.

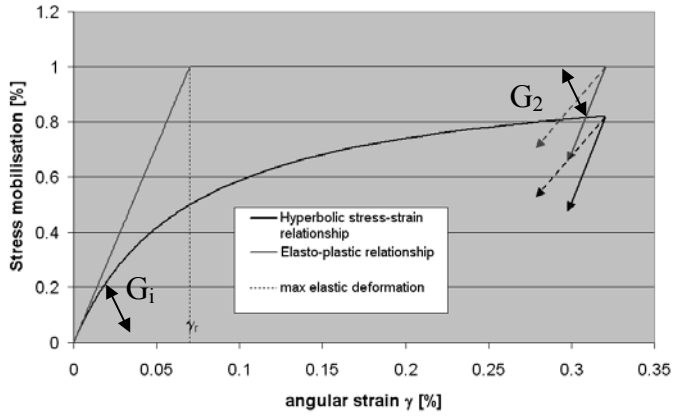

Figure III-3 : τ–γ relationship proposed for the shaft reaction

A smooth formulation may be established in order to progressively introduce plasticity. Kondner (1963) proposes the hyperbolic law (Equ. III-12), where the stress tends asymptotically to the ultimate shear stress τ_{ult} with increasing deformation. This relationship smoothly indicates the transition between linear to non-linear behaviours and respects the elastic behaviour in case of small strains, and the plastic deformation in case of large strains.

The unloading phase follows a linear path characterised by the initial shear modulus G_i or a different modulus given by the ratio: $\frac{G_i}{G_2}$ (Figure III-3).

Stress-displacement relationship (τ,displ)

The stress-displacement relation for the shaft is obtained after integration of the angular distortion of the soil. This integration must be performed on a finite domain in order to give a finite displacement:

$$displ_p = \frac{\tau_p \cdot R_p}{G_i}\int_{R_p}^{\infty}\frac{dr}{r} = \frac{\tau_{pile} \cdot R_p}{G_i}\ln(r)\,|_{R_p}^{r=\infty} = \infty$$ **Equ. III- 13**

- R_p is the pile radius [m];
- τ_p is the stress mobilized at the pile shaft [Pa].

Randolph & Wroth (1978) suggest the decomposition of the soil behaviour in a half space accounting for the base resistance and a layer of depth D accounting for the friction. They also reduce the infinite layer to a finite space with an outer boundary. This limit is fixed to a distance, called R_m, where the soil vertical stress induced by the vertical displacement of the pile is considered as negligible:

$$R_m = 2.5D \cdot (1-\upsilon)$$ **Equ. III- 14**

- D is the embedded pile length or the soil layer thickness [m];
- υ is the Poisson ratio [-].

Using this boundary, Equ. III- 13 becomes:

$$displ_p = \frac{\tau_p \cdot R_p}{G_i}\int_{R_p}^{R_m}\frac{dr}{r} = \frac{\tau_p \cdot R_p}{G_i}\ln\left(\frac{R_m}{R_p}\right) = \frac{\tau_p \cdot R_p}{G_i}\cdot\ln(\frac{R_m}{R_p})$$ **Equ. III- 15**

That is the stress-displacement relationship at the pile shaft for an elasto-plastic law.

If the hyperbolic law proposed by Kondner (1963) is used, the same process gives:

$$displ_p = \int_{R_p}^{R_{m1}}\gamma \cdot dr = \frac{\tau_p R_p}{G_i}\ln\left(\frac{\frac{R_m}{R_p} - \eta_p}{1-\eta_p}\right)$$ **Equ. III- 16**

- τ_p, $displ_p$ is the pile shaft stress-displacement state;
- η_p is the mobilization ratio at pile shaft ($\frac{\tau_p}{\tau_{ult}}$).

This approach allows also the direct introduction of the hysteretic damping by the introduction of a completely elastic unloading phase respecting the stiffness of the elastic spring (with a possible factor accounting for the modification of the shear modulus for the unloading : $G_i \rightarrow G_2$).

The static term, for both elastic or plastic deformations is completely described with three parameters:

- The ultimate shear resistance τ_{ult};
- The initial shear modulus G_i;
- Poisson's ratio υ.

It can be modelled by a non linear spring with a plastic slider in case of the use of an elasto-plastic relationship (Figure III-4).

2.2.2.2 Elastic and plastic deformations under dynamic solicitations

The shaft model acts under dynamic solicitations with two terms linked to the loading rate:

- A viscous damping supposed to represent the dissipative energy lost at the interface;
- A radiation damping supposed to represent the energy lost in the surrounding soil.

The sum of all terms (static + viscous + radiation) is limited to a velocity dependent term.

The viscous damping

As observed by numerous researches (see chapter 2), there is an increase of soil resistance due to an increasing loading rate. This term is velocity dependent following a non-linear relationship (a power law) and proportional to the static soil reaction:

$$\tau_{visq} = J.v^{N}.\tau_{stat} \qquad \textbf{Equ. III- 17}$$

τ_{visq} is the viscous stress [Pa]; N s the exponent expressing the non-linear dependency [-];

v is the pile velocity [m/s]; J is the damping factor [s/m^N].

τ_{stat} is the static soil reaction [Pa];

The law has an empirical origin and its parameters, J and N are based on the literature. N is generally set to 0.2 and J is function of the site, pile and soil types.

The radiation damping

The radiation damping is introduced in chapter 2, based on Novak et al.'s work (1978). That work concerned the analysis of the harmonic vibration of an infinite and rigid cylinder in an infinite medium. A complex stiffness of the medium has been found to represent the soil response. The imaginary part of this expression model the radiation of the energy into the soil and is simplified by the following expression for high frequencies:

$$c = \frac{G_i}{V_s} = \sqrt{\rho \cdot G_i} \text{ [Pa.s/m]} \qquad \textbf{Equ. III- 18}$$

Where ρ is the volumetric mass of the soil [kg/m] and G_i is the initial shear modulus [MPa].

The larger the frequency of the signal, the more dampened the pile motion due to the soil effect (increase of the importance of imaginary part compared to the real part of the soil stiffness).

Holeyman (1984) supposes that the pile/soil system creates a plastic zone around the pile under large dynamic solicitations and this disturbed zone is located in the close vicinity of the pile shaft. So, the radiation is reduced and almost vanished when the plasticity rate increases. Holeyman takes this

property into account by replacing the initial shear modulus of Equ. III- 18 by tangent shear modulus of the static stress-displacement relationship. Its evolution with η is given by:

$$G = G_i \cdot (1-\eta)^2 \qquad \textbf{Equ. III- 19}$$

- G is the local tangent shear modulus [Pa];
- G_i is the initial tangent shear modulus [Pa];
- η is the mobilization ratio [-].

The plastic slider

The plastic slider models the natural limitation of the soil resistance. This threshold is influenced by the loading rate and follows the well known non-linear velocity dependency as described in chapter 2.

$$\tau_{rheol} \le \tau_{ult,rheol} = \tau_{ult} \cdot \left(1 + J.v^{0,2}\right) \qquad \textbf{Equ. III- 20}$$

The parameters J and N are set equal to those of the viscous term but they should be different (especially for the parameter J that determines a typically different behaviour).

2.2.2.3 The rheologic shaft soil reaction

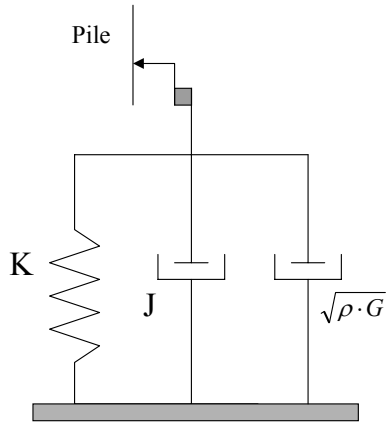

Figure III-4 : rheologic shaft model

The shaft friction model is summarized in Figure III-4. The static term is based on the hyperbolic law and the non linear stiffness k is related to the level of soil mobilization. It describes the low and large static strains. The first dashpot determines the viscous part of the soil reaction (relative to the loading rate effect). This dashpot is non-linear since the relationship is a power-law of velocity. The second dashpot represents the radiation damping. The dashpot is non linear since the shear modulus value decreases when the rate of mobilization increases. The slider is the rheologic ultimate resistance of the soil limiting the sum of all terms.

2.2.3 Base model

Similarly to the shaft modelling, the base model is composed of a static and a dynamic term which are described hereafter. The model is built to represent the soil response at low and large solicitations.

2.2.3.1 Small deformations under static and dynamic solicitations

As described in chapter 2 (section 4.2.1.), the base response is based for small strain Lysmer and Richart analogue (1966) that represents the response of an elastic half-space medium under harmonic solicitations applied on the centre of a circular and rigid footing resting on an elastic and homogeneous

half-space (Figure III-5). The footing has a radius R, a mass m and the medium has an initial shear modulus G_i, a soil density ρ and a Poisson's ratio υ.

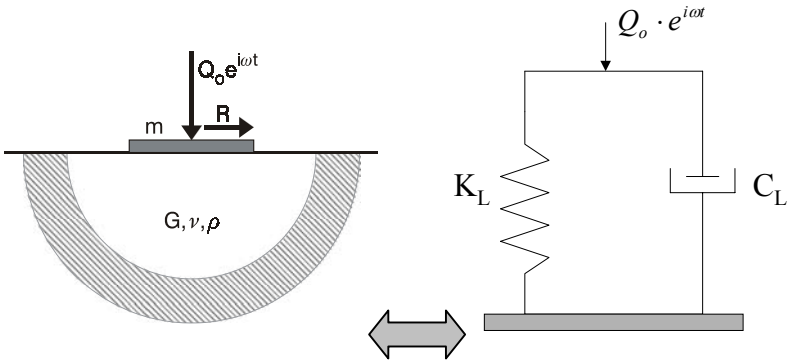

Figure III-5 : Lysmer analogue

The Lysmer analogue is composed of a spring for the static term of the reaction and a linear dashpot representing the energy losses by radiation in the soil beneath the pile base. This model can be applied to the pile base reaction by considering the footing radius as the pile base radius and the footing mass as the pile mass (without shaft effects). The stiffness and the dashpot factors are given by:

$$K_H = \frac{4G_i R}{(1-\upsilon)}$$ **Equ. II- 21**

$$C_H = \frac{3.4R\sqrt{G_i \rho}}{(1-\upsilon)}$$ **Equ. II- 22**

- K_H is the spring stiffness [N/m];
- C_H is the damping factor [Ns/m];

2.2.3.2 Large deformations under static and dynamic solicitations

Since the model based on the Lysmer analogue is only valid for homogeneous and elastic media. Holeyman (1984, 1985) modifies it to account for a heterogeneous half-space and a non-linear behaviour of the soil response. Figure III-6 represents an equivalent solid supposed to take account of these elements. The equivalent axisymetric solid rests below the footing and the model finally rests on a half-space medium governed by the analogue of Lysmer (K_H & C_H). The finite lateral extents are determined to have a correct response model under static and dynamic conditions (Holeyman, 1984). In this equivalent solid, only the vertical mode of deformation is considered and the cone mass density is equal to the soil medium. The vertical modulus of elasticity E_v is given by:

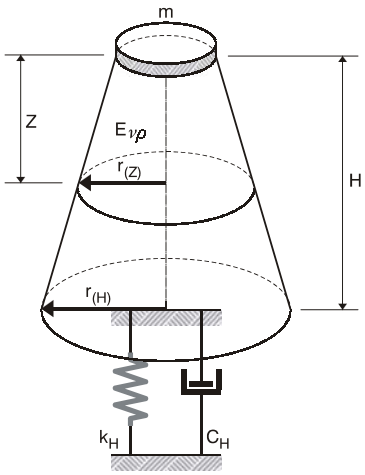

Figure III-6 : Concept of the equivalent solid (after Holeyman, 1988)

$$E_v = \frac{G_i}{0.85 \cdot (1-\upsilon)^2} = \frac{E_i}{1.7 \cdot (1-\upsilon)^2 \cdot (1+\upsilon)} \qquad \textbf{Equ. III- 23}$$

- E_i is the initial modulus of elasticity [MPa];

This relationship is due to the respect of the equality between the impedances of the half-space medium and the equivalent solid section (Holeyman, 1984). The evolution of the cone radius r(z) is function of the depth z, the pile radius r_0 and the Poisson's ratio:

$$r(z) = r_0 + \frac{1-\upsilon}{\sqrt{0.85}} \cdot z \qquad \textbf{Equ. III- 24}$$

This relationship is due to the combined action of the respect of impedances (dynamic condition) and the respect of elasticity condition (static condition) with the static settlement of the Lysmer analogue. The model has the advantage to be easily discretized in lumped parameter accounting for the local properties (non-homogeneity) of each layers (Figure III-7)

The cone is divided into n elements of same thickness and the stiffness used in the calculus correspond to those located in a mid position between two masses. An equivalent stiffness, similarly to Equ. III- 8 is used. Half an element mass is added to the pile last element and the last element before the half space has also a half mass. The base model does not accept tension stress; this is a direct consequence of the physical situation where the pile base acts in compression but not in tension. Consequently, the stress base response is set to 0 if the stress state beneath the pile base is in tension. The non-linear response of the soil, typical for large deformations, is integrated in the intermediate elements with the hyperbolic law (Kondner, 1963) adapted to the axial deformation and stresses.

This model is characterized by an elastic unloading phase (stiffness equal to the initial modulus) defining the hysteretic damping of the pile behaviour. This unloading path is defined as linear (with the same stiffness than the initial one, or modified similarly to the shaft model by using another stiffness ruled by a ratio E_i/E_2).

2.2.3.3 Viscous damping

A viscous effect is accounted for into the equivalent solid, function of the soil velocity and of the static soil reaction similarly to the shaft model.

$$\sigma_{rheol} = \sigma_{stat} \cdot \left(1 + Jv^N\right) \qquad \textbf{Equ. III- 25}$$

Where J and N are the rheologic parameters of the base reaction.

The radiation damping

The radiation damping is accounted for by the geometry of the cone and the masses of the lumped elements. The behaviour at the base of the cone is assumed as low strain as sufficient in order to use the Lysmer analogue defined for an elastic behaviour.

The plastic slider

The plastic slider models the natural limitation of the soil resistance. This threshold is influenced by the loading rate and follows the well known non-linear velocity dependency as described in chapter 2.

$$\sigma_{rheol} \le \sigma_{ult,rheol} = \sigma_{ult,stat} \cdot \left(1 + J.v^{0,2}\right) \qquad \textbf{Equ. III- 26}$$

2.2.3.4 The rheologic base soil reaction

The model is summarised by Figure III-7.

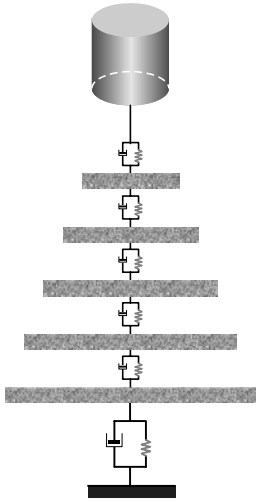

Figure III-7 : Rheologic base model

The soil response is given by an equivalent solid allowing heterogeneity and non-linearity lying on a half-space represented by a Lysmer analogue modelling the elastic response of the soil in the far field. The settlement of the base response is given by the settlement of the all cone and the settlement of the elastic half-space:

$$S_\infty = \Delta S + S_H \qquad \textbf{Equ. III- 27}$$

- ΔS is the settlement of the cone;
- S_H is the settlement of the half-space medium.

The stress is given by the stress undergone by the first cone element. The inside model is composed of a spring of which the stiffness corresponds to the non-linear static soil response and is function of the mobilization ratio and the relative displacement between cone elements; the hysteretic damping is included. The damping represents the viscous and strain rate or velocity dependent term regarding to the relative motion between cone elements. The plastic slider accounts for the static ultimate soil resistance and the loading rate effects. The cone base reaction follows the Lysmer analogue.

2.2.4 Parameters management

The soil is described by layers for both shaft and base reactions. The number of layers is limited to 5 for both shaft and base resistances.

- Shaft resistance parameters: each layer is characterized by its depth z_i, the ultimate shear strength $\tau_{ult,i}$, the initial tangent shear strength G_i and the damping factor corresponding to both viscous and ultimate rheologic forms J_i. The unloading modulus G_2/G_1 is set for all layers.

- Base resistance parameters: each layer is characterized by the same set of parameters : z_i, $\sigma_{ult,i}$, E_i, J_i and a ratio E_2/E_1 for the unloading (for all the layers). The soil is also divided in layers even if the only parameters used are those of the layers intersected by the cone of soil. The coefficient of Poisson and the mass density are required for the cone set-up.

- Pile and model parameters: pile parameters required: geometry (radius, length, type of section, expanded base, …) and material description (elastic modulus, mass density,…) and model parameters required: the mathematical and processing assumptions impose a number of parameters as the number of pile elements, the description of the cone (number of elements, height), the duration of the studied signal or the time increment precision.

2.2.4.1 Set of parameters : Input and sorting

The values of the soil parameters are the main unknowns of the back analysis problem. They can be characterized by a level of uncertainty and a level of influence in the dynamic pile response evaluation. Each parameter has a proper weight determined by its influence on the pile model response. The first set of parameters is used to describe the pile/soil system and allows one to calculate a first response for a given solicitation. This first estimation of the parameters is based on different sources. The most common is to use the geotechnical information available on site. If some of them are missing, existing correlations with known parameters are possible.

The number of parameter to be optimised is too large and a rational approach has to be undertaken in order to reduce this number. One idea was to sort the parameters in categories based on the level of reliability of their values. The number of parameters is reduced and also the complexity of the process.

The parameters are classified by categories: pile geometric and mechanical data, geomechanical data, rheological data (load rate effects parameters), test data and modelling parameters.

The pile geometric data are known *a priori* for most piles to be tested. The level of certainty varies from high to medium if the pile is a prefabricated driven pile (every dimensions are known) or if the pile is a cast-in-place one with enlarged base. Some of the parameters could be optimised but in an independent process, using methods built for this purpose (like the integrity method,…). In general the pile geometric data in the back-analysis process are assessed as known parameters.

Laboratory tests, literature, direct analysis of the measured signals or personal experience can give a good knowledge *a priori* of the pile mechanical parameters. In function of the source, the reliability is more or less important. But since the methods can be compared, and the theory allowing the calculation of the different parameters well established, their first evaluation does not seem to be far from the real solution. These parameters are not integrated to the general back-analysis problem.

The geomechanical parameters defining the fundamental soil relationships are the main unknowns of the problem and also the main objective. Besides these parameters, the type of relationships chosen to model the pile/soil interaction is also one of the main assumptions. The whole back-analysis process, performed manually or automatically, is focused on these parameters. As explained before, laboratory tests or geo-technical *in situ* tests can give a first estimation but contrary to the pile properties, the soil characteristics are dependent of the stress history and the environment within they are evaluated. Laboratory tests, CPT tests or other resources cannot exactly reproduce the conditions in the soil after

or during driving. This is a major reason why these parameters are highly uncertain and need a specific back-analysis in order to be evaluated in the field conditions[1].

The rheologic parameters (J and N) are linked to the loading rate effects. This behaviour is still poorly understood either for the specific value of J and N or for the behaviours they represent. Chapter 2 is focused on the research undertaken in this domain. Since these parameters (or preferably this behaviour) have a large influence on the dynamic load test results, the back analysis will try to estimate the best value for these parameters according to the assumptions of the chosen model.

The test data are function of the firm that performs the tests and the observation of the testing system before the dynamic loading test. Correlation with measurements made by transducers can confirm these values. They do not require an optimisation process.

The model parameters are connected to the numerical stability of the code, and the precision required for the results. They have to be chosen with discernment and do not have to be optimised.

Summary of the parameters

Figure III-8 presents a summary of the parameter classification and the importance to be accorded into the back-analysis process.

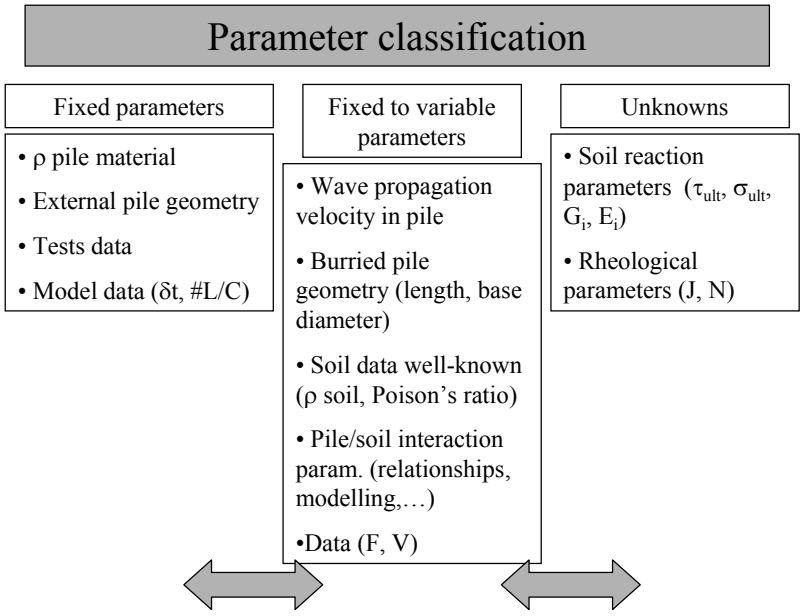

Figure III-8 : Classification of parameters according to their reliability

The arrows mean that the parameters located in the middle column can move from a position of variable parameter to fixed or unknown categories.

[1] Assumptions are made to equal the field conditions for static and dynamic cases (namely to compare the simulations of SLT with the real SLT). This can be partially correct for the installation influence but there remains a big uncertainty on the test consequences because of the loading rate effect on the soil state.

2.3. Algorithms – scheme of resolution – SLT simulation

2.3.1 The back-analysis process

The back-analysis process is fully described in chapter 5. It is based on the cross-matching of two signals (force and velocity measured at the pile head during the blow). These signals are compared to the corresponding model responses. An adjustment of the pile/soil parameters is performed in order to optimise the quality criterion. Once the matching fulfils the stop criterion, the soil's parameters are used to simulate the static load-settlement curve.

2.3.2 The static load-settlement curve simulation

The same pile/soil model is used to simulate the static load-settlement curve. The optimised set of parameters determined in the dynamic analysis is used to evaluate the bearing capacity of the pile under the constant settlement of the pile into the ground (from 10^{-2} to 10^{-5} m/s in order to have a simulation close to the real SLT). Consequently, the simulation is a constant rate of penetration test. The system solves the balances of forces at each node and at each time step for a monotonically increasing displacement. The soil reactions (shaft and base) are stored and the corresponding curves are plotted.

The modulus of elasticity of the pile used in the simulation is also different compared to the modulus used in the dynamic analysis. The empirical formulations of Mortelmans (1984) allowing to determine the dynamic and static elastic moduli from the concrete strength ($R'_{w,j}$) are used to evaluate the static modulus from the dynamic one introduced in the model for the dynamic analysis.

$$E_{stat} = 5200\sqrt{0.96R'_{w,j}} \qquad \textbf{Equ. III- 28}$$

$$E_{dyn} = 5600\sqrt{0.96R'_{w,j}} \qquad \textbf{Equ. III- 29}$$

$$E_{stat} = E_{dyn} \cdot \frac{5200}{5600} = 0.93 \cdot E_{dyn} \qquad \textbf{Equ. III- 30}$$

2.4. Decomposition of the rheologic shaft friction stress into static and velocity dependent terms

2.4.1 Presentation

In order to illustrate the rheologic response of the pile/soil system and especially the order of magnitude of each term, a damped harmonic signal of velocity (frequency ω, damping ξ and initial velocity V_o) is imposed to the pile model similarly to a measured dynamic signal during a DLT test (Figure III-9). The pile is modelled with one rigid element and the soil is a sole layer characterised by:

- τ_{ult} = 0.2 MPa;
- υ = 0.35;

- G_i = 100 MPa;
- J = 1 s/m & N = 1;

The reference signal is given by:

$V(t)=V_o \cdot e^{(-\xi\omega t)} Sin(\omega t)$ → Velocity (Figure III-10) **Equ. III- 31**

$$U(t)=\int V(t)dt=\frac{V_o}{-\xi\omega}\cdot\omega\cdot e^{(-\xi\omega t)}\frac{\left(Sin(\omega t)-\frac{\omega}{-\xi\omega}Cos(\omega t)\right)}{1+\frac{\omega^2}{(-\xi\omega)^2}}$$ → Displacement (Figure III-10) **Equ. III- 32**

$$Acc(t)=\frac{\partial V(t)}{\partial t}=V_o\cdot\omega\cdot e^{(-\xi\omega t)}\left(-\xi\cdot Sin(\omega t)+Cos(\omega t)\right)$$ → Acceleration **Equ. III- 33**

- Vo = 1.45 m/s;
- ξ = 0.233 s^{-1};
- ω = 272 rad/s.
- V_{max} = 1.03 m/s
- u_{max} = 7.4 mm
- u_{min} = 5.05 mm
- a_{max} = 391 m/s²

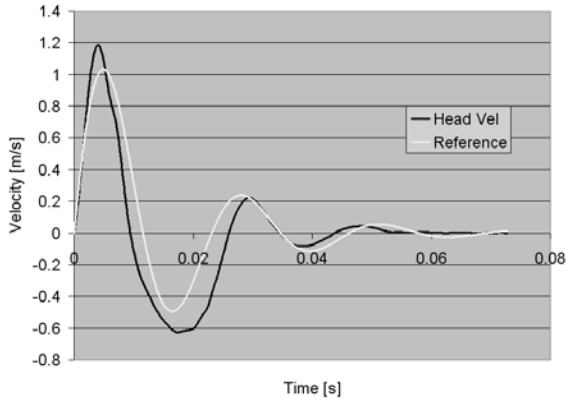

Figure III-9: Measured and reference velocities signals along the pile (blow B8-009 - Limelette)

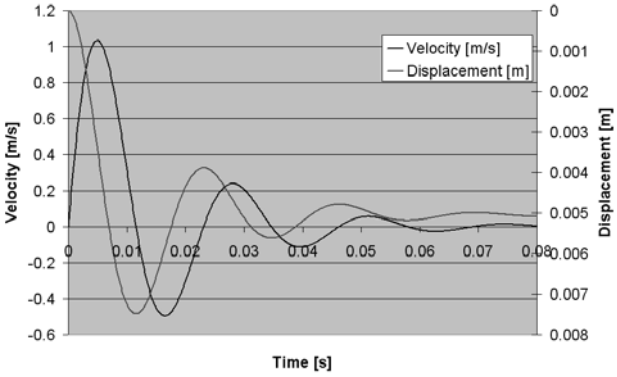

Figure III-10 : Plot of the reference velocity and displacement signals

The fundamental static stress-displacement relationship (Figure III-11) is hyperbolic and the rheologic soil resistance accounts for the static, the viscous and the radiation terms, all of them being limited by the velocity dependent rheologic ultimate stress. The tangent stiffness degrades with the soil mobilization towards the stress asymptotic value = 0.2 MPa and the unloading path is linear until the stress becomes negative. Afterwards, the hyperbolic progression starts again in the opposite stress sign.

Figure III-12 shows the terms of the rheologic stress already presented in the model: the static, the viscous and the radiation one (noted T_{stat}, T_{visq} & T_{rad} for τ_{stat}, τ_{visq} & τ_{rad}). The progression of the radiation stress is very fast and very stiff due to the high value of the radiation damping factor $\sqrt{\rho G}$ in the first part of the mobilization (when G is not degraded yet). After, with the progress of the static mobilization, the radiation damping decreases even before the velocity has reached its peak and the relative influence of the radiation damping decreases.

The viscous effect is relatively low, directly connected to the velocity and proportionally to the static soil reaction. The sum of all terms is also plotted and is mainly led by the radiation damping at the very beginning with a strong influence on the initial stiffness. This is also observable on the pile load testing dynamic curves. The soil material is characterized by an intrinsic resistance ($T_{rheol,ult}$), also velocity dependent to account for the load rate effect. This limit can never be exceeded by the sum of three terms. If the case happens, the value taken into account in place of the sum is the theoretical threshold. Figure III-13 represents the plots of the theoretical formulation of this limit and the sum of three terms.

The model uses the minimum value of those both terms (the yellow trace) also called the ultimate soil reaction. The rheologic term equals the static one when the velocity vanishes and there are angular points in the radiation trace when the static curve changes its behaviour from loading to unloading because of the change from hyperbolic loading to a linear unloading.

2.4.2 Observations

The break point in the progress of the rheologic soil reaction (green circle on Figure III-13) highlights the evolution of the soil mobilization from a continuum state (description of the intrinsic stress-displacement and velocity relationships) to a failure mode (slippage of the pile into the soil→ slider). Moreover, the failure occurs for very low static mobilization.

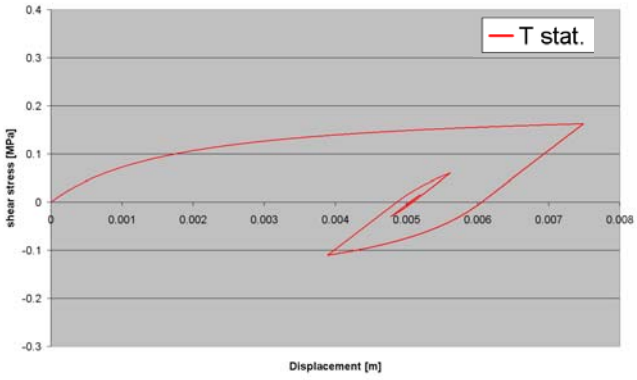

Figure III-11 : Static shear stress-displacement curve

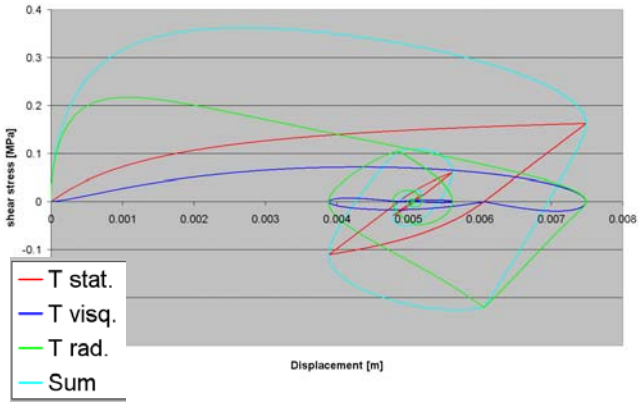

Figure III-12 : Static, viscous and radiation shear stress-displacement curves + sum of the three terms

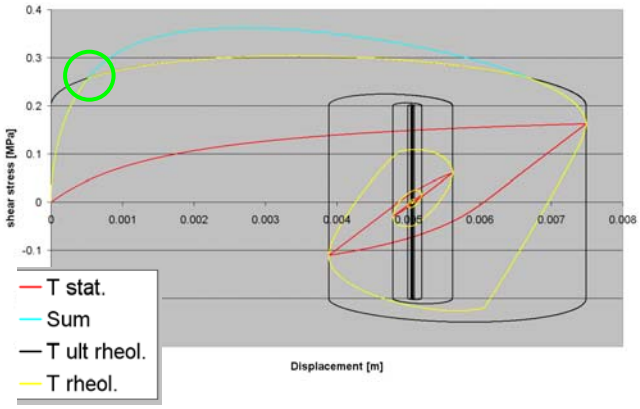

Figure III-13 : Static shear stress-displacement curve + sum of the three terms (static + viscous + radiation) + ultimate rheologic soil resistance + used rheologic stress-displacement curve

Figure III-13 expresses that the radiation has a strong and quick influence on the failure and the time needed to reach failure. The rheologic soil reaction appears to be almost linearly velocity dependent during the first part of the loading directly followed by a non–linear power relationship of velocity expressed by the formulation of the ultimate rheologic resistance when the limit of resistance is

exceeded. Since this breakpoint and the relative dependency of different terms is conditioned by the loading rate and the mobilization rate, it could be interesting to investigate the influence of different loading rates on the rheologic stiffness from the start of mobilization until failure. This break in the continuity of the rheologic soil reaction could also be interpreted as a quake (without knowledge of the radiation damping). However, the quake is linked to the static and intrinsic behaviours of the soil, whereas this event is rather related to the velocity and the level of static mobilization. Both behaviours are linked to the passage from soil mobilization state to failure mode but the former is connected to the displacement field (the quake), and the 2nd to the velocity field.

The influence of the velocity dependent terms is significant for the measured applied load and the deduced soil reaction but both terms (viscous and radiation terms) influence also the initial stiffness of the stress-displacement curve that can be easily compared to a load-settlement curve without taking the inertial effects into account.

2.4.3 Influence of a variation of the velocity and frequency of the loading signal

Since the loading description has a strong influence on the form of the load-settlement curve (especially at the very beginning), it is proposed to investigate the effects on the initial stiffness of a variation of velocity amplitude V_0 and frequency ω that modify both loading duration and magnitude. The velocity signal described in section 2.4.1. (Equ. III- 32 to Equ. III- 33) is imposed to the pile in contact with one soil layer. Obviously, both of them influence the time needed to generate a given displacement, the higher or the longer the maximum velocity, the longer the displacement mobilized.

2.4.3.1 Variation of magnitude

The velocity synthetic signal is limited to the first half phase (Figure III-14). The velocity starts from zero, increases until its maximum and decreases to zero. The signal evolves by modifying V_0 from 0.2 to 2 m/s. The plots of displacement & velocity vs. time, velocity vs. displacement and soil reaction vs. displacement are displayed on Figure III-14 to Figure III-17. The displacement curve is a damped cosinus characterised by the same parameters (ω, ξ and V_o).

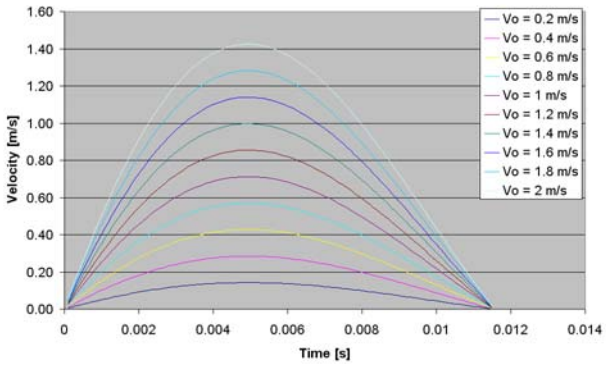

Figure III-14 : Variation of Vo: Velocity vs. time

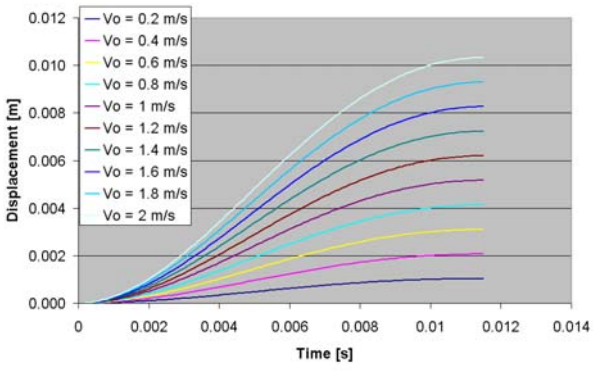

Figure III-15 : Variation of Vo: Displacement vs. time

The rheologic stresses (Figure III-17) are evaluated by the superposition of the static, the viscous and the radiation terms limited by the velocity dependent ultimate rheologic resistance and the radiation term is function of the mobilization ratio.

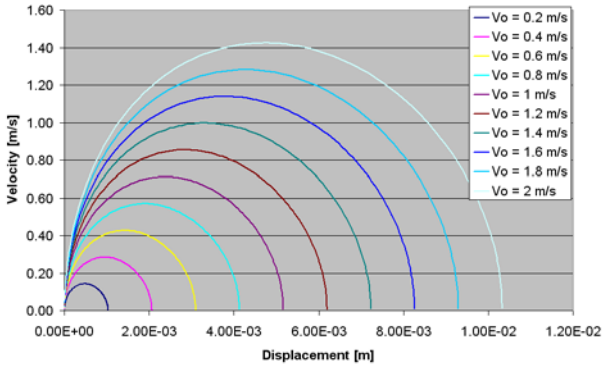

Figure III-16: Variation of Vo: Velocity vs. displ.

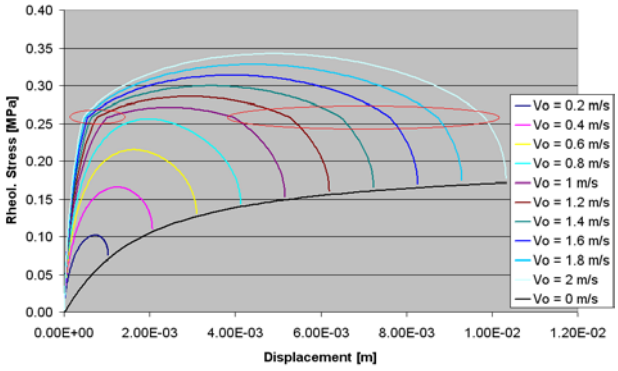

Figure III-17 : Variation of Vo: Stress vs. displ.

The red ellipses on Figure III-17 surround the break points defining the passage from the description of the continuous media to the failure mode (and the slippage conditions). This failure zone is conditioned by Equ. III- 34 also illustrated in the velocity-stress plot (Figure III-18). This last figure highlight the fact that there is a limiting value v_{lim} of the velocity corresponding to the failure or the beginning of the slippage.

$$\tau_{stat,ult}\frac{s}{s+\frac{\tau_{stat,ult}}{G_i}}\left(1+J\cdot v_{\lim}\right)+\left(1-\frac{\tau_{stat}}{\tau_{stat,ult}}\right)\sqrt{G_i\cdot\rho}\cdot v_{\lim}=\tau_{stat,ult}\cdot\left(1+J\cdot v_{\lim}\right) \qquad \textbf{Equ. III- 34}$$

- s is the displacement [m];
- G_i is the initial tangent shear modulus [MPa];
- τ_{stat} is the static stress [MPa].
- ρ is the mass density [kg/m³];
- J is the damping factor [s/m].

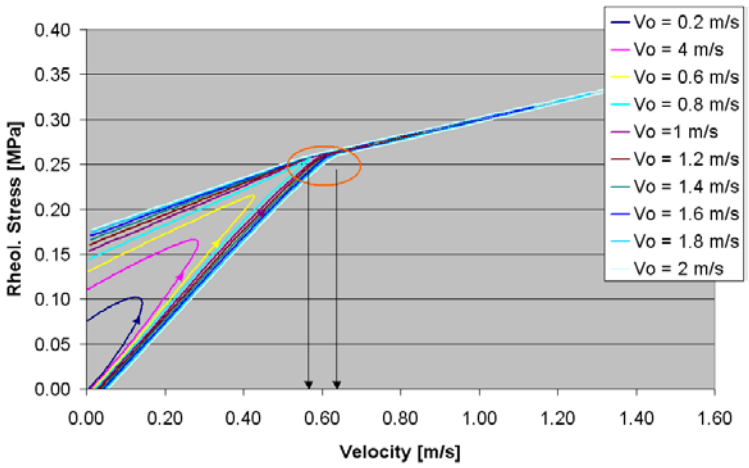

Figure III-18: Variation of Vo: Stress vs. velocity

This range of velocity concerned by the failure passage is very narrow and can be thought as characteristic of the chosen pile/soil model. The difference of behaviour characterizing the state before and during the failure is also well pronounced with the evolution of the curve slopes. The failure zone appears to be linear due to choice of N=1 in the imposed pile/soil model. The influence on the

resulting initial stiffness of the stress-displacement curve is pronounced even for low velocities (compared to the equivalent static curve).

2.4.3.2 Variation of frequency

After the analysis of a variation of velocity magnitude V_0, next observation concerns the frequency ω in order to lengthen the duration of the load application (ω varies from 25 to 300 rad/s). The velocity magnitude is kept constant. The velocity and displacement vs time and stress-displacement relationship figures are given in Figure III-19 to Figure III-21. The generated displacements are displayed in Figure III-20 with a longer duration and a larger reached displacement for simulations performed with a smaller frequency.

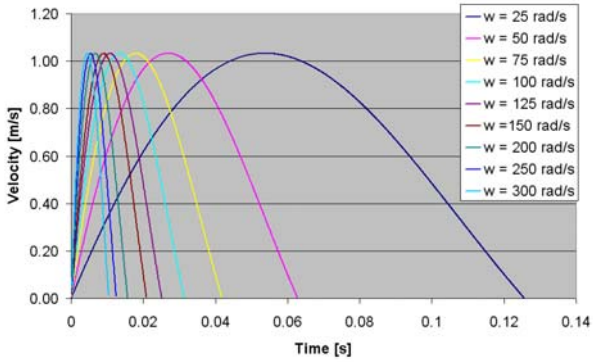

Figure III-19 : Variation of the frequency of the synthetic velocity signal

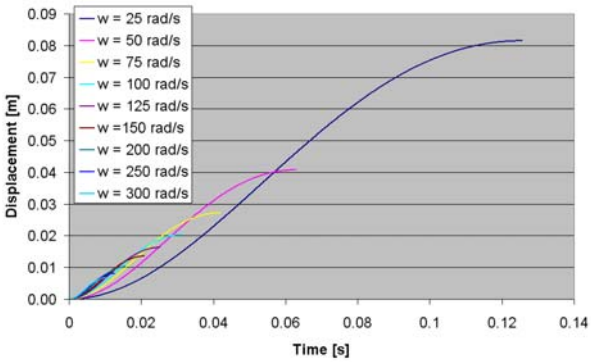

Figure III-20 : Variation of the frequency of the velocity : influence on the generated displacement

Since the maximum velocity is kept constant, the lengthening of the loading means an increase of energy transmitted to the pile and consequently a larger displacement and soil mobilization.

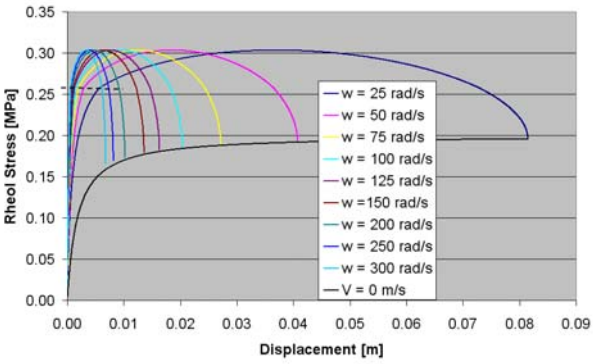

Figure III-21: Variation of the frequency of the velocity : influence on the mobilized rheologic stress

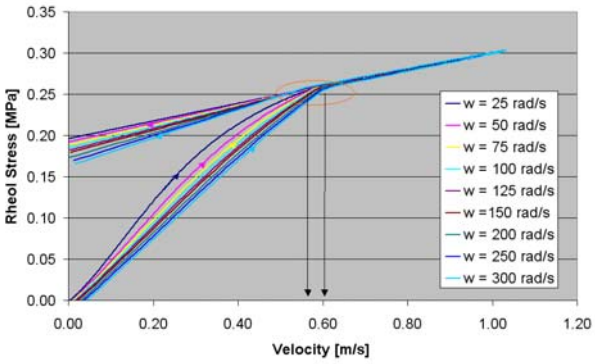

Figure III-22: Variation of the frequency of the velocity: velocity vs. rheologic stress

Equally to the previous case, Figure III-21 and Figure III-22 highlight the variation of initial stiffness, the narrow range of velocity for which the soil slippage condition kicks in (about 0.6 m/s).

3. Dynamic load test measurement: project description and signal analysis

After the description of the pile/soil model including the fundamental relationships, the parameters classification and the particular attention put on the rheologic stress and its developments, the focus is set on the real measurements performed on field. These data are here described. First, the projects from where the measurements were extracted are shortly described with a special attention to the geotechnical data usable in this research. After, a strict analysis of the maximum quantities measured is proposed with relationships existing between measured force, velocity, energy and settlements. Finally the quality of the signal is introduced in order to appreciate the sensitivity of the result only based on the quality of the measurement.

3.1. The Screw Pile projects

3.1.1 Genesis of the project

Within the framework of the setting-up of the Eurocode 7 relating to the Geotechnical Design, the Belgian Building Research Institute (BBRI) has organised in 1998 an ambitious research program with the financial support of the federal Ministry of Economic Affairs aiming to involve all Belgian piling companies installing cast in situ soil displacement screw piles plus representatives of organisations concerned by foundation design. The main topics of this program were to execute an experimental test campaign with cast-in-place screwed piles able to lead a proposal of semi-empirical design methods using installation coefficients. This program is organised equally in two representative types of soil encountered in Belgium: the tertiary overconsolidated Boom clay and a sandy bearing stratum (Bruxellian sand) underlying soft sedimentary layers.

3.1.2 Sint-Katelijne-Waver program

In the Boom clay site at Sint-Kathelijne-Waver (Belgium), 5 existing screw piles systems plus precast driven piles[2] without base enlargement were installed with the purpose to be tested dynamically and statically and by the statnamic method (intermediate loading rate or kinetic loading – Middendorp (1992)). Before the pile installation, an extensive geotechnical survey has been carried out on the site with most of the tools used by laboratories and contractors and required for design: Cone Penetration Tests (CPT) (including different types of cone and process), Standard Penetration Tests (SPT), Pressuremeters Tests (PMT), Dilatometers Tests (DLT), geophysical tests (SASW, seismic cone, seismic refraction) and a boring with undisturbed samples allowing for laboratory tests. Integrity testing of the piles was also carried out. Due to the Belgian practice, the CPT tests represented the largest part of the available information. A huge amount of analysis and most of the results have been compiled in the proceedings of the symposium organised in Belgium in 2001 (Holeyman, 2001).

Schittekat (2001) describes in detail the Boom clay under several aspects (geology, stratigraphy, geomechanic and geotechnical characterization). The Rupelian clay, or Boom clay is a marine deposit

[2] The precast pile is considered as the reference for Belgian design methods

of Middle Oligocene age (35 m.y.). The total thickness of the original clay formation could have been well above 100. Later erosion has removed part of the clay to leave typical thickness of 70 m in Antwerp. The removed overburden in the Antwerp area is estimated to be 90m. Consequently, the Boom clay may be considered as an overconsolidated clay.

Geological observations show the existence of fissures, diapir structures and septaria all related to the stress relief. These features might be at the origin of the scatter of the results of the *in situ* tests. It is admitted that cone resistance values of a CPT should steadily increase with depth in stiff fissured clays and remains in the range of 2.8 MPa to 4.4 MPa.

The testing site is 50x25 m² and was completely covered by all the investigation tests performed. The site layout is described in Figure III-23.

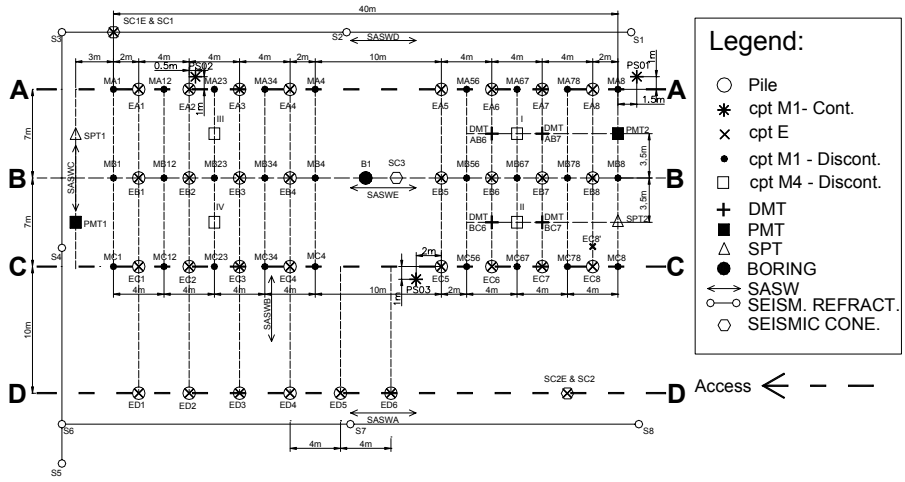

Figure III-23 : Sint-Katelijne-Waver : testing area layout (after Mengé, 2001)

3.1.3 Limelette program

In the second phase of the BBRI research program, a similar test campaign was organized in Limelette (Belgium) where the subsoil consists of 8 m of quaternary silty layers (loam) and tertiary Ledian-Bruxellian sand. The groundwater can not be found in the shallow layer layers investigated. A similar testing program than for the clayey site was followed: 30 pile load tests composed of 12 static load tests, 12 dynamic load tests and 6 statnamic tests. Besides this load testing program, an extensive soil investigation campaign was still organized with CPT, SPT, PMT, DLT, geophysical tests and a boring with undisturbed samples (lab tests) during different phases of the project. Similarly to Sint-Katelijne-Waver, a symposium was organised in 2003 in Brussels (Huybrechts and Maertens, 2003) wherein all the information and the analysis about the pile loading and the geotechnical campaigns are abundantly described.

Between the Asse Clay and the Ypresien clay layers, the layer of Brusselian sand (a serie of Lutetian sand) outcrops in the area of Brussels (Belgium). This sand results from a deposit during the Eocene age in a coastal area of probably a tropical sea. The layer is about 50 meters thick and presents a large panel of different sands with different grain size distribution, grain shape and carbonate content. The

layer is more or less horizontal with a gently slope towards the North. These sediments are covered by quaternary silts formations with a thickness up to 6 m. The Brusselian sand is characterized by numerous facies changes not only at a regional scale but also at a local scale.

The test layout is organised similarly to the Sint-Katelijne-Waver site in order to reduce the risk of variability of soil properties due to distance. The site is divided in two parts: a static test field where the static load tests were performed and a dynamic test field designated for the dynamic load and statnamic tests.

3.1.4 Sites Characterization

3.1.4.1 Sint-Katelijne-Waver

The tests results presented herein are those used in the present research: CPT results - geophysical conclusions (wave propagation velocity V_s and shear modulus G_o) - physical characteristics of the soil.

CPT results

The CPT results presented on Figure III-24 and Figure III-25 show typical CPT profiles from both sites. The traces represent the envelopes of 30 and 18 tests, respectively. The scatter is more pronounced for the silty site than for the clayey one. Both q_c and f_s results (cone resistance and local shaft friction) will use as input set of data for the pile/soil interaction back analysis procedure (see chapter 5). R_f is the ratio of f_s on q_c.

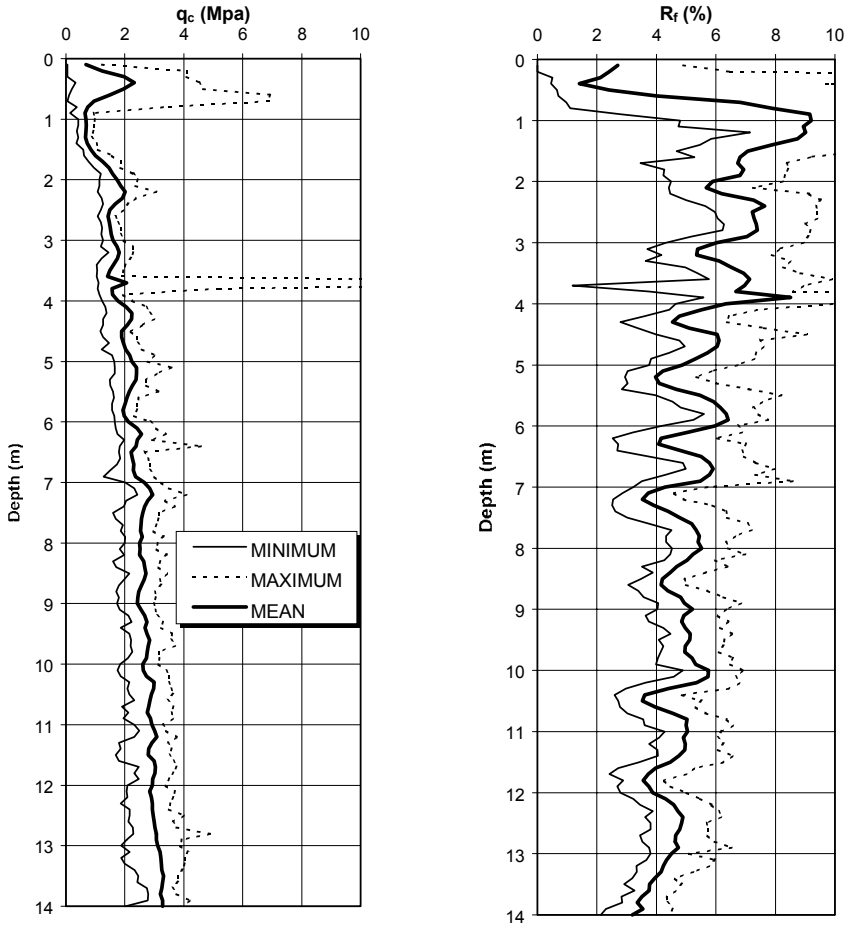

Figure III-24 : Mean, min and max q_c and R_f values from Sint-Katelijne-Waver (after Mengé, 2001)

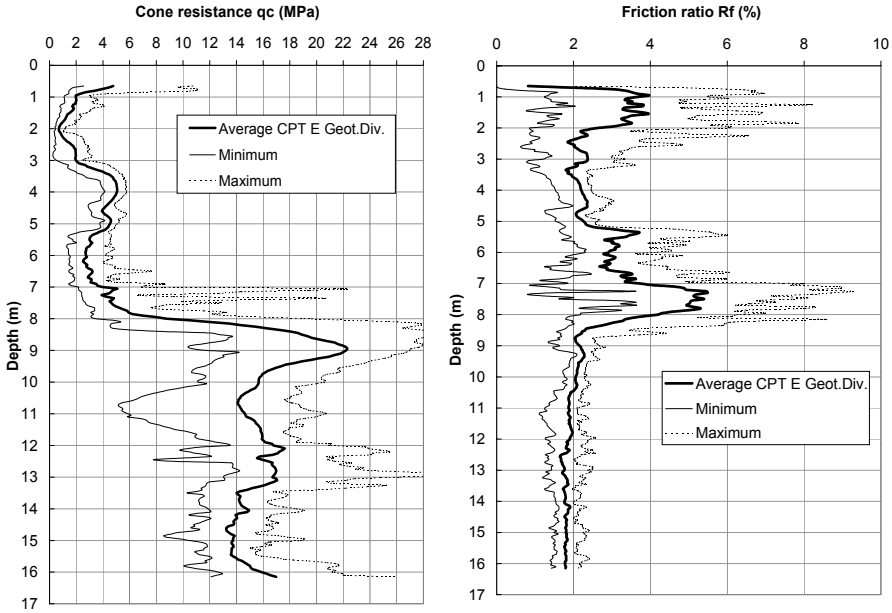

Figure III-25 : Mean, min and max q_c and R_f values from the dynamic test field of Limelette (after Van Alboom & Whenham, 2003)

Geophysical investigation

The values of G_o presented in Figure III-26 and Figure III-27 summarize the results of 3 geophysical *in situ* tests and 1 lab test:

- The seismic cone penetration test;
- The seismic refraction tests;
- The SASW test (Surface Analysis of Surface Waves).
- Laboratory tests, namely triaxial tests (Bender elements).

When studying Figure III-26 and Figure III-27, a large scatter of G_o values is found for both sites. It is known that V_s and consequently G_o are influenced by several factors: the main direction of the particle movement or the anisotropy of the studied soil, the stress level, the soil density and the soil structure.

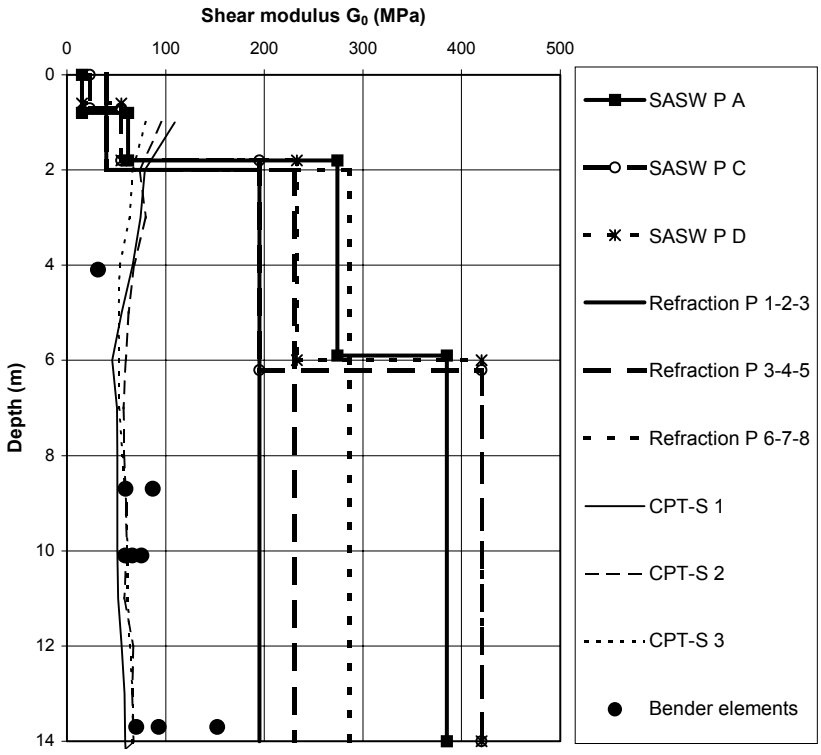

Figure III-26 : Shear modulus G_0 derived from in situ and laboratory seismic tests (Sint-Katelijne-Waver) (after Mengé, 2001)

The particular over-consolidated state of the Boom clay could be involved in the scattering shown in Figure III-26.

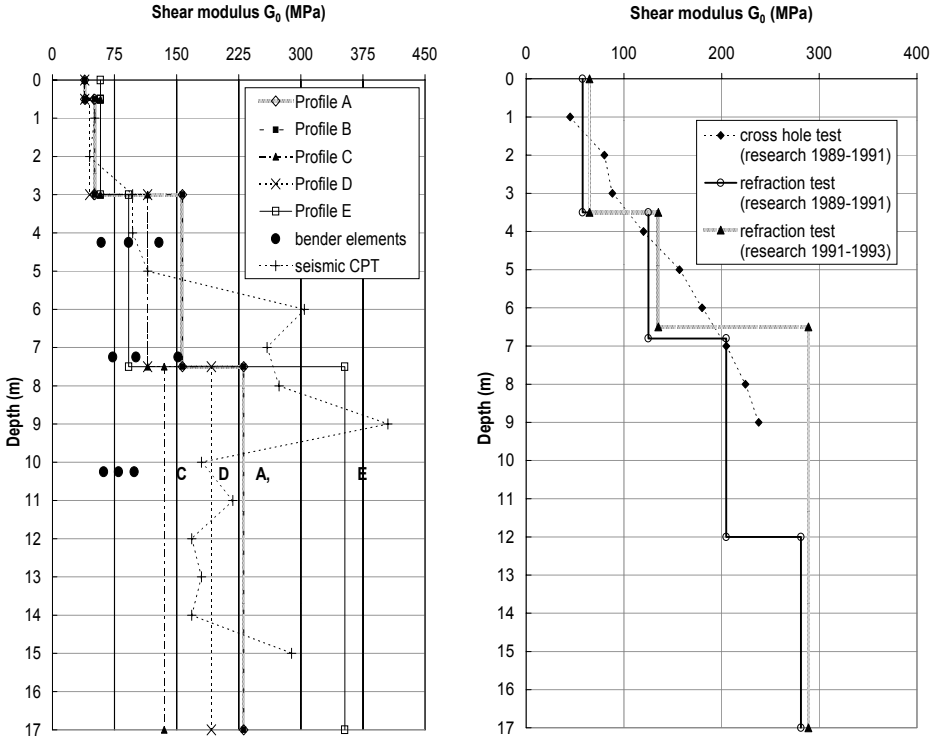

Figure III-27 : Shear modulus G_0 derived from in situ and laboratory seismic tests (Limelette) (after Van Alboom & Whenham, 2003)

In Limelette, seismic refraction tests were performed in 1989-1991 and 1991-1993 at a distance about 50m to 150m from the test site. Also a cross hole test was conducted during the research project of 1989-1991. The concordance between both methods is very good and remains also in accordance with SASW results of the 2002 research (Figure III-27).

The G_o profile is extremely uselful for the interpretation of dynamic load test in the description of the fundamental soil relationships.

Boring and laboratory tests

Table III-1 provides the results obtained for the UU and CU-triaxial tests of Sint-Katelijne-Waver. The watertable at the test site is found at 0.5 m to 1.0 m below ground level.

Characteristic	Sample depth 4.50 m – 4.90 m	8.50 m – 8.90 m	10.50 m – 10.90 m	13.50 m – 13.90 m
γ_d (kN/m³)	15.7	15.3	15.5	15.4
γ_n (kN/m³)	19.7	19.3	19.5	19.4
w (%)	25.3	26.0	25.8	26.1
Sr (%)	(101.8)	99.2	(100.9)	(101.0)
w_L (%)*	72.2	65.1	75.9	71.8
w_P (%)*	25.4	25.3	26.2	26.0
I_P (%)*	46.8	39.9	49.7	45.8
φ' (°)	26	28	26	27
c' (kPa)	20	30	40	15
c_u (kPa)	88	129	158	188

Table III-1 : Physical characteristics and results of triaxial tests of the Boom Clay at Sint-Katelijne-Waver (after Mengé, 2001)

(*) These tests were performed on samples recovered 0.50 m higher.

Table III-2 provides the main results of the physical tests and the results obtained for the CU and CD triaxial tests of the Limelette site. The watertable at the test site is not found.

Characteristic	Sample depth 4.00 m – 4.50 m	7.00 m – 750 m	10.00 m – 10.50 m
γ_d (kN/m³)	16.4	18.4	13.8
γ_n (kN/m³)	18.8	20.8	15.0
w (%)	14.8	12.9	9.0
Sr (%)	67.6	82.3	27.0
w_L (%)*	27.6	30.2	23.4
w_P (%)*	18.7	15.0	20.7
I_P (%)*	8.9	15.2	2.7
φ' (°) CU	34	34	34
φ' (°) CD	35	-	35

Table III-2 : Physical characteristics and results of triaxial tests of the Bruxellian sand at Limelette (after Van Alboom & Whenham, 2003)

3.1.5 Pile Loading Tests

Within the present research, the pile load tests data used from dynamic and static tests only concern the prefabricated pile type considered as reference in the BBRI projects. The reasons of this choice was the wish to limit the size of the treatments to be processed, the need of a certain homogeneity in the data and results and to limit the uncertainty linked to the cast-in-place piles. Moreover, the knowledge of the exact geometry and the mechanical properties of the prefabricated piles is a great help for the interpretation. The following information is required to use, describe and model the pile:

- A geometric and a mechanical description of the installed piles;
- A presentation of the static load results.

The geometric and mechanical description of the concerned piles is available in chapter 4. The 3 static tests involved in this research (comparison with the simulations issued from the dynamic analysis) are displayed in Figure III-28 to Figure III-30.

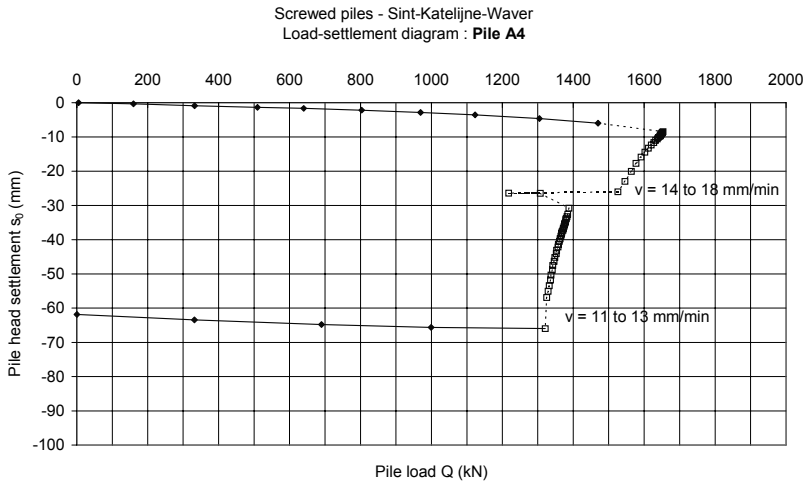

Figure III-28 : Load-settlement plot - Driven prefab pile A4 (SKW) (after Maertens & Huybrechts, 2002)

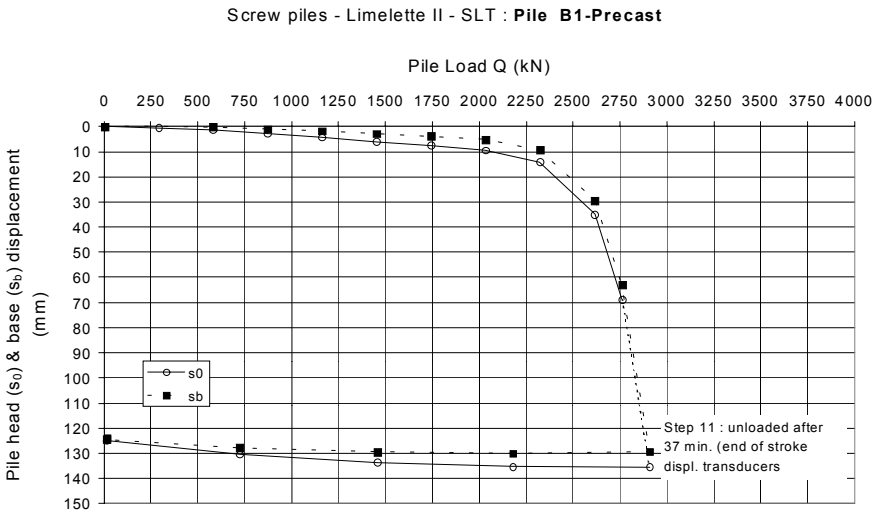

Figure III-29 : Load-settlement plot - Driven prefab pile B1 (Lim.) (after Maertens & Huybrechts, 2003)

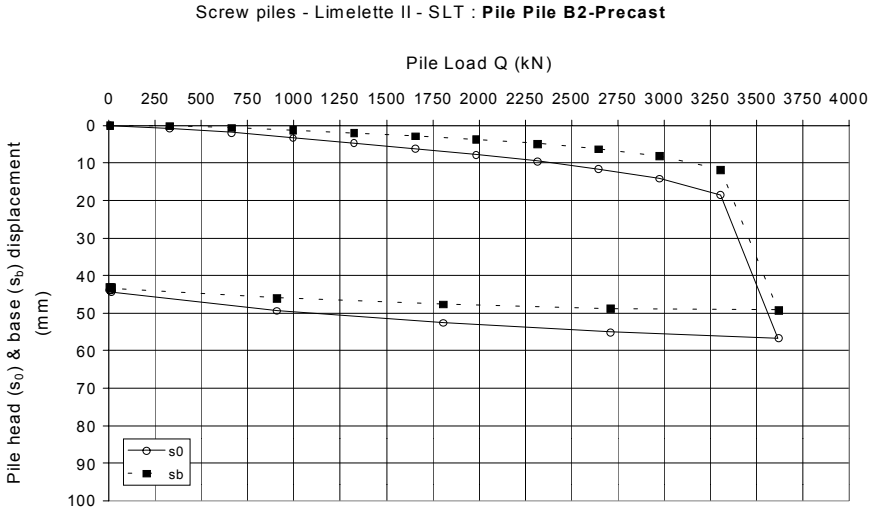

Figure III-30 : Load-settlement plot - Driven prefab pile B2 (Lim.) (after Maertens & Huybrechts, 2003)

◆ = pile head settlement at the end of a constant loading, unloading or reloading step;

❍= pile head settlement during failure of the pile under a constant pile head penetration rate;

□= pile head settlement during failure of the pile under a non-constant pile head penetration rate.

A dashed type of line has been used to connect the last completed (after 60 minutes) load step (indicated with the symbol ◆) with the next non completed load step during which failure occurs (indicated with symbols ❍ or □), as well as for the connections between the points illustrating the failure of the pile.

3.2. Pile presentation

This section is focused on the study of data directly measured on field during dynamic loading tests (DLT). This presentation summarizes the main characteristics of these signals. So as to be precise in this description, it concerns only one kind of pile: the long prefabricated concrete pile driven into the soil a few month before testing. The advantages to only present the results of this pile are numerous:

- The pile geometry is known and equal for all piles: length, diameter all along the pile;
- Except for a failure during driving, the mechanical quality of the pile is assessed over the all length (no weak zone in the concrete strength profile);
- The concrete in all piles of a same site has similar properties and the same age;
- The pile driving provides dynamic data to be compared with the specific testing;

Consequently, the study of these piles reduces the number of potential unknowns and allows a fine comparison between piles which is more difficult with cast-in-place screwed piles.

The same model of pile has been driven in Sint-Katelijne-Waver (called "SKW") and Limelette (called "Lim"). No pile head has been installed on pile during driving and for dynamic pile testing. The piles are 13 m (SKW) and 11 m (Lim) long, with a square section of 35x35 cm² .

The length dimensions are summarized in Table III-3:

	Static Load Test		Dynamic Load Test		Statnamic Load Test	
	SKW	Limelette	SKW	Limelette	SKW	Limelette
Buried length [m]		Variable-D	Variable-D 10.88	Variable-D 8.7 – 8.71	Variable-D 10.8	Variable-D 8.73
Distance transducer -base		9.8	12.2	9.8 – 9.8	12.2	9.8
Radius [m] shaft-base		0.446 0.395	0.446 0.395	0.446 0.395	0.446 0.395	0.446 0.395

Table III-3 : Summary of the dimensions of the prefabricated piles

- The buried length corresponds to the depth of base minus the excavation depth;
- "Variable-D" corresponds to the variable buried depth reached during driving.

There are two long piles tested dynamically in Limelette and one in Sint-Katelijne-Waver.

The dynamic data available for the study are for Sint-Katelijne-Waver:

- 7 drops in 1999 and 13 one year later.

And for Limelette:

- 16 drops for the pile B8 and 20 for the pile B9.

3.3. Relationships between maximum quantities

3.3.1 Heights of drop and dynamic settlements

The dynamic loading tests can be summarized by the schedule of drop heights. This height is related to the transmitted energy, the maximum velocity and also the settlements observed during the tests. The heights of drop during a testing procedure are generally increasing with an alternating succession of smaller drop heights. Table III-4 summarizes the dropping schedule for both sites and concerned piles.

	A7 – SKW (99)	**A7 – SKW (00)**	**B8 - Limelette**	**B9 - Limelette**
Blow No	**Drop Height [m]**	**Drop Ht. [m]**	**Drop Ht. [m]**	**Drop Ht. [m]**
1	0.4	0.2	0.4	0.4
2	0.8	0.4	0.6	0.6
3	1.2	0.6	0.8	0.6
4	0.8	0.6	0.8	0.8
5	1.2	0.6	1.0	1.0
6	1.6	0.8	0.6	0.6
7	0.8	1	1.2	1.2
8		0.7	0.8	1.2
9		1.2	1.4	1.2
10		0.7	0.6	0.8
11		1.3	1.6	1.4
12		0.6	1.0	0.6
13		1.4	1.8	1.6
14			1.8	1.0
15			2.0	1.8
16			2.0	1.8
17				2.0
18				2.2
19				2.6
20				2.6
Min	***0.4***	***0.2***	***0.4***	***0.4***
Max	***1.6***	***1.4***	***2.0***	***2.6***

Table III-4 : Summary of the drop heights (dynamic loading test results)

The height ranges are 1.4 m wide in clay up to 2.2 m in sand. This is due to the estimated bearing capacity and the concrete strength not to be exceeded in order to keep safe the pile integrity.

This section proposes a short analysis of the maximum and permanent displacements generated by the blows on the piles. Table III-5 and Table III-6 give the settlements evaluated from the signals, Figure III-31 and Figure III-33 illustrate the curves giving these values and Figure III-32, Figure III-34 and Figure III-35 summarize the results as pile displacements versus drop heights.

Beforehand, it is important to explain that the settlements occurring during the dynamic loading test are not measured but evaluated from the measured acceleration signals. Consequently, a correction is sometimes (often) performed in order to correct for the hypothetic errors of derivation due to the integration constants. It appears that the maximum displacement “measured” does not vary with these corrections, contrarily to the permanent displacement. This is due to the double integration process and the fact that the final settlement is evaluated at the end of the recorded signal (~ 0.2 s) more influenced

by the corrections made. A fair confidence is given to the maximum settlement listed, and a slight variation is possible around the permanent settlement. However the trends remain valid.

	A7 – SKW (I)	A7 – SKW (I)	A7 – SKW (II)	A7 – SKW (II)
Blow No	**Max Setl. [m]**	**Perm Setl. [m]**	**Max Setl. [m]**	**Perm Setl. [m]**
1	3.6	0.3	2.1	0.1
2	6.2	1.2	3.9	0.2
3	8.6	2.7	5.2	0.3
4	6.6	1.2	5.2	0
5	9	3.1	5.3	0.6
6	10.9	3.9	6.7	1.2
7	6.8	1	7.9	1.6
8			6.5	1
9			9.6	3.2
10			6.5	1.2
11			10.5	3.6
12			5.8	0.2
13			10.9	3.5
Min	***3.6***	***0.3***	***2.1***	***0***
Max	***10.9***	***3.9***	***10.9***	***3.6***

Table III-5 : Maximum and permanent settlements during DLT for SKW site

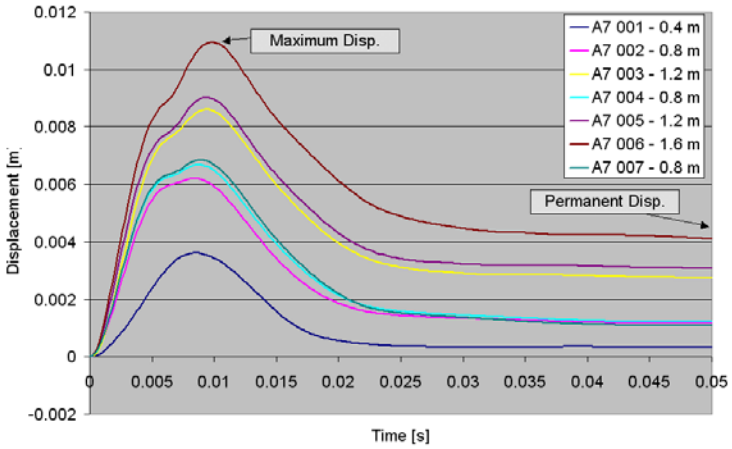

Figure III-31 : Plot of the displacement curves for A7 (99) of SKW

The curves of Figure III-31 present the displacements of the 1st set of tests performed in 1999. The influence of the drop height is evident, for both amplitudes and curve shapes. Moreover, the curves corresponding to similar drop heights provide similar responses. The curves are quickly dampened, with no subsequent oscillations after the first loading and unloading. This is due to the clay damping behaviour.

Figure III-32 represents the evolution of the maximum and permanent settlements (Table III-5) vs. drop height (Table III-4). This kind of figure is useful in the driving analysis. It allows the evaluation of the rebound of the pile (difference between permanent and maximal settlements) and the height required to obtain a given pile settlement.

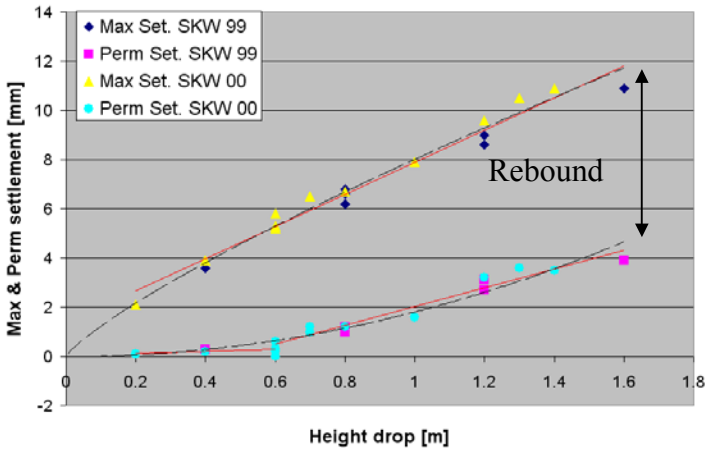

Figure III-32 : Heights of drop vs. maximum & permanent settlements (pile A7 - SKW)

The maximum settlement curves are characterized by a downward slope from the origin up to a given drop height and a constant slope for any superior drop heights. The permanent settlement curves are characterized by a null slope from the origin followed by an upward slope until both curves (max and perm settlement curves) becomes almost parallel (dashed lines on Figure III-32). This point, from where the maximum and permanent settlement curves evolve in parallel, is called the critical height h_c (Holeyman, 1984). Consequently, all tests carried out with a height drop inferior to approximately 0.6 m have no chance to generate permanent settlements, namely, no chance to exceed the "equivalent quake" of the pile in Boom clay.

The SKW results are also interesting because they authorize the comparison of two sets of tests performed on the same pile with a temporal gap of one year. The displacements remain in the same range for both maximal and permanent categories. There is no distinction between pile/soil system responses from both years.

The same data have been generated for the piles B8 and B9 in the Bruxellian sand of Limelette. The maximum values of both series are slightly different because the drop height schedule is different (until 2.6 m for pile B9 where it is only 2.0 m for pile B8).

	B8 - Limelette	B8 - Limelette	B9 - Limelette	B9 – Limelette
Blow No	**Max Setl. [m]**	**Perm Setl. [m]**	**Max Setl. [m]**	**Perm Setl. [m]**
1	3.3	0.4	3.5	0.2
2	5.4	0.5	5.3	0.2
3	6.2	0.4	5.4	0
4	6.5	0.4	6.3	0.4
5	7.1	0.1	7.3	0.7
6	5.9	0.3	5.4	0.2
7	7.7	0.4	8	0.7
8	6.8	0.4	8.3	0.3
9	8.7	0.1	8.5	0.5
10	6.1	0.5	6.8	0
11	9.4	0.9	11	0.7
12	7.9	0.7	6	0
13	9.5	0.8	10.1	1.9
14	11	2.5	8	1

15	11.9	3.9	11.3	3.5
16	11.8	4.4	9.6	2.6
17			9.8	2.2
18			12.5	5.2
19			14.8	6.6
20			14.9	7.1
Min	***3.3***	***0.1***	***3.5***	***0.2***
Max	***11.9***	***4.4***	***14.9***	***7.1***

Table III-6 : Maximum and permanent settlements during DLT for Limelette site

Figure III-33 shows the curves of displacement based on the measured signals of acceleration for the pile B8. The attenuation is less pronounced than for the tests in clays (more than 1 oscillation before stabilization of the signals). On the other hand, the permanent settlement does not increase with the drop height as faster as for the tests in clay. Figure III-34 confirms that the trends observed for the tests in clays are confirmed: evolution of the slopes and a constant settlement gap (the rebound) between both curves from a certain drop height called the critical height. But the height of drop required to have a significant permanent settlement increases to 1.3 – 1.5 m. Consequently, a major part of the tests performed in Limelette do not present significant permanent settlements.

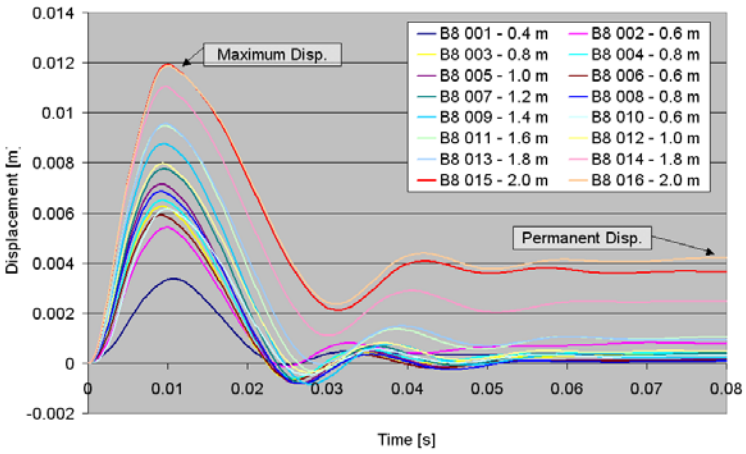

Figure III-33 : Plot of the displacement curves for the pile B8 of Limelette

Figure III-35 compares both results (drop height vs. max & perm settl.) from tests in clay and sand.

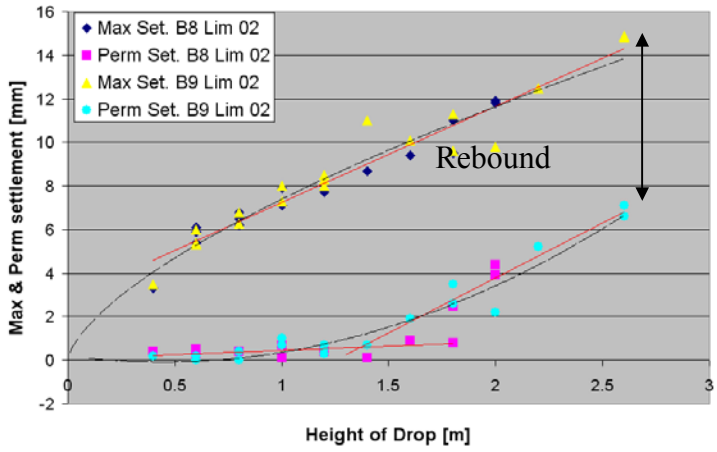

Figure III-34 : Heights of drop vs. maximum & permanent settlements (Piles B8-B9 - Lim)

The maximum settlement trends seems to be complementary since the Limelette's points look like following the SKW's points. On the other hand, the permanent settlements trends show typical behaviours for both types of soil. The critical height is higher for sand and their slope seems to be stiffer as well. This is characteristic of the soil type: the more resistant the soil, the higher the drop to cause a significant driving.

The height of drop is linked to the energy transmitted or the work done by the pile with regards to the efficiency rate of the hammer, ram or any machine providing the dynamic force on the pile head. However this efficiency is not known and can be variable, influencing the above analysis.

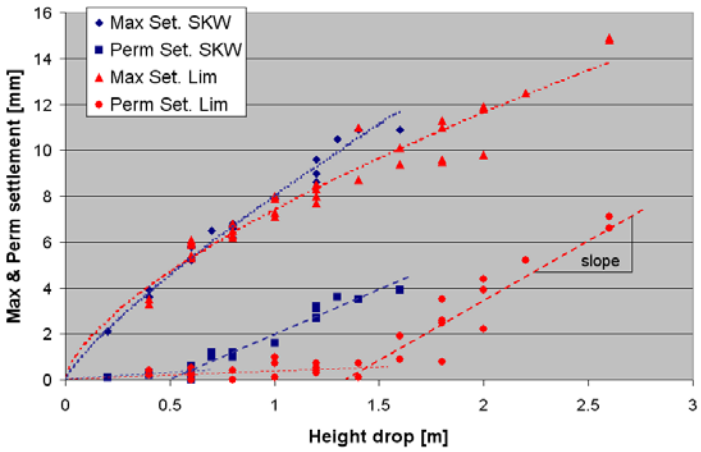

Figure III-35 : Heights of drop vs. maximum & permanent settlements (Sites SKW - Lim)

The following section approaches a more rational point of view. Instead of drop height in the previous figures, the maximum velocity of the pile head, the maximum force or energy transmitted to the pile are used vs. settlements.

Gossuin (2001) analysed the response of the pile/soil system to driving by using the program GRLWEAP© and simulating the equivalent of Figure III-32 for a variation of shaft and base resistances. He particularly studied the influence of these changes in the required height to produce a significant permanent settlement, on the rebound and on the slope of the permanent settlement trace. He concludes that the critical drop height needed to produce a permanent settlement is highly dependent of the ratio of shaft resistance in the total capacity: the higher the ratio and the lower the critical height. What is recovered in Figure III-35 where the critical height is inferior in the clayey site compared with the sandy site. He also concludes that the slope of the permanent settlement must decrease if both the total resistance and the ratio Q_{frot}/Q_{total} increase. This last conclusion is in opposition with the observations made herein since the total capacity in the sandy soil is superior to the corresponding one in clayed soil and the ratio Q_{frot}/Q_{total} is also inferior for sandy soil but the slope appears to be higher. However, it can be concluded that the observations made for the specific driving analysis can be used for the analysis of dynamic load test data.

3.3.2 Maximum velocities and dynamic settlements

Table III-7 provides the maximum velocities of the pile head for all tests investigated.

	A7 – SKW (99)	A7 – SKW (00)	B8 - Limelette	B9 - Limelette
Blow No	**Max Velocity [m/s]**	**Max Vel. [m/s]**	**Max Vel. [m/s]**	**Max Vel. [m/s]**
1	0.66	0.42	0.54	0.57
2	1.46	0.83	0.97	1
3	1.87	1.14	1.15	1.05
4	1.58	1.16	1.19	1.22
5	1.97	1.1	1.31	1.42
6	2.23	1.39	1.09	1.02
7	1.61	1.7	1.39	1.53
8		1.51	1.26	1.56

9		2.05	1.58	1.61
10		1.5	1.11	1.28
11		2.27	1.65	1.67
12		1.37	1.46	1.14
13		2.28	1.74	1.84
14			1.9	1.49
15			2	1.96
16			1.98	1.71
17				1.72
18				2.06
19				2.24
20				2.27
Min	***0.66***	***0.42***	***0.54***	***1.14***
Max	***2.23***	***2.28***	***1.98***	***2.27***

Table III-7 : Maximum velocities during DLT for both sites

Based on the results of Table III-4 and Table III-7, for a given drop height, the maximum velocity is superior in clay. However, even if the type of soil is of importance, the efficiency of the dropping system (manual dropping by the crane operator) is certainly also involved.

Figure III-36 shows the comparison of the maximum velocities vs. drop heights for both sites. Figure III-37 shows the curves of the velocities evaluated from the measured signals of acceleration of the pile A7 of Sint-Katelijne-Waver during the 1st set of tests (1999). The traces confirm the increase of the peak velocity with the drop height, the relative repeatability for same drop heights (even if the posterior tests performed at the same height of drop present a slight higher peak velocity) and the quick attenuation of the signal (over a period of 0.04 s).

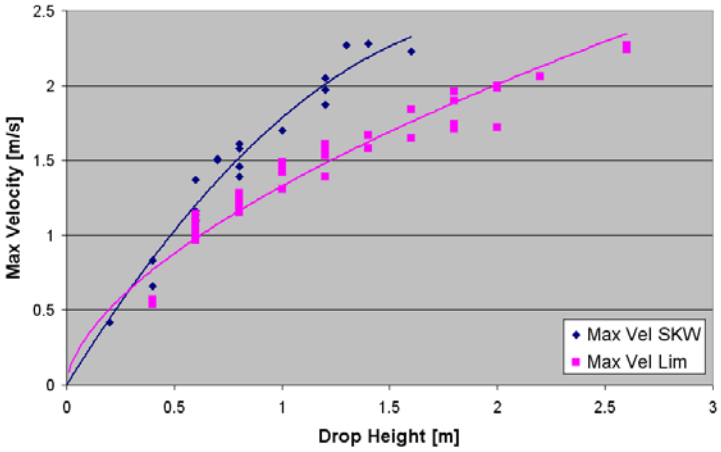

Figure III-36 : Height of Drop vs. maximum velocity (Sites SKW - Lim)

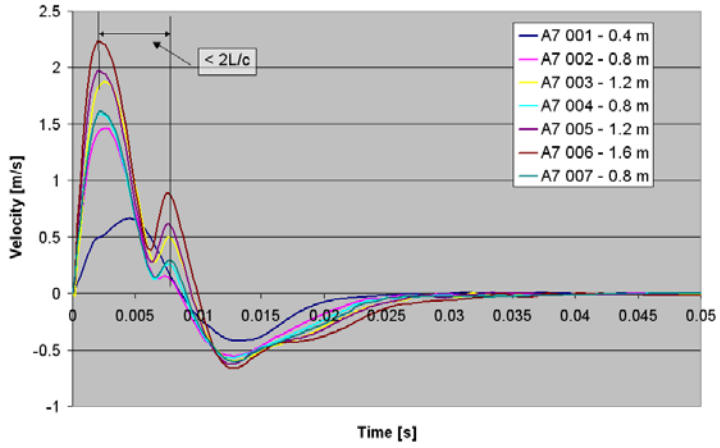

Figure III-37 : Plot of the velocity curves for A7 (99) of SKW

The curves show a second peak most probably connected to the return of the wave after reflection on the base. Figure III-38 exhibits the maximum and the permanent settlements vs. the maximum velocity of the pile head during the test for the clayed site of Sint-Katerijne Waver. The maximum velocities present a trend very well fitted with a straight line almost crossing the origin but this behaviour can also be fitted with a set of two consecutive straight lines (the first, from the origin, and the second, stiffer, when the permanent settlements start to be generated).

Moreover, the permanent settlement indicates clearly two pronounced behaviours marked by the velocity 1.2 – 1.3 m/s (critical velocity?).

As for Figure III-37, Figure III-39 presents the traces of velocity measured on the pile B8 in sand. The signals corresponding to a same drop height evolves with the chedule of drop height: the traces are amplified maybe denoting a certain degradation of the soil response (a smaller resistance along the pile shaft and a highr velocity) due to the loading history.

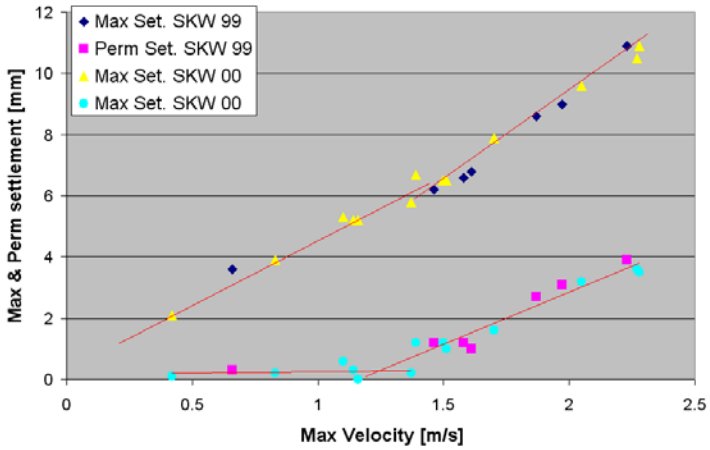

Figure III-38 : Maximum velocity vs. maximum & permanent settlements (Pile A7 (99 & 00) - SKW)

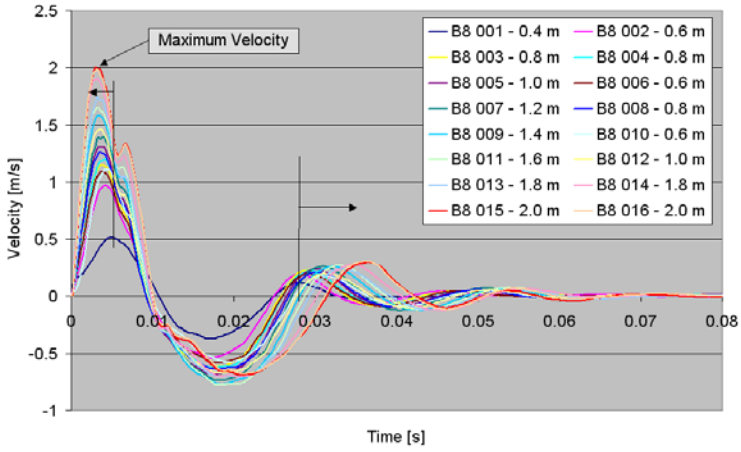

Figure III-39 : Plot of the velocity curves for the pile B8 of Limelette

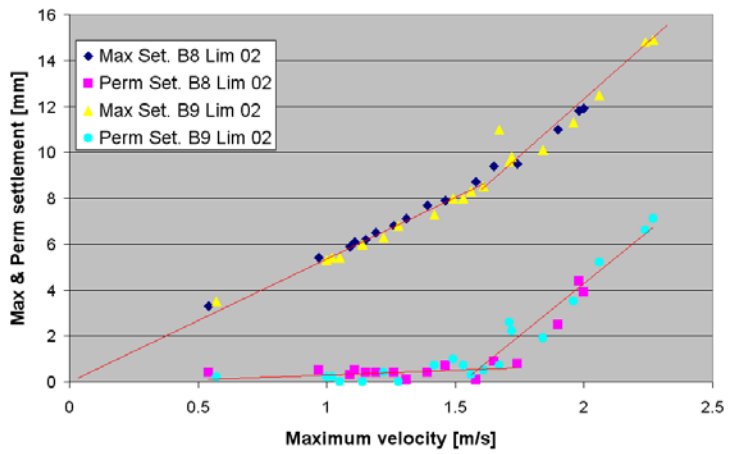

Figure III-40 : Maximum velocity vs. maximum & permanent settlements (Piles B8-B9 - Lim)

The signals attenuate slowly compared to the clayed site: the signals seem to be stabilized for only t = 0.08 s. Globally, the frequency of the damped sinus evolves (decreases) when the drop height and the peak velocity increases. The first peak of velocity arrives more rapidly if the velocity is high and the second velocity peak "recedes". Figure III-40 is the mirror of Figure III-38 for the tests performed in sand. The trend of the maximum settlement is also almost linear with velocity but an increase of slope in the range of high velocities indicates a modification of behaviour when significant permanent settlements start to be generated. The permanent settlement traces show two distinct behaviours marked for a maximum velocity of ~ 1.6 m/s. There is no difference between the results of piles B8 and B9. The trend is similar.

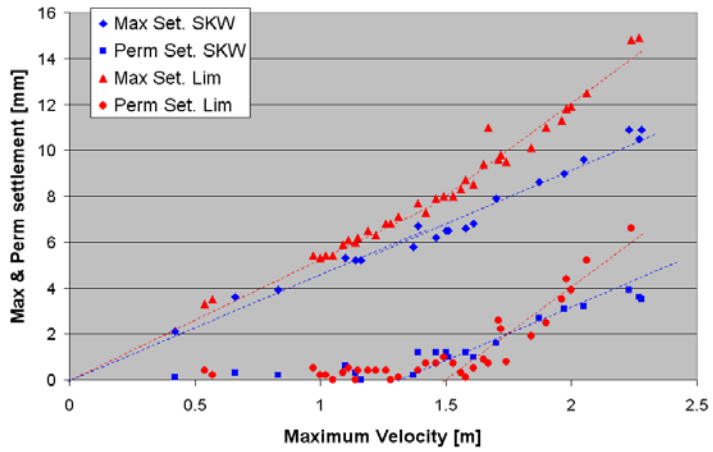

Figure III-41 : Maximum velocity vs. maximum & permanent settlements (Sites SKW - Lim)

Figure III-41 gathers Figure III-38 and Figure III-40. Both classes of settlement (perm and max) present a linear relationship of the max velocities in both soil types. It is also shown that the ratio of settlement by unit of velocity is higher for sand than for clay.

Finally, a link can be done between the drop height (linked to the potential energy) and the maximum velocity measured (linked to the kinetic energy). The velocity of the pile head can be expressed, theoretically and for an infinite pile, to the ratio of ram and pile impedances and to the impact velocity (Holeyman, 1984). This impact velocity is itself linked to the drop height by the kinetic energy and the efficiency of the impact system. If this efficiency is noted η_i, the drop height is linked to the maximum velocity by:

$$\sqrt{2g \cdot h} \cdot \eta_i = v_i = f(v) \qquad \textbf{Equ. III- 35}$$

Where v_i is the impact velocity.

The plot of $\sqrt{2g \cdot h}$ vs. the measured maximum velocity gives:

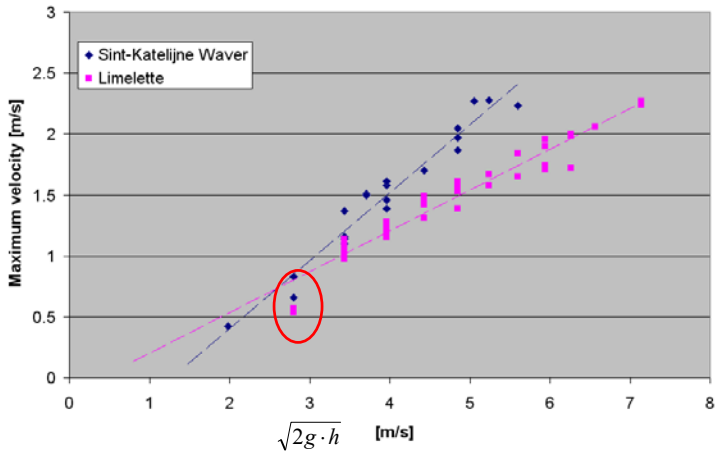

Figure III-42 : Relationship between the maximum velocity measured and the drop height

The trend is linear for both sites but the regression straight line does not cross the X axis at the origin for the clayed site. This may be due to the fact that in clay, when the velocity reaches its maximum, the effects of the first layers of clay could have already influenced the velocity by reducing it (upwards waves and reduction of the measured velocity). The sand shows a similar trend for the first two points (corresponding to the first blows on both piles B8-B9) where the velocity is inferior to the expected result given by the regression line. At this moment, the first layers still influence the total resistance, but after, this effect vanished and is degraded and the maximum velocity remains not influenced by the friction upward waves of the first layers of soil.

3.3.3 Force and energy

Contrarily to the settlement (maximum and permanent) and the maximum velocity used previously that are both based on the acceleration signal, the force is coming from the second signal measured on site: the strain. This signal is less reliable than acceleration because of its sensitivity to the eccentricity of the impact on the pile head and also due to the higher variability of the parameters required to transform the strain into force compared to the integration procedure of the acceleration. All these developments will be presented with more details on the section focused on the quality of the signal, but it is important to introduce this point here because of the bad quality of 8 of 13 signals of the second phase of tests of the pile A7 of Sint-Katelijne-Waver. The signals of the drops #6 → #13 are consequently not presented in the force and energy analysis. The details of this malfunction are presented in the quality section. This section is focused on the force and energy (or Enthru) signal s analysis.

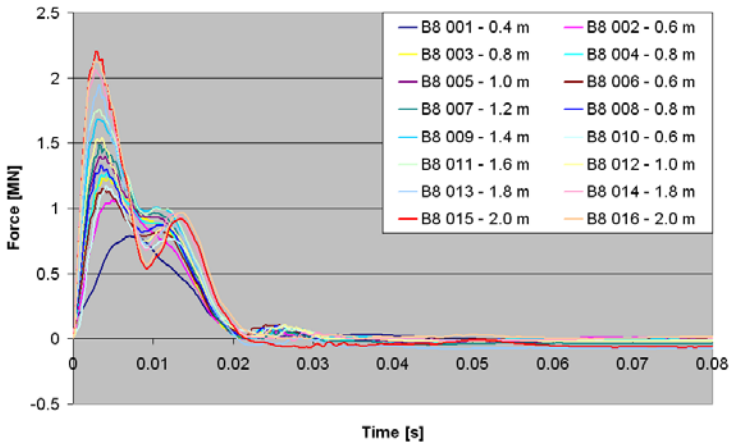

Figure III-43 : Plot of the force curves for the pile B8 of Limelette

Figure III-43 presents the traces of the force measured at the pile head for the pile B8 of the site of Limelette. The figures of the site of SKW are comparable but higher in magnitude and shorter in duration (width of the force pulse). Table III-8 summarizes the maximum values for both sites. Both maximum and minimum specific values are superior for the clayed site. This is due to the stronger load rate effects in clay compared to the sand response. The force traces are (almost) always positive or null. That confirms that the pile does not undergo traction during the test. The small negative values are the result of to the averaging of the measurements from the two transducers (and including the eccentricity effects).

	A7 – SKW (99)	A7 – SKW (00)	B8 - Limelette	B9 – Limelette
Blow No	**Max Force [MN]**	**Max Force [MN]**	**Max Force [MN]**	**Max Force [MN]**
1	1.576	1.039	0.787	0.833
2	2.264	1.571	1.061	1.138
3	2.751	1.933	1.237	1.154
4	2.344	1.863	1.274	1.358
5	2.794	1.897	1.400	1.537
6	3.112	Not Valid	1.157	1.116
7	2.358	Not Valid	1.492	1.670
8		Not Valid	1.329	1.725
9		Not Valid	1.687	1.787
10		Not Valid	1.173	1.415
11		Not Valid	1.762	1.823
12		Not Valid	1.541	1.248
13		Not Valid	1.950	2.025
14			2.062	1.632
15			2.207	2.164
16			2.132	1.874
17				1.883
18				2.236
19				2.450
20				2.659
Min	***1.576***	***1.039***	***0.787***	***0.833***
Max	***3.112***	***1.933***	***2.207***	***2.659***

Table III-8 : Maximum forces measured during DLT for both sites

Figure III-44 presents the comparison of the maximum measured force vs. the maximum and permanent settlements. Similar observations than for the velocity analysis can be made: the driving behaviour is conditioned in two “linear” phases. The first phase is characterized by an absence of final settlement until reaching a certain level of force. This value is fixed to 1900 to 2000 KN for clay and 1700 to 1800 KN for sand.

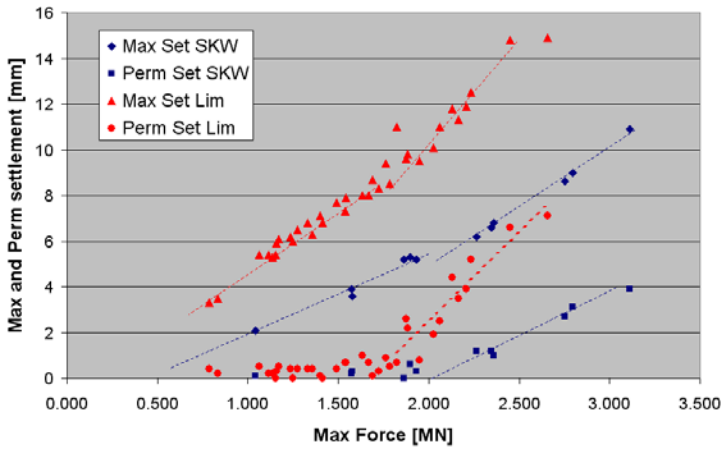

Figure III-44 : Maximum force vs. maximum & permanent settlements (Sites SKW - Lim)

The behaviour of the maximum settlement regarding to the force seems to be also influenced by this particular value, changing the slope of the regression straight line. Once the permanent settlement reaches not-null values, the evolution of both settlements (perm and max) is nearly parallel but stiffer for sand than for clay.

When the maximum force is compared to the maximum measured velocity, the trend observed must reflect the nominal impedance of the pile (wave equation section in chapter 1).

Figure III-45 shows the plot of these points for both sites and parallel trends are highlighted by the linear regression (in black). The dashed red line corresponds to the slope of the nominal impedance and is nearly perfectly parallel to the lines based on measurements. However, the data of the clayey site exhibit a linear relationship that does not reach the origin. The explanation can be the same that for Figure III-42: the velocity signal is reduced by the upward waves, and on the other hand, the force is also modified in the opposite way (increase of force due to the upwards waves), both effects brings out a permanent gap.

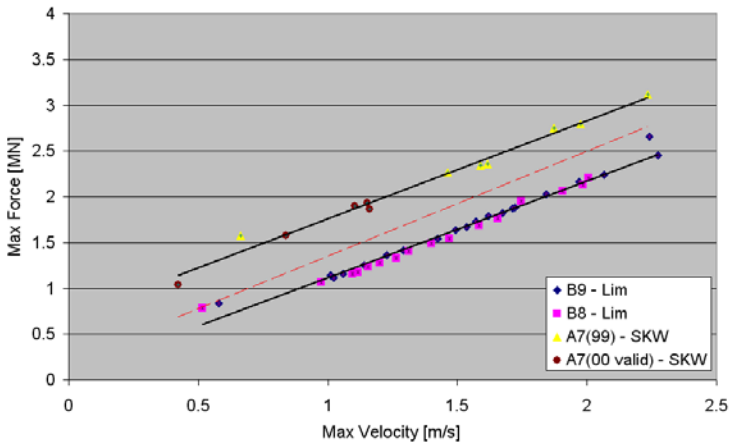

Figure III-45 : Max force vs. max velocity (SKW - Lim)

The energy transmitted to the pile is called “Enthru”. It is defined as the integration of the product of both force and velocity signals until the end of impact (t_f)

$$Enthru = \int_0^{t_f} F(t) \cdot v(t) \cdot dt$$ **Equ. III- 36**

Figure III-46 shows the traces of Enthru for the pile B8 of Limelette. As expected, the transferred energy increases with the height of drop.

The value taken into account is the maximum peak value corresponding to the integration of the positive pulse of velocity without considering the negative part of the velocity. Table III-9 summarizes the results of the maximum enthru calculated for both sites.

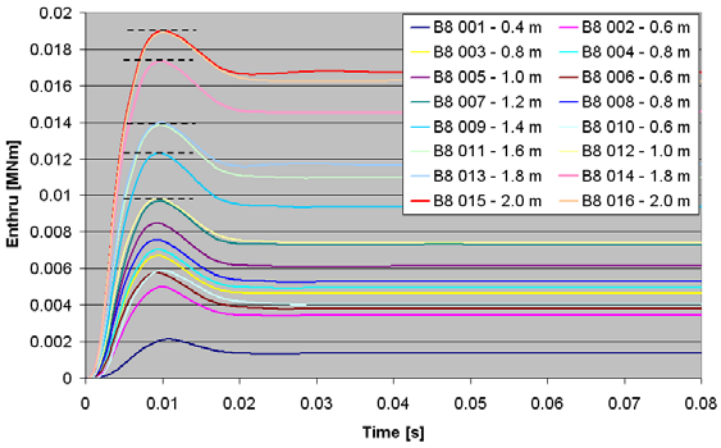

Figure III-46 : Plot of the energy transferred curves for the pile B8 of Limelette

	A7 – SKW (99)	A7 – SKW (00)	B8 – Limelette	B9 - Limelette
Blow No	**Enthru [MNm]**	**Enthru [MNm]**	**Enthru [MNm]**	**Enthru [MNm]**
1	0.004387	0.001634	0.002122	0.002336
2	0.012107	0.004907	0.004995	0.005185
3	0.019608	0.008370	0.006698	0.005286
4	0.013299	0.008270	0.007035	0.00721
5	0.020539	0.008147	0.008492	0.009536
6	0.026425	Not valid	0.00575	0.00502
7	0.013638	Not valid	0.009692	0.011064
8		Not valid	0.007566	0.011844
9		Not valid	0.012320	0.012296
10		Not valid	0.005879	0.007937
11		Not valid	0.013855	0.013307
12		Not valid	0.009827	0.006207
13		Not valid	0.013991	0.016149
14			0.017376	0.010663
15			0.019025	0.018445
16			0.018919	0.014176
17				0.014405
18				0.02072
19				0.027035
20				0.028390
Min	***0.004387***	***0.001634***	***0.002122***	***0.002336***
Max	***0.026425***	***0.00837***	***0.019025***	***0.02839***

Table III-9 : Maximum enthru during DLT for both sites

Figure III-47 presents the comparison of the Enthru and the permanent and maximum settlements. The same observations than previously are still valid. The trend curves are not linear but are similar to the drop height analysis (section 3.3.1). The instant slope of the maximum curve decreases from origin to almost stabilize. The energy values of slippage starting are 0.008 to 0.01 MNm for clay and 0.012 MNm for sand.

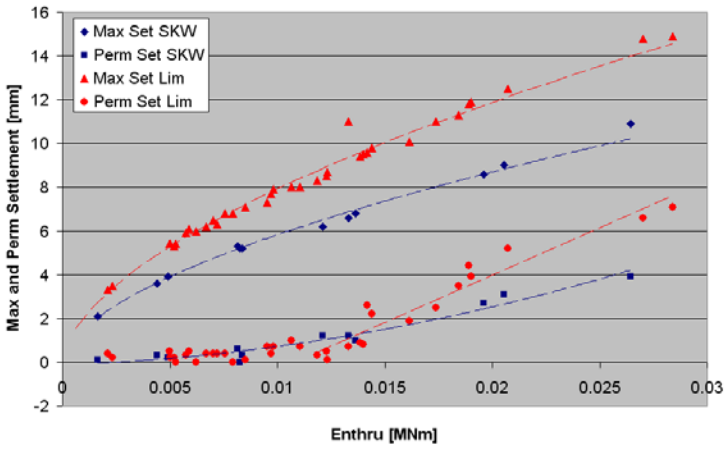

Figure III-47 : Maximum enthru vs. maximum & permanent settlements (Sites SKW - Lim)

The comparison of the Enthru with the potential energy (Figure III-48) illustrates the efficiency of the testing system. The data are arranged linearly for both sites. The dashed lines correspond to the data regression of each sites. The efficiency is the ratio of the Enthru by the potential energy (slope of the dashed lines). The efficiency in Sint-Katelijne-Waver is 48 % and the ratio in Limelette is equal to 27 %.

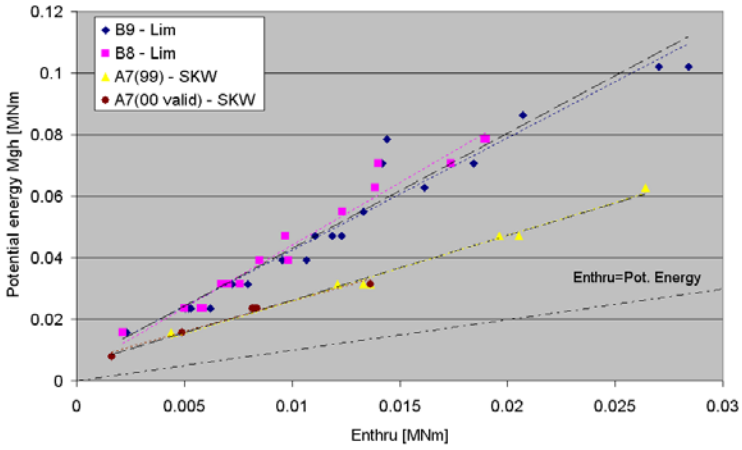

Figure III-48 : Maximum enthru vs. theoretical potential energy (Sites SWK - Lim)

3.4. Visualisation of the dynamic motion signal along the pile

The dynamic testing of pile is characterised by the wave propagation effect into the pile. It can give a tomography of the pile in depth if the reception of the wave in time at the pile head is analysed with this purpose (see chapter 1, section 3.2.3.3.). This phenomenon is rendered by the spring mass system supposed to model the axial pile behaviour under axial solicitation. Considering this model and considering a real signal injected at the head (for example the velocity signal). The visualization of the motion of all pile elements vs. time may represent the wave propagation.

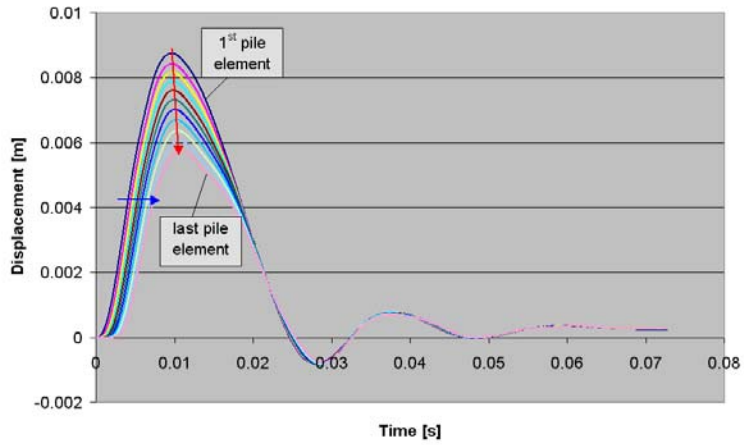

Figure III-49 : Pile elements displacement during a dynamic load test

The displacement figure is very explicit. The wave propagation (blue arrow) is coupled with the load transfer generating a differential shortening of each pile element. After a period of about 20 ms, all the pile elements are synchronised and the pile moves as a rigid body due to the wave propagation into the pile. The red arrow gives an information about the load transmitted to the pile base: the reduction in displacement between the maxima is due to the elastic shortening of the elements and to the dynamic load transmitted to shaft and base, respectively.

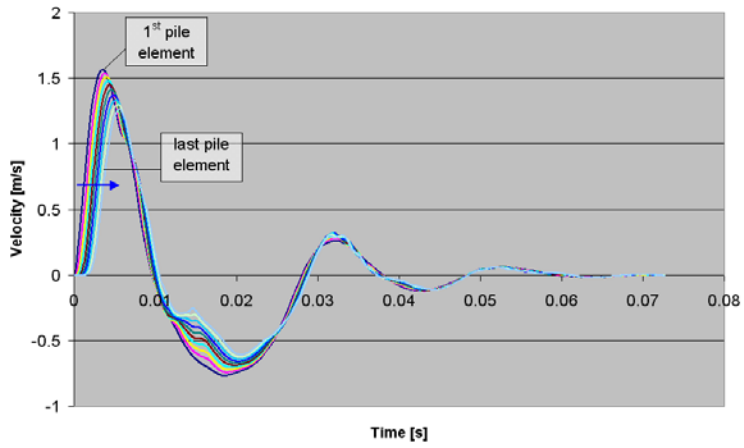

Figure III-50 : Pile element velocity during a dynamic load test

The velocity figure shows the same situation. The velocity traces evolve together after the same duration of about 20 ms like in Figure III-49. The main trend of each element's trace illustrates the general behaviour of the pile and is coming from the input signal at the pile top (blue trace in detail (a)-Figure III-51). Consequently, the information "goes down" the pile with the wave propagation. Sometimes the information can come from the bas reaction due to a particular reflection and the information goes up to the top (grey trace in detail (b)-Figure III-51).

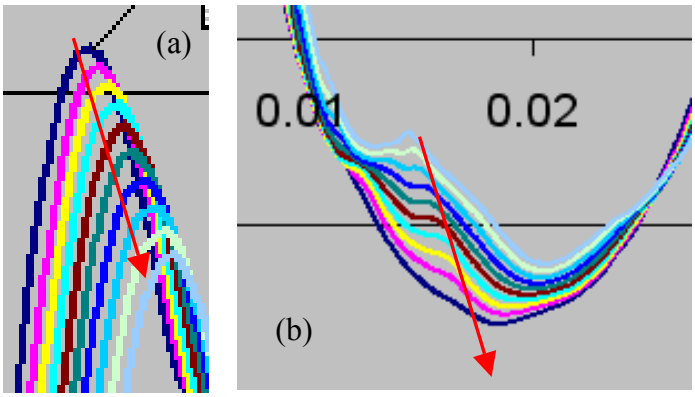

Figure III-51 : Propagation of the information from the top (a) or from the base (b)

3.5. Signal quality check

The signal quality check is an essential part of the process of analysis of the dynamic data. This analysis needs fair data representative of the measured behaviour. This obvious remark requires hypothesis, verifications and good evaluations of certain quantities.

First, the data must be correctly measured and the blow must be correctly given to the pile head. To ensure this fact, several operations can be done:

- On field, the observation of the complete progress of the test is needful, including the control of the alignment of the mass and the pile axis, the correct fixation of the transducers, the verification of the data acquisition chain and the verification of the height and the free fall behaviour of the dropping system;
- The strain and the acceleration are both measured on two independent channels placed diametrically opposite on the pile shaft. Their comparison allows to check the potential eccentricity of the blow;
- The data of acceleration and strain are measured with respect to time. The storage starts before the blow and ends after stabilization of the pile. Consequently, both acceleration and strain values have to be equal to zero at the start and at the end of each blow.

After, the acceleration and the strain are transformed in velocity and displacement, and in force respectively. These operations also need hypothesis.

3.5.1 The field measurements

A. The acceleration is measured with accelerometers (2) generally fixed on the pile shaft. Figure III-52 presents the traces of both measured signals and the average one used in the analysis. The following remarks can be pointed out in parallel with the marks on the figure.

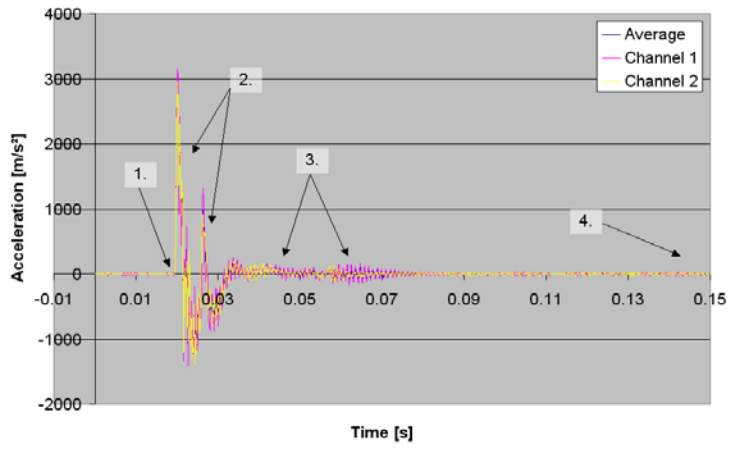

Figure III-52 : Acceleration measurements (2 channels + average)

1. The impact: both signals start at the same time with the same slope. Good synchronisation;

2. When the blow has just impacted the pile head, the accelerations are also in phase;

3. After the main part of the signal, the pile starts to vibrate. The opposition of phases indicates that it is probably a parasite vibration due to a slight eccentricity in the horizontal plan. The averaging corrects this influence but can generate spurious velocity;

4. The end of signal, the acceleration has to be equal to zero in order to generate correct velocity and displacement after integration.

This average signal renders correctly the single ones as it is generally the case for acceleration. This kind of signal is very stable to eccentricity.

B. The strain is measured with strain gages fixed on the pile shaft 2 or 3 diameters below the pile head to avoid the local stress generated by the geometrical particularities.

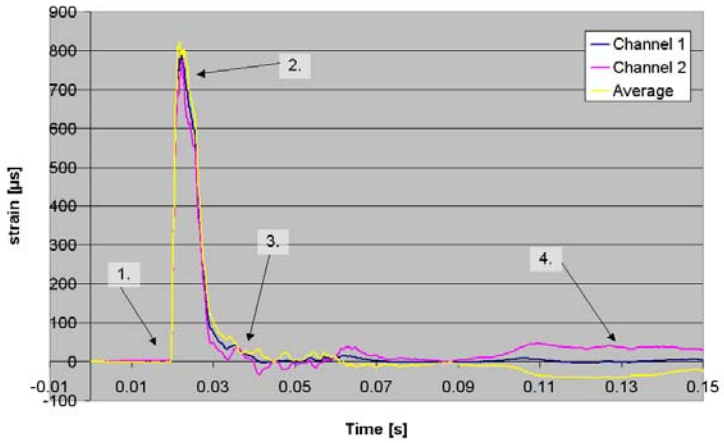

Figure III-53 : Strain measurements (2 channels + average)

Figure III-53 shows the stress measurements from both transducers. The graph plots the single traces and their average used in the analysis. The following remarks can be given:

1. Synchronization of the signals at the start;

2. The major part of the signal is similar for the three traces;

3. The end of the energetic part shows a differentiation that corresponds with the vibrations appeared in the acceleration figure (Figure III-52). The pile vibrates around its vertical axis and generate slight tensions. A slight eccentricity is brought out;

4. The end of the signal exhibit opposed behaviours averaged with a expected null value. That corresponds probably to the blow eccentricity or the pile horizontal vibrations.

The strain signal is more sensitive to the eccentricity than the acceleration. Generally, the average trace of both signals is considered as the correction to this eccentricity. This is true for a small difference such as the difference seen in Figure III-53. But if the eccentricity becomes pronounced or located in another vertical plane than the plane defined by both transducers, the average can introduce errors that generally over or under-estimate the force signal. The data withdrawn from the analysis in section 3.3.3 of this chapter were improper because of the effect of eccentricity to the force measurements:

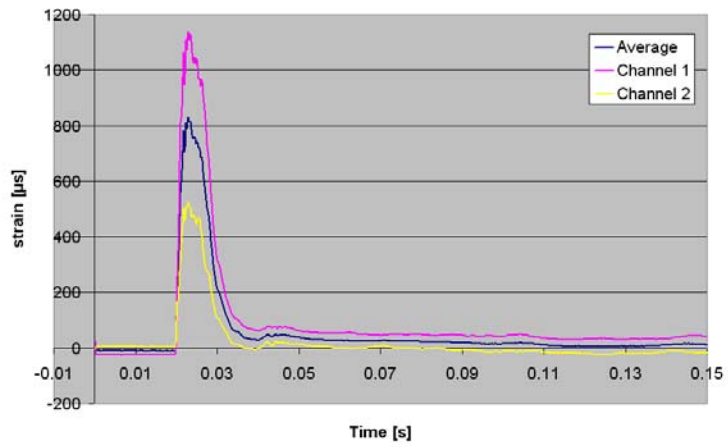

Figure III-54 : Bad strain measurements (2 channels + average)

Figure III-54 shows the effect of a strong eccentricity: a large deviation between both stress measurements, and a large uncertainty on the average data measured. The origin of this eccentricity can be variable: e.g. a misalignment of the ram with the pile axis or the failure of the pile causing a differential settlement. The consequences can lead to a bad interpretation of the signals. The consequences on the relationships between the measured force and the Enthru (Figure III-45 to Figure III-48) are obvious and illustrated here below.

Figure III-55 and Figure III-56 express clearly that the forces measurements are badly influenced. The dashed red arrows indicate the large consequence if only one signal of force is used instead of the average trace. The force chosen is the smallest one and is probably under-estimated in comparison with the real one. The "corrected" value should reach the trend of the old A7 results.

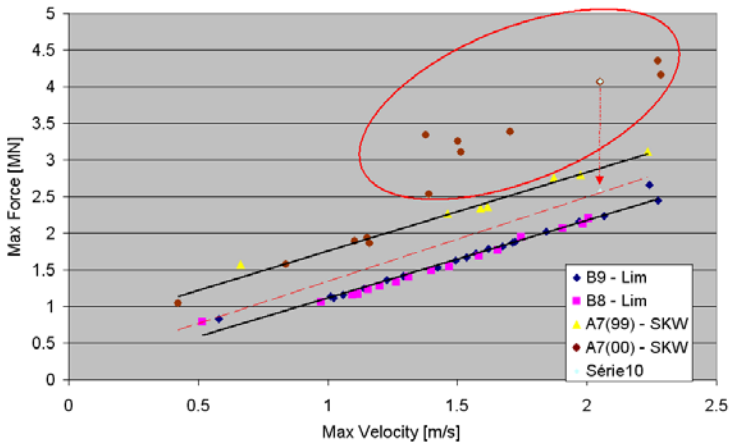

Figure III-55 : Addition of questionable data to Figure III-65 to highlight the effects of large eccentricity on the quality of data

It is also shown on Figure III-54 that the initial and the final values of the strain measurements are not equal to zero what is a serious indication of the quality of the measurements.

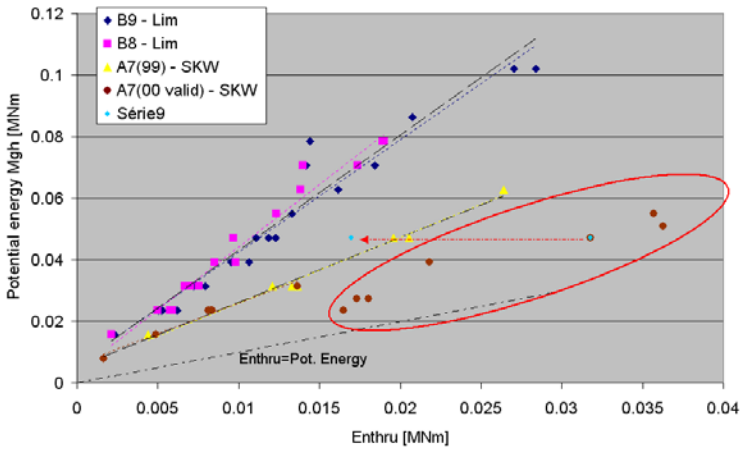

Figure III-56 : Addition of wrong data to Figure III-68 to highlight the effects of large eccentricity on the quality of data

3.5.2 The post-treatment

If the measurements are estimated reliable, the post-treatment needs also to be correctly performed because of the assessment required for this post-treatment.

3.5.2.1 From strain to force

The force is linked to the strain by the Hooke's law:

$$F = A \cdot E \cdot \varepsilon$$ **Equ. III- 37**

- A is the pile normal section [m²];
- ε is the strain [-];

and E the elastic modulus is given by: $E = v_p^2 \cdot \rho$ **Equ. III- 38**

- v_p is the wave velocity [m/s];
- ρ is the mass density of the pile material [kg/m³]

Compared to the pile head velocity that is almost directly measured, the force signal depends on the pile section and especially on the wave propagation velocity. However, the latter parameter is more variable[3] than the mass density and the pile section. The wave propagation is directly connected to the concrete strength that depends on the type of cement and on the age of concrete after casting.

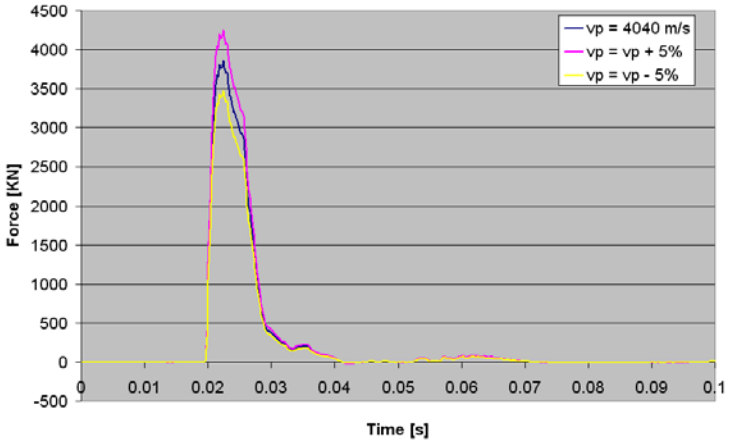

Figure III-57 : Influence of v_p on the force precision

Figure III-57 presents the influence

[3] For concrete

of the modification of 5% (fewer or extra) of the wave propagation velocity on the force evaluated. Since the force is used directly as input or reference in the back-analysis process, the importance of this step is highlighted. But possibilities exist to evaluate the wave propagation velocity:

- Laboratory methods (empirical relationships);
- Ultrasonic method (wave auscultation);
- Analyse of the signals measured.

The last method uses two properties of the wave equation analysis applied to piles:

- as already explained (chapter 1 and section 3.2.3.3.) the force and the velocity are proportional with respect to the pile nominal impedance (I) during the first instants of the blow when the upwards waves of the first shaft layers do not perturb the measurements yet:

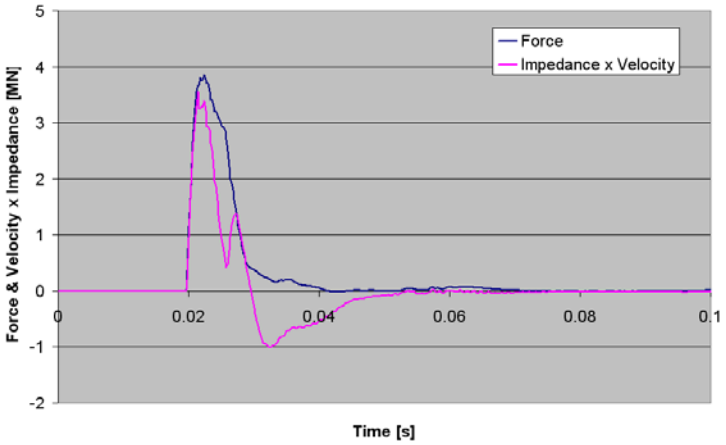

Figure III-58 : Relationship between force and velocity x impedance

$F = VI$ and $I = \rho \cdot v_p \cdot A$ **Equ. III- 39**

In the case of a pile where this duration is sufficiently long, a matching procedure of both signals in order to best fit the first part of them can inform for the value of v_p (Figure III-58).

- Another method is to analyse the upwards waves given by:

When the upwards wave presents a local peak, it corresponds to the end return of the information reflecting to the base. This return may be characterized by the time needed to travel 2 pile lengths. This time is equal to $2L/v_p$ giving an information on the value of the propagation velocity v_p (Figure III-59).

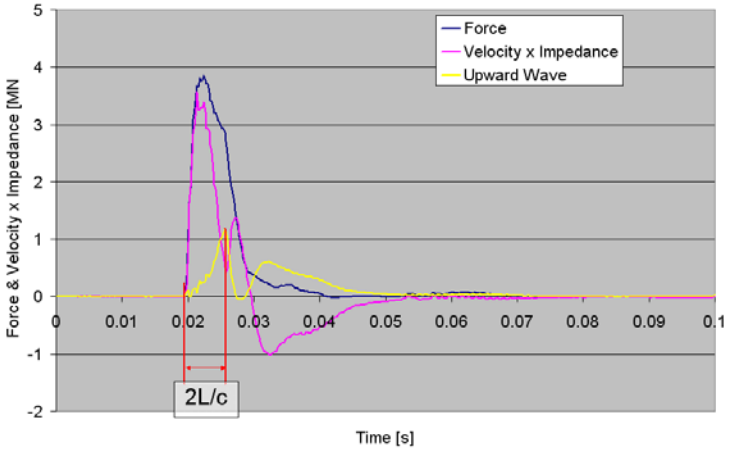

Figure III-59 : Use of the upwards wave to evaluate the wave propagation velocity

$$F \uparrow = \frac{1}{2}(F - VI) \quad \textbf{Equ. III- 40}$$

3.5.2.2 From acceleration to velocity and displacement

The acceleration is integrated with respect to time to evaluate the velocity and the displacement. However, the integration procedure can be perturbed by the miss of the constants of integration during those two processes. This correction is taken into account by the possibility to equal the permanent settlement to a fixed value. This operation is visual and allows to correct the kinetic data.

4. Conclusions

Mainly based on the pile/soil model, the first part of this chapter describes the distinct shaft and base soil reactions by defining the specific terms linked to the small and large deformations and the static and dynamic solicitations. Afterwards, a special attention is put on the classification of the parameters in order to reduce their number before the optimization process. Finally, a parametric study of two dynamic parameters (the main frequency and the magnitude of the dynamic solicitation) allowed to described the influence of each term involved in the load rate effect at different steps of the load-displacement curve (initial stiffness, failure, …). It appears that, in the range of the dynamic solicitations, the radiation damping influences greatly the magnitude and the initial stiffness of the dynamic soil reaction compared to the viscous term.

The second part of this chapter is mainly focused on the measurements made during a dynamic load test. The date used in this research come from a national research program organized by the BBRI which is shortly described. Afterwards, a specific analysis is carried out upon the measurements. This strict analysis is based on the reached maxima of quantities such as displacement or settlement (perm or max), velocity, force or transferred energy on the top of the pile that bring similar results between couple of quantities. Figure III-32, Figure III-34, Figure III-38, Figure III-40, Figure III-44 and Figure III-47 illustrate with the same accuracy that there is a need for a minimal drop height, velocity and force of energy to develop a substantial permanent settlement. This settlement develops later quasi in parallel with the evolution of the maximum reached settlement. Depending on the quantity used, the curves present two types of behaviours. The maximum settlement curve presents a convex evolution in function of height of drop or the Enthru. On the other hand, the maximum settlement curve presents a concave[4] evolution in function of the velocity or the maximum force. A summary of the required quantities to develop a significant permanent settlement is given by:

	Sint-Katelijne-Waver	Limelette
Drop Height [m]	0.5 – 0.7	1.3 – 1.4
Maximum Velocity [m/s]	1.2 – 1.4	1.5 – 1.6
Maximum Force [MN]	1.9 – 2.0	1.75 – 1.8
Energy [MNm]	0.007	0.012 – 0.03

Table III-10: Summary of the critical quantities to get significant permanent settlement

[4] Or a sum of two straight lines with the stiffer in second position.

The analysis of the measurements has also highlighted theoretical results expected between measured quantities. For example the relationships between force and velocity measured at the pile head or energy transmitted and the drop height (translated in potential energy).

Another good result is the repeatability of same tests performed on a pile. Despite the fact that a slight trend to degradation of resistance is observed when several blows of same height drop were compared (especially in Limelette), in general the same response is measured after submission to a similar solicitation. Moreover, in each site, an internal comparison allows the comparison of the effects of the pile resting in the soil during one complete year for Sint-Katelijne-Waver and the comparison of the behaviour of two identical piles installed in the same soil and tested similarly in the same day for Limelette. The results bring no clear distinct trends for both particular comparisons what is remarkable and allows conclusions to be given only for soils and sites.

CHAPTER 4
Back-analysis and optimisation

1. Introduction

This chapter aims to describe the main principles of the back-analysis applied to the resolution of the dynamic pile testing analysis. This process is the main tool used to extract the parameters of the pile/soil interaction system from the dynamic measurements obtained in the field.

The general principle followed is described including the type of data involved in the process, the quality criterion leading the optimisation, the details of the analysis in the duration and pile/soil characterization and the way used to visualize the results of the optimisation. Afterwards, an automatic method of matching is presented, described and validated with a short analysis of the uniqueness of the obtained solution. Some guides are also given to accelerate, improve or validate the matching procedure. The matching procedure and the back-analysis works with a variable set of parameters. Within this group, some parameters have a larger influence compared to others. A section is dedicated to the sensitivity analysis allowing to classify the parameters and to use this classification to improve the reliability of the back-analysis. Finally, a sequence of dynamic load tests from Sint-Katelijne-Waver and Limelette are analysed .

2. The back-analysis system used in the dynamic pile testing analysis

2.1. Principle

The main principle of the back analysis uses the fact that the pile/soil model described in chapter 3 is able to calculate the system response for a given impetus. This input signal is an event measured during the dynamic test. The pile response is compared to the measured one and the gap between

curves is considered as a measure of the imperfection ofthe simulation. The smaller the difference, the best the calculated response. Consequently, if the pile/soil interaction is known, simulations of other solicitations are possible (like Static load settlement curve).

The main goal of the technique is to adjust the parameters characterizing the pile/soil model chosen in order to fulfil a criterion based on the measured data issued from the dynamic test. When the criterion is achieved, the model is considered as describing the pile/soil system. The criterion commonly used by numerous procedures works with the force or velocity signal as input and control data of the matching procedure. The procedure follows those steps:

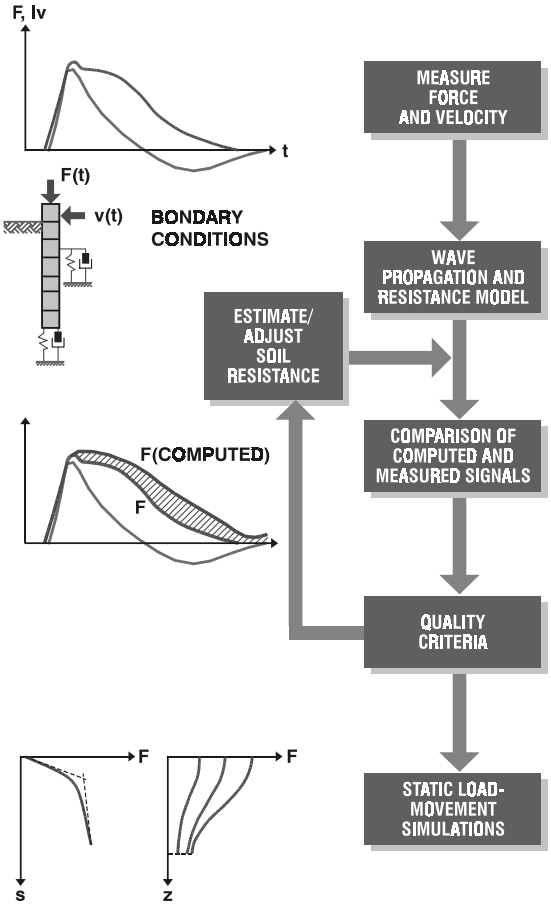

Figure IV-1 : NUSUMS procedure (Holeyman, 1992)

- Either the force or the velocity[1] is imposed as a stimulus at a boundary of the model;

- The model uses this stimulus and calculates the pile/soil response. Either the velocity (if the force is used as stimulus) or the force (if the velocity is used as stimulus) is calculated;

- The computed signal and the measured signal (not used as a stimulus) are compared and a quality criterion determines the degree of agreement between both signals;

- If the matching agrees, the procedure is stopped and the used parameters are considered to describe the pile/soil model for the analysed test in the configuration of the chosen model;

- If the quality criterion does not fulfil the requirements of agreement, the model parameters are re-estimated and a new loop is launched in order to improve the matching agreement.

Figure IV-1 describes the resolution algorithm and is called NUMSUMS for NUMerical Simulations Using Measured Signals.

The present chapter describes the improvements brought during this research to this important step of the analysis and this particular section aims to describe the general tools and characteristics of the back-analysis process.

[1] Or a combination of signals like the downwards and the upwards forces waves

2.2. Used signals and quality criterion

The dynamic measurements are of two types: the dynamic (the strain (force) at the pile head) and the kinetic (the acceleration (velocity) at the pile head) ones. Both of them are incorporated in the back analysis process. These signals can be used either as input or as reference for the comparison step. If the force is imposed as boundary condition, the velocity of the pile head is calculated and compared to the measured one, while if the velocity is chosen as impetus, the force is used as reference for the comparison and the matching quality evaluation.

It is also possible to mix the force and the velocity signals in order to impose the downwards wave and to compute the upwards wave to be compared with the measured upwards wave.

The force and velocity data are measured independently with transducers (strain gage and accelerometers). When the fitting between curves is achieved by using one signal as input and the other as reference, the simple fact to invert the signals used as input is a check of the quality of the result.

Both signals are imposed as boundary condition and as reference. The average gap between the measured and calculated curves is evaluated for both couples of curves and their sum represents the general quality criterion to be minimized. By this way, the crossing check is realized each time and the set of parameters giving the best fit between curves optimises both possible approaches (force or velocity imposed to the system):

$$D_p = D_{pF} + D_{pV} \qquad \textbf{Equ. IV- 1}$$

Where:

- D_{pV} is the normalized average gap between the measured and calculated velocity traces;
- D_{pF} is the normalized average gap between the measured and calculated force traces;
- D_p is the normalized gap equal to the sum of both normalized distances of the force and velocity signals and considered as the quality criterion.

D_p means normalised gap for the set of parameters p, as follows:

$$D_{pV} = \frac{\sum_t (V_m - V_c)^2}{\sum_t (V_m)^2} \quad [\%] \qquad \textbf{Equ. IV- 2}$$

$$D_{pF} = \frac{\sum_t (F_m - F_c)^2}{\sum_t (F_m)^2} \quad [\%] \qquad \textbf{Equ. IV- 3}$$

F_m is the discrete measurement of force; V_c is the discrete calculation of velocity;

F_c is the discrete calculation of force; t is the duration of the analysis.

V_m is the discrete measurement of velocity;

Figure IV-2 and Figure IV-3 provide the result of an optimisation. The shaded zones represent the gap between curves to be minimized.

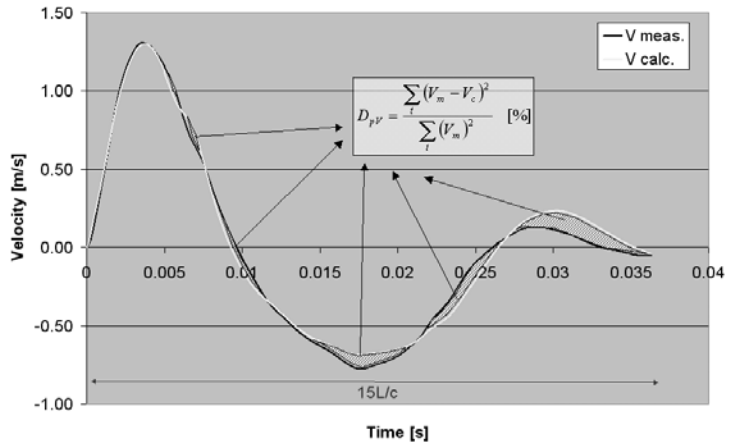

Figure IV-2 : Measured and calculated velocity signal

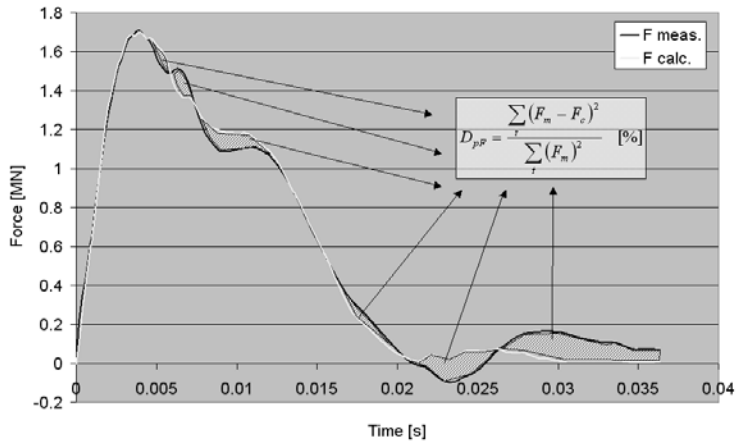

Figure IV-3 : Measured and calculated force signal

The gap is normalized in order to allow the sum of the gaps between signals of different units (force or velocity) and to allow comparison of analysis performed on tests of different energy (drop heights increasing → vel and force increasing). The square function is applied to avoid the negative values problem. This has an influence on the evaluation of the best solution. The minimization of this function favours the decreases of the higher gaps in comparison to the smaller ones (because of their higher relative weight in the general sum).

Others methods of gap evaluation exist in the literature:

- The automatic matching procedure of CAPWAP® described in Rausche et al. (2000) uses a normalized and weighted sum of the difference existing between both measured and calculated curves. The purpose is to minimize this value by changing the parameters.

$$D_C = \min \sum_t |Dif| = \int_t |F_m - F_c| \cdot dt \qquad \textbf{Equ. IV- 4}$$

The normalization is made with respect to the temporal integration of F_m. The match over a period of 3ms following the first return of the stress wave from the pile toe is given a double weight in the summation because of its importance for a total capacity determination.

- El Naggar and Baldineli (1998) minimize the squared difference between computed and measured displacements (ΔD):

$$D_{EN} = \min \sum_{t} \left[\frac{D_c - D_m}{D_m} \right]^2$$ **Equ. IV- 5**

This is almost the same formulation than the one presented in this section, but the use of the quotient inside of the summation includes high risks of divergences when the discrete value of D_m is close to 0.

- Berzi (1994, 1996, 1999) defines the observed and the simulated system responses as represented by two curves in a 2-D system and by m discrete points (1, …, m) with coordinates x_i and y_i (I = 1 to m). The deviation between both curves is quantified by the area Dp equal to the sum of the partial area r(p). The partial area is defined as the area of the quadrangle among the j-1th and the jth point (j < m) (Figure IV-4). The areas are evaluated in a normalized coordinate system: gap

$$\begin{bmatrix} (x) \\ (y) \end{bmatrix} = \begin{bmatrix} \frac{x - x_{\min}}{x^0_{\max} - x^0_{\min}} \cdot W \\ \frac{y - y_{\min}}{y^0_{\max} - y^0_{\min}} \cdot \frac{1}{W} \end{bmatrix}$$ **Equ. IV- 6**

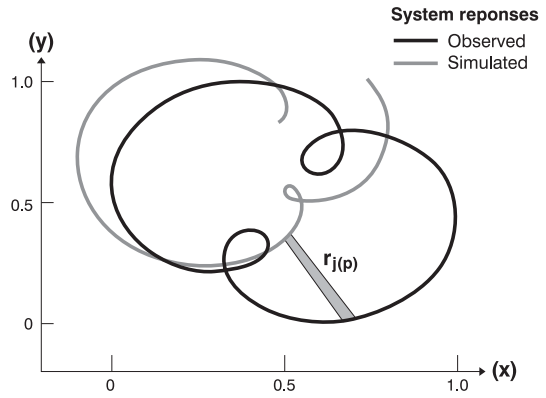

Figure IV-4 : Definition of the distance between system responses (after Berzi, 1999)

$x_{min,max}$ are the min and max values of the x coordinates; The term W is a weight factor;

$y_{min,max}$ are the min and max values of the y coordinates; (x) and (y) are the normalized coordinates.

the superscript "0" referred to the observed response;

The quality criterion becomes:

$$D_B = \min \sum_{i}^{1 \to m} \left| r_i(p) \right|$$ **Equ. IV- 7**

- TNOWAVE® uses also an automatic matching procedure but the authors do not describe the quality criterion used with accuracy. The literature informs that the convergence criterion can be a small residual between calculated and measured signals, a small update for the parameters or a maximum number of iterations.

The duration of analysis has a certain influence on the value of the quality criterion. All signals (force, velocity, …) stabilize faster or slower depending of the type of signal and the type of soil: the clay dampens the pile oscillations faster than the sand and the load signal is the shortest one compared to the acceleration, the velocity and the displacement, respectively placed in an increasing duration order.

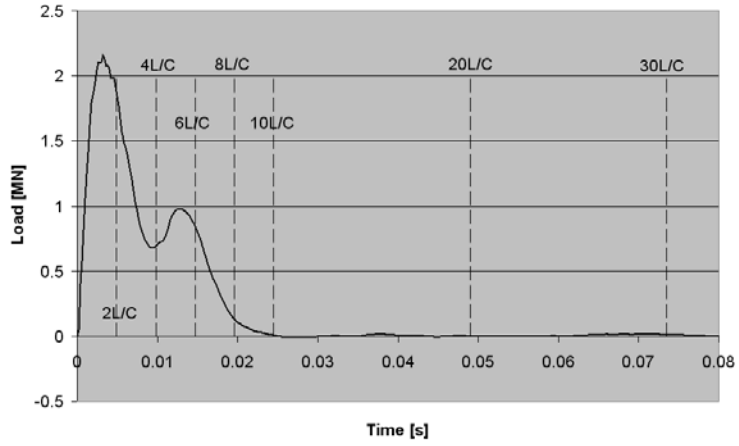

Figure IV-5 : Load signal marked with multiples of travel duration

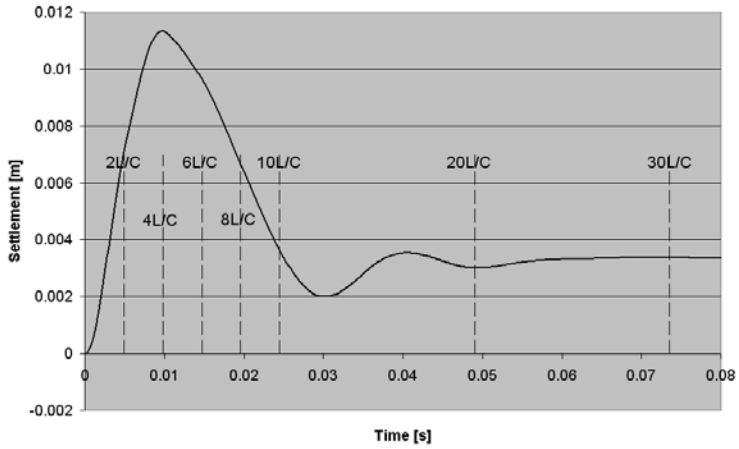

Figure IV-6 : Settlement signal marked with multiples of travel duration

Figure IV-5 and Figure IV-6 exhibit the difference existing between the load and the settlement time histories. The time determined to perform the back analysis depends on the parameters to be optimised and the time available to analyse the signals. The longest the signal to be analysed, the longest the analysis duration due to the time processing. Moreover, the first part of the signal only concerns the loading, the unloading parameters can not be optimised. Time processing management and choice of parameters to be optimised are two antagonist steps in the general process.

In the following treatments, the duration of analysis is defined by the number of travelling of the wave into the pile. The time needed to a wave to travel from the to the base is determined by the pile length (L) and the wave propagation velocity (c):

$$t = \frac{L}{c}$$ **Equ. IV- 8**

Consequently, the time fixed to perform the back analysis is determined in multiple of this duration:

$$t = \frac{4L}{c}, \frac{6L}{c}, \frac{10L}{c}, \frac{20L}{c}, \ldots$$

2.3. Results and comparison of signals

The result of the optimisation is given in percent [%] (the value of D_p). But different graphical results can confirm the quality of the optimisation. The load-settlement trace is the most used in the future developments to represent the quality of the optimising procedure (Figure IV-7). This curve summarizes both measured information: force and settlement. The best optimisation must be reliable in both domains and the comparison of measured and computed curves is a good way to check the quality of the back-analysis and the potential zones of erroneous modelling.

Figure IV-7 displays the data and the three possible representations of the pile/soil response:

- The force calculated with the settlement measured;
- The force measured with the settlement calculated;
- The force calculated with the settlement calculated.

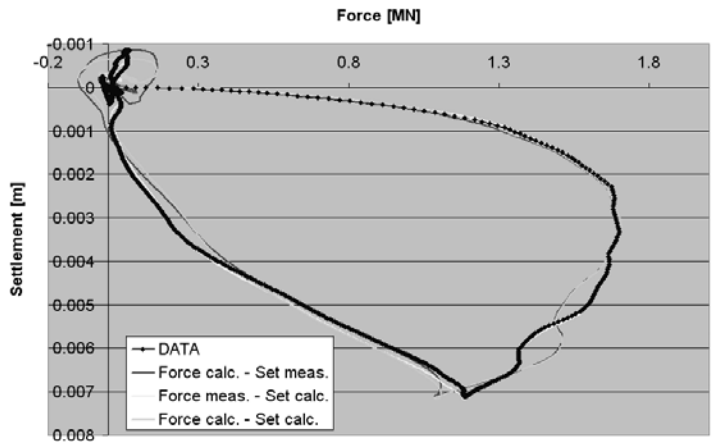

Figure IV-7 : Result of the optimisation : the load settlement curves

The imposition of the motion causes uncertainties in the evaluation of the force during the start of the unloading and at the end of the signal and the generation of the displacement based on the force signal [force meas. - set calc.] seems to be very successful and give a very good agreement with the original trace. The comparison of the measured signal with the double calculated signal [force calc.- set calc.] is the sign of a very good agreement but is not used to characterize the matching.

The time histories of each quantity is also a good way to confirm the quality of the matching procedure. Figure IV-2 and Figure IV-3 give an overview of these results for the signals of force and velocity. But it is also possible to check the settlement or acceleration agreements. The energy transferred to the pile (Enthru) can also be used as indicator of the quality of the matching procedure but instead of one sole curve as for the others quantities, the modelled enthru is function of the chosen function force and velocity (calculated or measured) used in its equation.

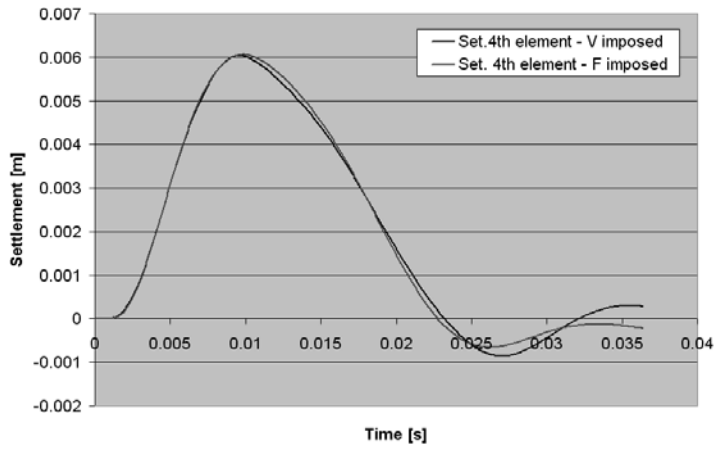

Figure IV-8 : Result of the optimisation : the settlement curves of the 4th pile element

The comparison of quantities at the pile head allows to compare the pile/soil response with the measured data. It is also possible to check the same quantities with depth along the pile. Since there is no possibilities of comparison with a real value, the comparisons only concern the signals generated by both types of signal imposition. The traces must be the most similar as possible.

2.4. Pile/soil system input

The pile soil system has to be introduced in order to give a first response. This description of the pile/soil system must be as relevant as possible in order to reduce the time needed to get an acceptable matching and to ensure a solution compatible with the pile/soil environment and logic with the quantity orders of magnitude: e.g. the soil parameters (ultimate resistance, initial stiffness, …) must be included in a well known range due to the knowledge of the soil constitution. The section dedicated to the parameters management in chapter 3 sorts the parameters in classes in function of their reliability and potential of variability. Essentially the soil parameters are concerned by the back-analysis process. The pile and test related parameters can be assessed with confidence.

The description of the subsoil is given by:

The shaft resistance parameters: maximum 5 layers with for each layer the depth z_i, the value of the ultimate shear strength $\tau_{ult,i}$, the initial tangent shear strength G_i, and the rheologic parameter J_i called the damping factor. A general value for the unloading modulus G_2/G_1 [-] is set for all the layers as the exponent of the viscous and rheologic ultimate terms fixed to 0.2.

The base resistance parameters: maximum 5 layers despite the fact that only the layers intersecting the cone of soil are taking into account. Each layer is characterized by the depth z_i, the value of the ultimate compression strength $\sigma_{ult,i}$, the initial modulus of elasticity E_i, and the damping factor J_i. As for the shaft, a ratio E_2/E_1 informing the unloading stiffness of all the layers is fixed. The Poisson ratio and the mass density are also required especially for the cone set-up.

Those soil parameters can be issued from several sources: geotechnical information from site, laboratory tests results, geophysical survey on field, experience of values by knowing the soil type or correlations between some of those quantities, are methods allowing to introduce a first pile/soil system description called the input of parameters.

Within this research, both sites of Sint-Katelijne-Waver (Boom clay) and Limelette (Bruxellian sand) have been extensively investigated with a large range of geotechnical tools and laboratory tests. The depths and the ultimate strengths for both shaft and base soil reactions are based on the electric cone penetration test (CPT-E) performed in the pile axis. The initial shear modulus and the initial modulus of elasticity are evaluated from the geophysical survey informing about the profile of wave propagation velocities V_p and V_s with depth. The typical soil parameters as Poisson's ratio and the mass density are based on the literature concerning the well documented soil types: Boom clay and Bruxellian sand. And the damping factors for shaft and base descriptions are fixed to 0.5 and 1 $s/m^{0.2}$ respectively, according to the literature.

The following figures summarize the data used for the analysis of the dynamic tests performed on the piles A7 of Sint-Katelijne-Waver and B8 of Limelette.

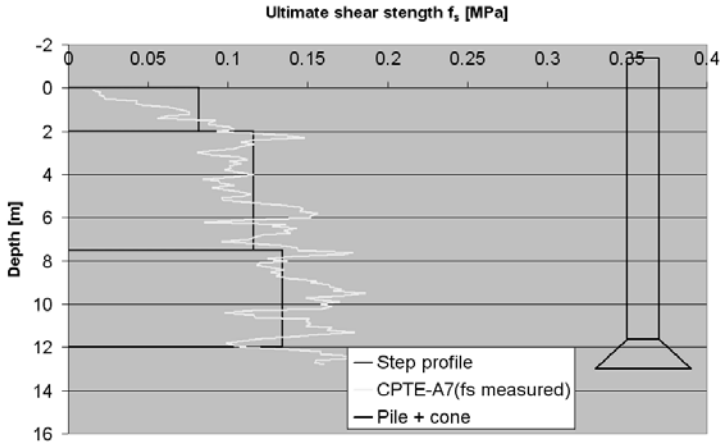

Figure IV-9 : Local friction strength from CPTE measurement and ultimate shear strength profile used in the back-analysis (SKW – pile A7)

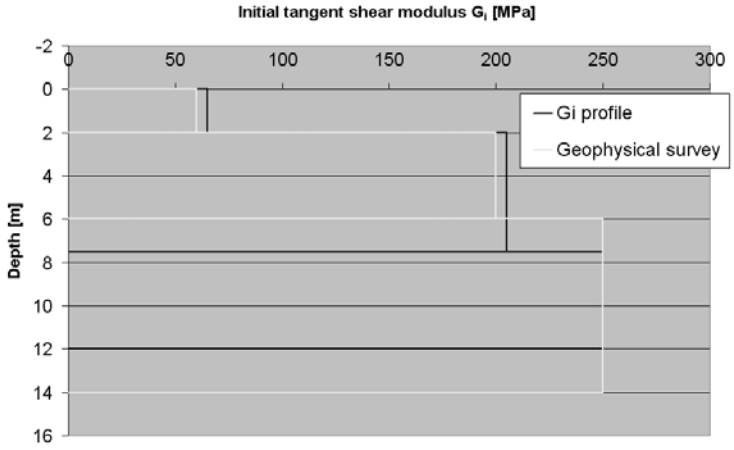

Figure IV-10 : Initial shear modulus from geophysical survey and initial shear modulus profile used in the back-analysis (SKW – pile A7)

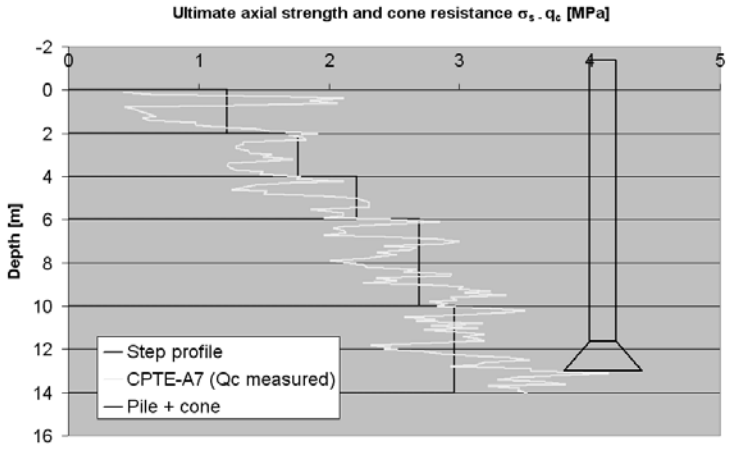

Figure IV-11 : Cone resistance from CPTE measurement and ultimate vertical stress profile used in the back-analysis (SKW – pile A7)

The ratio of modulus either for the shaft friction or the base resistance are both equal to 1 for this input definition and for both sites. the exponent N is also fixed according to the literature to 0.2 for the shaft viscous and ultimate soil resistance formulations and to 0.2 or 1 for the base viscous and ultimate soil resistance formulations.

The modulus of elasticity is based on the relationship linking the shear modulus to the elastic modulus and function of the Poisson ratio:

$$E = 2G \cdot (1 + \upsilon) \qquad \textbf{Equ. IV- 9}$$

For the concerned depths, the value of the initial modulus of elasticity in Sint-Katelijne-Waver is equal to 675 MPa and for Limelette to 800 MPa. The corresponding Poisson ratio are 0.35 and 0.45 respectively. The mass density of both materials is fixed to 2000 Kg/m³.

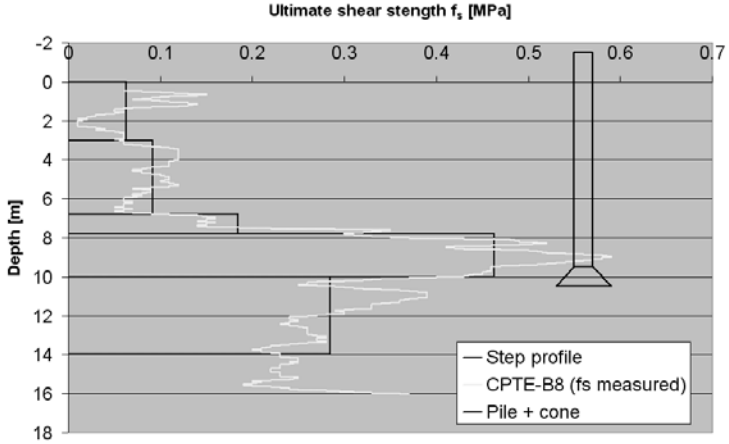

Figure IV-12 : Local friction strength from CPTE measurement and ultimate shear strength profile used in the back-analysis (initial) (Limelette – pile B8)

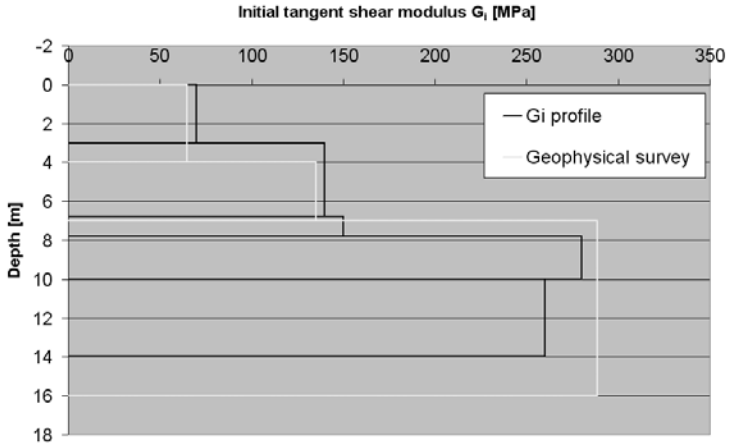

Figure IV-13 : Initial shear modulus from geophysical survey and initial shear modulus profile used in the back-analysis (initial) (Limelette – pile B8)

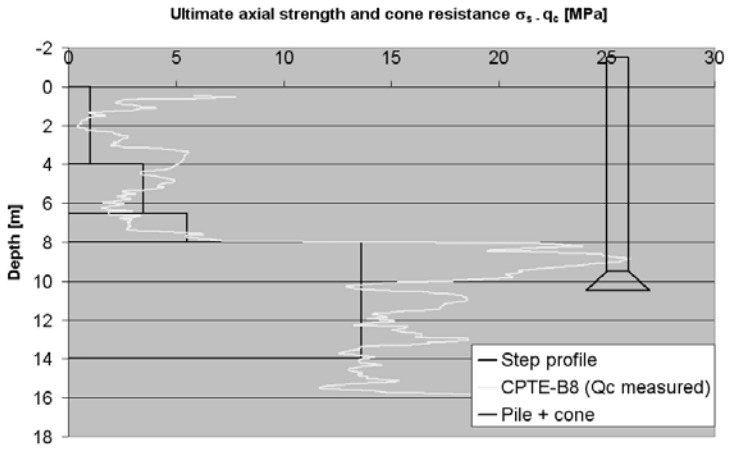

Figure IV-14 : Cone resistance from CPTE measurement and ultimate axial stress (σ_v) profile used in the back-analysis (Limelette – pile B8)

This first description is used as start of the matching procedure. It gives the first point of the optimisation process. It seems to be logical to have the same point with all the analysis related to the same pile. It will be approached in a further section the question of the uniqueness which is directly linked to the relevancy of this point. These future developments highlight the importance to have a coherent input for the pile/soil characterization. The pile B9 of Limelette, located just next to the pile B8 uses the same input than the pile B8 as described here above.

3. Automatic optimisation system

3.1. Requirement

The condition to perform the back analysis are as follows:

- the signals are of good quality;
- the pile geometry is well known and well described;
- the pile is well shaped and its integrity reliable;
- the wave propagation velocity inside of the pile material is well evaluated;
- the pile/soil model is correctly built (choice of the fundamentals relationships, of the pile discretization and the numerical procedure).

With these assessments , the back-analysis can be launched with the modification of the resistance and the rheologic parameters in order to fulfil the agreement between measured and calculated curves.

In some previous procedures, this operation was conducted manually and concerned only the values of the ultimate strengths. All the other parameters (rheologic, thickness of the soil layers, initial shear modulus and modulus of elasticity) were not modified directly. Their changes were not supposed to be influential. If it is true that the ultimate soil resistance is a very powerful class of parameters in the

matching procedure, it will be shown that the others parameters have their own influence and there is real danger to forbid them to be variable during the back-analysis. However, the number of parameters is directly function of the difficulty to find out an acceptable solution. 2 to 5 layers of soil x 4 unknowns (τ_{ult}, z, J, G) for the shaft reaction plus 1 or 2 layers of soil x 4 unknowns (σ_{ult}, z, J, E) for the base reaction plus the unloading moduli (2) give a total of 14 to 30 unknowns to be optimised with the only guide of two couples of curves to fit in between.

This set of n parameters $\mathbf{p}=\{p_i\}$ and their respective range of variability gives a response of the pile/soil model for each combination of them. This response is evaluated with the criterion D_p as:

$$D_p = f(p_1, p_2, ..., p_i, ..., p_n) \qquad \textbf{Equ. IV- 10}$$

This function is a surface of dimension n (according to the number of parameters to be optimised) in the system of dimension n+1 (Figure IV-15). The purpose is to find the minimum of this surface and to respect the domain of validity of each parameter and some physical constraints.

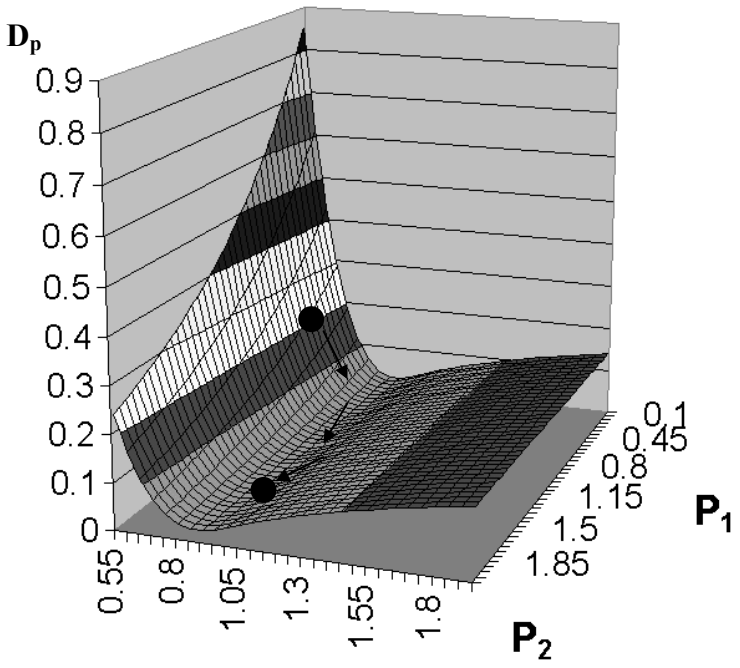

Figure IV-15 : Surface of the matching quality factor function of 2 parameters (p_1 & p_2)

The modification of one parameter modifies the influence of the other parameters on the pile/soil system response. The relative influence of each parameters is given by the partial derivation of the function with respect to the chosen parameter. That can be translated as the slope of the surface in the direction of the parameter axis. If the operator modifies one of the parameter manually, all the others are influenced in function of the distance travelled on the surface. There is a need to investigate all the parameters at the same time and to chose the best way to reach the solution in function of the variability of each parameters. But this operation is not achievable without an automatic operation managing all the parameters or allowing to do it for a given number of them.

Moreover, the optimisation requires a large number of iterations and small modifications of parameters in order to find a stable and best final characterization of the pile/soil system. Indeed, a large modification generally prevents to stabilize the process and to refine the solution. This high number of iteration requires also the setting up of an automatic procedure.

Finally, the need to study the sensitivity of the pile/soil response to particular modifications of some parameters and the necessity to ensure an impartial process imposes also this approach.

3.2. Literature

Several authors and methods use an optimisation process based on a self made algorithm or an existing method developed in the applied mathematics domain.

CAPWAP® uses an iterative algorithm based on the modification of resistance parameter in order to minimize the deviation given in Equ. IV- 4. The signal is optimised either on the force or on the upward wave signal (imposition of the velocity or downward wave as boundary input, respectively).

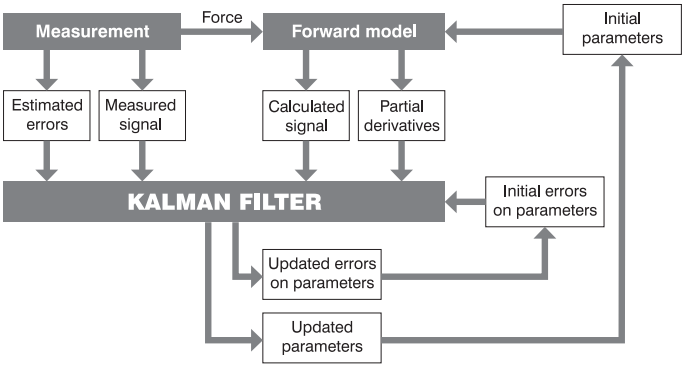

Figure IV-16 : TNOWAVE algorithm of matching (after Van Foeken et al., 1998)

TNOWAVE® uses a pile soil response from the imposed boundary condition based on its typical pile/soil model (chapter 1). It is called the "forward model" (Van Foeken et al (1998) & Courage & et al (1992). An algorithm called the Kalman fiter (Kalman (1960); Hendriks et al. (1990) and Courage et al. (1990)) is used in order to estimate the unknown parameters values and their a posteriori covariances so that a good agreement is found between the measured data and the forward model response. The a posteriori covariances inform about the reliability of the values found. With the impact signal and initial parameters description, the forward model computes the pile/soil response. This response, together with the measured one is supplied to the Kalman filter. Based on the difference between both signals and the partial derivatives of the responses with respect to the parameters (using a perturbation method) and the covariance of the measurements, the parameters and the chosen model, the Kalman algorithm calculates a gain to update the parameters and their covariance. The procedure is repeated until a convergence criterion is met. In dynamic signal matching, the match is done on the upward travelling wave.

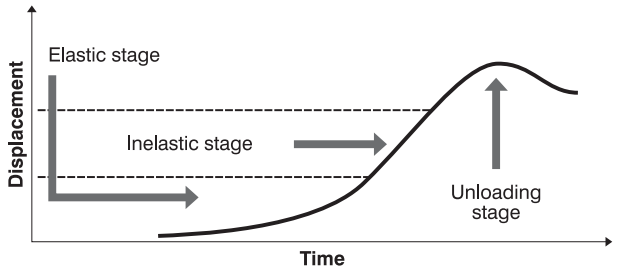

Figure IV-17 : Typical displacement-time history curve (after El Naggar et al., 1998)

El Naggar and Baldinelli (1998) describe an iterative automatic matching technique focused on the statnamic load test optimisation based on the decomposition and the fitting of the displacement signal into 4 distinct phases. The method uses the pile/soil model of El Naggar and Novak (1994) describing the response of pile under dynamic loading (see chapter 2). This model and the initial set of parameters calculate a response of the pile to the statnamic load introduced as boundary condition. The computed displacement response is compared with the

measured one. Each one is fitted with a set of polynomial functions and connected to a few number of parameters significant in this part of the curve and adjusted with priority:

- The elastic stage of the displacement time history is fairly linear, is governed by the stiffness of the soil medium and derived from the elastic properties such as shear modulus and mass density. The function modelling this phase is a linear function;

- The inelastic stage is faily non-linear due to the pile response at higher load level. The end of this stage is associated to the time of maximum applied load when the unloading phase begins. This phase is governed by the soil resistance parameters and depend of the chosen rheologic model. A quadratic function represents the pile response during this stage.

- The unloading phase is also non-linear and divided in two sections. The first is between the maximum load instant and the peak of displacement. This section is modelled by a quadratic function, and the next phase starts at the peak displacement and ends at the moment the displacement becomes constant around its permanent value. This section is also modelled by a quadratic function. The ultimate soil resistance, the shear modulus at the base and the eventual post peak soil resistance govern the unloading stage.

After fitting the stages of the displacement signals, measured and computed, with the appropriate functions, the convergence criterion is calculated (Equ. IV- 5). The constant of the regression analysis and the area of each curve are used to adjust the soil parameters in each iteration. After fulfilment of the convergence, the parameters, which resulted in the best fit, are used to model the pile response to any solicitation.

Berzi (1994, 1996 & 1999) developed an efficient secant-method based algorithm for solving non-linear least squares problem presenting a good stability and convergence properties even with large number of unknowns. He applies this resolution technique to the dynamic pile/soil interactive system. The method is based on the willingness to fit a structured mathematical model to available data expressed by a surface in the n +1 dimension system composed by the n parameters of the structured mathematical model. He transforms the parameter identification problem in a non-linear least squares problem in which the solution is given for parameters values providing a minimal deviation between observed and simulated system response and the normalized error. His algorithm is based on the works of Wolfe (1959) with an improvement of the convergence with a special selection of the search direction. The non linear system is function of the pile/soil interaction system through the definition of the gap between the observed system and the simulated response. The latter is function of the system definition and the parameters values:

If - $\mathbf{p} = [p_1, p_2, \ldots, p_n]$ the n parameters of the system (1, …,n);

- $\mathbf{p}^0$ = the initial set of values for **p**;

- D**(p)** = the gap (normalized) between the observed and simulated pile/soil responses;

- r_J**(p)** = the partial area between two corresponding couples of points of the observed and simulated pile/soil response (1 to m) (Figure IV-4

- the observed and simulated pile/soil response are composed of m points;
- **r(p)** = the vector of r_j**(p)**.

then, the parameter identification problem can be formulated as a system of non linear equations:

$$r(p) = 0 \quad r : \Re^n \rightarrow \Re^m \quad m \geq n \qquad \textbf{Equ. IV- 11}$$

The basic idea is to replace the non linear system of Equ. IV- 10 by a linear problem. It consists of linear interpolations through n+1 solutions [$\mathbf{p^i}$, $\mathbf{r(p^i)}$] (I=0, …, n).

The management and the choice of the successive [$\mathbf{p^i}$, $\mathbf{r(p^i)}$] represents the algorithm leading to the solution **p*** minimizing **r(p)**.

All these methods propose good ideas that were integrated partially or not in the development of the following optimisation method.

The method proposed by El Naggar and Baldinelli (1998) seems to be very attractive for statnamic tests because of the high number of data available for the different stages described. It is more difficult to apply this procedure to dynamic tests due to the quick loading and the small number of points available before the last stage, namely the unloading phase.

The methods used in CAPWAP® and TNOWAVE® seem to be very attractive but look like a black box procedure with a few details on the evaluation of the parameters gain at each step of the procedure. Consequently, the need of a global and automatic optimisation procedure remains like the need to develop it.

Finally the Berzi method is well described and defines the problem of the parameter identification with back analysis in a theoretical way. But the method looks like too mathematical. Moreover, the purpose is also to evaluate the path used by each parameter before reaching the optimal position in the R^n system and to integrate the procedure in a global program based on a explicit method of resolution and not a method based on matrix resolution. But the system should be developed and compared with other methods of optimisation.

3.3. Algorithm

The method developed in this research is inspired of a process used to analyse the sensitivity of the neighbourhood of the optimal solution in order to evaluate the potential local minimum and to evaluate the influence of variability of each parameter around the found solution. As explained in section 3.2, Berzi developed this approach in 1996.

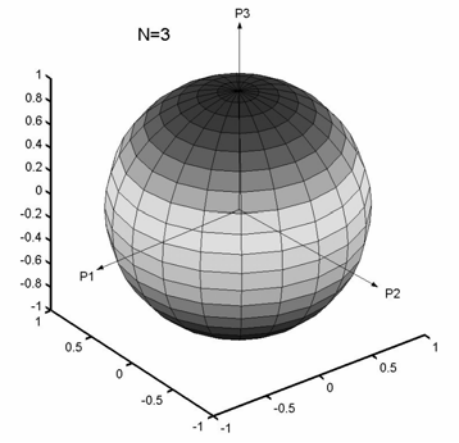

Figure IV-18 : Analysis of the neighbourhood of the optimal solution

The neighbourhood of the optimal solution **p*** is systematically explored. With 3 parameters, if the solution **p*** is given, the systematic exploration around this point is a sphere of radius Δ (Figure IV-18). The exploration is made randomly in the parameters space R^n. The pile/soil response is evaluated with D**(p)** determined for each combination of parameter values and associated to the vector **p**. Generally, the point environment is investigated with successive and decreasing values of Δ. The collection of points and the corresponding values of D**(p)** characterize the quality of the interpretation and the effects this interpretation on the simulation of the static load settlement curve.

The principle is the following:

Each parameter p_i is modified such as $p_i = p_i^* + \Delta p_i$ **Equ. IV- 12**

Where Δp_i is the variation added to the parameters p_i^*. Δp_i can be positive or negative.

The condition allowing to quantify this variation for each parameter of **(p)** is the radius of the n-ball in the parameters space R^n:

$$\Delta = \sqrt{\sum_{i=1}^{n}\left(\frac{\Delta p_i}{p_i^*}\right)^2} = Const. \qquad \textbf{Equ. IV- 13}$$

Δ is limited to the range [0,1] because the parameters values can not be negative due to the physical meaning of the parameters, so that the ratio $\frac{\Delta p_i}{p_i^*}$ must be lower than 1.

Determining randomly the combinations of the vector Δ**p** but respecting the rule of Equ. IV- 13 allows to know the effect of a determined variation of the parameters on the quality criterion D**(p)** and possibly on the simulated load-settlement curve. A large number of these vectors are generated and the result of D**(p)** is sorted as a function of the radius Δ used and as a function of an unequivocal quantity evolving with the variation of parameters e.g. the ultimate soil resistance, … This method is called the *multidimensional parameter perturbation sensitivity analysis* (Berzi, 1996).

The use of this technique in the optimisation process is based on the extensive random study around a particular value of **p** and the systematic evaluation of D**(p)**. Instead of analysing the variation of D**(p)** around $\mathbf{p}^*$ optimal, the minimum of D**(p)** is sought around the vector **p** which is not the optimal solution.

If the pile/soil system is characterized by the vector $\mathbf{p}^0$ defined by the input (page 8) and the corresponding D$(\mathbf{p}^0)$, the value of the quality criterion for this configuration, a systematic study of its

neighbourhood for a given radius Δ and k combinations of **p** according to Equ. IV- 13 can evaluate each $\mathbf{D(p^i)}$ and find the best vector **p'** amongst all the tested combinations of **p** such as:

$$D(p') \le D(p^i) \quad (i = 0...k) \qquad \textbf{Equ. IV- 14}$$

When the best solution is found for the random set of combination of **p** around $\mathbf{p^0}$, the new set of parameters characterizing the pile/soil interaction system is changed from $\mathbf{p^0}$ to **p'**:

$$p^0 = p' \qquad \textbf{Equ. IV- 15}$$

And the set process is started again until reaching of the minimum minimorum. This method is illustrated by Figure IV-19 for two parameters and resumed by the algorithm Figure IV-21.

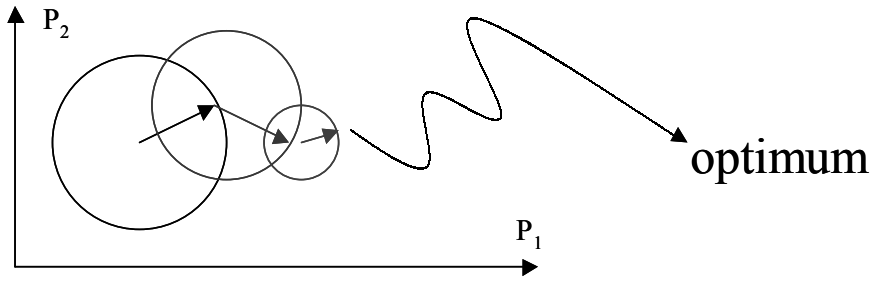

Figure IV-19 : Schematic procedure of optimisation for 2 parameters

There are conditions for the evaluation of the number of the combinations k tested around $\mathbf{p^0}$, for the definition of the radius Δ, for the end of process conditions and for the evaluation of the optimum value of $\mathbf{D(p^i)}$ in each loop of the optimisation process. All these steps are described in next sections.

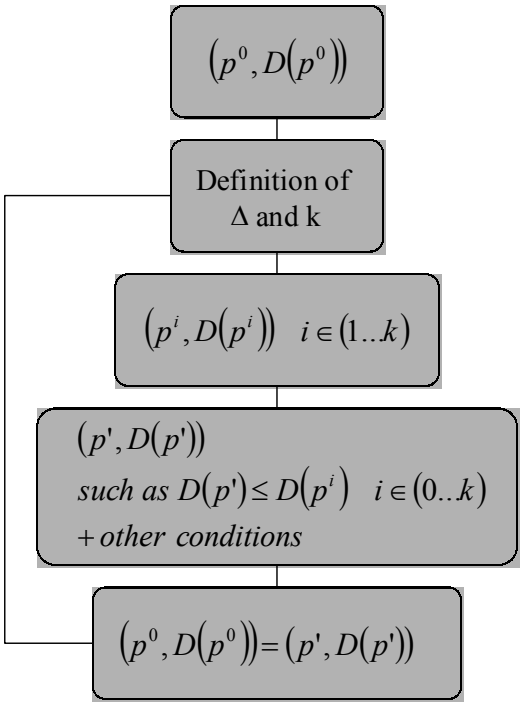

Figure IV-20 : Algorithm of the sensitive method of optimisation

This method have the following advantages:

- The step by step way of resolution allows a control on the parameters inside of their range but also in comparison with the environment and the other parameters;

- All the parameters evolve at the same time. A procedure that optimised the parameters one by one was also tested during this research, but the correlations between parameters influenced the quality criterion. The simultaneous upgrade of two parameters is often more benefit than the sole and consecutive modification of the same parameters;

- This method, open and explicit, allows to store the evolution of the optimisation in order to check the variation of each parameters. The relative weight of each one can be assessed in function of the optimisation progress. Moreover, the path followed is known and

attests of an evolution or an erratic progression.

There is also disadvantages:

- The random evaluation of a large number of combinations can be a waste of time and does not represent an advanced methodology;
- There is no certainty that the best combination is not a local minimum

These disadvantages must be taken into account by the setting up of methods improving the choice of the best combination by testing the combination with respect to the a priori knowledge of the pile/soil system, by checking out the path followed in order to identify a trend in the parameters evolution and by rendering more reliable the method of construction of the combinations.

Two methods were tested in order to carry out this algorithm. The first one is rigid and the second is more open. They differ by the choice of k, Δ, and the choice of the of **p'**.

The first approach imposes the values of k and the schedule of Δ investigated. That means the algorithm follows a determined sequence of radius. The optimisation starts always with the larger radius in order to progress as fast as possible; this radius is progressively reduced until reaching the end of the sequence.

The schedule of Δ allows to test the same radius several times before changing and reducing it. For each radius, a determined number of combinations is tested and the set of parameters giving the best result amongst all these combinations (according to the criterion of quality) is chosen as new reference for the following steps. The procedure ends when the last radius envisaged is tested. This method generates a lot of non-used evaluations for one sole modification in each step. But this choice of the best combination can be made with statistical methods because the large number of succeeding combinations allows it. This method lasts also longer than the next one.

The second approach is more sensitive. A start radius is determined, generally rather large, and for each combination $\mathbf{p}^i$ tested, a comparison is made with the previous criterion of quality (D(p)). If all the recommendations testable agree, the modification is performed immediately and the new position of reference in the n-system becomes this new found combination of **p**. The radius Δ does not change until a particular criterion is fulfilled: if a certain number of combinations is attempted without improvement of D(p), the radius is automatically reduced. The optimisation procedure ends when the determined lower radius is reached and no improvement have been noted since a fixed number of trials. This method is faster and generates more intermediate changes, but only small number of tests can be applied on each particular successful combination to check its validity. For each method, it is possible to choose the parameters to be optimised. A list is composed before the start of the procedure. This allows to refine some parameters less influent when the best solution is almost reached.

3.4. Uniqueness of the back-analysis response

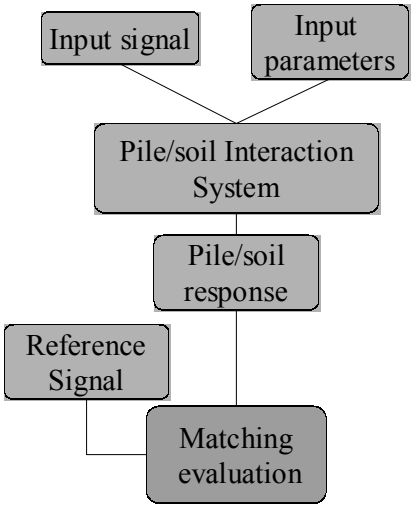

Figure IV-21 : Scheme of the back-analysis process

Since the pile/soil interaction characteristics are back-calculated from the results of dynamic loading test in order to simulate the load-settlement relationship, the reliability of the latter depends on both the quality of the measured data and the quality of the analysis. The quality of the data has already been discussed earlier (chapter 3). The precision inherent to the analysis is function of the validity of the pile/soil interaction model chosen to represent the real system and of the method used for the "signal matching" and the back-analysis. It is known that the solution of the inverse problem is never unique due to the measurement noise and modelling inaccuracies (Berzi, 1996). Nevertheless, this problem is linked to the hypothesis assessed and not to the system supposed to perform the analysis.

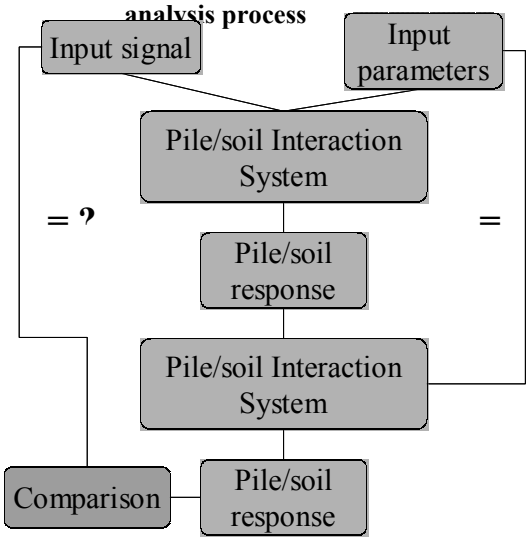

Figure IV-22 : Scheme of verification of the system (#1)

It is proposed in this section to briefly validate the system and to check the reliability of the back-analysis process (Figure IV-21) with a double crossed analysis of a real test (Figure IV-22 & Figure IV-24):

1. The test consists to impose the input signal and the input parameters to the system, and to re-inject the pile/soil response obtained in the pile/soil system to compare the result with the first input signal. If the system is reliable, both signals agree perfectly (Figure IV-22). A signal of force measured on field during the Limelette campaign is used as first input signal (B9-013).

Figure IV-23 shows both signals of forces: the imposed and the computed ones. The agreement between both curves is perfect. This test validates the system and allows to use crossing signals to characterize the matching process.

2. A second test is based on the back-analysis itself. Is the process repeatable? Is the solution or the area in the n-space of parameters representing the unique solution? In order to test this assumption, the algorithm described in Figure IV-24 is followed. A force signal is injected as input in a given pile/soil system characterized by the input parameters set #I. The pile response is re-injected in a second pile/system from where the parameters are back-analysed in order to have a perfect agreement between the first input signal and the last pile/soil response. The input characterisation of the second pile/soil system (#II) is set completely different from the solution in order to check a different path. The purpose is to compare the initial input I with the result of the back analysis (Figure IV-24).

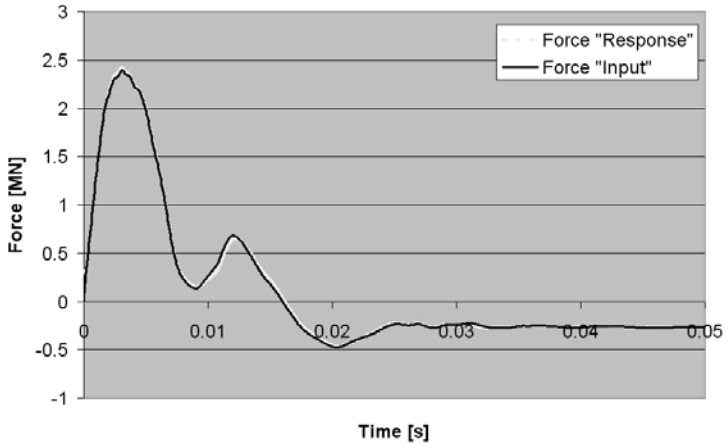

Figure IV-23 : Validation of the system : comparison of forces measured and calculated

Three optimisations with three types of input characterisation are successively performed. the reference input is displayed on Figure IV-27 to Figure IV-30 and Table IV-1 with the label "Reference" (from the Limelette measurements previously used (B9-013):

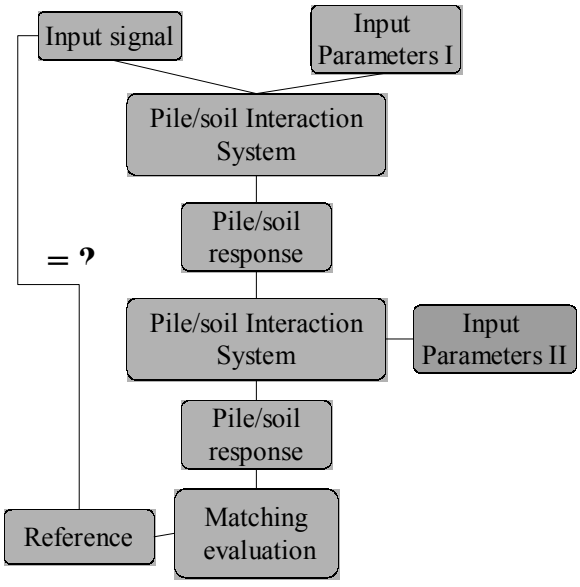

Figure IV-24 : Scheme of verification of the back analysis tool (#2)

- "Optim1" is proposed with a profile of ultimate shear strength constant with depth and equal to 0.15 MPa. The ultimate base resistance is set to 13 MPa;
- "Optim2" is proposed with a shaft inverse profile (the maximum resistance close to the pile top, and the weakest to the pile bottom). the ultimate base resistance is set inferior to the reference one (about 1.4 MPa);
- "Optim 3" has simply the same ultimate resistance profiles (base and shaft) than the reference one but doubled.

The depth, stiffness and damping factor profiles do not have been modified. The ultimate resistance parameters have the most significant influence on the matching process and too much changes bring a misunderstanding of the results.

After optimisation, the quality criteria are very low: D(p) less than 0.16 % for optim1, 0.73% for optim2 and 0.26 % for optim3 for a study duration of about 20L/c. Moreover, the load-settlement curves (Figure IV-25) and the acceleration and velocity traces are almost superimposed (Figure IV-26). In a strict matching aspect, the process is successful and the back analysis gives theoretically the same pile/soil characterization characterizing the pile/soil interaction. It remains to compare the parameters profiles to check the most important: the reliability of the process in the parameters determination.

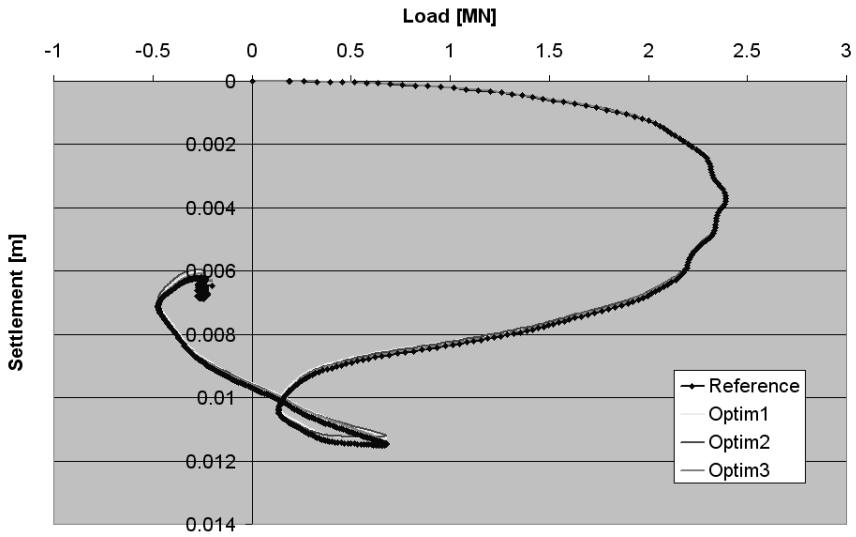

Figure IV-25 : Validation of the back-analysis procedure – comparison of the measured and calculated load settlement curves

The acceleration traces (Figure IV-26) present a small difference, especially the optim2 case, compared to the reference. Globally the matching is very good, but there is a slight perturbation between the instants 0.007 and 0.023 s. Since the problem is almost concentred on the optim2 case, this could be a sign of quality of the back-analysis process. The acceleration traces remain very difficult to match. However the quality of the matching is particularly remarkable because of the length of the study (more than 50 ms), due to very low value of D(p) for all attempts and also due to the almost perfect agreement between calculated and measured signals for all quantities (force, displacement, velocity and acceleration).

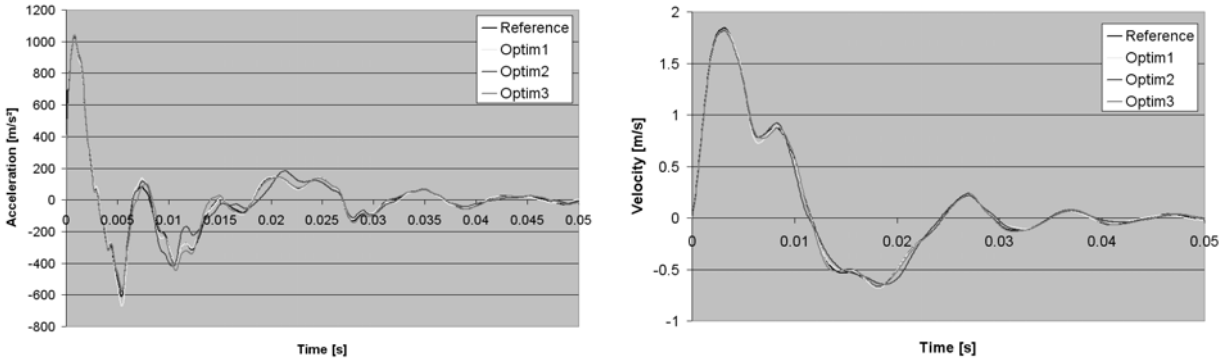

Figure IV-26 : Validation of the back-analysis procedure – comparison of the measured and calculated acceleration and velocity curves

The velocity traces are also well modelled. The trace related to the 2nd optimisation is still the worst.

Figure IV-28 to Figure IV-32 display the result of the back-analysis in terms of parameter profiles after the optimisation stages. Figure IV-28 and Figure IV-29 present the ultimate and the maximum reached static shear stresses obtained. Figure IV-31 shows the integration of the soil reaction along the pile shaft plus the base static soil reaction. Finally Figure IV-30 gives the detail of the reached maximum vertical stress at pile base for each optimisation process and the ultimate value obtained and Figure IV-32 gives the ratio in % of the maximum shaft friction reaction and total soil reaction with the corresponding reference.

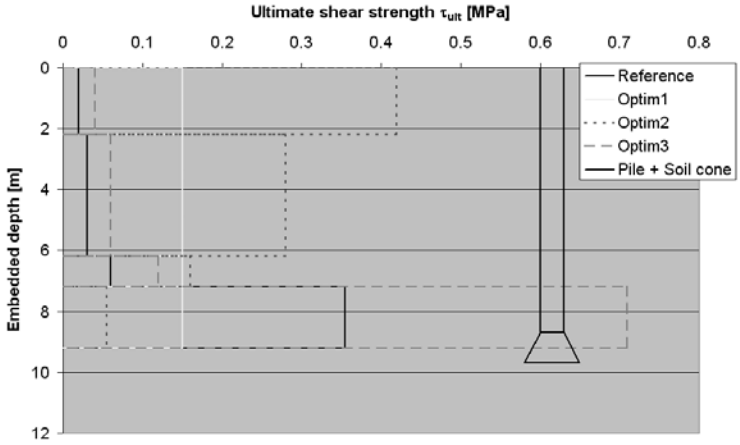

Figure IV-27 : Ultimate shear strength initial profiles

The profiles are displayed with reference to a Prefab pile from Limelette. The only embedded part of the pile (without excavation) is represented.

The profiles of ultimate shear resistances (Figure IV-28) present a mutual general profile and variable discrete values. Taking into account that the input profiles were very well differentiated, the global shape of each result present an evident similarity with the reference, which is an extremely good result. The soil profile remains unchanged (a weaker soil layer along almost the all pile and a stronger layer close to the base: this profile is noted “reference” on Figure IV-28) and can be determined from a dynamic load test with the back analysis process. On the other hand, the net values are rather variable:

the ultimate shear resistances of the strongest soil layer vary from 0.29 to 0.46 MPa. The thickness of the layers is also quite different. The thicker the strongest layer, the less resistant the corresponding ultimate shear stress.

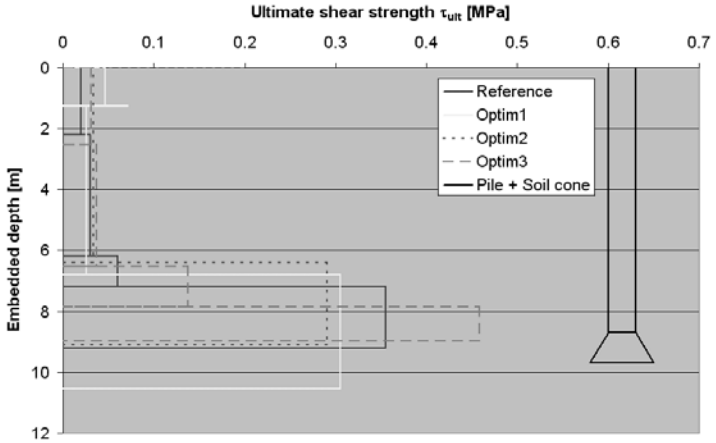

Figure IV-28 : Ultimate shear strength profiles

Most of the soil layers, especially along the pile shaft, are fully mobilized during the pile loading. But this is not the case for the base resistance and the strongest soil layer because the displacement imposed is not sufficient. Figure IV-29 presents the maximum shear stress reached for each pile element during optimisation. As expected, the weakest zone completely mobilizes the soil resistance and the last layer presents smaller values of soil reaction than their ultimate corresponding. However, a difference remains between the optimisations, what is relatively problematic within the framework of the static load-settlement relationship (max stresses reached vary from 0.23 to 0.42 MPa) even if the corresponding thickness seems to be inversely correlated to this variation.

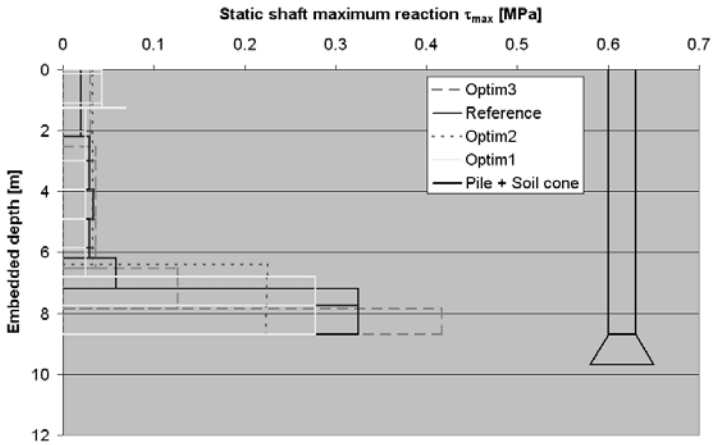

Figure IV-29 : Maximum shaft friction τ_{max} profiles

Figure IV-30 present the maximum reached vertical stress at pile base and the values of the ultimate vertical stress obtained with the back-analysis. optim1 and optim3, which have started from a higher value than the reference one (for both ultimate and maximum values) are very close to the reference result. On the other hand, the 2nd optimisation is inferior for both maximum and ultimate values. This corresponds to the worst quality of this matching process seen on the signals traces (Figure IV-26).

Moreover, the two remaining trials have an ultimate base resistance superior but not excessively. These observations may indicate that the base ultimate resistance must be set superior to the estimated one in order to have a correct evaluation and that the ultimate values are of importance but the max values reached during the test are more important. This is confirmed by Figure IV-31.

	Ultimate static base resistance σ_{ult} [MPa]
Reference	5
Optim 1	13
Optim 2	1.4
Optim 3	10

Table IV-1 : Ultimate base strength values

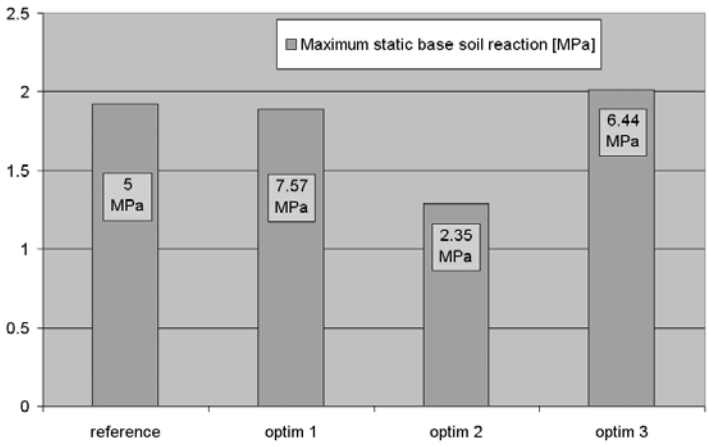

Figure IV-30 : Maximum vertical static stress

Since a balance may exist between the thickness and the maximum shear stress reached for each optimisation, it seems to be evident to integrate the reached stresses along the pile shaft plus the base mobilization and to compare the four results with respect to depth (Figure IV-31). The comparison and the results are remarkable. The curves present the same behaviour, quickly modelled by an addition of two straight lines defining two types of soils. The depth of change is also conserved (about 7 m).

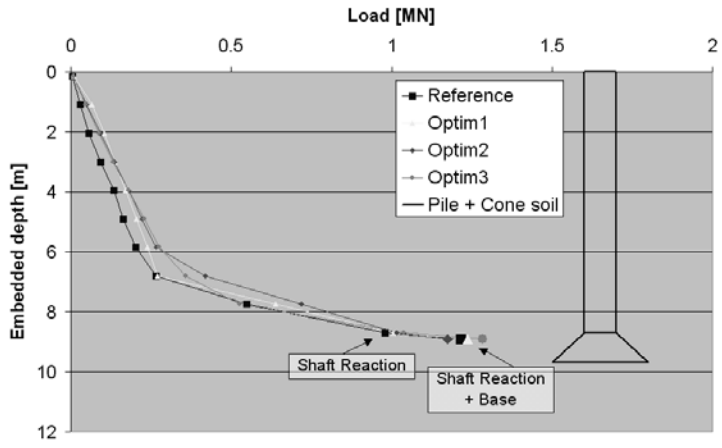

Figure IV-31 : Cumulated load along shaft + base

These results confirm the fact that the most important in the modelling and the back calculation is not the ultimate stress, neither their maximum reached stress but the all resistance in function of the depth along and beneath the pile. Only the profile of the second optimisation seems to be slightly different by a start of the strong soil layer a few earlier than the other cases. This is probably to compensate the lack of resistance coming from the base at the start of the optimisation. This fact highlights the importance of the quality of the initial Input in value and profile.

This result is extremely good. The final results of the back-analysis evaluate the same soil reaction along the pile depth even if the input characterizations are rather different. Figure IV-32 presents the ratio of loads for both shaft and total details with the corresponding reference. The results are very close to the reference one. Only the influence of the weakest base of the 2nd trial causes a small difference.

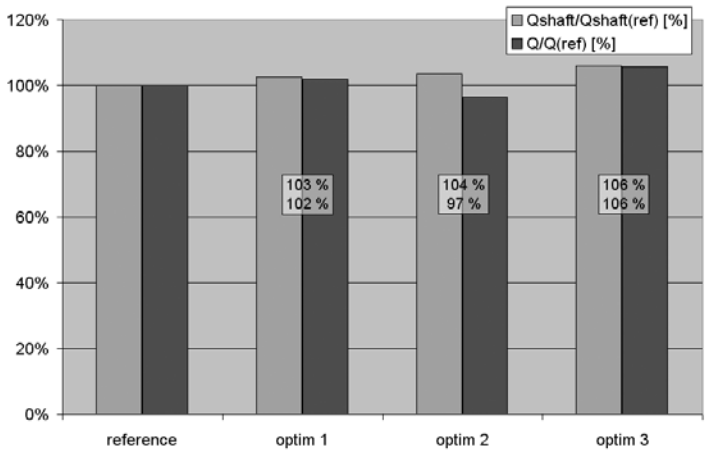

Figure IV-32 : Evaluation of the shaft and total soil reaction compared to the reference (in %)

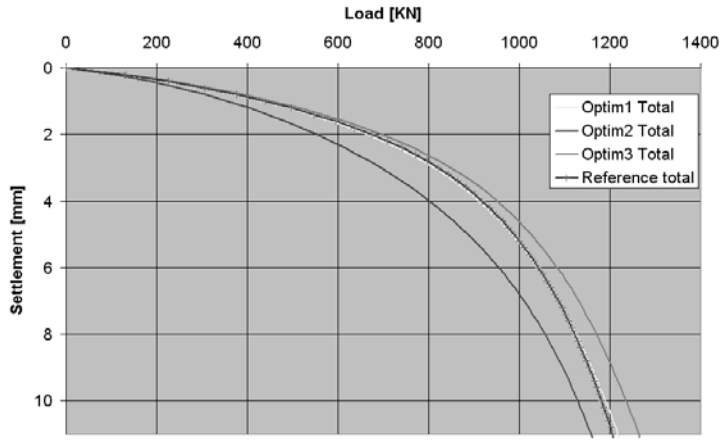

Figure IV-33 : Simulated static load-settlement curves

Finally, Figure IV-33 displays the simulations of the static load-settlement curves until the depth of the maximum settlement reached during the test. It can be seen that optim1 is almost perfectly superimposed to the reference simulation and optim3 is slightly overestimated (but not significantly). The most pronounced difference is seen with the 2nd optimisation due to the weakest base soil reaction. For the others, the curves are remarkably grouped.

This result allows one to conclude that the back-analysis process is globally reliable in the total soil reaction mobilized point of view. The ultimate resistance evaluated must be taken into account with interest in order to assess of the global evolution of the profile but there is a balance occurring between the thickness of each layer, their ultimate resistance and the maximum reached resistance in order to balance the total mobilized reaction that seems correspond to a invariant amongst the results of the three back-analysis. Moreover, the strict result of the matching procedure is a needed condition to have a good back-analysis process but not a sufficient condition.

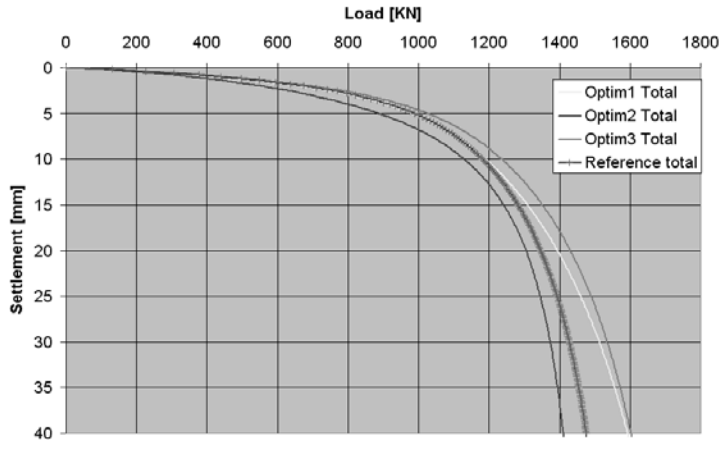

Figure IV-34 : Simulated static load-settlement curves

Another test is needed to confirm the good result of a successful matching between dynamic curves. For example the profile obtained must be correlated with an external source of information (geotechnical, …).Finally the simulated curves are valid for the only settlement mobilized during the dynamic test. If larger settlements are taking into account, the mobilization of the base is completely estimated and not checked out by comparison with measured data. That causes a more spread out result (Figure IV-34).

4. Sensitivity of the result to a parameter variation

4.1. Sensitivity analysis and representation of the matching quality

It is known that the solution of the inverse problem is never unique due to the measurement noise and modelling inaccuracies (Berzi, 1996). It just has been observed in the previous section that the back-calculated values of the parameters can vary following a certain combination of each other allowing to obtain a given matching quality. Instead of having discrete and inalienable parameters values from signal matching, the optimisation result is more a combination of the whole parameters representing a cloud within the n-space of parameters.

Some of the parameters are more influential than others. The same percentage of variation does not influence the signal matching result with the same magnitude. That determines the shape of the cloud in the n-space. The size of this cloud is determined by the required precision in the matching procedure. Finally the precision required for the parameters to ensure a certain accuracy in the matching procedure influences subsequently the simulation of the static loading procedure. Consequently, it is important to characterize this variation in order to qualify the influence of each parameter and the influence of each category of parameters on the matching process and on the simulation of the static load-settlement curve.

The method used to investigate the influence of the variability of each parameter or its sensitivity is based on the *multidimensional parameter perturbation sensitivity analysis* (Berzi, 1996) (see section 3.3). The point of which the neighbourhood is investigated remains constant and is the optimal solution **p***. The exploration is made randomly in the n-space R^n only defined by the radius Δ.

The modifications of the parameters p_i follow the same process than in Equ. IV- 13 & Equ. IV- 14.

The pile/soil response is evaluated with D**(p)** and each combination of parameter values $\mathbf{p_i}$ is associated with the corresponding D(p).

Δ	N
0.8	600
0.7	600
0.6	500
0.5	500
0.4	400
0.3	400
0.2	300
0.1	200
0.05	100

Table IV-2 : Sensitivity analysis

Generally, the point environment is investigated with successive and decreasing values of Δ. The values of Δ and the number of generated vectors are selected so that the size of the statistical sample is suitable for analysis. Table IV-2 summarises the advised size of the samples needed with respect to the radius Δ.

The results can be expressed in several forms. The classical representation of the sensitivity analysis is given by the variation of D(p) in function of the variation of one parameter.

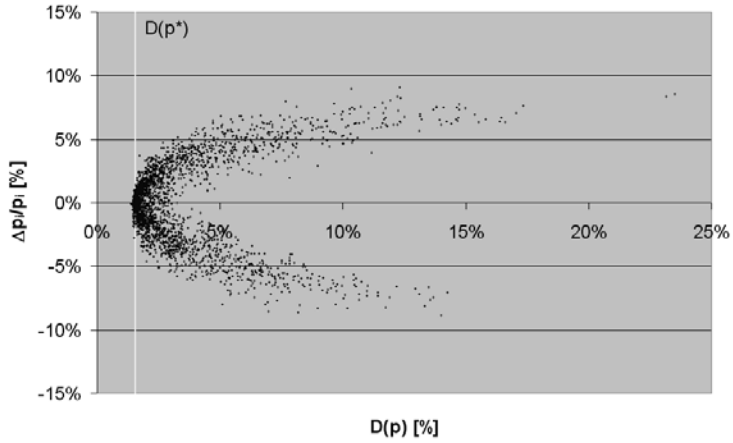

Figure IV-35 : Variation of D(p) vs. the variation of an influent parameter

Figure IV-35 to Figure IV-37 represent the variation of the matching quality factor D(p) with respect to the imposed variation of one parameter ($\frac{\Delta p}{p}$).

The analysis presented in the following figures is based on the result of the optimisation of the 13th blow of the pile B9 of Limelette. The result of the optimisation give a result of D(p) of about 1.57% (the minimum value is marked with a vertical line on the figures). The sensitivity analysis has been performed using the radius Δ of 5, 10, 25, 50, 65, 80 and 90 %. The analysis was applied on 25 parameters and based on a total of 2900 generated points. A lot of points are located in the close vicinity of the matching optimum: 273 combinations (9.4%) give a better matching and more than 40% of the combinations represent a matching inferior to 2%.

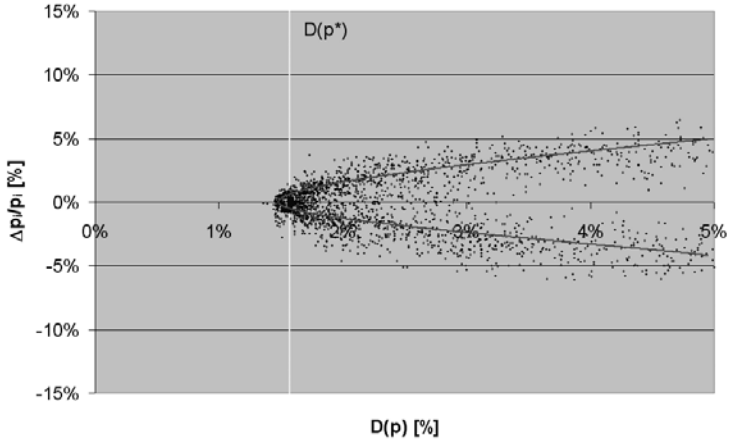

Figure IV-36 : Variation of D(p) vs. the variation of an influent parameter (Zoom)

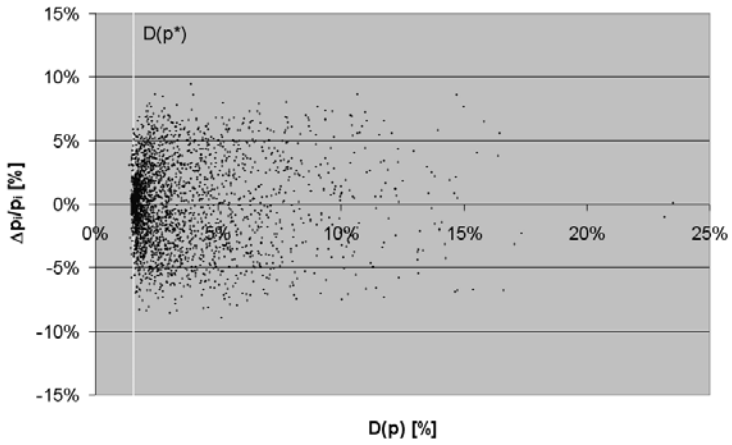

Figure IV-37 : Variation of D(p) vs. the variation of a non-influent parameter

Figure IV-35 and Figure IV-36 present the classical representation of an influent parameter and Figure IV-37 the typical cloud observable for a less influent parameter. The parabolic form highlighted by the line on Figure IV-36 marks the behaviour of an influent parameter on the matching quality. When this parameter moves away from its optimal position, either due to an increase or a reduction, there is a direct influence on the matching quality, the value of D(p) increases. Obviously, the match quality depends on the combination formed by the other parameters. On the other hand, Figure IV-37 displays the classical behaviour of a non influent or less influent parameter. It consists of a cloud with no clear trend. Most of the points are located close to the initial state (no variation, $\Delta p_i/p_i = 0$) and in the close vicinity of D(p*). That means that the current value is close to an optimised value and if the parameter is not too much modified, the matching remains in a range of good quality. Nevertheless, the lack of trend in the cloud of point indicates a poor influence of this parameter or its smaller influence compared to another parameter (like the preceding one).

For the analysis of the n parameters, only the most influent (often only one) governs the general quality of the matching. That means that only one or a few parameters presents a shape comparable to Figure IV-35 and Figure IV-36. Sometimes, when the optimisation is not completely done yet, the influent parameters display a general trend which is not a parabola centred on $\Delta p_i/p_i = 0$ but it can be a trend tending to the correct value of p_i. This trend could be linear or almost linear (Figure IV-38). Generally, when this case is observed, there is about half the total number of combinations that improve the matching quality. Figure IV-38 presents about 48% of the points enhancing D(p).

In conclusion, the parabola denotes an influent parameter close to its equilibrium position or optimised value. A straight line expresses a trend to be followed by an influent parameter and the cloud of points express a lack of relationships between the parameter variation and the matching fitting or the existence of a more influent parameter in the same sensitivity analysis.

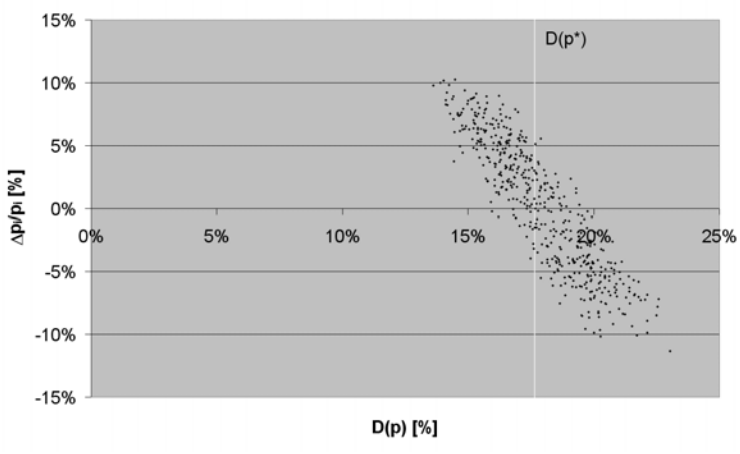

Figure IV-38: Variation of D(p) vs. the variation of a influent parameter

The variation of either the matching quality criterion or the variation of the sole parameters can be confronted with an another quantity linked to the main purpose of the analysis.

These quantities could be:

- The ultimate state of the soil reaction mobilized along and beneath the pile (Figure IV-39);
- The load corresponding to a given settlement (Figure IV-40);
- The settlement corresponding to a given applied load;
- The secant stiffness of the simulated load settlement curve for a given load or displacement;
- Other quantity depending of the parameters studied.

Figure IV-39 and Figure IV-40 present two possibilities of these combinations: the variation of the ultimate soil reaction expressed as a function of the matching quality factor and the evolution of the load corresponding to a settlement of 15 mm as a function of the variation of a parameter of the model

The calculation of the load for a given settlement and inversely, the calculation of the settlement for a given load are two algorithms developed by the author and allowing to know a particular point of the static load-settlement curve without the construction of all the curve.

When the matching quality factor is close to its minimum and the set of parameters is in the area of its optimum, Figure IV-39 and Figure IV-40 look like a parabola.

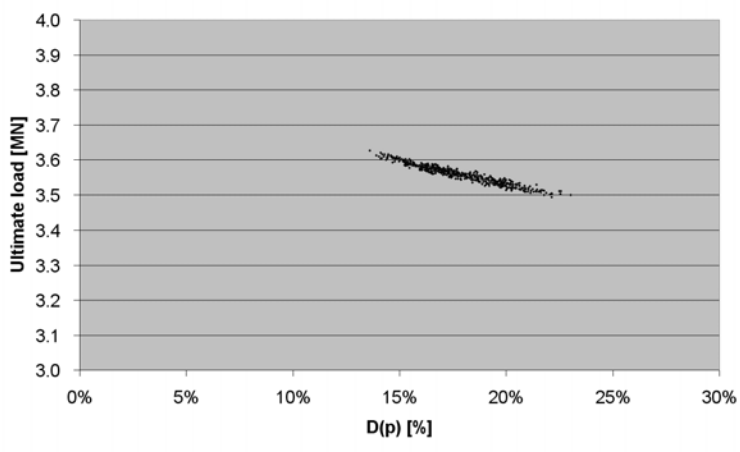

Figure IV-39 : Variation of the estimated ultimate pile capacity vs. the matching quality factor D(p)

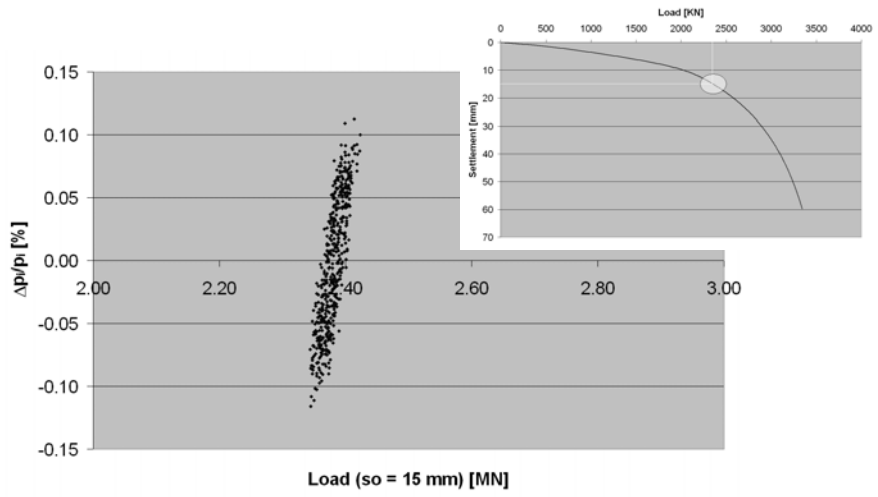

Figure IV-40: Variation of an influent parameter vs. the load corresponding to a head settlement of 15 mm.

4.2. Classification of the parameters due to their relative influence

Since all the parameters influence differently the pile/soil response, and since the most influential parameters lead the optimisation process, it is important to identify the weight of each parameter on the matching process in order to select them correctly and to find out the best solution for each of them. After a complete analysis of real cases from Sint-Katelijne-Waver and Limelette, it appears that the most influential parameters are characterized by a parabolic cloud of generated points similarly to Figure IV-36 and that the others parameters do not show a particular trend like on Figure IV-37. Figure IV-41 to Figure IV-44 present the results of clayey and sandy sites for both influent and non-influent parameters.

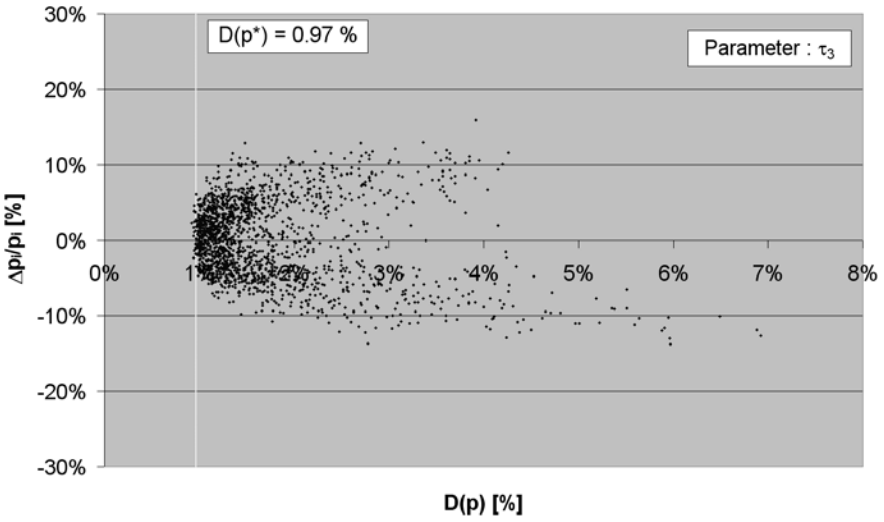

Figure IV-41: Variation of the parameter τ_3 (ultimate strength of the 3rd layer) vs. the matching quality factor D(p) – clayey site

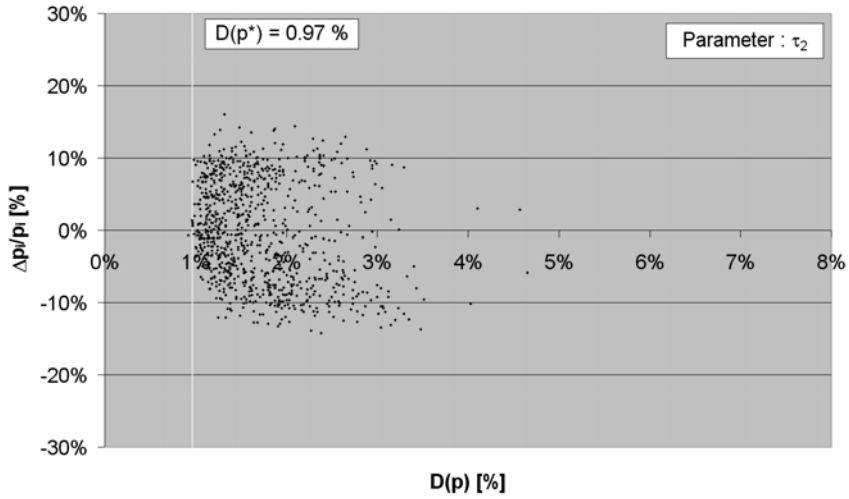

Figure V-42: Variation of the parameter τ_2 (ultimate strength of the 2nd layer) vs. the matching quality factor D(p) – clayey site

The consequence of this influence is a good optimisation of the concerned parameters (the most influential) and a poor optimisation of the others parameters. The less influential parameters remain almost unchanged after processing.

Nevertheless, it is possible to improve their optimisation by retrieving the most influential parameters and by launching a new optimisation process on the remaining parameters. A new balance between parameters is performed and a classification can be done based on this hierarchy of influent parameters. A major consequence is that the less influent parameters, like the damping factors J_i at the base and along pile shaft, can be optimised.

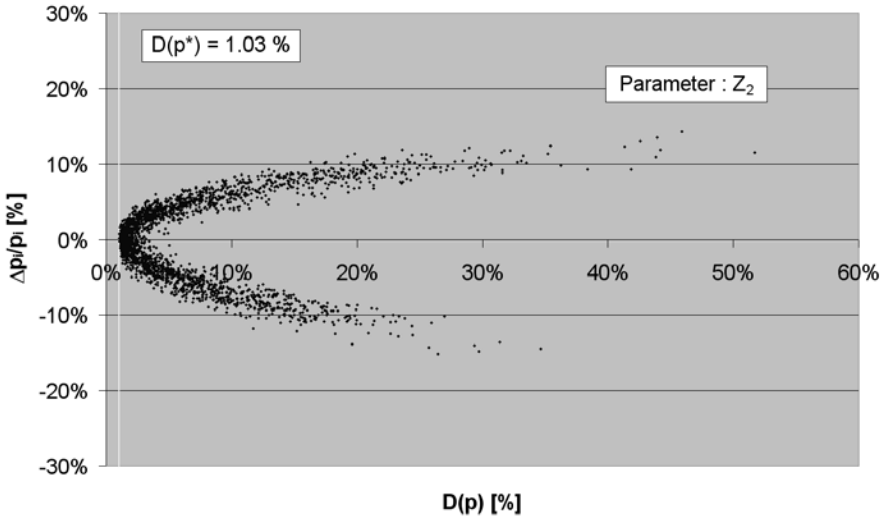

Figure IV-43: Variation of the parameter Z_2 (depth of the 2nd layer) vs. the matching quality factor D(p) – sandy site

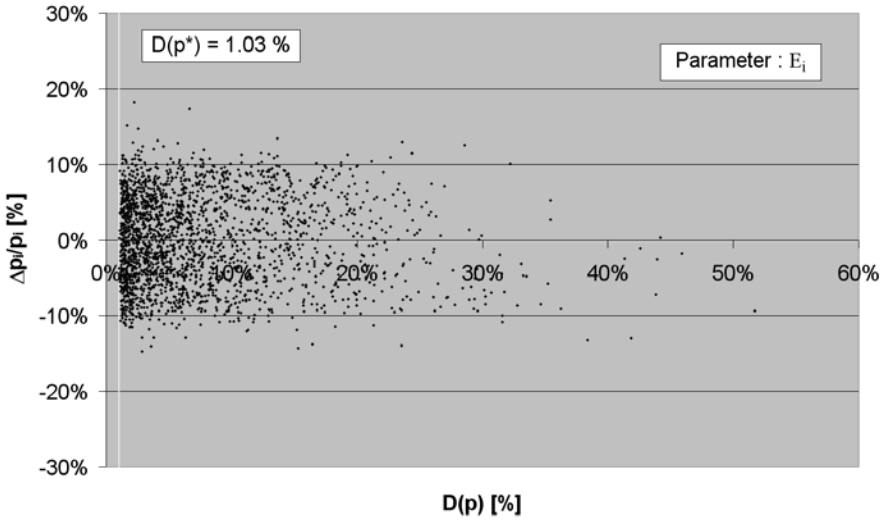

Figure IV-44: Variation of the parameter E_i (elastic modulus at the pile base) vs. the matching quality factor D(p) – sandy site

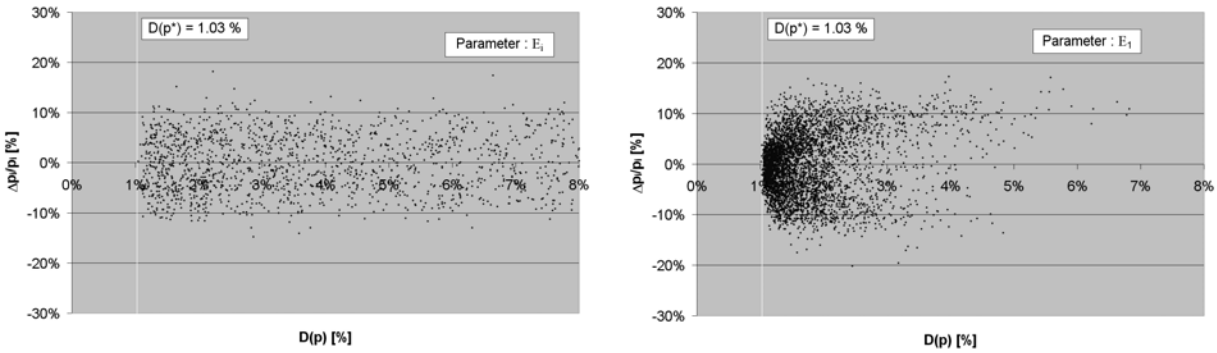

Figure IV-45: Comparison of the variability of E_i with and without a more influential parameter – sandy site

Figure IV-45 highlights the hierarchy existing between the parameters through their relative influence on the pile/soil response. Both figures show the analysis of the same parameter with and without a most influent parameter. the left figure presents a cloud without trend, the right figure highlights the influence and allow to refine its optimisation.

Despite the large influence of some of the parameters (principally the parameters linked to the static soil resistance like the thickness of the shaft layers or the ultimate strength of the shaft layers), it is possible to perform an optimisation on all the pile/soil model parameters, even the less influential like the rheological ones.

Figure IV-46 and Figure IV-47 present similar figures where the same parameter is shown with and without the influence of a more influential parameter. This allows the discernment of an optimised value.

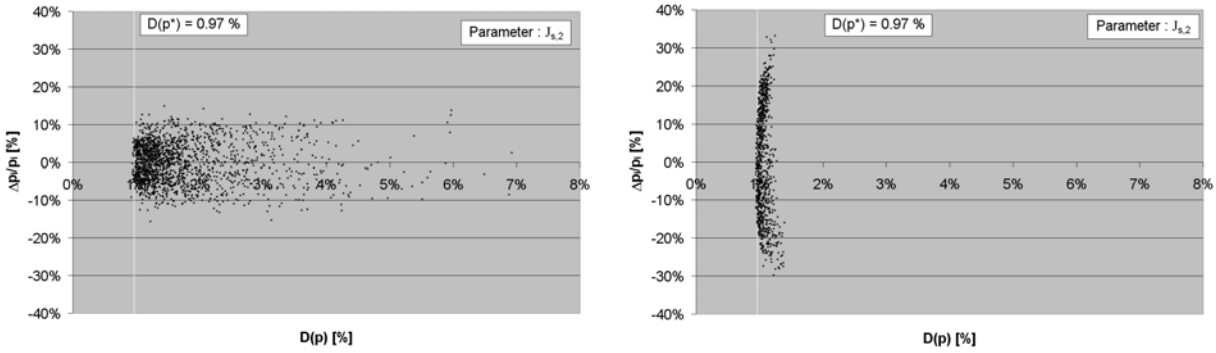

Figure IV-46: Comparison of the variability of $J_{s,2}$ (shaft damping factor of the 2nd layer) with and without a more influential parameter – clayey site

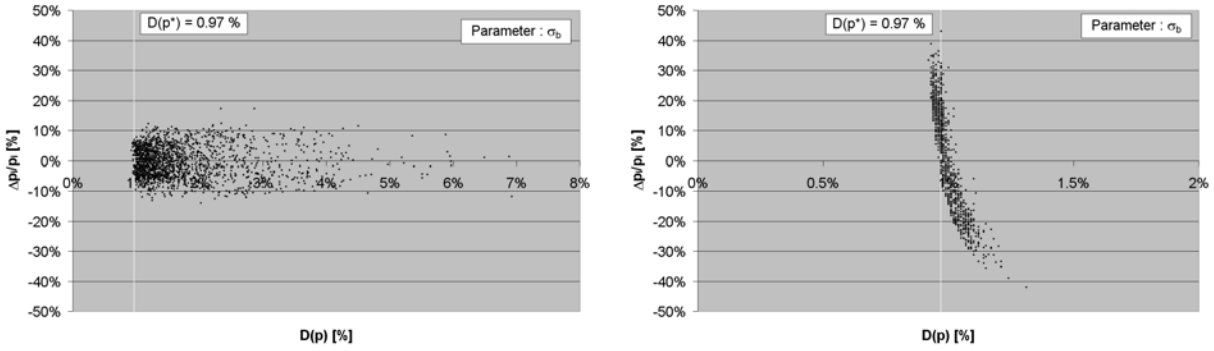

Figure IV-47: Comparison of the variability of σ_b (ultimate vertical stress at the pile base) with and without a more influential parameter – clayey site

5. Results of the back-analysis on real measurements

In order to illustrate the back-analysis process, the dynamic tests performed on the two sites are analysed. A complete set of DLT blows has been analysed for each type of soil and the results are displayed in the two next sections. One for the Sint-Katelijne-Waver (Boom clay) and one for Limelette (Bruxellian sand).

5.1. Analysis of the dynamic tests from Sint-Katelijne-Waver

The tests analysed are those already studied in chapter 3. It concerns the long prefabricated pile A7 described in detail in section 3 of chapter 3. The pile is 13 m long and its embedded part is 10.9 m long. The base is located at 11.63 m of depth.

The modelled pile is decomposed in 10 elements, the pile modulus of elasticity is fixed to 38000 MPa (c = 3940 m/s) and the surrounding soil is described by the input set of parameters (Figure IV-9 to Figure IV-11). The exponents N of the velocity dependent power laws are fixed to 0.2 for the shaft and 1 for the base according to the results obtained in literature. These values are not optimised and remain fixed during all the process. The ratio of shear modulus G_2/G_i describing the unloading is fixed to 1 and authorized to be optimised. The input set of parameters is the same for each analysis. Each blow is considered as an independent study.

The pile A7 was tested twice with about one year of delay between the testing campaigns. The first has been carried out in 1999 and the second in 2000. As it was described in section 3.3 of the chapter 3, only the first blows of the second campaign are valid because of an extreme eccentricity. But the blows of both campaigns are similar with no pronounced difference. Since the first blows of the 2000's campaign were very weak (0.2 m to 0.6 m of drop height) the three first blows analysed come from this campaign, they are called A7b-00i. After, tests of the 1999's campaign with higher drop heights are analysed (called A7-00i). Table IV-3 informs of the chosen blows, of the drop heights and of the maximum and permanent settlements reached during each blow according to the analysis of the acceleration measurements at the pile top (more details in section 3.3 of chapter 3). There are 6 blows from 0.2 m to 1.6 m.

	Drop Height [m]	Max Settlement [m]	Perm Settlement [m]
A7b-001	0.2 m	0.0021 m	0.0001 m
A7b-002	0.4 m	0.0039 m	0.0002 m
A7b-003	0.6 m	0.0052 m	0.0003 m
A7-002	0.8 m	0.0062 m	0.0012 m
A7-003	1.2 m	0.0086 m	0.0027 m
A7-006	1.6 m	0.0109 m	0.0039 m

Table IV-3: Summary of the analysed blows and of the reached settlements.

The back analysis is processed by the automatic algorithm proposed in this research. The matching procedure is performed by optimisation of all the parameters in the same time: since it is possible to refine the optimisation procedure to a certain number of parameters, Table IV-4 lists about the concerned parameters: 16 parameters.

Shaft (x 3 layers) :	$\tau_{ult,i}$	z_i	G_i	Js_i	G_2/G_1
Base 1 layer :	$\sigma_{ult,i}$	E_i	Jb_i		

Table IV-4: List of optimised parameters

The optimisation procedure start with a radius Δ of 90%, there are 10 reductions authorized and the last radius analysed is 5%. The number of iterations/radius without improvement of the matching quality factor D(p) is fixed to 100. The matching is processed on a duration of 15L/c which is sufficient for the tests in clay because of the dampening of the soil.

Table IV-5 presents the results of the matching procedure. D(p) is listed in %. This value is the sum of the weighted and averaged distance between the measured and calculated curves of force and velocity (Equ. IV- 2 and Equ. IV- 3). It can be seen that the quality decreases with the drop height.

	Matching factor D(p) [%]	Max inferred base settlement [m]	Difference max settlements pile top & base [m]
A7-001b	0.61 %	0.0007 m	0.0014 m
A7-002b	0.79 %	0.002 m	0.0019 m
A7-003b	0.98 %	0.0033 m	0.0019 m
A7-002	0.64 %	0.0045 m	0.0017 m
A7-003	1.06 %	0.0069 m	0.0017 m
A7-006	1.66 %	0.0092 m	0.0017 m

Table IV-5 : Results of the matching procedure (matching quality factor D(p)) and maximum base settlement obtained for each test.

Figure IV-48 to Figure IV-53 display the result of the matching procedure in terms of force-settlement curves. The measured one (Force measured – Set calculated) is compared to both calculated: "Force measured – Set calculated" or "Force calculated – Set measured". The quality is remarkable and the matching is successful for all blows. Nevertheless, it can be pointed out that the calculated settlement curves (based on the force signal as input) fit much better with the reference curve than the calculated force curves (based on the settlement as input). This trend increases with the height of drop and corresponds to the wave return after reflection at the pile base. The final maximum and final settlement are conserved. The energy (integration of the curve) is also well fitted. The matching is performed until stabilisation of the pile.

Figure IV-54 exhibits three couples of velocity curves: each couple includes the measured and the calculated curves of the blow #b001, b003 and 006. The agreement is perfect for the tests with small drop height (#b001, b003), and the agreement is less perfect with the more energetic blow, the second peak of velocity is particularly difficult to be modelled where this peak is almost missing in the two others curves. Since this second peak is a consequence of the wave propagation and especially the reflection of the wave at the pile base and free top, it must be correlated.

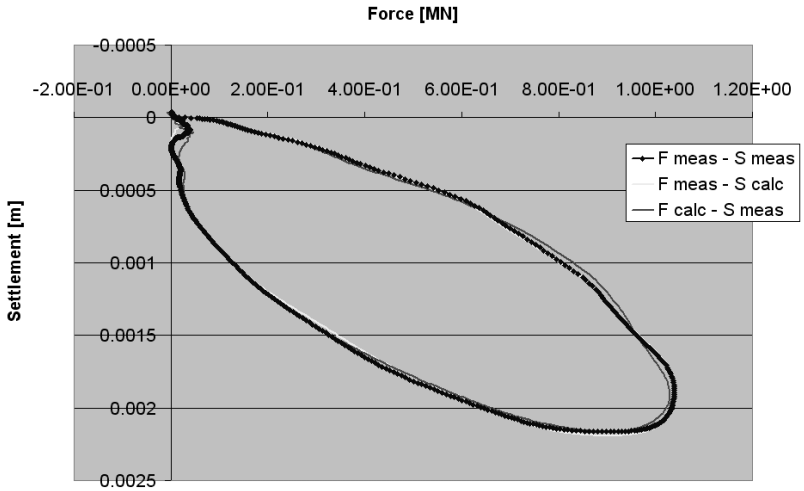

Figure IV-48 : Force-settlement curves (measured, and optimised (2 curves)) – blow A7b-001/ 0.2 m.

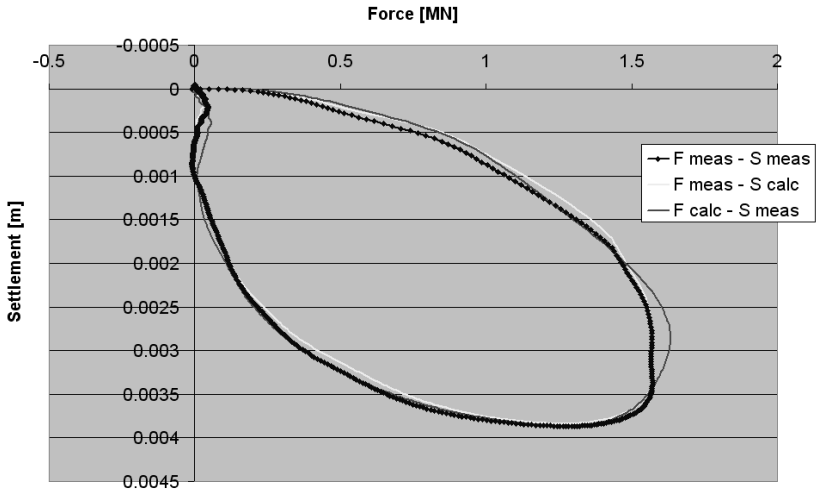

Figure IV-49 : Force-settlement curves (measured, and optimised (2 curves)) – blow A7b-002/ 0.4 m.

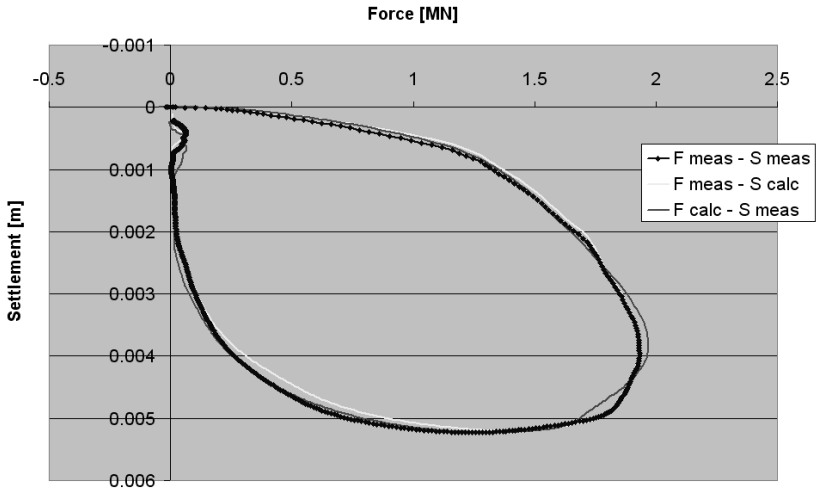

Figure IV-50 : Force-settlement curves (measured, and optimised (2 curves)) – blow A7b-003/ 0.6 m.

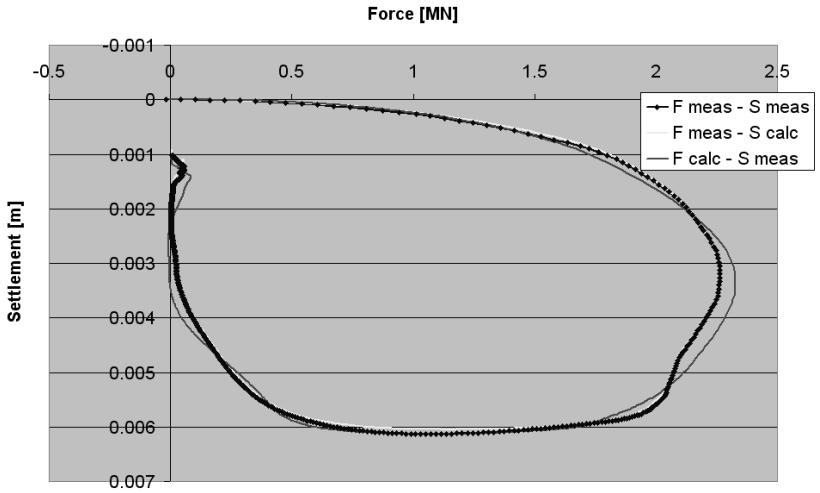

Figure IV-51 : Force-settlement curves (measured, and optimised (2 curves)) – blow A7-002/ 0.8 m.

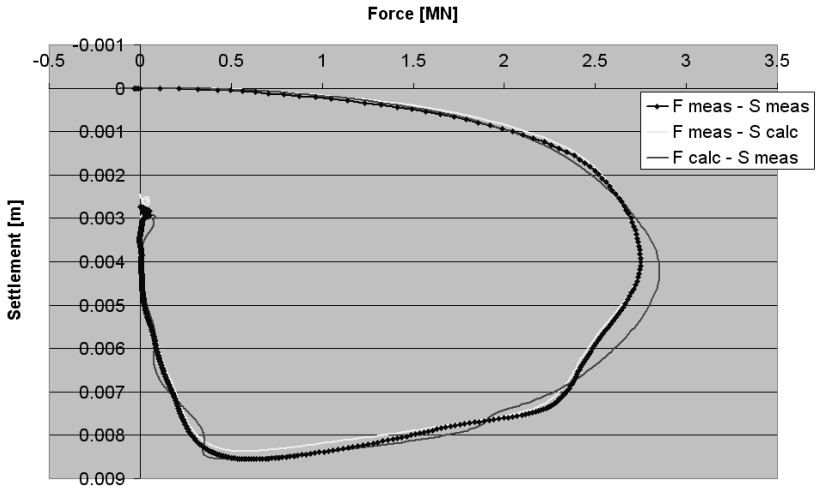

Figure IV-52 :Force-settlement curves (measured, and optimised (2 curves)) – blow A7-003/ 1.2 m.

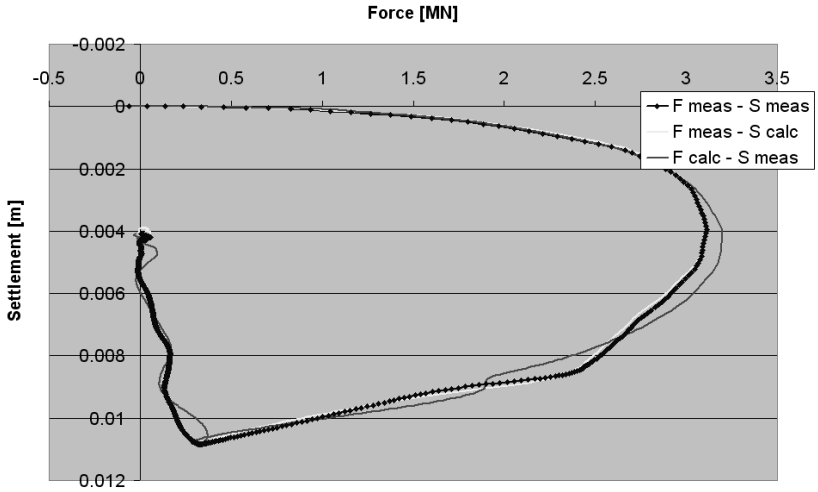

Figure IV-53 : Force-settlement curves (measured, and optimised (2 curves)) – blow A7-006/ 1.6 m.

The code allows to check the fundamental stress-displacement relationship mobilized for all pile elements by selecting one of them to observe the plot or by storing it. The behaviour of the last element close to the pile base was investigated and the maximum settlement of this last element is listed in Table IV-5 for each analysis. The maximum settlement increases with the drop height. Hence, the transfer of load to the base is also increasing. The total shortening of the pile is the difference between both maximum settlements and is listed in Table IV-5. It is seen that this shortening is constant for the three tests of the first campaign (002-003 & 006) and also constant for the two higher drops of the 2nd test campaign. this difference, even small, can correspond to a change in the pile/soil interaction system (distribution of load, or modification of the ultimate soil resistance, or stiffness). But the constancy of the shortening for all blows is also the mark of the constancy of the mobilization of the soil reaction along the pile shaft. It can be assumed that if the mobilized shaft reaction is constant, that means it could correspond to the ultimate one. More details are available with the integration of the reaction mobilized along the pile (Figure IV-69).

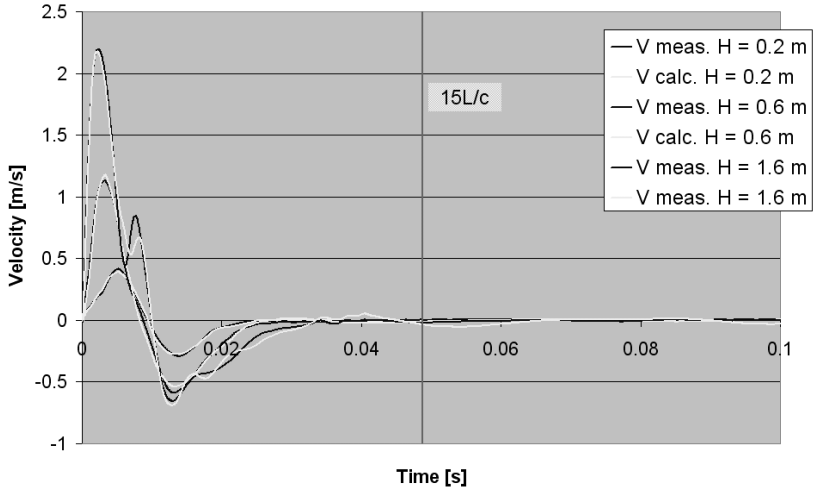

Figure IV-54 : Velocity curves (measured, and optimised) – blows A7b-001/ b-003 & 006

Before describing the distribution of the soil reaction along the pile shaft, most resistant part of the pile capacity for a pile in clay, Figure IV-55 presents a summary of the result of the base parameters optimisation. The histograms display 4 types of data, the height of drop being reminded for each blow:

- The maximum static stress reached at the base during the test σ_{max};
- The base damping factor J_b;
- The initial elastic modulus E_i;
- The ultimate vertical stress under the base, labelled in text box in the middle of the bars σ_{ult};

Trends, expected or not, can be highlighted.

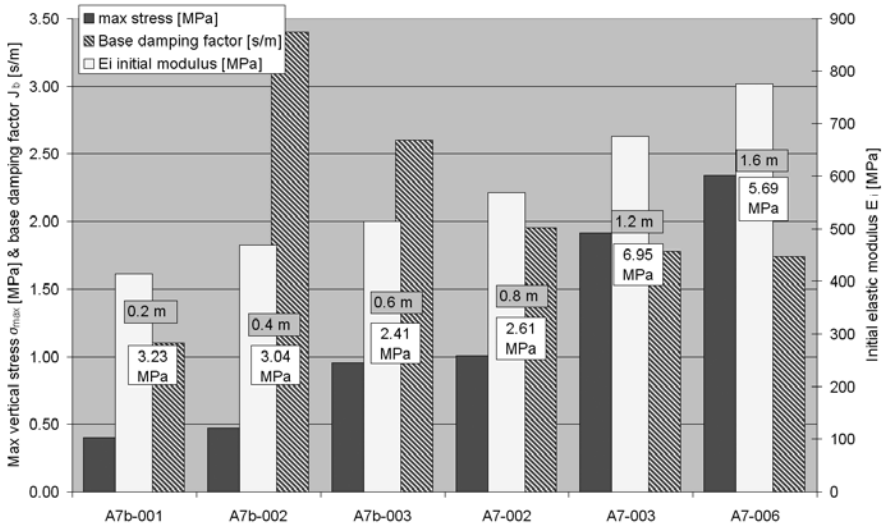

Figure IV-55 : Description of the base parameters after optimisation

The maximum stress σ_{max} reached increases with the drop height, as expected and denotes an increasing base mobilization but the corresponding ultimate value σ_{ult} increases as well what is not

wished. The base damping factor has no influence in the first test because the base is almost not mobilized by the load transmitted through the pile. The load is almost completely transmitted to the shaft (displacement of max 0.7 mm for the base for the blow A7b-001). But from the drop height of approximately 0.8 m, the sensitivity analysis of the base damping factor shows a pronounced trend of about 1.8..1.75 s/m which is stable and significant compared to the smallest drop height. It is remarkable tot see that the base damping factor decreases with the increasing drop height from a very high value (J_b = 3.4 s/m) to a stable one for large drop height. On the other hand, the initial elastic modulus has an upwards trend with the height of drop which can be linked to the stiffening of the soil.

The soil reaction along the pile shaft is summarized with all the data available:

- The profile of the local shear strength f_s measured with the CPT;
- The step profile introduced as input (in dashed lines) τ_{ult};
- The step profile of the ultimate shear strengths obtained after optimization τ_{ult};
- The step profile of the maximum reached shear stresses along the pile shaft τ_{max};
- The values of the initial shear modulus G_i for each soil layer;
- The value of the shaft damping factor J_s corresponding to each soil layers.

There is one figure per test (Figure IV-56 to Figure IV-63). In order to perform a global analysis, each figure is analysed individually and afterwards, the main remarks are summarized.

A7b-001: 0.2 m

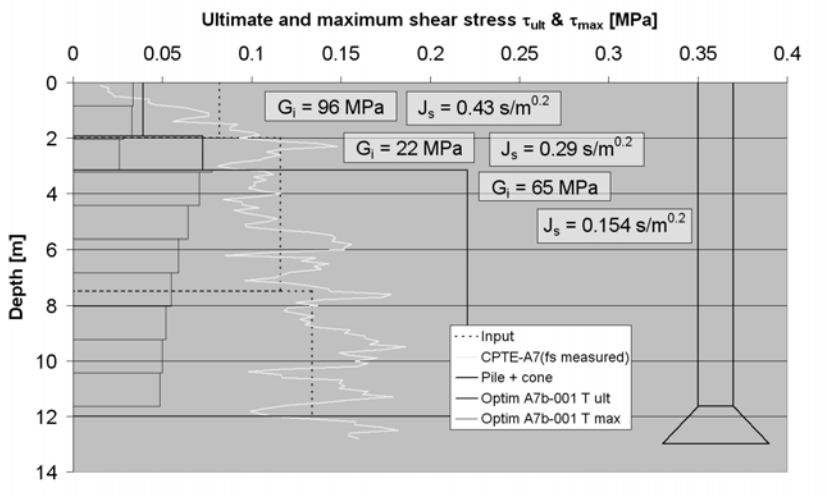

Figure IV-56: Summary of the parameters of the soil reaction along pile shaft for the blow A7b-001

Remarks:

- The ultimate profile optimised is rather different compared to the reference one but it is expected due to the small height of drop, the small settlement generated (0.2 m – 21 mm at the pile head – 0.7 mm at the pile toe) and the consecutive soil mobilization;

- The values of the shear modulus G_i are abnormal, especially for the 2nd and the 3rd layers. 22 and 65 MPa are not high enough;

- The profile of the maximum reached shear stress is increasing with the layers but decreasing with depth in the same layer. This is due to the shortening of the pile element and the reduction of the their respective motion; However, the small value of the second maximum reached stress is inferior to the first one; this is not correct and due to the low value of the shear modulus $G_{i,2}$;

- The levels of reached stresses are low compared to their corresponding ultimate values. This is a direct consequence of the small shear modulus and the reduction of the pile elements motion with depth;

- The values of J_s for the three layers can be characterised by a sensitivity analysis (Figure IV-57). Only the first damping factor has a significant influence on the matching quality (not necessarily an improvement, but a trend like those observed on Figure IV-35 and Figure IV-36). The two next ones do not mobilize their ultimate rheologic resistances, mainly because the level of velocity of each pile element is not sufficient to generate a radiation term of importance able to exceed the ultimate rheologic resistance. Since the maximum static reached stress of the first layer is close to its ultimate one, the failure occurs. The value of $J_{S,1}$ minimizing the matching quality factor is equal to 0.43 s/m$^{0.2}$ +/- 15%.

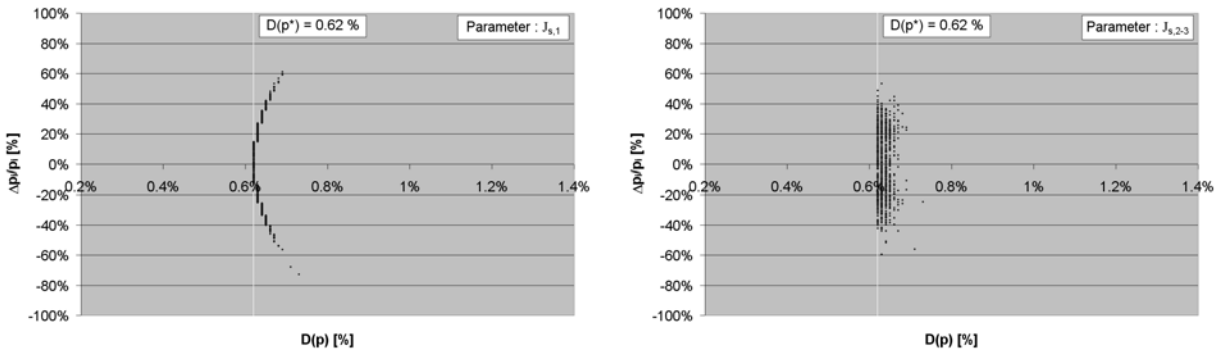

Figure IV-57 : Sensitivity analysis of the shaft damping factors $J_{s,I}$

A7b-002 : 0.4m

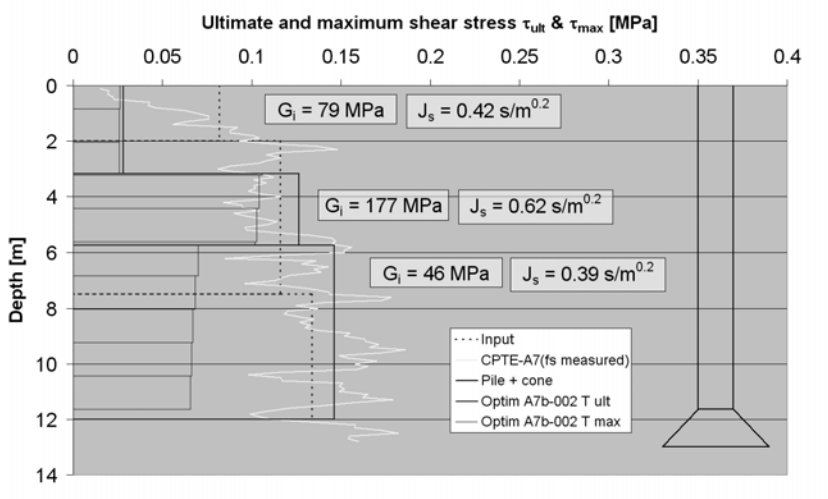

Figure IV-58 : Summary of the parameters of the soil reaction along pile shaft for the blow A7b-002

Remarks:

- The optimised ultimate shear stress profile is close to the CPT and the reference ones;
- On the other hand, the maximum reached values profile displays a decreasing trend with depth; this is not expected;
- The first layer of soil is fully mobilized in static, and also in dynamic. The shaft damping factors of the two first soil layers are both considered as influent on the matching quality criterion (Figure IV-59); $J_{S,1}$ and $J_{S,2}$ are fixed to 0.42 s/m$^{0.2}$ and 0.62 s/m$^{0.2}$ respectively. These values, and especially $J_{S,2}$ must be kept in mind for the future characterisation of the dynamic properties of the Boom clay.
- The profile of initial shear modulus G_i is still odd. The second layer is 4 times stiffer than the layer underneath. The stiffness evolution with depth is rather unusual and does not correspond to the reality.

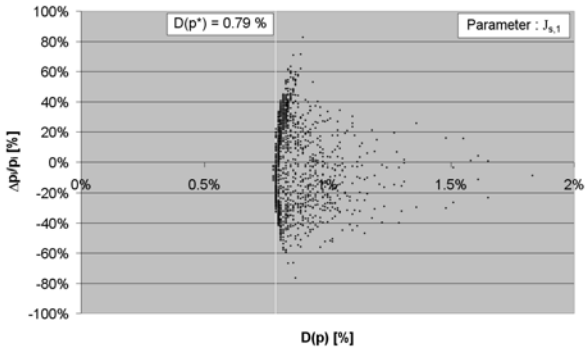

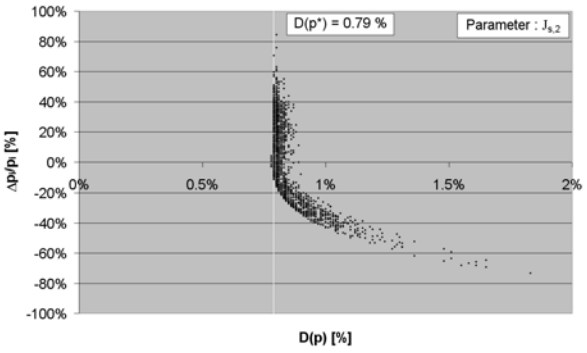

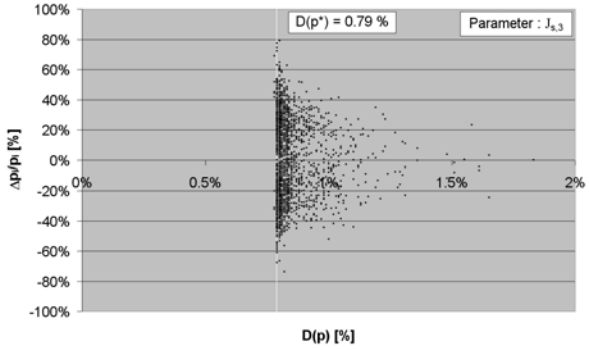

Figure IV-59 : Sensitivity analysis of the shaft damping factors Js,i

A7b-003: 0.6 m

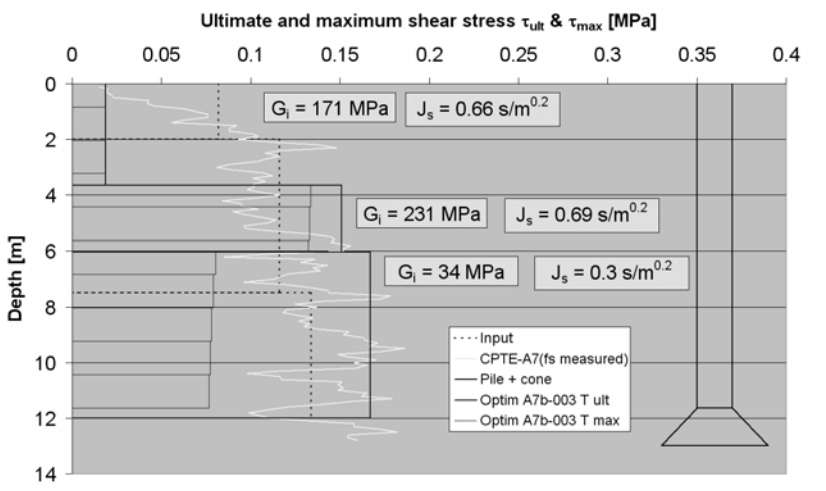

Figure IV-60 : Summary of the parameters of the soil reaction along pile shaft for the blow A7b-003

This analysis exhibits the same remarks than the previous ones:

- A good ultimate stress profile. But the first layer becomes more and more degraded;
- An illogical profile of stiffness with the lower value close to the pile base;
- A profile of maximum reached shear stresses also inverted;
- Values of shaft damping factors significant for the two first layers and insensitive for the third one (result obtained by means of a sensitive analysis similarly to Figure IV-59).

A7-002: 0.8 m

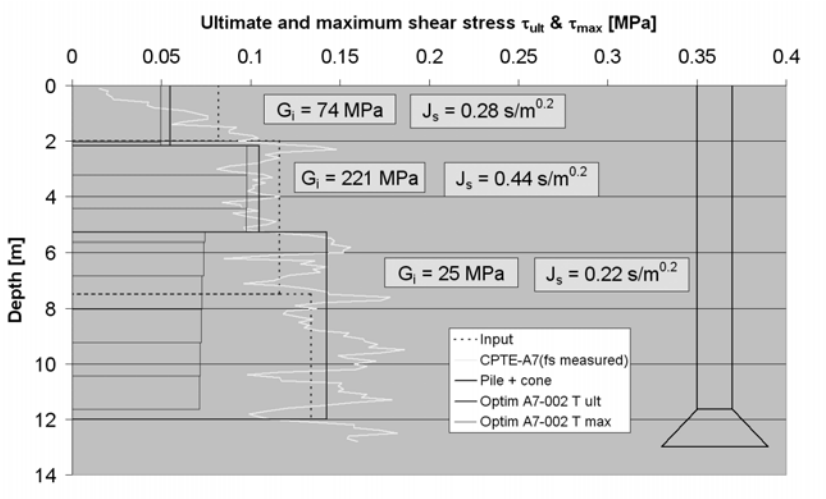

Figure IV-61 : Summary of the parameters of the soil reaction along pile shaft for the blow A7-002

The main results are similar to the previous ones. The 3rd layer starts to slightly influence the matching quality. This is due to the increasing velocity at the pile top and along the pile shaft. This increases the relative influence of the radiation damping in the rheologic stress evaluation. On the other hand, the 1st layer has less influence because of its small thickness compared to the pile length and the relative influence of the others layers.

A7-003 : 1.2 m and A7-006: 1.6 m

Still the same remarks with a smaller value of the shear modulus of the 3rd layer (14 and 15 MPa respectively).

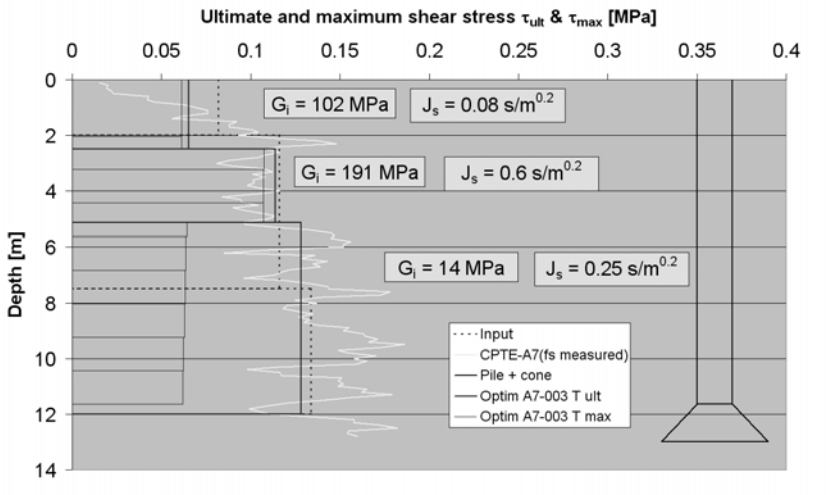

Figure IV-62 : Summary of the parameters of the soil reaction along pile shaft for the blow A7-003

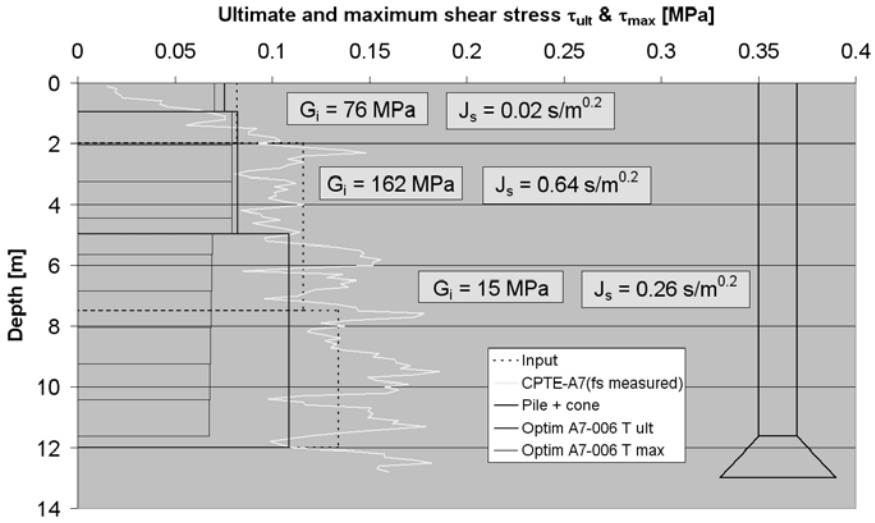

Figure IV-63 : Summary of the parameters of the soil reaction along pile shaft for the blow A7-006

Summary:

- The ultimate profile is remarkably close to the theoretical situation in the field but both maximum reached shear stress and shear modulus profiles are illogical and irrealist.

- The shaft damping factors are also remarkably stable through all the analysis performed. If only the second layer can be considered as reliable due to the expected values of shear resistance and shear modulus, the value of 0.6 $s/m^{0.2}$ can be representative of the site (including the pile, the soil type and the level of energy). Moreover, these values were refined after the first phase of optimisation by mean of a sensitivity analysis allowing a precise optimisation of a few number of parameters (Figure IV-57 and Figure IV-59). Nevertheless, the unusual profiles, the low values of G_i prevent to be categorical.

The ratio of shear modulus G_2/G_i [2] are listed for all the tests:

	G_2/G_i
A7-001b	0.64
A7-002b	0.29
A7-003b	0.25
A7-002	0.25
A7-003	0.28
A7-006	0.3

Table IV-6 : List of unloading shaft ratio G_2/G_i

These values are extremely small and do not support a physical behaviour, because of energy considerations.

The combination of the initial shear modulus, the ultimate shear stress, the ratio of shear modulus G_2/G_i and two hypotheses of the pile/soil model allow to bring some insight into the situation. These

[2] The quotient of the unloading initial shear modulus to the loading one. If the quotient is >1, the unloading is stiffer than the loading; the expected situation is a ratio > 1.

two hypothesis express that the ratio of shear modulus G_2/G_i is the same for all soil layers, and that the pile is moving into a fixed soil considered as motionless. Since the soil reaction is determined by its mobilization, the stress generated at the interface with the pile is determined by both relative displacement and velocity. Since the soil is motionless, the relative displacement becomes the pile displacement. There is no possibility of slippage, because the slippage is, by definition, the relative movement of a body with respect to another. So, the stress of a soil particle and the displacement of this soil particle are linked.

However, the pile motion is determined by the input condition (integration of the velocity of the pile head). There is also a force balance at the pile head between the external force (from the blow) and the internal forces (from the soil reaction). This balance acts at the pile top but also influences each node of the pile. Finally, since the pile is mechanically known (pile material elastic modulus, dimensions, stiffness,…), the pile top constraints are transmitted at each node (force and displacement) according to the local modifications (elastic shortenings,…). So the pile must globally respect a force equilibrium and a settlement balance corresponding to the input information. And, the soil must respect the same constraints.

The soil behaviour is characterized by its stress-displacement relationship. This relationship is function of 3 interconnected parameters[3]:

- The ultimate soil resistance;
- The initial shear or elastic modulus;
- The unloading ratio of shear or elastic moduli.

Since the pile displacement and then, the soil displacement is defined by the settlement balance at each node, since the reached stress is also defined by the force equilibrium, the only parameters variable in order to minimize the matching quality factor are the ratio of shear modulus, the initial shear modulus and the combination of the three parameters in order to keep constant the two conditions.

The pile element settlements during the blow A7-002 are plotted on Figure IV-64. All the elements follow the same trend led by the imposed signal at the pile head. The shortening of the pile and the progression of the wave into the pile are highlighted with the progression of the maximum settlement. The residual stresses generated along the pile shaft at the end of the blow are highlighted by the difference of permanent settlement of each pile's element. Those displacements are also the soil particle displacements at the interface. In order to ensure this displacement and the force equilibrium at each node during all the analysis duration, the variable parameters of the soil-displacement relationships are optimised[4]: the ultimate soil resistance and the initial stiffness for each soil layer, and the ratio of loading-unloading modulus. The result is given for two pile's elements on Figure IV-65 and Figure IV-66. The ratio G_2/G_1 is small and unphysical but imposed by the settlement and stress path conditions. If Figure IV-65 seems to be correct and representing an expected behaviour, on the

[3] In case of a hyperbolic or an elasto-plastic relationship.

[4] Plus the rheologic parameters

other hand, Figure IV-66 is completely illogic, especially during the unloading phase when the stress path goes over the loading stress path. That means that the unloading phase creates energy. This is physically impossible.

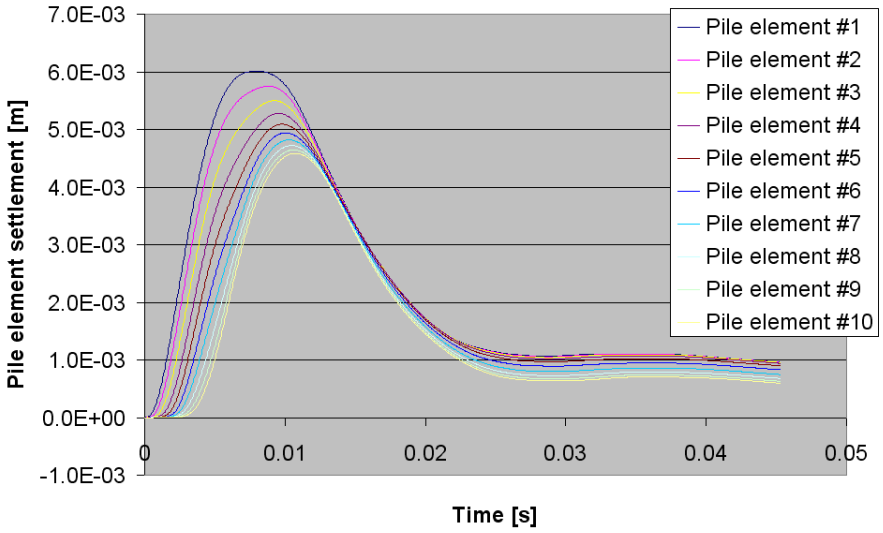

Figure IV-64 : pile's element settlement of A7-002

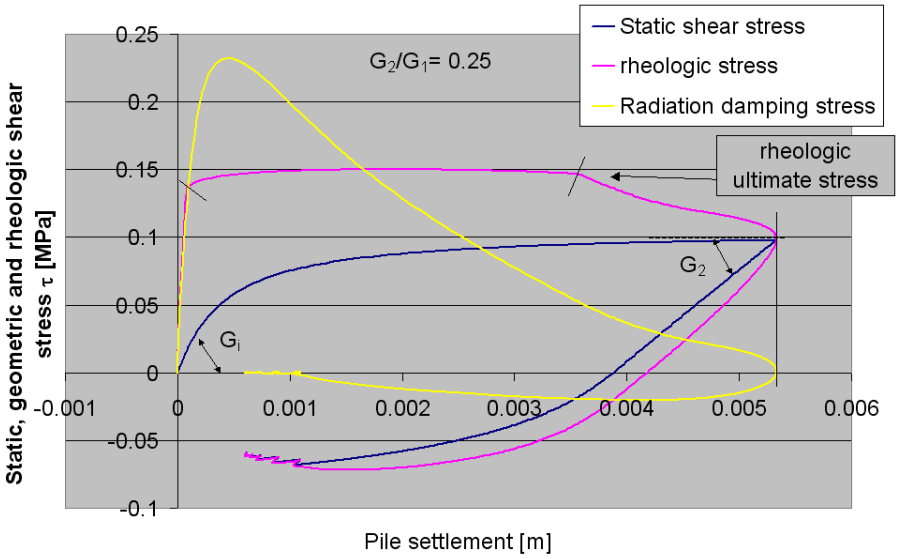

Figure IV-65: Detail of the soil reaction along the 4th element of the pile (blow A7-002)

The difference of behaviour is a result of the level of mobilization and the initial stiffness of the load-displacement curve.

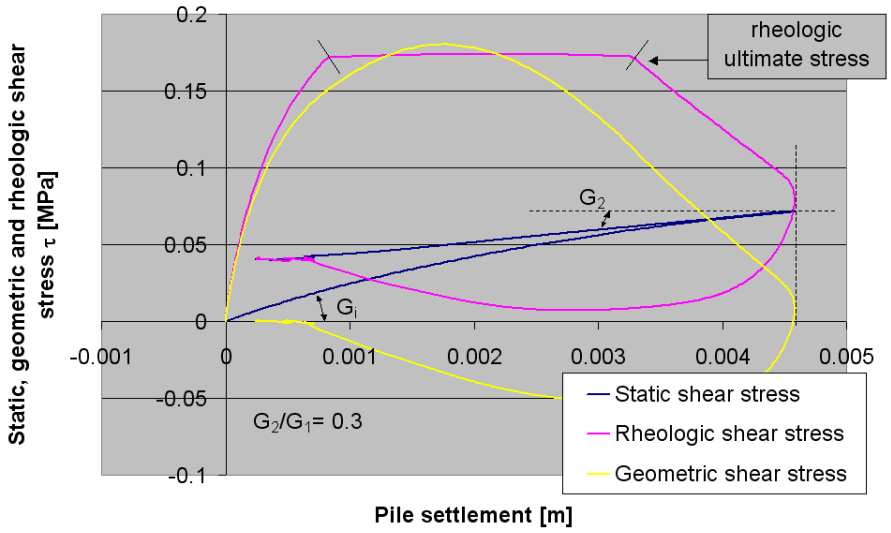

Figure IV-66: Detail of the soil reaction along the 13th element of the pile (blow A7-002)

If the initial shear modulus G_i are maintained fixed as given by the input, the optimisation gives a result where the ratio G_2/G_i is reduced to a very small value, the ultimate shear resistance of the last soil layer before the base is multiplied per more than 8 and the corresponding maximum stress of this layer reach unrealistic value compared to the real soil resistance (>> f_s (CPT)). Moreover, the matching quality can not be considered as successful (D(p) > 5%).

If the ratio of modulus G_2/G_i is fixed to 1 and maintained fixed during the optimisation, the last layer of soil describing the friction reaction includes almost all the pile length, the initial shear modulus is very low (less than 13 MPa) and the ultimate shear resistance is superior to the expected one (>0.3 MPa). However, the matching quality is correct and the pile's element settlement histories are very close to Figure IV-64.

The pile/soil model used does not allow to render the real behaviour of the pile/soil interaction. Whatever the initial conditions, it is impossible to have a final result respecting the ultimate resistance, the initial shear modulus profiles and an acceptable unloading modulus together in agreement with the reality. However, these conditions must be fulfilled in order to have the opportunity to optimise the rheologic parameters. Consequently, this problem must be solved by another way:

- To allow an independent unloading modulus for each pile soil element and to multiply the number of soil layers along the pile shaft;
- To work on a shorter duration including only the loading phase or the rebound stage of the settlement curve;
- To change the pile/soil model;

The first solution proposed was not followed because it does not answer to the underlying problem linked to the reliability of the modelling. If it is possible to match two curves by increasing the number of parameters, it is appropriate to improve the matching result by improving the model quality.

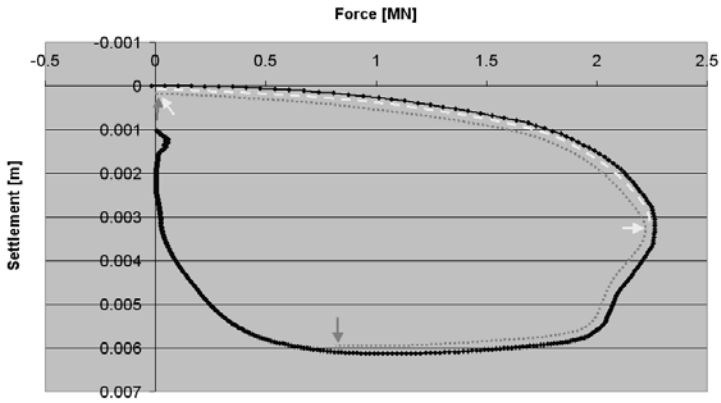

Figure IV-67 : Optimization duration investigated

The second solution was widely investigated. The main idea was to focus the matching procedure on the reliable data. If the optimisation procedure is perturbed by the unloading stage, it can be possible to only analyse the loading stage, or the increasing part of the settlement (Figure IV-67). Unfortunately, the number of points before these two points is very low (less than 1L/c for the F_{max} analysis and less than 3.5 L/c for the S_{max} analysis) and does not enable a good optimisation process as possible.

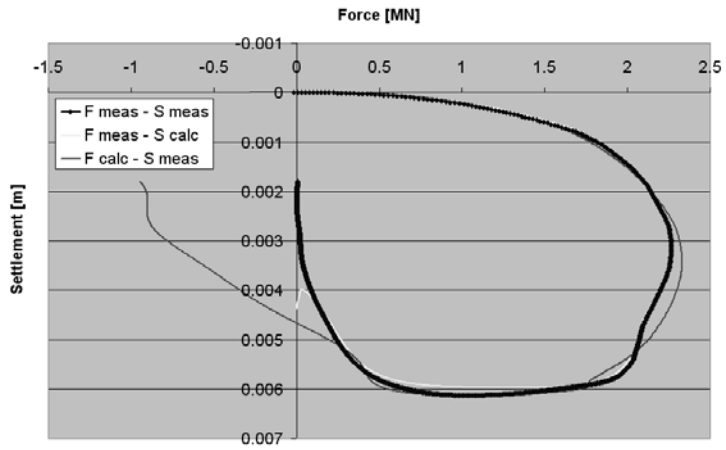

Figure IV-68 : Influence of the optimisation duration on the matching quality

The following trend is noted: the longer the duration, the more pronounced the influence of G_2/G_1. If the duration is small enough, the unloading phase can be without importance. But if a short analysis allows one to optimise the parameters without modifying the initial modulus, the matching is relevant for this short duration and absolutely not for the rest of the signal (Figure IV-68).

Finally, the last solution proposed is the chosen one. Since the soil is considered motionless, the pile/soil interaction is lead by the pile motion without taking into account of the slippage into the formulations. This constraint links the loading and the unloading phases to the pile settlement. By authorizing the pile and the soil to move in an independent way, the interface motion between both media starts to have a certain magnitude when the pile slips into the soil. The pile/soil interaction must evolve to allow that. When the rheologic stress exceeds the ultimate rheologic resistance, the pile and the soil become uncoupled and both media behave independently (such an improvement is developed in the next chapter).

Other interesting results are available:

If the integration of the maximum stresses reached (static mobilization) during the blow along the pile and beneath the base is performed, Figure IV-69 summarises all the analysed blows. The points inform about the evolution of the shaft friction with depth and the last point adds the base to the shaft soil reactions. The curves exhibit the evolution of the shaft friction mobilization with the height of drop. The blow A7b-001 (0.2m) shows a poor mobilization an a quasi nil base soil reaction. The A7b-002's

(0.4 m) shaft friction evolves and its base reaction increases a little. From the blow A7b-003 (0.6 m), the friction becomes almost identical for all the blows, only the base reaction presents an upwards trend.

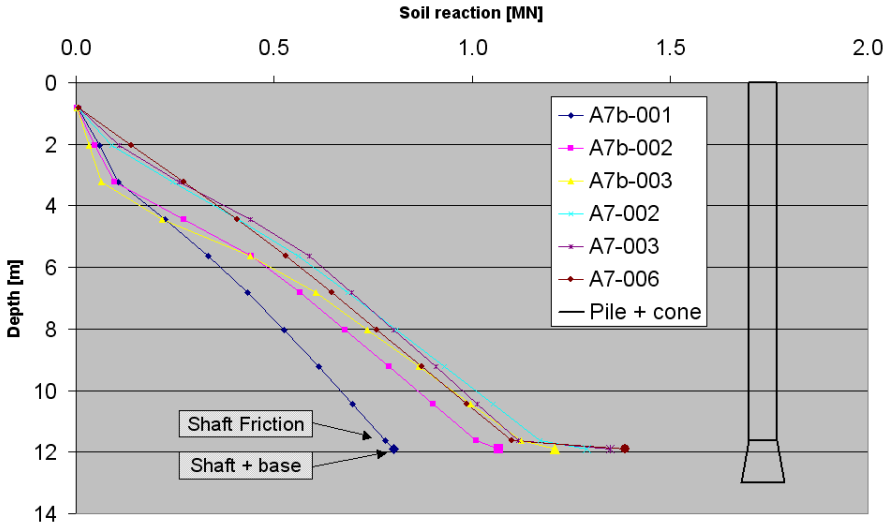

Figure IV-69 : Integration of the reached stresses along the pile and beneath the base for the analysis of Sint-Katelijne-Waver DLT tests

Despite the caution required due to the initial loading and unloading modulus problem (see above), the evolution of the blow analysis respects an expected trend: the progressive and quick mobilization of the shaft reaction, and the slower base reaction mobilization. This evolution isplotted vs. the maximum settlement measured of each blow (Table IV-3). Figure IV-70 exhibits this representation plus the separation of the total soil reaction in shaft and base terms and the corresponding static load-settlement curve measured during the Static Load Test performed on a identical pile in the close vicinity of the pile tested dynamically. The evolution of the integrated soil reaction is very close to the behaviour expected on clay: a very weak base resistance and a strong friction one quickly mobilized. The total soil reaction can be modelled by a hyperbolic curve which tends to an ultimate value of 1.7 MN. The comparison with the real curve prompts several observations:

- The initial stiffness is perfectly recovered;
- The large soil reactions are under-estimated compared to SLT result;
- The shaft friction curve present a recess after reaching a peak similarly to the observed behaviour during the static tests;
- The shaft friction seem to be fully mobilized after a settlement of about 6 mm, namely 1.5% of the pile diameter.

The same caution than previously must be kept in mind with this analysis due to the likely influence of the modelling of the initial modulus and the unloading phase on the integrated soil reaction. However, this representation has the advantage to condense all the analysis into a single figure (1 point/1 analysis).

Moreover, this kind of result is easy to plot and understand and is a usable result to easily compare the DLT conclusions to the SLT classic load settlement curve.

Besides the problem already approached, the under estimation could come from:

- The possible variation in the geotechnical profiles between the DLT and SLT locations;
- The base modelling with the cone of equivalent soil that underestimates the base soil reaction;
- The influence of the inertial and the load rate effects on the measured maximum settlements (overestimation of the measured settlement);
- The influence of the loading rate effect on the measured static load-settlement curve (overestimation of the measured load);
- Degradation of Boom clay under repeated impacts.

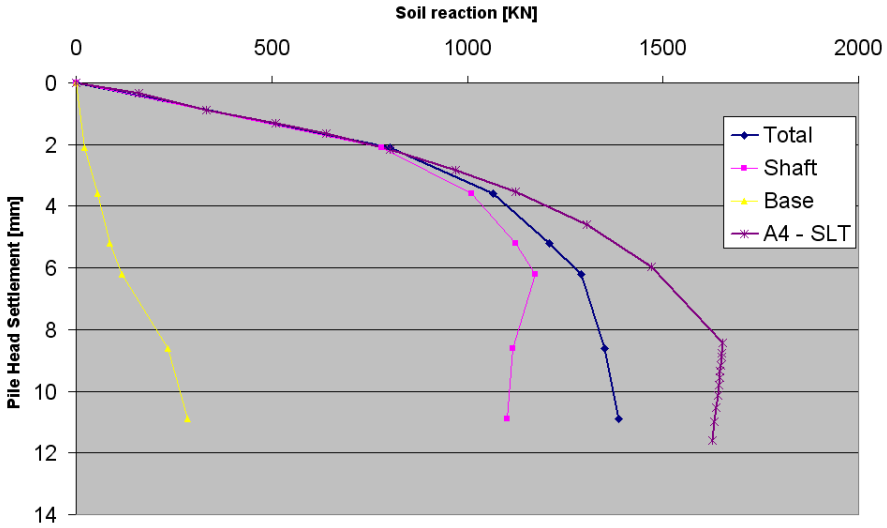

Figure IV-70 : Maximum mobilized load vs. maximum settlement for the sequence of blows A7 of SKW

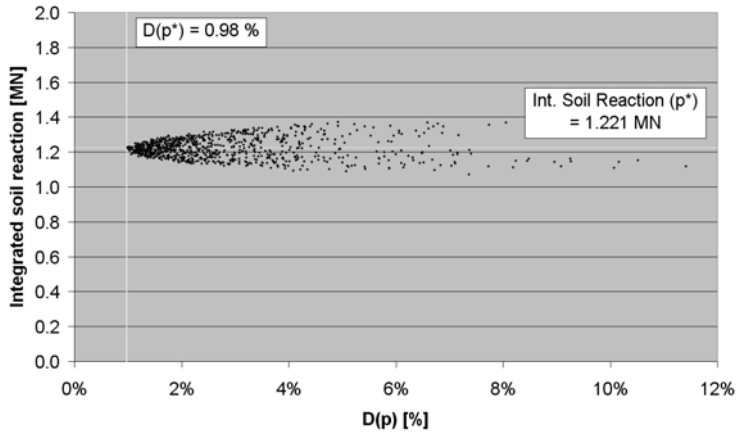

Figure IV-71 : Sensitivity of the integrated soil reaction of the blow A7b-003 around the optimal solution p*

A sensitivity analysis can be performed on the integrated soil reaction by varying all the parameters all around their optimal combination (p*) and to measure systematically the corresponding value of D(p) and the integrated soil reaction. Figure IV-71 exhibits this analysis for the blow A7b-003. The plot highlights the optimisation of the integrated soil reaction with the matching quality factor. That means that there is global balance

between all the parameters to obtain a given matching linked to a certain soil reaction whatever the differentiation in shaft and base.

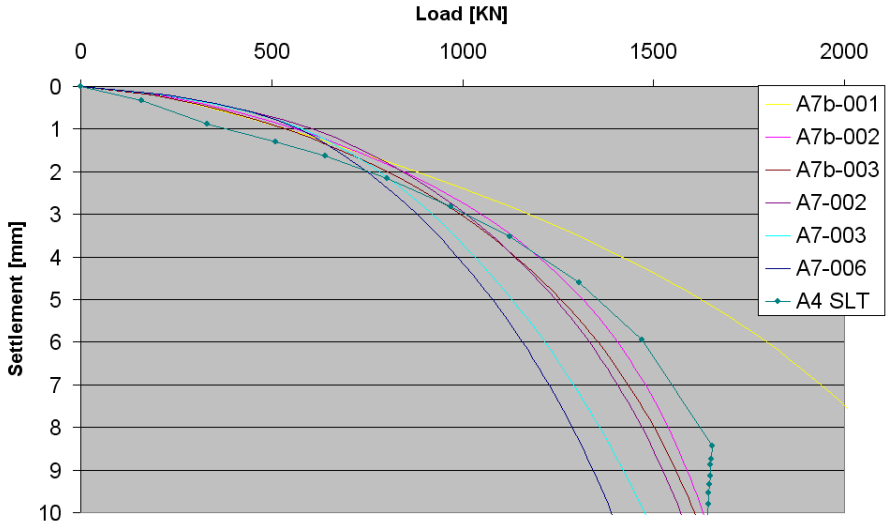

Figure IV-72 : Simulation of the static load-settlement curves based on the individual analysis of the A7's blows

Finally, Figure IV-72 summaries the simulations of the static load-settlement curves obtained from the individual analyses. The settlement axis is limited to 10 mm what is the maximum settlement reached during the dynamic tests analysed. The curve of the blow A7b-001 overestimates the static load settlement curve but the simulated curve must be compared until the mobilized settlement corresponding to the blow, namely 2.1 mm. At this settlement, the difference is not important. On the other hand, the curves of the higher drop heights are underestimated. It is probably a direct influence of the loading-unloading modulus. The others curves are very similar and present a good quality of simulation in the range of the concerned settlements. The initial stiffness of the curve is higher than the SLT due to the high values of initial shear modulus in the first layers, but this tangent stiffness decreases rapidly due to the small value of G_i of the third and resistant soil layer.

5.2. Analysis of the dynamic tests from Limelette

The analysis is less complete than the previous one because the conclusions are similar. All the figures are not presented but the main ones are described and detailed in order to comment all the analysis.

The tests analysed have already been studied in chapter 3. It concerns the long prefabricated pile B8. The pile is 11 m long and its embedded part is 8.7 m long. The base is located at 9.5 m of depth.

The modelled pile is decomposed in 10 elements, the pile modulus of elasticity is fixed to 42000 MPa (c = 4140 m/s) and the surrounding soil is described by the input set of parameters (Figure IV-12 to Figure IV-14). The exponents N of the velocity dependent power law are fixed to 0.2 for the shaft and 1 for the base according to literature. The ratio of shear modulus G_2/G_i describing the unloading is fixed to 1 and authorized to be optimised. Similarly to the SKW analysis, the input set of parameters is the same for each analysis but each blow is considered as an independent study.

The pile B8 was dynamically tested in 2002. the blows analysed are the blows #001, 002, 003, 007, 011 and 015. this sequence ensure a progressive increase of drop height from 0.4 m to 2 m. Each height is tested for the first time. They are called B8-00i. Table IV-7 informs of the chosen blows, of the drop heights and of the maximum and permanent settlements reached during each blow according to the analysis of the acceleration measurements at the pile top (more details in section 3.3 of chapter 3).

	Drop Height [m]	Max Settlement [m]	Perm Settlement [m]
B8-001	0.4 m	0.0033 m	0.0004 m
B8-002	0.6 m	0.0054 m	0.0005 m
B8-003	0.8 m	0.0062 m	0.0004 m
B8-007	1.2 m	0.0077 m	0.0004 m
B8-011	1.6 m	0.0094 m	0.0009 m
B8-015	2 m	0.0119 m	0.0039 m

Table IV-7: Summary of the analysed blows and of the reached settlements

The back-analysis is processed by the automatic algorithm proposed in this research and the following results are obtained. The matching procedure is performed by optimisation of all the parameters in the same time: since it is possible to refine the optimisation procedure to a certain number of parameters, Table IV-8 informs about the concerned parameters: 24 parameters.

Shaft (x 5 layers) :	$\tau_{ult,i}$	z_i	E_i	Js_i	G_2/G_1
Base 1 layer :	$\sigma_{ult,i}$	E_i	Js_i		

Table IV-8: List of optimised parameters

The optimisation procedure starts with a radius Δ of 90%. There are 10 reductions authorized and the last radius analysed is 5%. The number of iterations/radius without improvement of the matching quality factor D(p) is fixed to 100. The matching is processed on a duration of 25L/c which is longer than for the clay because the sand dampens less the signals (see Figure IIV-53 and Figure IIV-60). Table IV-9 contains the results of the matching procedure: D(p) is listed in %.

	Matching factor [%]	Max base settlement [m]	Difference max settlements pile top & base [m]
B8-001	0.74 %	0.0017 m	0.0016 m
B8-002	0.98 %	0.003 m	0.0024 m
B8-003	0.89 %	0.0035 m	0.0027 m
B8-007	1.18 %	0.0049 m	0.0028 m
B8-011	1.2 %	0.0063 m	0.0031 m
B8-015	0.91 %	0.0094 m	0.0025 m

Table IV-9 : Result of the matching procedure (matching quality factor D(p)) and maximum base settlement obtained for each test

Figure IV-73 to Figure IV-75 display the result of the matching procedure in terms of force-settlement curves for three analysis: B8-001, B8-007 and B8-015 corresponding to the drop heights of 0.4 m, 1.2 m and 2 m. The measured curve (Force measured – Set calculated) is compared to both calculated: "Force measured – Set calculated" and "Force calculated – Set measured". The matching is successful for all blows (see Table IV-9). Nevertheless, it can be pointed out that the calculated settlement curves (based on the force signal as input) fit much better with the reference curves than the calculated force curves (based on the settlement as input). There is a gap between those two curves between the

maximum force and the maximum settlement (especially in Figure IV-74). The maximum and final settlement are conserved and the second peak of force is also well modelled (Figure IV-75). The matching is performed until stabilisation of the pile (about 25L/c).

The settlement behaviour of the last element close to the pile base (Table IV-9) does not show a constant behaviour like for the site of Sint-Katelijne-Waver but an upwards trend with the drop height and with a decreasing rate: the maximum settlement increases like the shortening of the pile's element (except for the last test #015). Consequently, the transfer of load to the base is also increasing and the mobilization of the shaft friction is not complete but tends to be.

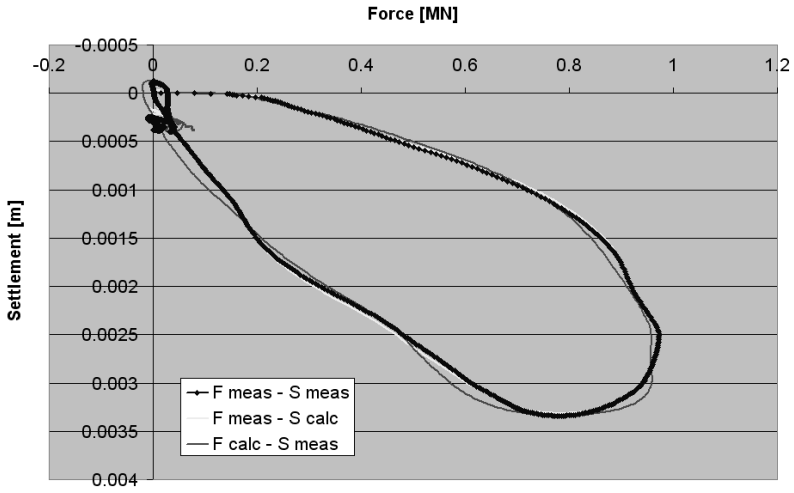

Figure IV-73 : Force-settlement curves (measured, and optimised (2 curves)) – blow B8-001/ 0.4 m

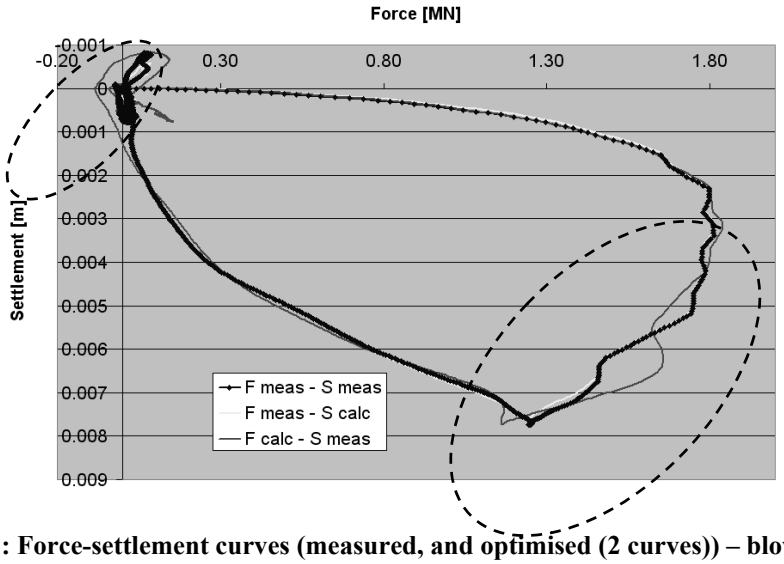

Figure IV-74 : Force-settlement curves (measured, and optimised (2 curves)) – blow B8-007/ 1.2 m

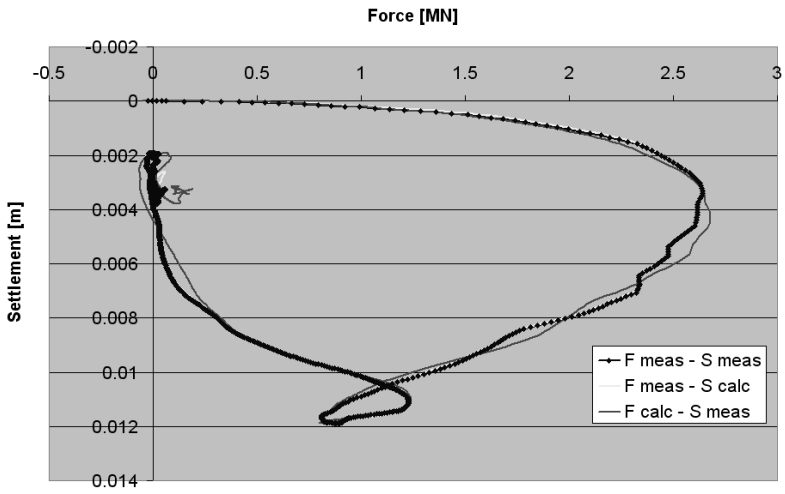

Figure IV-75 : Force-settlement curves (measured, and optimised (2 curves)) – blow B8-015/ 2 m

Figure IV-74 shows a good matching between curves, but there are two parts of the "Force Measured – Set calculated" curve that do not fit very well. The first one is systematic in the other analysis and correspond to the part of the curve between both maximum of measured force and settlement where the velocity is positive and decreasing (positive effect on the measured force) and the acceleration is negative (negative effect on the measured force). The second is also typical but corresponds to the part of the signal where the load has reached a quasi nil level and not the velocity (and consequently the settlement). The matching is difficult in this portion and is a question of radiation, essentially. The velocity curves matching (Figure IV-76) is also of very good quality except for the local maximum and minimum where a small gap exist. The first dashed ellipse on Figure IV-74 is located in the first decrease of the velocity (H = 1.2 m) marked with a grey arrow. The measured velocity presents a little threshold not modelled by the calculated curve.

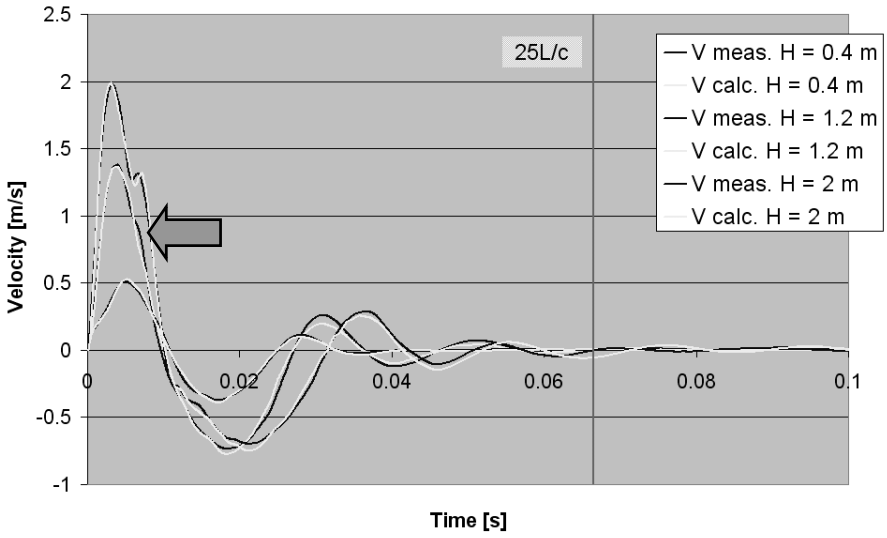

Figure IV-76 : Velocity curves (measured, and optimised) – blow B8-001/ -007 & 015

Figure IV-77 summarizes the data of the base parameters for the 6 blows analysed:

- The maximum reached stresses increase with the drop height denoting an increasing base mobilization. The range is from 0.3 MPa to more than 7 MPa;
- The ultimate soil resistance fluctuates between 12.26 and 22.46 MPa, but since the real stress mobilized reaches only max 53% of this value, the variability can be accepted. Moreover, an equilibrium exist with the initial elastic modulus to respect the settlement path of the pile base;
- The initial elastic modulus E_i reaches very high values, unrealistic and not physical (> to 2500 MPa). The reason is the same than for the previous analysis on the Sint-Katelijne-Waver data, there is an obligation to respect the settlement path and the load balance imposed as input and transmitted into the pile. Since this parameter is manifestly too high, the proposed values for σ_{ult} and σ_{max} are uncertain;
- The base damping factor J_b starts the sequence with a very high value (> 2.9 s/m) and decreases to stabilize for the higher drop height to about 0.85… 0.9 s/m; this value does not concern the ultimate soil resistance limit, but only the viscous term definition;

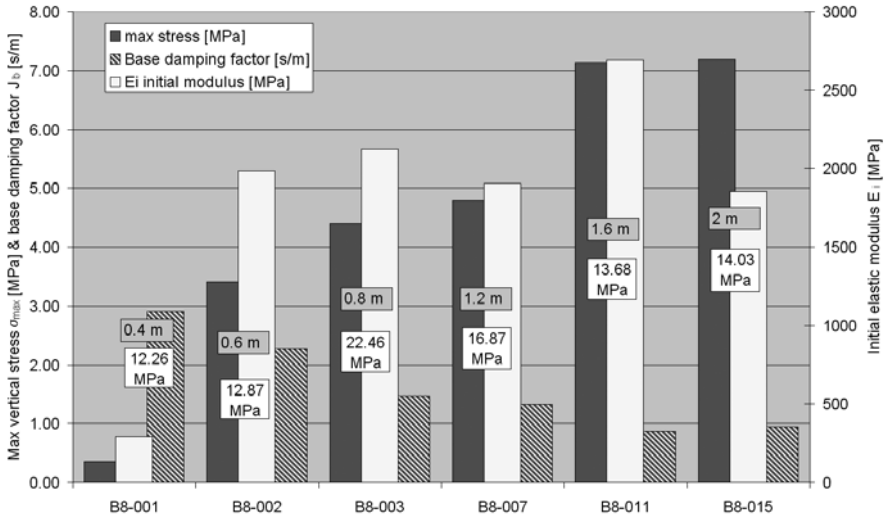

Figure IV-77 : Description of the base parameters after optimisation

The next three figures (Figure IV-78 to Figure IV-80) summary the soil reaction along the pile shaft with one sole figure per analysis. only the the blows #001, 007 and 015 are resumed (0.4 m, 1.2 m and 2 m respectively). The following information is available into the figures.

- The profile of the local shear strength f_s measured with the CPT;
- The step profile introduced as input (in dashed lines) τ_{ult};
- The step profile of the ultimate shear strengths obtained after optimisation τ_{ult};
- The step profile of the maximum reached shear stresses along the pile shaft τ_{max};
- The values of the initial shear modulus G_i for each soil layer;

- The value of the shaft damping factor J_s corresponding to each soil layers.

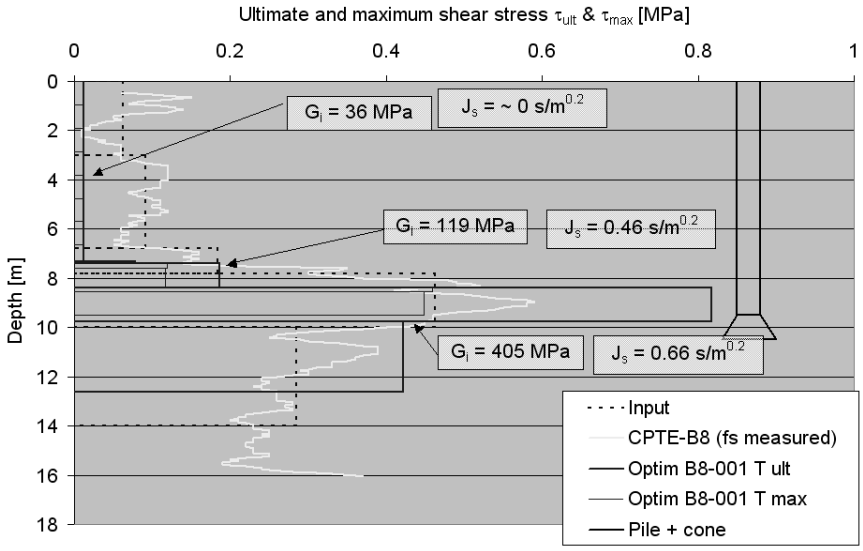

Figure IV-78 : Summary of the parameters of the soil reaction along pile shaft for the blow B8-001

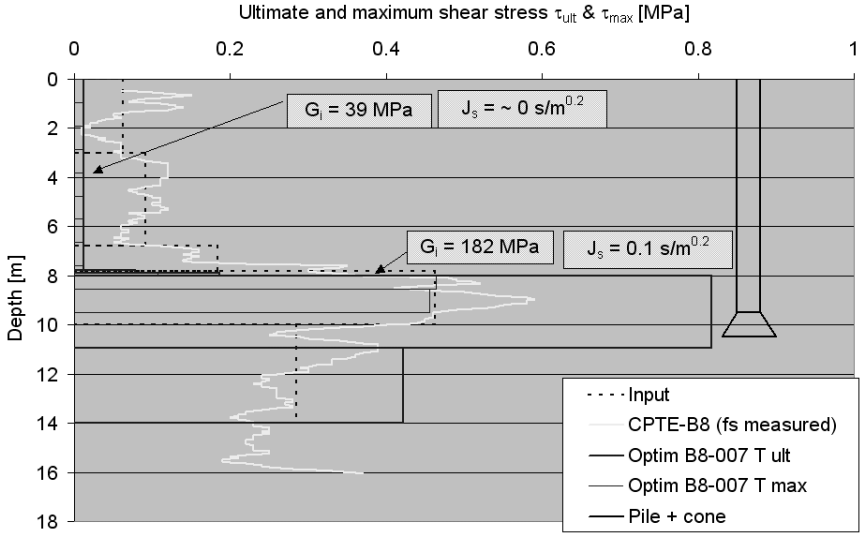

Figure IV-79 : Summary of the parameters of the soil reaction along pile shaft for the blow B8-007

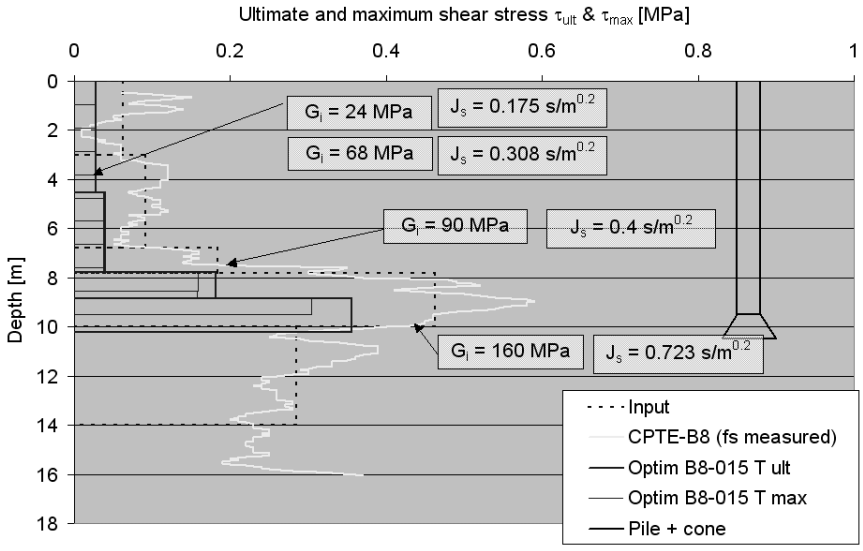

Figure IV-80 : Summary of the parameters of the soil reaction along pile shaft for the blow B8-011

The following remarks can be enounced:

- The profile of the CPTE measurement f_s is respected. The layer of resistant sand in which the pile is embedded is found for all the piles. The optimisation process finds remarkably well the depths of soil resistance change of importance. However, the net ultimate values are not respected completely. The order of magnitude is ok, not the precise value. This is due to the settlement path to be respected and the balance existing between the stiffness and the resistance parameters that gives the shape to the hyperbolic curve;

- The first layer, until a depth of about 7.5 m defining the start of the sandy layer, is completely mobilized and also modelled inferior to the reference profile (f_s from CPTE); it is maybe due to the degradation of this weak layer or still an indirect consequence of the unloading shear modulus trouble; the last test (Figure IV-80) is slightly superior to the previous analysis but it is also shown that the sandy layer reaction has been reduced. There is a general equilibrium of the soil resistance along the pile in order to match the curves;

- The G_i profiles are more logical even if they present a downwards trend with the increasing drop height, the balance with the ratio G_2/G_i is less pronounced because the major part of the soil reaction is focused on the sandy layer close to the pile base. Hence, the balance between the modulus of the loading and unloading stages is performed on this sole layer and the initial shear modulus vary less than for the multi layers analysis of the clayed site. The values of the ratio of shear modulus (Table IV-10) exhibits a decreased trend with the drop height due to the fact that the maximum settlements to be respected increase with the soil mobilization but not the permanent settlement. Consequently, as observed on the Figure IV-81, the unloading modulus is adjusted to link both values.

	G_2/G_i
B8-001	0.46
B8-002	0.47
B8-003	0.4
B8-007	0.38
B8-011	0.25
B8-015	0.22

Table IV-10 : List of unloading shaft ratio G_2/G_i

- Despite the fact that the poor first layer of soil is completely mobilized, there is no need of an added viscous reaction in most of the blows. All the first layer rheologic reaction is equivalent to a static reaction, the optimised values of J_{s1} can be equal to 0 $s/m^{0.2}$. The sandy layer presents a shaft damping factor that oscillates between 0.1 $s/m^{0.2}$ and 0.72 $s/m^{0.2}$. These values, and especially the last one, are confirmed by a sensitivity analysis around this position but are highly influenced by the optimised value of the ultimate soil resistance (τ_{ult} > 0.8 MPA for B8-007 and < 0.4 MPA for B8-015). Since the shaft damping factor mainly influences the rheologic soil reaction parameters into the ultimate formulation instead of the viscous one, the ultimate soil resistance has a strong influence. The real value of J is probably between 0.1 $s/m^{0.2}$ and 0.72 $s/m^{0.2}$ but need to be confirmed with a pile/soil system where the slippage is authorized and the troubles affecting the loading and unloading stiffness

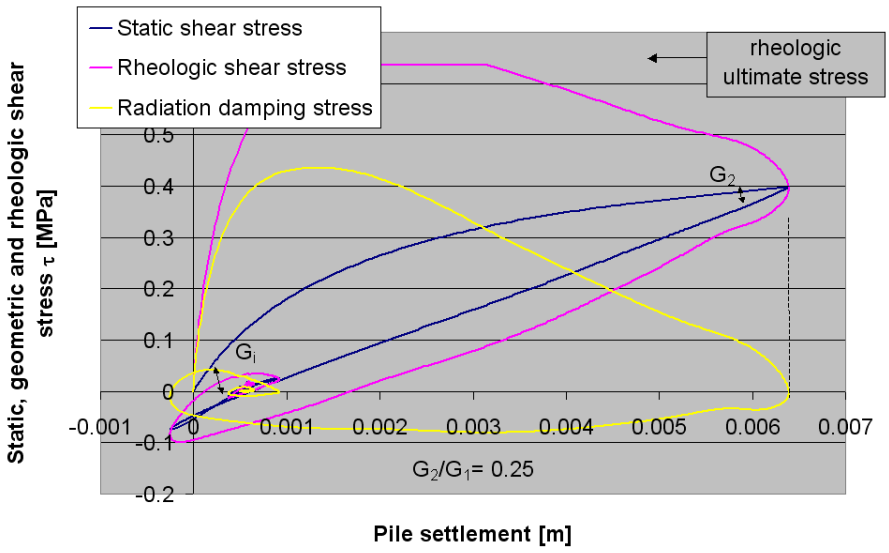

Figure IV-81 : Detail of the soil reaction along the 11th element of the pile (blow B8-011)

Figure IV-82 shows the detail of the settlements modelled of all the pile's elements for the blow B8-011 after optimisation. This is also the displacement path to be followed by each soil layer in contact with the pile's elements.

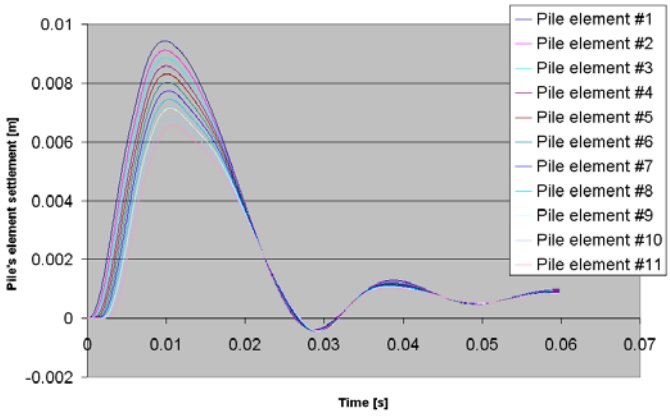

Figure IV-82 : pile's element settlement of B8-011

The trouble pointed out by the analysis of the Sint-Katelijne-Waver site still concerns the sandy site of Limelette. The need to dissociate both media, pile and soil becomes essential to perform a precise back analysis.

Similarly to the previous analysis, the integration of the maximum stresses reached during the blow along the pile and beneath the base (Figure IV-83) informs about the evolution of the shaft friction with depth and the last point adds the base to the shaft soil reactions. The first layer, described as of very small resistance gives a very poor soil reaction until the depth of 7.5 m. The same response is found for the 5 first analysis. Only the last one presents a more resistant soil reaction but this trend is balanced by a reduction of resistance in the sandy soil layer.

The figure highlights the quick mobilization of the shaft friction and the increasing mobilization of the base with the drop height.

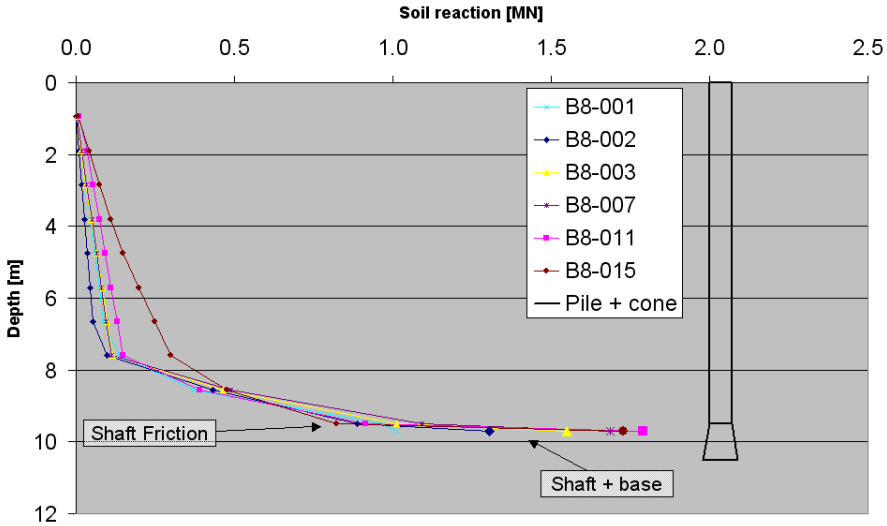

Figure IV-83 : Integration of the reached stresses along the pile and beneath the base for the analysis of Limelette

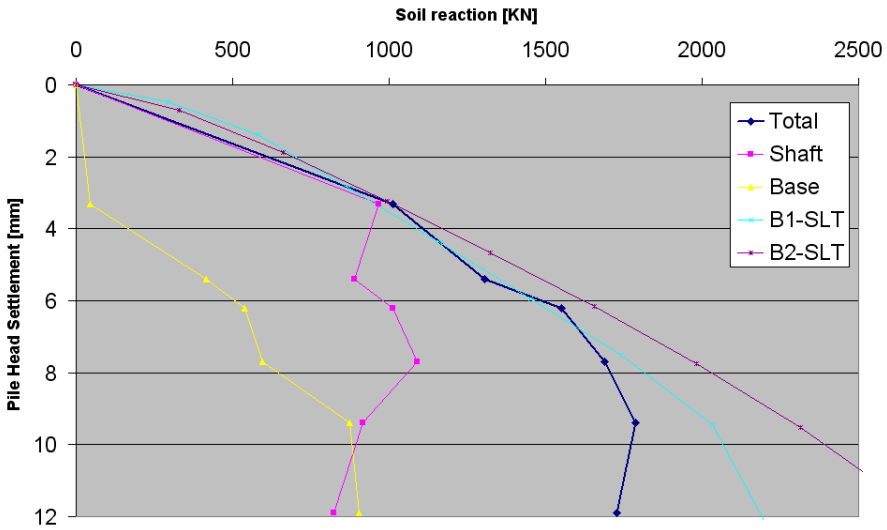

Figure IV-84 : Maximum mobilized load-maximum settlement curve for the sequence of blow B8 of Limelette

This evolution can be plotted vs. the maximum settlement measured of each blow (Table IV-7). Figure IV-84 exhibits this representation plus the separation of the total soil reaction in shaft and base components and the corresponding static load-settlement curves measured during the Static Load Tests performed on identical piles in the close vicinity of the pile tested dynamically (B1 & B2).

The initial stiffness agrees perfectly with the measured static curves. The shaft resistance is quickly fully mobilized (3.5 … 4 mm or 1% of the pile diameter) and the total shaft soil reaction is about 1 MN (oscillations around this value and equilibrium with the base reaction). The base reaction is increasing and is going to be superior to the shaft resistance as expected in sand. Since for the clayed site, the points corresponding to the large soil reactions are under-estimated compared with the SLT result, the same reasons than previously can be enounced.

Obviously, a general caution must be kept in mind with the likely influence of the modelling of the initial modulus and the loading and the unloading phases on the integrated soil reaction.

Finally, Figure IV-85 summaries the simulations of the static load-settlement curves obtained from the individual analysis. The settlement axis is limited to 10 mm what is the maximum settlement reached during the dynamic tests analysed. All the curves underestimate the static load settlement curves from both static load tests performed on the piles B1 and B2. The best fitted curve is the blow B8-003. the worst are the blows B8-001 and 015. If the first agrees perfectly with the SLT curves on the settlement mobilized (3.3 mm), it is not the case for the higher drop height blow.

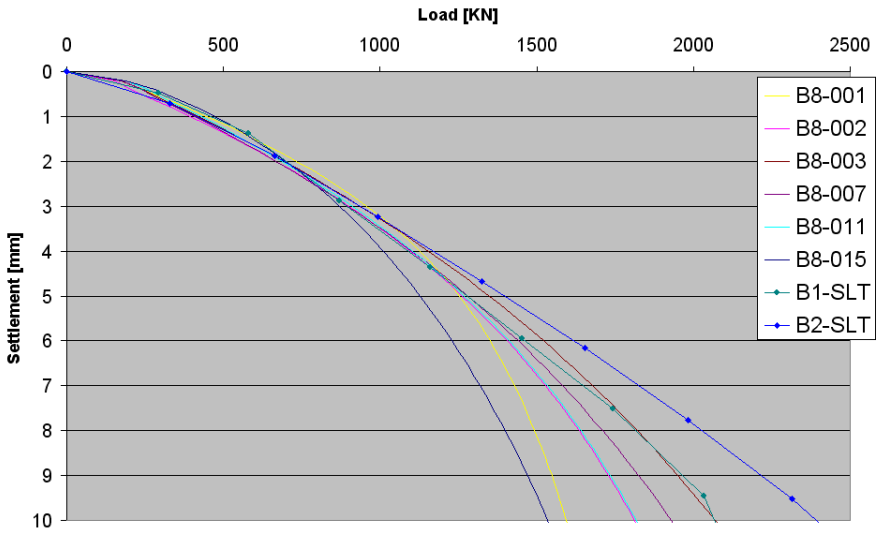

Figure IV-85 : Simulation of the static load-settlement curves based on the individual analysis of the B8 blows

6. Conclusions

This chapter is focused on the back analysis and the optimisation procedure used to analyse the dynamic measurements and to simulate the static load settlement curve to be compared with the measured one.

The principles of the matching procedure, the details and the requirements to have an objective and rapid method to perform it was presented: in order to have a better knowledge of the loading rate effect and especially on the parameters supposed to characterize it, all the parameters have to be optimised following a hierarchy based on of their relative weight.

The multi dimensional parameter perturbation sensitivity analysis developed by Berzi (1999) in order to explore the close vicinity about a point (defining a combination of n parameters in their R^n space) is used to systematically find the best combination improving the matching quality factor defining the matching process. When a new combination improving the matching is found, this value is set as new position of reference and a new perturbation analysis is undertaken until a stop criterion was achieved. The final combination is considered as the solution of the back-analysis.

This method is adapted to the back analysis of dynamic measurements from loading tests. The number of parameter to be optimised is free, and the solution can be tested by the sensitivity analysis in order to check its variability in its close environment. The consequences of this sensitivity on the simulated load settlement curves can be studied. This automatic procedure was tested and validated. The matching procedure converges.

The sensitivity analysis of the solution allows one to sort the parameters according to their relative weight in the matching procedure. Since the matching is successful and the combination converges towards the final solution, it is possible to refine in the later stages the less influential parameters by only selecting and optimising them. An analysis on the dynamic load test measurements from Sint-Katelijne-Waver and Limelette allows one to classify the rheologic parameters as not influential, except for the case where they are optimised together. The parameters leading the static soil reaction (τ_{ult}, thickness of the soil layers) appear to be leading the optimisation.

This automatic analysis was applied to the real data of the dynamic load tests of Sint-Katelijne-Waver and Limelette. The matching procedure is generally successful for all blows analysed. The back-analysis results are less reliable. The dynamic load tests analysis presents soil resistance profiles comparable to the CPT one (used as reference). The global static pile/soil response can be extracted and generally the simulated static load settlement curves are similar to the measured ones.

However, a systematic error hampers the optimisation of the loading and unloading initial shear moduli. Since the pile and soil motions are coupled by definition of the pile/soil system, the pile settlement path is imposed to the stress-displacement relationship of the soil. In order to match the measured and calculated curves of velocity, the constitutive soil relationships have to follow this settlement path. However, there is also a stress balance at each node of the pile/soil system between the rheologic soil reaction and the internal forces coming from the pile top. In order to fulfil this double constraint, the matching process influences the optimisation of the free parameters left in the soil-displacement relationship: the initial shear modulus for the loading and unloading stages and the rheologic parameters. Since the modulus influences greatly the stress generated for a given settlement, this parameter undergoes the consequences of the uncoupled behaviour of the pile and soil motions.

To avoid this trouble and to have a chance to succeed in the matching procedure and in the back analysis process, the slippage between pile and shaft must be authorized and both motions have to be independent during this slippage.

Nevertheless, except for the strict quality of the back analysis and despite the fact that there are some uncertainties on the results, there are some good results coming from the analysis of both sequences of DLT tests of the sandy and the clayey sites:

- The evolution of the soil mobilization with the drop height is as expected. First, the shaft friction mobilization, until a settlement of approximately 1% or 1.5% of the diameter where the shaft friction seems to be fully mobilized and afterward, progressively, the base reaction. The balance between base and shaft friction is also respected for the clayey and sandy sites;

- The soil mobilization integrated along the pile vs. the max settlement reached during dynamic load test is a comparable curve in stiffness, shape and quantity to the corresponding static load settlement curve.

- The profiles of soil resistance with depth are also recovered after the automatic processing;

- The rheologic parameters are more influential in the clayey site than in the sandy one. With the appropriate caution, it is possible the give a value to the shaft and base damping factors corresponding to the sites investigated (including the pile, the soil and the loading types):

	Sint-Katelijne-Waver	Limelette
Shaft damping factor	0.6 s/m$^{0.2}$	0.1 to 0.75 s/m$^{0.2}$
Base damping factor	1.75 s/m	0.9 s/m

- The simulations of the static load settlement curves agree with the measured one but are probably influenced by the pile/soil motion coupling.

On can observe a general balance in the soil reaction along and beneath the pile. The parameters of resistance, of stiffness and the rheologic parameters combine with each other to respect the settlement path all along the pile. The equilibrium at the base is particularly significant: both terms of soil reactions (shaft friction and base) combine to have a similar response submitted to the last pile element. This combination can have a strong influence on the optimised parameters value from base and shaft and an equivalent influence on the matching quality factor.

Finally, one can point out that the load rate effects are more developed in clay compared to sand. It can be observed that a good matching is not a sufficient condition to have good back-analysis results. Guides must orientate the matching. The first one and the most important one is the comparison with a good geotechnical information about the soil environment. Automatic guides can be implemented, but the most relevant is engineering judgement.

CHAPTER 5
The Slippage Event

1. Introduction

It was previously observed (chapter 4) that the pile and the soil interaction suffered from a continuously coupled behaviour during the use of the simple 1D model (chapter 3). This modelling constraint perturbs the back-analysis process and the quality of the optimisation. It was concluded from these results that the slippage between the pile in the soil during a loading test was required and must be implemented in the pile/soil model. But the character of the 1D model prohibits this evolution since the model is developed in only one degree of freedom: the pile one.

Indeed, with the slippage modelling comes another need: the introduction of the soil motion, independently of the pile motion while slippage happens. This introduction brings on a second degree of freedom and complicates the scheme of resolution of the 1D model described in chapter 3. In order to introduce this second degree of freedom, assumptions must be set to describe the soil concerned. Is it only the soil reaction acting at the interface or the soil until a large distance where the effects of the pile loading are not felt?

This section intends to open different ways in order to take slippage into account in the shaft friction modelling and to study the behaviour of the soil in the direct vicinity of the pile during the slippage according to the modelling assumptions assessed. Two approaches are followed focused on the shaft friction modelling, only concerned by the slippage.

First, only the soil reaction in the direct vicinity of the pile is taken into account: the soil reaction interacting directly in the pile equilibrium. A model including the own motion of the soil is presented. This model is called the DDOF for Double Degree Of Freedom, to be compared with the 1D model of chapter 3 called in this chapter the SDOF model (for Single Degree Of Freedom). The DDOF model

has two motion systems, but no horizontal development. The soil behaviour concerns only the highly perturbed zone.

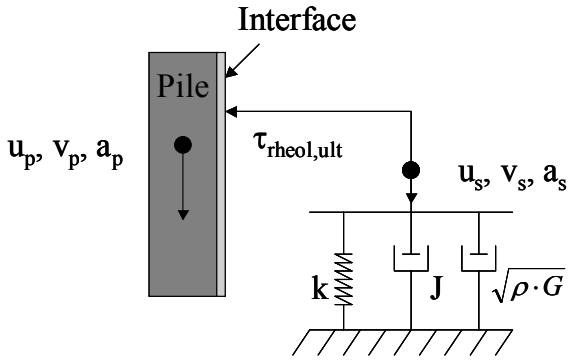

Figure V-1 : Schematic description of the ML model

The soil reaction is modelled similarly to the SDOF model by using mechanical devices: a non-linear spring and two dashpots for the viscous and the radiation term representing the soil impedance (Figure V-1). The slippage event is marked by the coupling and re-bonding of both pile and soil surfaces.

Second, the soil is described horizontally by means of a cylindrical development of the SDOF model (Figure V-2). The pile is located in the centre of concentric cylinders representing the soil. The cylinders are a set of rings with same thickness and increasing height. The last ring closes the model by an absorbing boundary respecting the theory of Novak et al, 1978. The Cylindrical model (or Cyl model) was first developed for the driving by Holeyman et al. (1984, 1996), further applied into vibratory driving by Vanden Berghe (2001) and extended to take the viscous soil reaction into account. The Cyl model allows the computing of the vertical displacements and the shear stresses induced in the soil into the far field due to the a dynamic pile solicitation.

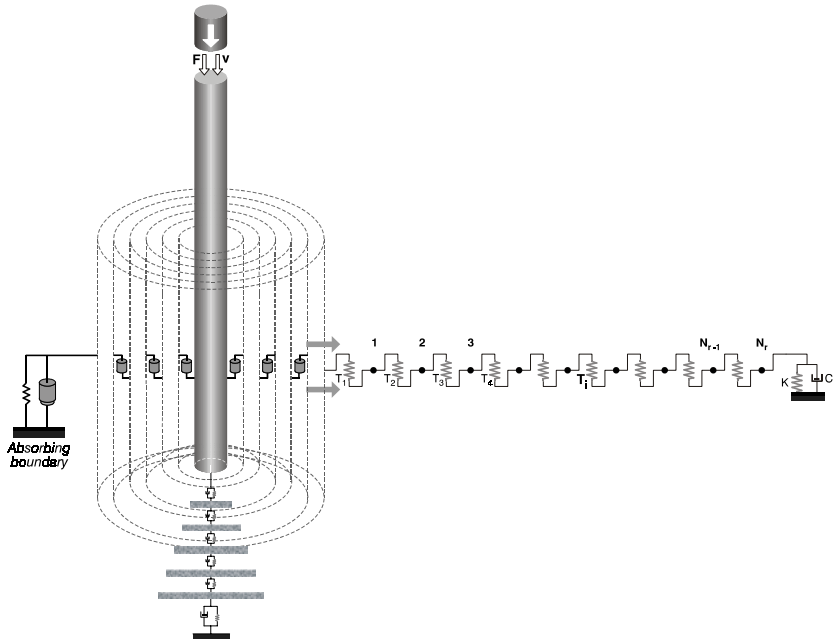

Figure V-2: Schematic view of the Cyl Model

Both models are focused on the shaft friction modelling and consider the pile as a rigid body influencing only one layer of soil. The pile imposes a vertical motion to the soil and according to the soil characterization, slippage occurs or not.

The models are solved with an explicit method. Accelerations are calculated based on the balance of the acting forces between media. These forces are computed (time t_i) with the displacement information of the preceding step (time t_{i-1}) (issued from the integration of the acceleration).

Both models were developed independently and some assumptions can be contradictory. Nevertheless, each approach brings conclusions that can be useful in the study of the influence of the loading rate.

2. The DDOF Model

2.1. Description

A new method has been developed in order to keep the advantages of the SDOF-model already presented in chapter 3 (time computing, simplicity, interest focused on the pile and of its direct vicinity and absence of reflecting waves) with the requirement to take into consideration slippage between the pile and the soil when the ultimate resistance is exceeded (required in chapter 4). This improvement only concerns the shaft friction and not the base soil reaction (not concerned by the slippage).

It must be possible to separate both medias, soil and pile, by considering their motions interdependently or not, without addition of a new horizontal element to the model. In other words, it is possible to take the soil motion into account at the close vicinity of the interface between pile and soil without modelling the soil up to a distance where it is not influenced by the pile motion.

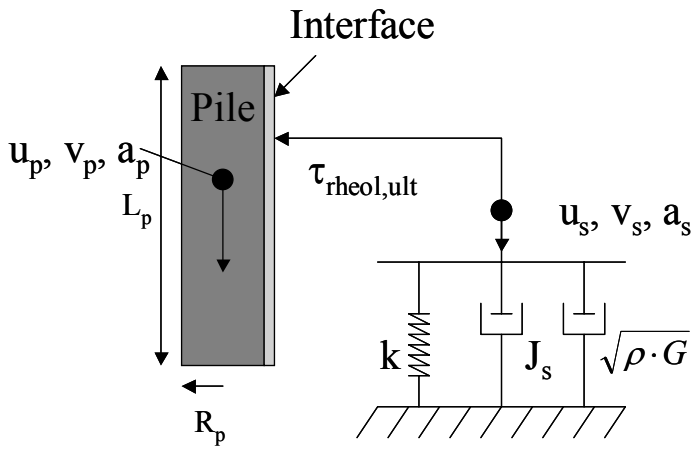

Figure V-3: Diagram of the new proposed shaft model

Nevertheless, without mass, there are some difficulties to estimate the independent motion of the soil when the slippage occurs. How to solve the equations of motion if the inertial term is eliminated or omitted? The proposed solution is based on the relation existing between the pile motion, the soil reaction and the ultimate value of the resistance acting at the interface of both medias (Figure V-3).

The pile moves according to its imposed motion and the balance with the external forces acting on itself. The soil follows this motion until the stress generated exceeds a variable threshold that determines the start of slippage and the uncoupling of both movements.

The soil reaction is represented by three terms. A spring, for the static behaviour, characterized by a hyperbolic stress-displacement relationship and a non linear stiffness k, a viscous dashpot representing the internal dissipation of energy, and a dashpot for the radiation term, characterized by a damping factor $\sqrt{\rho \cdot G}$. Those terms are already described in details in chapter 3 (Section 2.2.). The

fundamental difference concerns the displacement and the velocity used in these formulations. Instead of the pile motion considered as unique and used previously, the soil motion is used (velocity and displacement). Since the motions are differentiated during slippage, the soil reaction is different than previously calculated.

$$\tau_s = \frac{\tau_{stat,ult}\left(1 + J_s \cdot v_s^{0.2}\right)}{\frac{u_r}{u_s} + 1}$$ the static and viscous terms **Equ. V-1**

$$\tau_{rad} = v_s \cdot \sqrt{G_i \cdot \rho} \cdot (1 - \eta)$$ the radiation term **Equ. V-2**

$$\tau_{rheol} = \tau_s + \tau_{rad}$$ **Equ. V-3**

$$\tau_{ult,rheol} = \tau_{stat,ult}\left(1 + J \cdot \left(v_p - v_s\right)^{0.2}\right)$$ the ultimate terms **Equ. V-4**

Where:

- $\tau_{stat,ult}$ is the ultimate static shear strength of the soil [MPa];
- τ_{stat} is the static soil reaction [MPa];
- J_s is the viscous damping factor [$s/m^{0.2}$];
- J is the rheologic damping factor [$s/m^{0.2}$];
- u_r is the quake [m];
- G_i is the initial shear modulus [MPa];
- η is the level of static mobilization: $\frac{\tau_{stat}}{\tau_{stat,ult}}$ [-];
- ρ is the soil mass density [kg/m^3];
- u_p, v_p is the pile displacement and velocity [m, m/s];
- u_s, v_s is the soil displacement and velocity [m, m/s].

The soil reaction is described by the sum of all terms until a limit determined by the slider limit (Equ. V-4). The slider represents the rheologic ultimate resistance of the soil under dynamic solicitations.

Both damping factors (J and J_s) are used equal to 0.5 $s/m^{0.2}$ but they represents different behaviours.

There is a fundamental change in the meaning of the ultimate resistance corresponding to the value of the plastic slider limit. The plastic slider is not a constant value nor dependent of the only pile velocity. The limit varies with the velocity differentiated at the pile/soil interface. This velocity is different from the soil velocity chosen to describe the viscous and the radiation terms. The interface velocity is nil until the starting of the slippage. This is a relative velocity, contrary to the pile or soil velocities which

are absolute ones. The form of the equation is well known and generally used in the problems involved with loading rate effects.

The slider limit (the rheologic ultimate resistance) is equal to the ultimate static resistance (velocity independent) until a certain occurrence and becomes bigger and velocity dependent after this occurrence. The first limit, before the slippage occurs, is:

$$\tau_{rheol,ult} = \tau_{stat,ult} \qquad \textbf{Equ. V-5}$$

if $\tau_{rheol} \le \tau_{rheol,ult}$ **No slippage**

$$\tau_{rheol,ult} = \tau_{stat,ult} \cdot \left(1 + J \cdot \left(v_p - v_s\right)^{0.2}\right) \qquad \textbf{Equ. V-6}$$

if $\tau_{rheol} \ge \tau_{rheol,ult}$ **Slippage**

So, the threshold of soil resistance increases during the slippage with the interface velocity and the slippage starts when the resistance exceeds the static soil resistance. Before that, pile and soil, at the pile/soil interface, move with the same velocity, and are perfectly connected. When the slippage occurs, both behaviours start to diverge. The relative velocity (or interface velocity), (v_p - v_s), increases from zero to a certain value, positive of negative, defining the independent behaviour of both media. When the condition of Equ. V-6 is not achieved, both medias re-bond and v_p=v_s.

The slippage conditions are variable during the slippage but start and end with the same limit: $\tau_{stat,ult}$. It must be pointed out that the soil reaction is always velocity dependent, even if both pile and soil move coupled under the same solicitation. The rheologic stress is indeed function of two terms velocity dependent but linked to the soil motion: the viscous and the radiation terms.

The slippage is determined by the exceeding of a limit dependent of the interface velocity by a stress dependent of the soil velocity. The resolution of the problem is focused on the solving of v_s during the slippage event (u_p, v_p known – u_s, v_s unknown). The equilibrium of Equ. V-6 is used to obtain the value of v_s in an explicit scheme.

2.2. Algorithm

This algorithm describes the solving of v_s and u_s :

Equ. V-5 & Equ. V-6 are used:

When $\tau_{rheol} \le \tau_{rheol,ult}$ → $v_p = v_s$, $\tau_{rheol,ult} = \tau_{stat,ult}$ and $\tau_{rheol} = \tau_s + \tau_{rad}$

When $\tau_{rheol} \ge \tau_{rheol,ult}$ → $v_p \ge v_s$, $\tau_{rheol,ult} = \tau_{stat,ult} \cdot \left(1 + J \cdot \left(v_p - v_s\right)^{0.2}\right)$ and $\tau_{rheol} = \tau_s + \tau_{rad}$ and reduced to $\tau_{rheol} = \tau_{rheol,ult}$ so v_s and u_s are unknown.

The algorithm aims to find out v_s and u_s such as $\tau_{rheol} = \tau_s + \tau_{rad} = \tau_{rheol,ult} = \tau_{stat,ult} \cdot \left(1 + J \cdot \left(v_p - v_s\right)^{0.2}\right)$ during slippage.

Algorithm: calculation for t = t+ Δt

First time step after $\tau_{rheol} \geq \tau_{rheol,ult}$, v_p and u_p known.

Initial values: $v_s(t+\Delta t) = v_p(t+\Delta t)$

$$u_s(t+\Delta t) = u_s(t) + v_p(t+\Delta t)\cdot\Delta t$$

All the velocities and displacements expressed here below correspond to the time t+Δt.

1. Calculation of $\tau_{rheol} = \tau_s + \tau_{rad}$ (called **A**) with the initial values v_s and u_s;
2. Calculation of $\tau_{stat,ult}\cdot\left(1 + J\cdot\left(v_p - v_s\right)^{0.2}\right)$ (called **B**) with the initial values v_s and u_s;
3. Calculation of the difference **A-B = Δτ**;
4. Calculation $v_s^* = v_s - v_s\cdot\frac{\Delta\tau}{K}$;
5. Calculation of the corresponding displacement (u_s^*) and acceleration (a_s^*) for the proposed velocity (v^*_s) and using:

$u_s^*(t+\Delta t) = u_s(t) + \Delta t\cdot v_s^*(t+\Delta t)$ and $a_s^*(t+\Delta t) = \frac{v_s^*(t+\Delta t) - v_s(t)}{\Delta t}$

6. Test to validate the convergence criteria achievement $\left|v_s^* - v_s\right| \leq \varepsilon$;

   Where ε is the required limit of convergence between two consecutive values of soil velocity (10^{-6} …10^{-8} m/s)

7. Interchanging of the corresponding values: $v_s = v_s^*$, $u_s = u_s^*$ and calculation of **A**: $\tau_{rheol} = \tau_s + \tau_{rad}$;
8. Loop of the points 2 to 7 until the convergence criteria is achieved;
9. a_s, v_s and u_s known for the time t+Δt and different of a_p, v_p and u_p.

The point 4. means that the closer the velocity to the solution, the smaller Δτ and so the increment.

The intermediate velocity v^*_s is a temporary one used to ensure the convergence in the algorithm.

It is possible to check the last solution for v_s with the Equ. V-7:

$$v_s = -\left[\left[\frac{1}{J}\cdot\left[\frac{\left(\tau_s + \tau_{rad}\right)}{Q_{stat,ult}} - 1\right]\right]^{\frac{1}{0.2}} - v_p\right] \qquad \textbf{Equ. V-7}$$

The algorithm is summarized on Figure V-4.

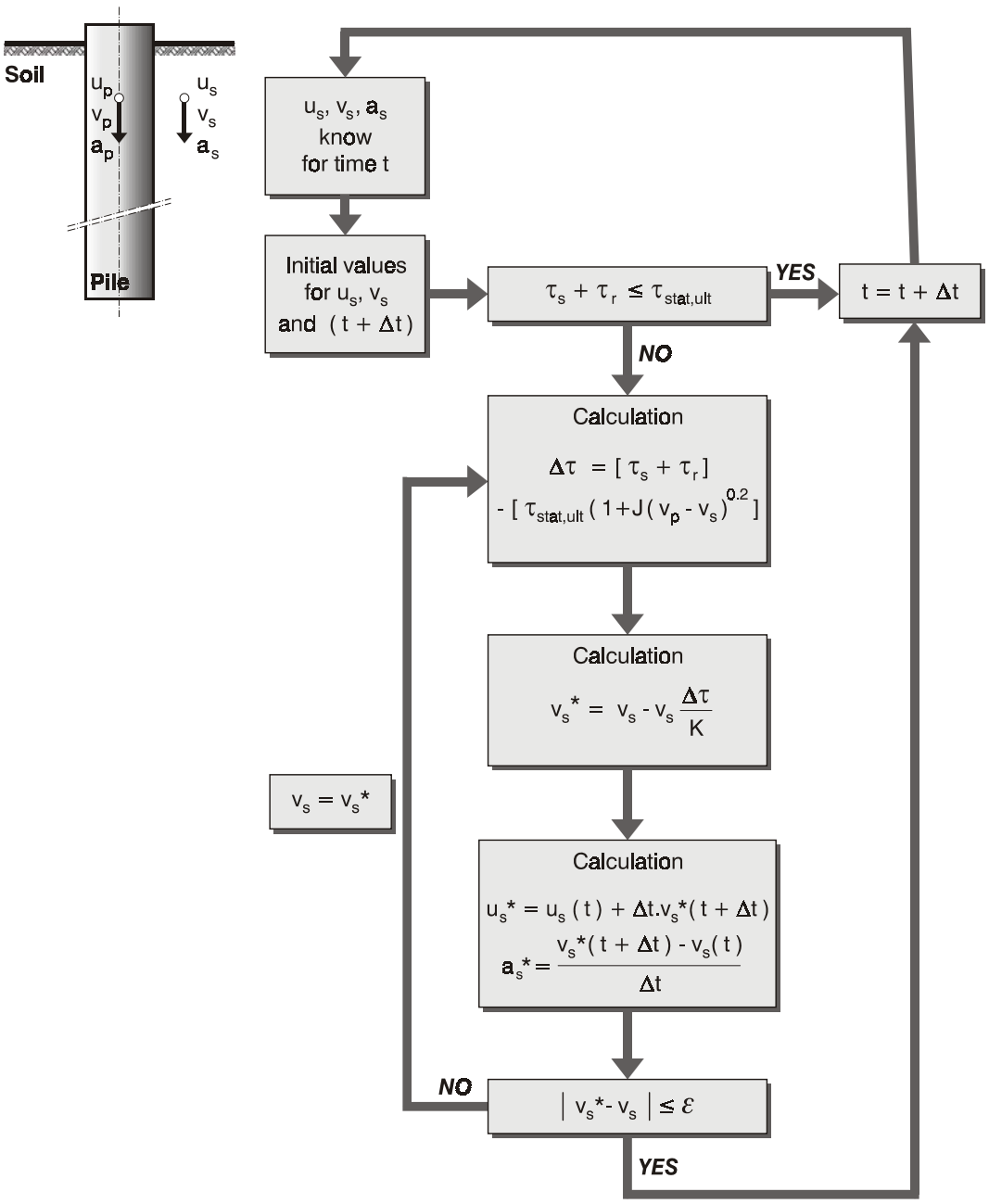

Figure V-4: algorithm of resolution for the DDOF model

The soil reaction during the slippage becomes:

$$\tau_{rheol} = \tau_s + \tau_{rad} = \tau_{stat,ult} \cdot \left(1 + J \cdot \left(v_p - v_s\right)^{0.2}\right) \qquad \textbf{Equ. V-8}$$

and allows to compute the pile motion for the next time step starting a new resolution loop of v_s .

The soil and pile re-bond when both velocities become equal ($v_p = v_s$) and when the soil reaction ($\tau_{rheol} = \tau_s + \tau_{rad}$) becomes inferior to the ultimate static resistance of the soil ($= \tau_{stat,ult}$).

The numerical convergence depends on the gap between **A** and **B** (points 3 & 4 of the algorithm). To ascertain this convergence, the constant K is introduced in order to smooth the variation imposed to v_s.

The value of K is set to 2…4 after a set of successful trials. The coefficient K has the same unit than $\Delta\tau$ so that the ratio $\frac{\Delta\tau}{K}$ is dimensionless.

The equations signs are significant to ensure the stability, the continuity and the convergence of the algorithm. The algorithm is relevant with the following rules:

If **A** =($\tau_s + \tau_{rad}$) > 0 and $v_s > 0$ then

$\tau_{stat,\,ult} > 0$

$$\Delta\tau = \mathbf{A} - \mathbf{B} = \left(\tau_s + \tau_{rad}\right) - \tau_{stat,ult} \cdot \left(1 + J \cdot \left(v_p - v_s\right)^{0.2}\right)$$

$$v_s^* = v_s - v_s \cdot \frac{\Delta\tau}{K}$$

If **A** =($\tau_s + \tau_{rad}$) > 0 and $v_s < 0$ then

$\tau_{stat,\,ult} > 0$

$$\Delta\tau = \mathbf{A} - \mathbf{B} = \left(\tau_s + \tau_{rad}\right) - \tau_{stat,ult} \cdot \left(1 + J \cdot \left(v_p - v_s\right)^{0.2}\right)$$

$$v_s^* = v_s + v_s \cdot \frac{\Delta\tau}{K}$$

If **A** =($\tau_s + \tau_{rad}$) < 0 and $v_s < 0$ then

$\tau_{stat,\,ult} < 0$

$$\Delta\tau = \mathbf{A} - \mathbf{B} = \left(\tau_s + \tau_{rad}\right) - \tau_{stat,ult} \cdot \left(1 - J \cdot \left(v_p - v_s\right)^{0.2}\right)$$

$$v_s^* = v_s + v_s \cdot \frac{\Delta\tau}{K}$$

If **A** =($\tau_s + \tau_{rad}$) < 0 and $v_s > 0$ then

$\tau_{stat,\,ult} < 0$

$$\Delta\tau = \mathbf{A} - \mathbf{B} = \left(\tau_s + \tau_{rad}\right) - \tau_{stat,ult} \cdot \left(1 + J \cdot \left(v_p - v_s\right)^{0.2}\right)$$

$$v_s^* = v_s - v_s \cdot \frac{\Delta\tau}{K}$$

The respect of this algorithm allows one to calculate the independent soil velocity without having to add a mass element to represent the soil in the close vicinity of the pile.

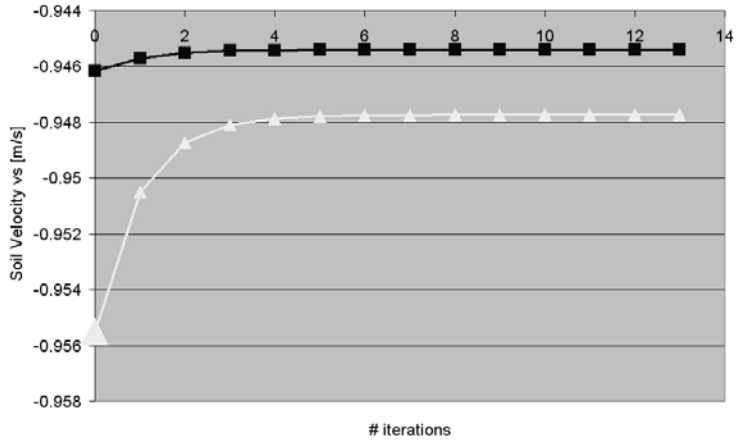

Figure V-5: Examples of v_s resolution

Figure V-5 shows two examples of resolution by using this algorithm. As shown, the convergence is achieved quickly and stably. The biggest marks at the beginning of each curves show the initial values for v_s.

In order to use an implicit method, Equ. V-8 has to be simplified by gathering the terms in u_s and v_s. The problems could be solved using the Newmark integration scheme if the

exponent N was set equal to 1 but not for N=0.2 as formulated.

After description of the algorithm, the results of simulations are presented in the following sections on a simplified model.

2.3. Simplified pile/soil model

This pile model only takes the shaft friction into account. The pile is geometrically characterized by a radius R and a length L. These two parameters are required to evaluate the static soil reaction (chapter 3, section 2.2.2 evaluation of the radius of influence R_m). A given synthetic motion is imposed to its head and transmitted to the soil. This motion is based on a real signal of velocity measured during a dynamic load test event. This modelling is described in details in chapter 3, section 2.4. and plotted in Figure V-6.

The velocity, the displacement and the acceleration signals are given by:

- $V(t)=V_o \cdot e^{(-\xi\omega t)} Sin(\omega t)$;
- $Acc(t)=\frac{\partial V(t)}{\partial t}=V_o \cdot \omega \cdot e^{(-\xi\omega t)}\left(-\xi \cdot Sin(\omega t)+Cos(\omega t)\right)$;
- $U(t)=\int V(t)dt=\frac{V_o}{-\xi\omega} \cdot \omega \cdot e^{(-\xi\omega t)} \frac{\left(Sin(\omega t)-\frac{\omega}{-\xi\omega}Cos(\omega t)\right)}{1+\frac{\omega^2}{(-\xi\omega)^2}}$.

Where ω is the circular frequency: 272 rad/s; V_0 is the initial velocity: 1.45 m/s and ξ is the attenuation coefficient: 0.233 rad^{-1}.

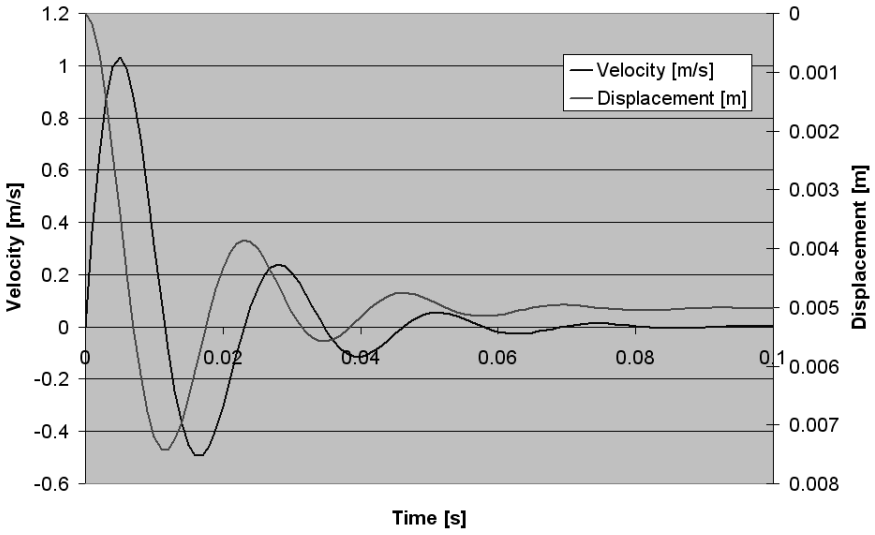

Figure V-6: Imposed motion (displacement and velocity)

The pile geometry parameters are given by:

- The pile length: 10 m;
- The pile radius: 0.2 m.

The pile is considered as rigid and the soil as one sole layer of which the characteristics are given by:

- Ultimate shear resistance $\tau_{stat,ult}$: 0.2 MPa;
- Poisson ratio υ: 0.35;
- Soil mass density ρ_{sol}: 2000 kg/m³;
- Initial shear modulus G_i: 100 MPa.
- Damping factor of the viscous term J_s : 0.5 s/m$^{0.2}$;
- Damping factor of the ultimate rheologic term J : 0.5 s/m$^{0.2}$;
- Velocity dependent power law exponent: 0.2.

The simplified model is described in Figure V-7 and called DDOF. A special attention is put to the interface behaviour (stress and motion).

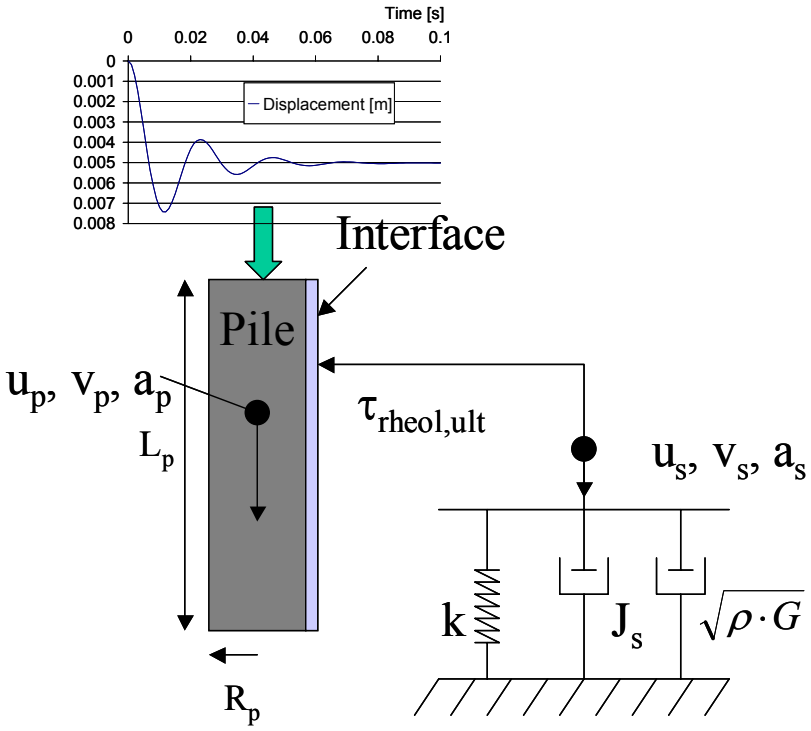

Figure V-7: description of the simplified pile/soil model

First, the results generated by this model are examined alone. After, a short analysis of the main parameters influencing the slippage or governing the interface velocity during slippage is proposed. Eventually, a comparison with the SDOF model, without slippage, in the same configuration, is performed.

2.4. Analysis of the DDOF Model results

Two sets of tests have been carried out to differentiate a case where the slippage is developed and a case where it is not. To allow this comparison, the static ultimate shear resistance $\tau_{ult,stat}$ is set to 0.2MPa and 2 MPa. The first soil resistance is too small and the second is sufficiently large to avoid the slippage. Those two cases allow the comparison with both typical behaviours concerned. The typical signals are pile and soil displacements; pile and soil velocities; interface soil reaction (static and rheologic) an the mobilization curves (soil reaction – soil/pile/interface displacement).

2.4.1 Comparison of the displacement curves

The first couple of figures (Figure V-8 et Figure V-9) show the displacement imposed to the pile (black trace), and the generated soil motion (white trace).

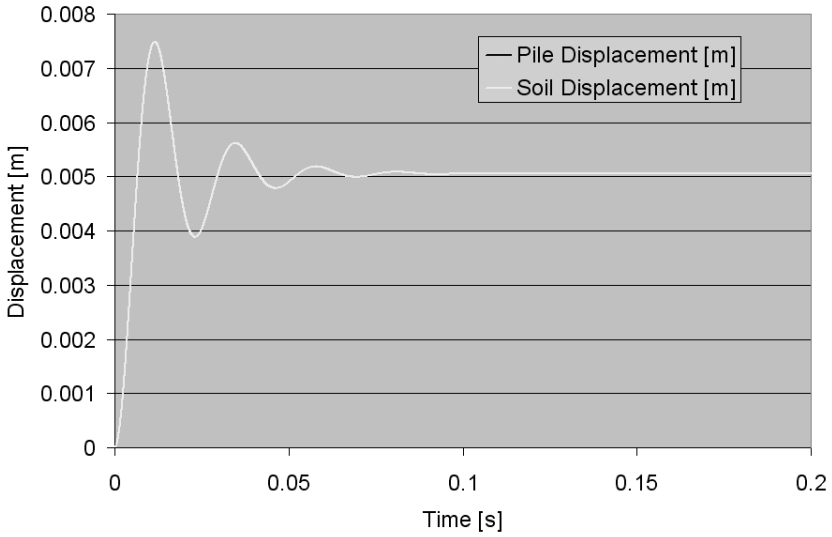

Figure V-8: Pile and soil displacements (DDOF model) - $\tau_{stat,\ ult}$: 2 MPa

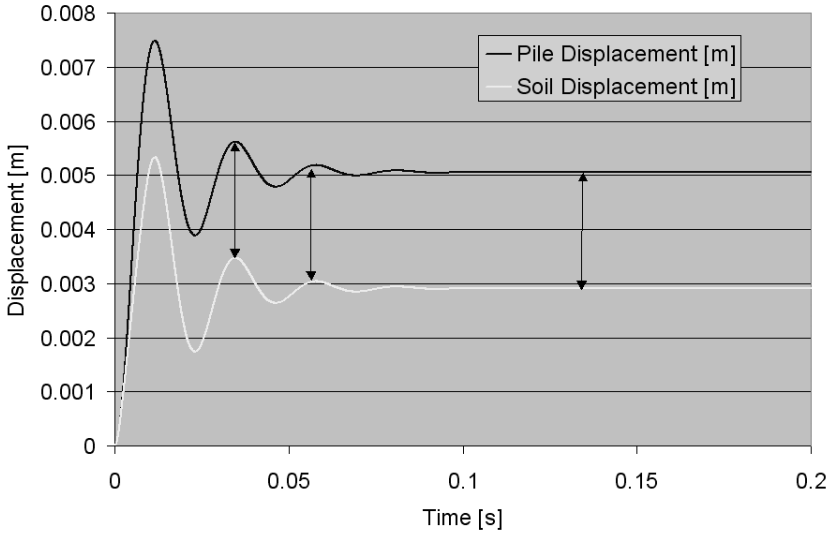

Figure V-9: Pile and soil displacements (DDOF model) - $\tau_{stat,\ ult}$: 0.2 MPa.

When the ultimate resistance is high enough, both elements, pile and soil, move coupled. Therefore, the displacement curves are superimposed (Figure V-8) and pile and soil in its direct vicinity undergo the same settlement path. On the other hand, the small strength threshold of the soil ($\tau_{stat,\ ult}$ = 0.2 MPa) influences directly the soil motion (Figure V-9). Both maximum and final displacements are influenced. The variation of displacement is working during the first part of the curve due to the strict period of slippage (differentiation of motion). After, both signals are perfectly parallel because the bodies are anew coupled (black arrows on Figure V-9). The difference of displacement is the effective penetration of the pile also called the permanent settlement.

2.4.2 Comparison of the velocity curves

Similarly to the displacement curves, when the ultimate resistance is too large, the pile and soil velocities are superimposed because they are continuously coupled (Figure V-10). Figure V-11 exhibits the result of the weakest soil. There are two occurrences of slippage during the first 30 ms.

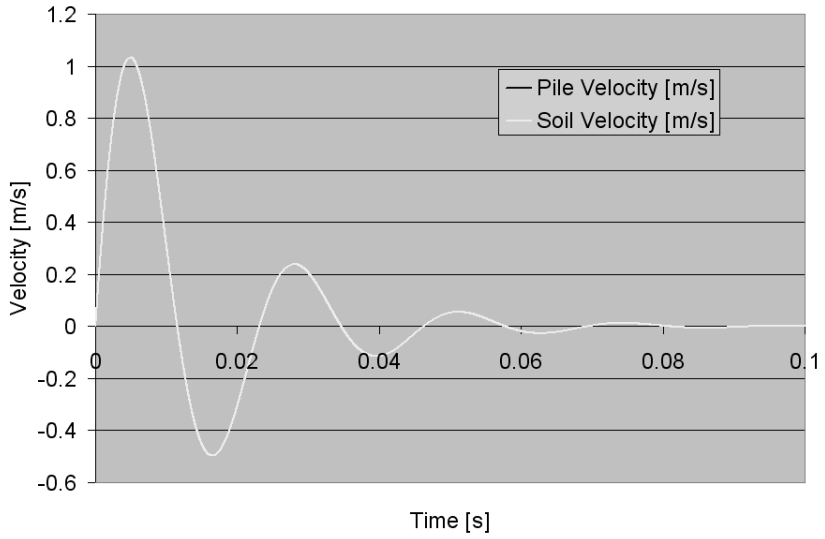

Figure V-10: Pile and soil velocities (DDOF model)- $\tau_{stat,\ ult}$: 2 MPa

The first slip event is clear and starts early in the motion evolution. The second is tiny and short and is barely visible on Figure V-11 (encircled).

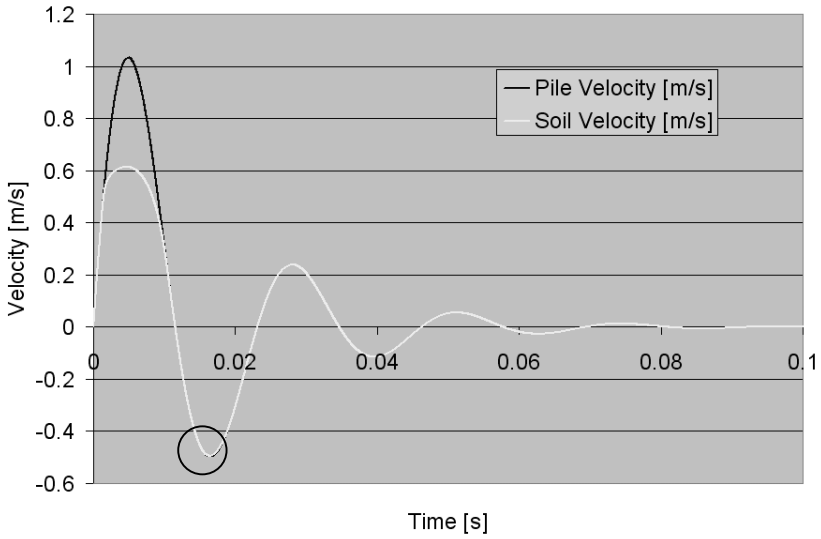

Figure V-11: Pile and soil velocities (DDOF model) – $\tau_{stat,\ ult}$: 0.2 MPa

The ultimate static resistance is exceeded twice during the simulation, once in the positive velocities field, once in the negative domain. Both modifications influence the soil and the pile behaviours. It is only during these periods that the pile settles down permanently compared to its direct vicinity. Figure V-12 is a zoom of the velocity curves focused where the velocities diverge. In order to have a better overview of the situation, this simulation has been performed with $\tau_{ult,stat}$ = 0.15 MPa highlighting a larger difference in the second slip occurrence. The light curve highlights the breaks in the continuity of the soil velocity history when the slippage starts and ends defining the passage to the failure mode and the slippage between the pile and the soil (two circles on Figure V-12).

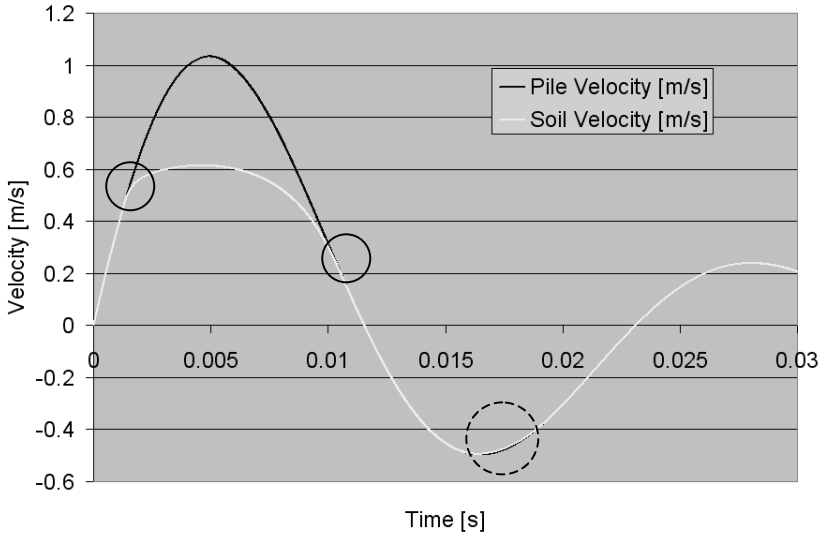

Figure V-12: Pile and soil velocities (DDOF model) – (zoom) $\tau_{stat,\ ult}$: 0.15 MPa

There is also a second break in the continuity of this trace (dashed circle on Figure V-12). During the second slip event, The first break point corresponds to the entrance in the failure mode. The second corresponds to the passage from positive static to negative static stresses. Since the soil velocity is nil

when the static stress is maximum (arrow v_s =0 on Figure V-13), the velocity dependent term influence the stress "negatively". When the static stress crosses the zero level, all the terms of Equ. V-3 are of same sign and the evolution is similar to the first slip event. The point 1 corresponds to the passage to the failure mode while point 2. corresponds to the equalisation of the stress signs.

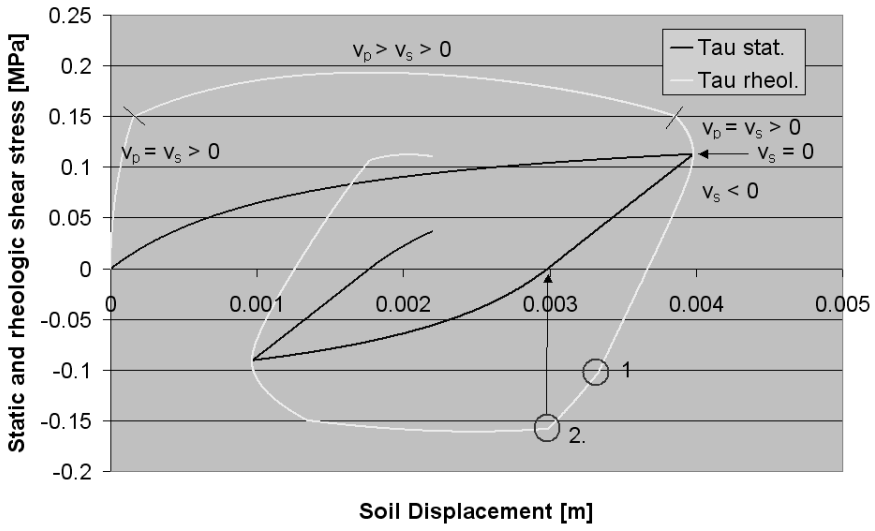

Figure V-13 : Static and rheologic shear stresses vs. soil displacement - $\tau_{stat,\ ult}$: 0.15 MPa

Figure V-14 exhibits the penetration velocity (v_p - v_s) in a simulation performed with $\tau_{stat,\ ult}$: 0.2 MPa. If this curve is integrated with respect to time, it wil result in the pile penetration. The differentiation of velocities (pile and soil) is similar to the Paquet approach (1988) (Figure V-15) wherein the interface velocity (v_p - v_s) is called the penetration or interface velocity. For Paquet, the final penetration of the pile (final gap between both displacement curves of Figure V-9) is connected to the penetration velocity. This differentiation of behaviours occurs when the slippage resistance is exceeded. The definitions of the limit and of the soil reaction are different but the methodology is similar.

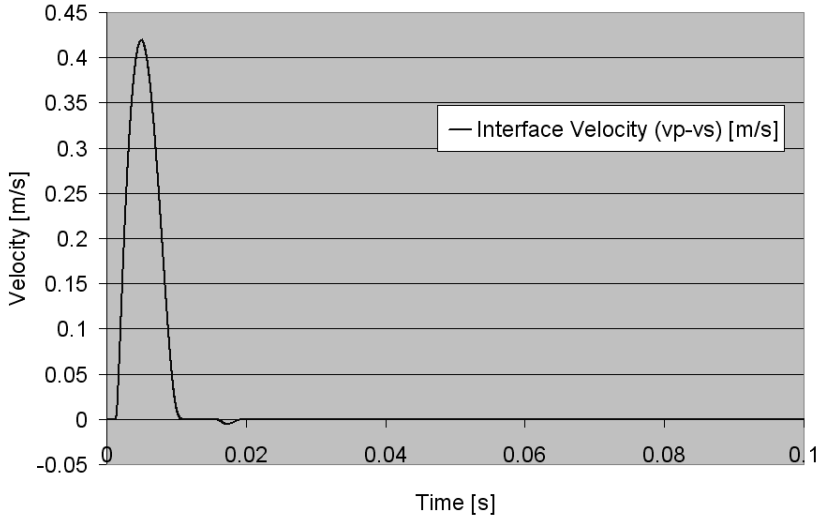

Figure V-14: Penetration velocity – $\tau_{stat,\ ult}$: 0.2 MPa

Paquet challenges the classic formulation where the soil reaction is modelled by an elastoplastic soil reaction plus a viscous coefficient J (the rheologic term of the SDOF model). According to him, this approach seems to draw more upon empirical considerations than physical characteristics. There is no clear differentiation between the movement of the pile and the movement of the soil. The dashpot associated with the pile movement can not represent the radiative type damping (linked to the movement of the soil) or the viscosity of the penetration (associated with the difference of movement between the pile and the soil). Paquet states that the displacements of pile and soil are perfectly differentiated and their difference is the pile penetration. The reaction of the soil is represented by a spring and a dashpot theoretically determined by the expressions given by Briard (1970) and Novak et al (1978). They are linked to the soil displacement and represent the impedance of the soil layer (Figure V-16).

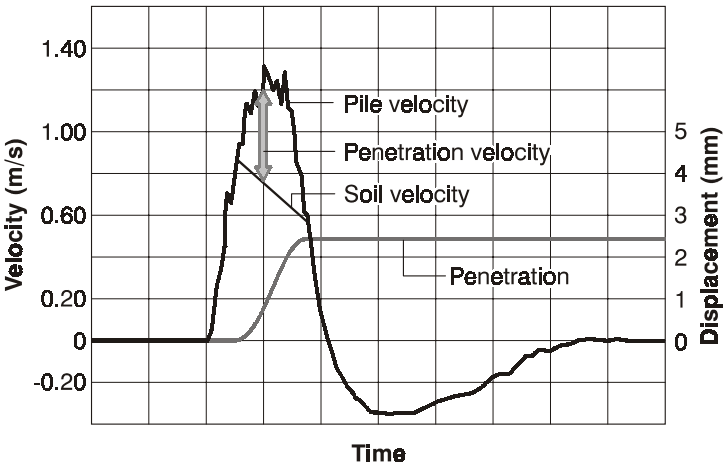

Figure V-15: Description of the Paquet model (Paquet, 1988)

Heritier and Paquet have shown that the failure can be obtained from the stress generated by the radiative component (Heritier and Paquet, 1984). To take this failure into account, a slider is added to the Paquet's model to represent the possible slippage between the pile and the soil when the stress generated in the soil becomes larger than the limit. For Paquet, this limit can be a function of the mean penetration velocity or the static ultimate resistance associated with a dashpot. This approach is particularly similar to the approach explained in this section.

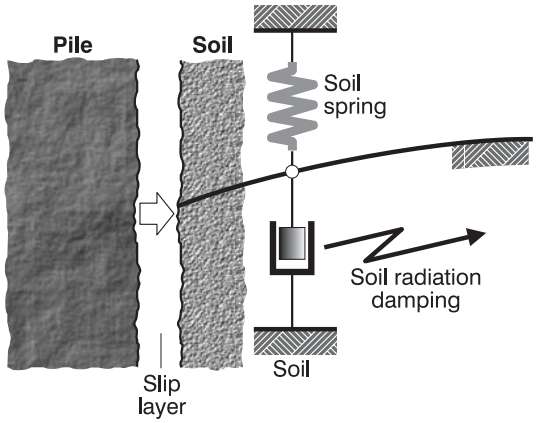

Figure V-16: Schematic Simbat model (Stain, 1992)

2.4.3 Comparison of the static and rheologic stress curves

The static and rheologic stresses can also be examined. The static stresses (related to the non linear spring via hyperbolic relationship) and the rheologic stresses (sum of all terms: static, viscous and radiative) are differentiated on Figure V-17 and Figure V-18 . These terms are linked to the soil motion (velocity and displacement). Since the ultimate soil resistance is large enough to avoid slippage in Figure V-17, the static stress curve looks like the displacement trace (even though the stiffness is not linear and decreases with the soil mobilization).

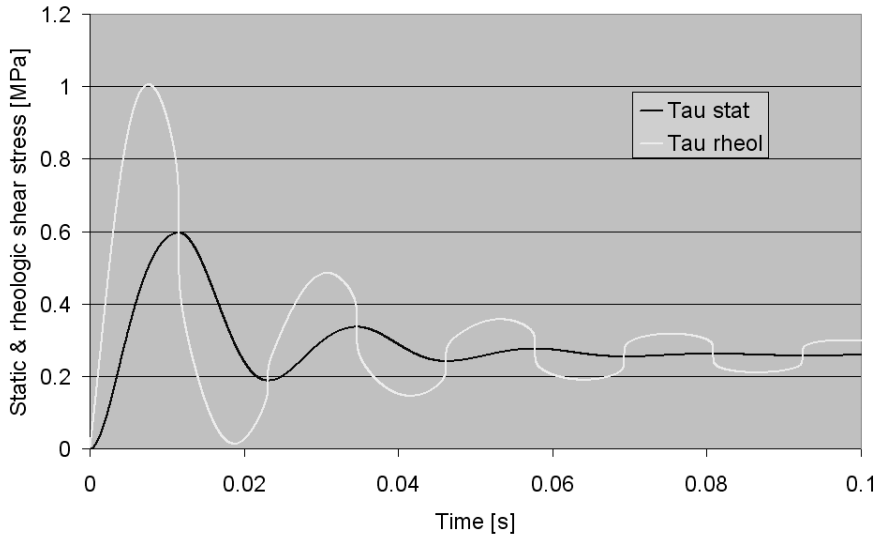

Figure V-17: Rheologic and static stresses (DDOF model)- $\tau_{stat,\ ult}$: 2 MPa

Both rheologic and static traces are characterized by a same frequency and a phase gap. Since the velocity is ahead of the displacement (Figure V-6), this influence is recovered in the displacement and velocity dependent terms of the rheologic stress. Figure V-18 highlights the influence of the slippage on the static stress. The soil motion is eased and the level of reached stresses is highly reduced (as expected). Figure V-18 is still itemized with the addition of the trace of the difference between the rheologic and the static stress traces (Figure V-19). The result exhibits the influence of the soil velocity and the predominance of the velocity dependent terms in the rheologic stress evaluation, especially in the beginning of the mobilization.

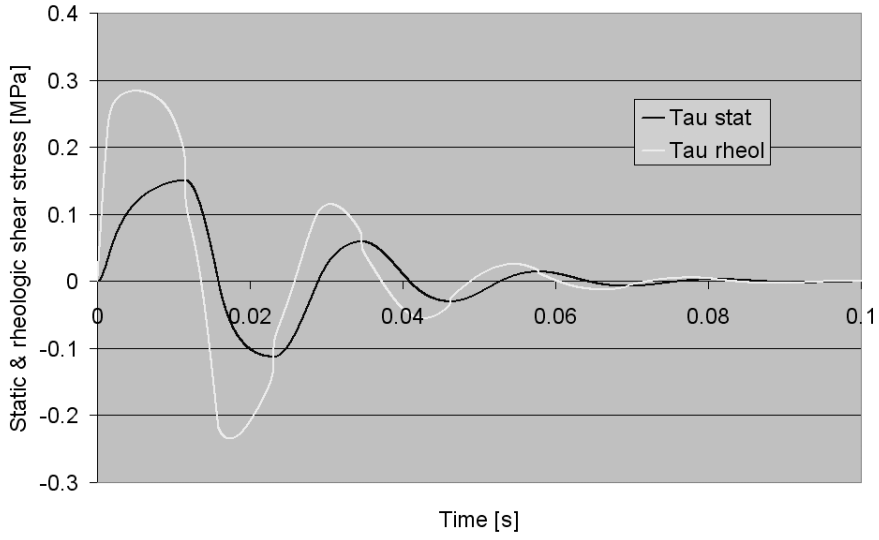

Figure V-18: Rheologic and static stresses (DDOF model)- $\tau_{stat,\ ult}$: 0.2 MPa

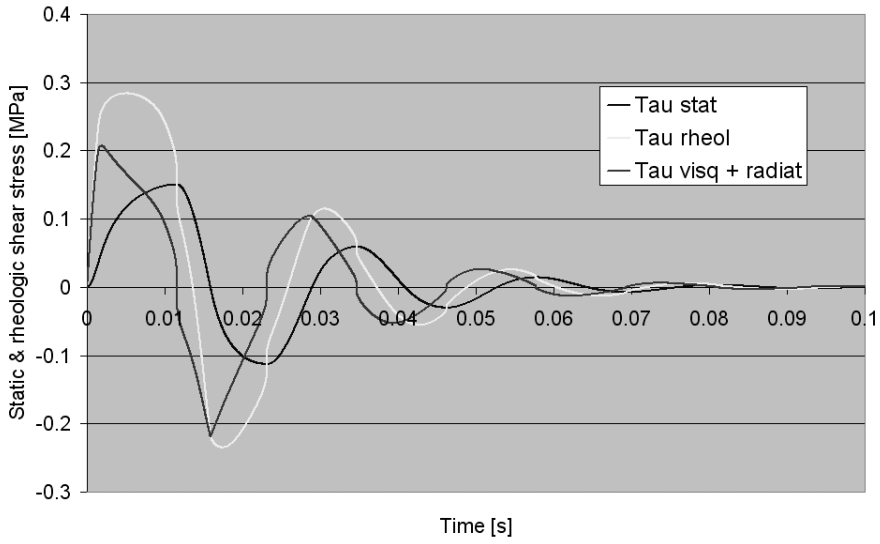

Figure V-19: Rheologic, static stresses and their difference (DDOF model)- $\tau_{stat,\ ult}$: 0.2 MPa

The final stress state of the soil is function of the soil reaction history and of the ultimate stress level of soil resistance. For a same motion imposed, if the first simulation ($\tau_{ult,stat}$ = 2 MPa) results in a certain state of residual stress along the pile shaft (about 0.26 MPa), the second proposition ($\tau_{ult,stat}$: 0.2 MPa) almost nullifies the final stresses around the pile. This parameter influences the final stress state of the pile/soil interaction (influence in the static equilibrium and the dynamic analysis during driving).

2.4.4 Comparison of the displacement-stress curves

The static behaviour of both simulations (τ_{ult} = 0.2 MPa and τ_{ult} =2 MPa) remains hyperbolic (Figure V-20 and Figure V-21) and the influence of the velocity dependent terms is greatly influenced by the sign of the soil velocity.

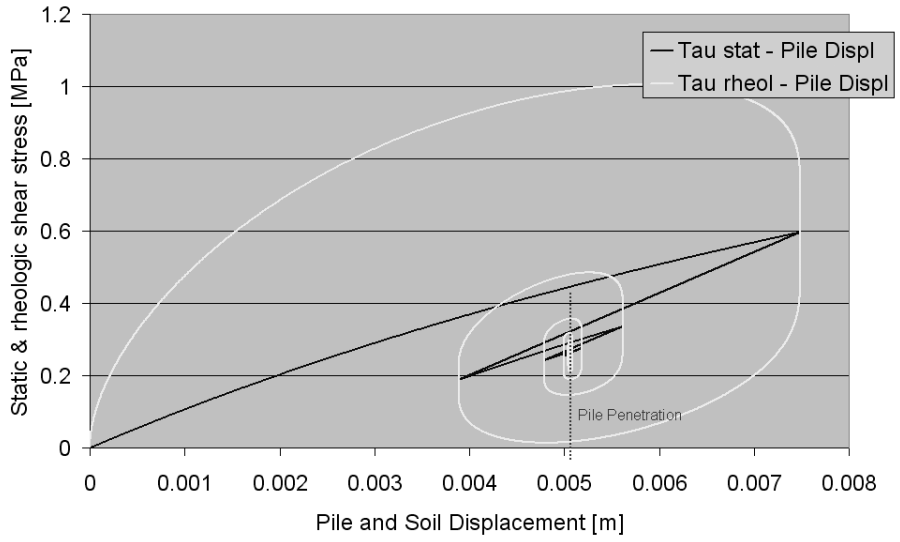

Figure V-20: Static and rheologic stresses vs. pile & soil displacements - $\tau_{stat,\ ult}$: 2 MPa

Figure V-20 shows the case without slippage ($\tau_{ult,stat}$: 2 MPa). The pile and soil displacements are coupled all the time and the four traces are superimposed two by two. The pile penetration is nil compared to the adjacent soil because both displacements are coupled but is equal to its final position compared to the initial referential.

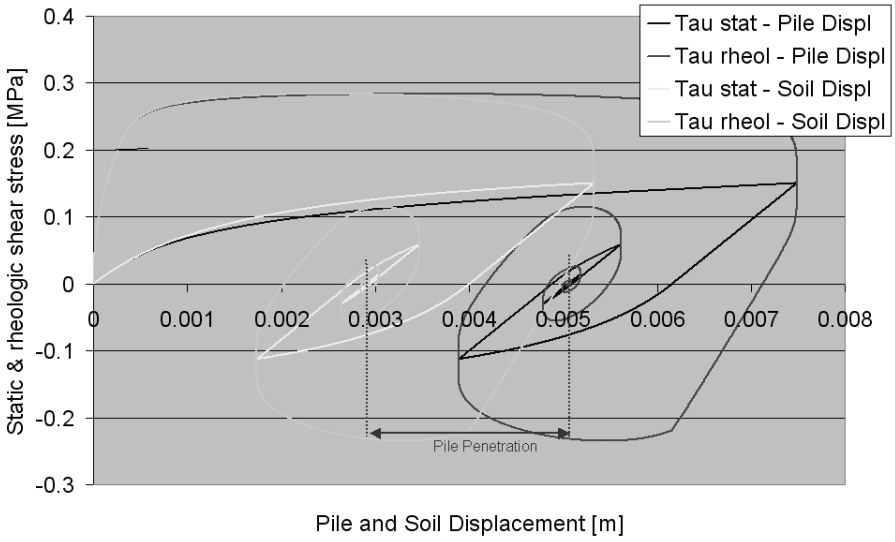

Figure V-21: Static and rheologic stresses vs. pile & soil displacements - $\tau_{stat,\,ult}$: 0.2 MPa

Figure V-21 exhibits the behaviour of the soil reaction with respect to the pile and the soil motions. The difference between both final settlements can be considered as the net settlement of the pile sliding into the soil. Nevertheless, compared to the initial referential, the final position of the pile is the final settlement. there is a settlement of the soil in the direct vicinity of the pile influenced by the pile motion. Since the final displacement is different, the settlement path does not influence the unloading parameters optimisation and the ratio of shear modulus G_2/G_i could be fixed to 1 without influence on the optimisation of the other parameters (to be checked with complete model). The first part of the traces is identical for both displacements because both behaviours are coupled at this moment and are only differentiated during the slippage. This slippage occurs for a rheologic stress superior to $\tau_{stat,ult}$ = 0.2 MPa as expected.

2.5. Influence of a variation of $\tau_{ult,stat}$

This section compares the evolution of the main curves already described (displacement, velocity, rheologic stress) for a variation of ultimate static soil resistances (from $\tau_{ult,stat}$: 0.02 MPa to 0.7 MPa). The parameters of the pile/soil system remain the same than listed in section 2.3. The response of the pile/soil system with $\tau_{stat,ult}$: 0.7 MPa corresponds to a situation where no slippage occurs (identical to case $\tau_{stat,ult}$: 2 MPa presented previously).

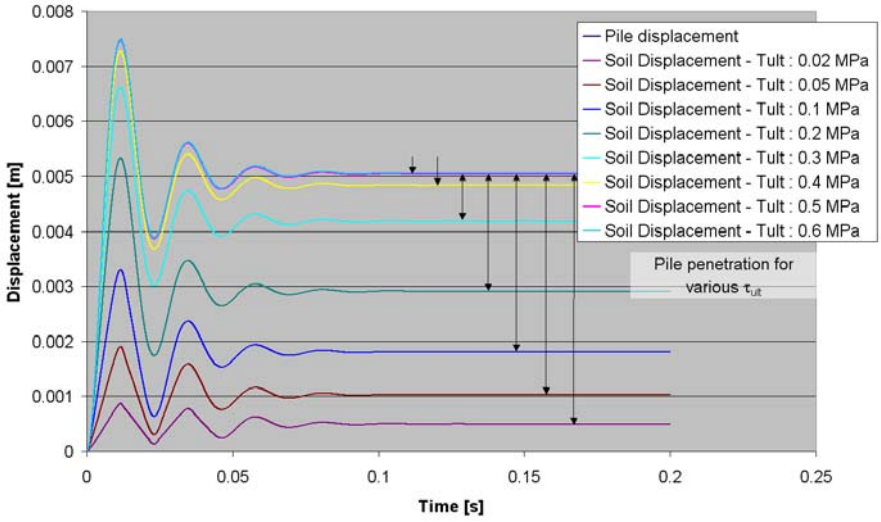

Figure V-22: Pile and soil displacements (DDOF model) - $\tau_{stat,\ ult}$: 0.02 to 0.7 MPa

Figure V-22 exhibits the traces of the generated soil displacement for each case of ultimate static shear stress proposed. The evolution is similar to the stress trend. The maximum soil displacement reached increases with $\tau_{stat,ult}$ like the final settlement of the soil. On the other hand, the pile penetration (u_p-u_s) (Figure V-23) decreases with $\tau_{stat,ult}$.

The evolution of the pile penetration with $\tau_{ult,stat}$ depends on the number of slippage events and their timing. If the slippage occurs when the velocity is positive, the reduction of the soil velocity compared to the pile velocity results in an increase of the final pile penetration. If the opposite situation is observed (slippage occurring during a period where velocities are negative), the consequence is a decrease of the pile penetration. This is illustrated by the evolution of the curve of Figure V-23 where the progression of the pile penetration is slowed down when two slippage events (the first in positive velocities and the second in negative velocities) perturb the pile/soil system response.

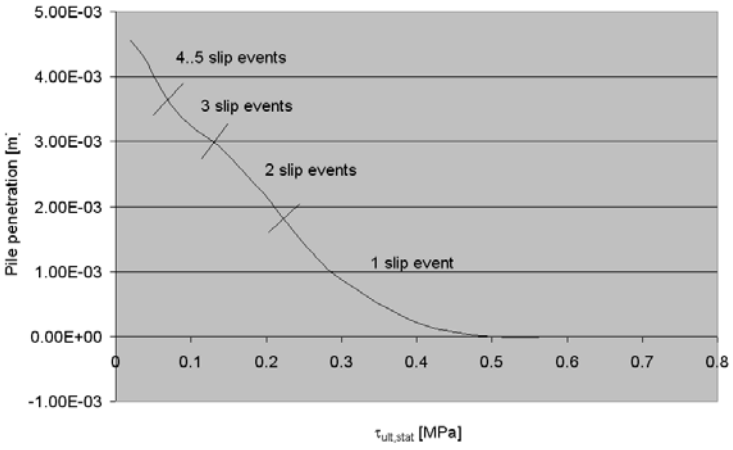

Figure V-23: Evolution of the pile penetration in the DDOF model for various τ_{ult}

As expected, the number of slippage events increases when $\tau_{ult,stat}$ decreases because the threshold of resistance to be exceeded to enable slippage decreases.

Figure V-24 shows the evolution of the soil velocity compared to the pile velocity for the same variation of $\tau_{ult,stat}$.

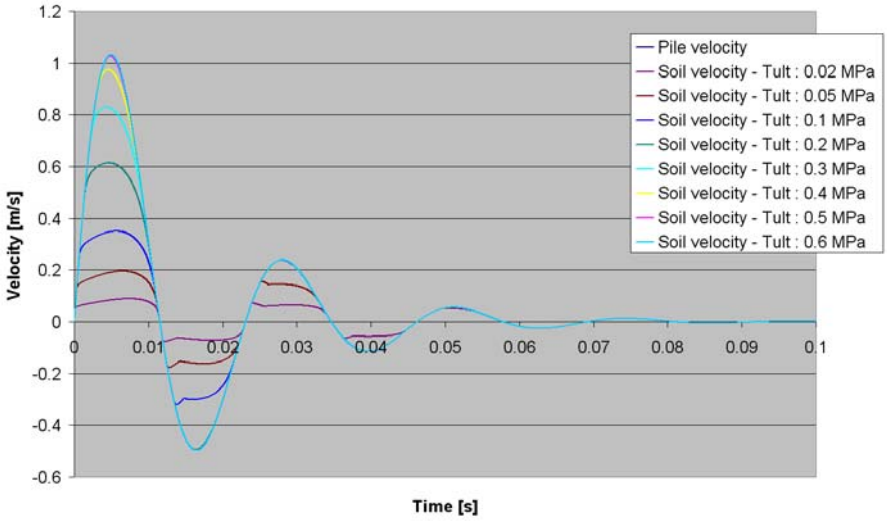

Figure V-24 : Pile and soil velocities (DDOF model) - $\tau_{stat,\ ult}$: 0.02 to 0.7 MPa

Figure V-24 exhibits the strong influence of the ultimate static resistance in the evaluation of the soil velocity with the proposed model. When the ultimate static resistance is reduced, the disconnections start more and more early and the number of slip events increases. If the soil resistance is very poor, the soil motion is greatly influenced and the corresponding soil velocity and displacement are very small for a same imposed pile motion. The pile and soil velocities remain of the same sign during the separations. There is a re-bonding before each change of velocity sign. The larger the ultimate resistance, the more similar the velocity curve compared to the pile one.

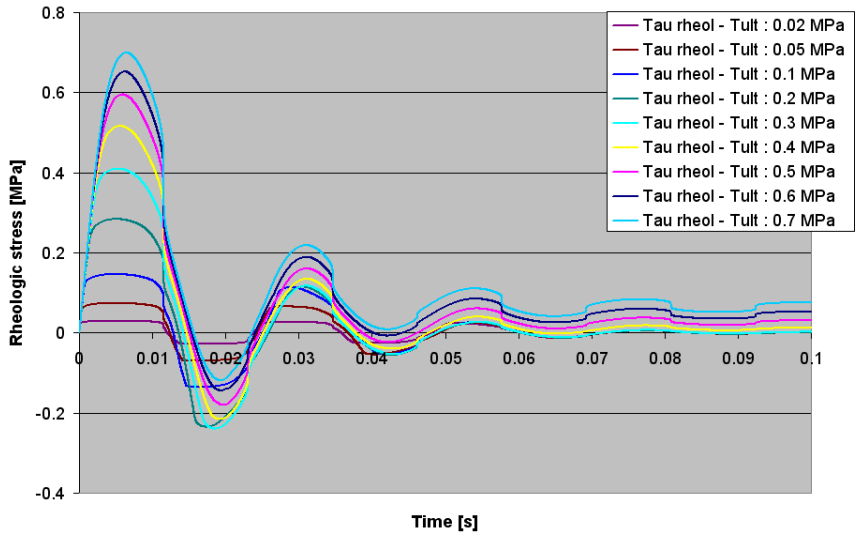

Figure V-25: Rheologic stresses (DDOF model) - $\tau_{stat,\ ult}$: 0.02 to 0.7 MPa

Figure V-25 describes the evolution of the rheologic stresses for a variation of ultimate static strength. The change of ultimate static stress influences more the peak value than the final state of the rheologic stress. The first peak illustrates this link because of the complete mobilization of the resistance and the development of the slippage resistance (dependent of the interface velocity). The final shear stress state remains approximately in the same range due to the small levels of velocities.

2.6. Influence of a variation of the rheologic parameter J

The pile/soil system response is defined by the equations Equ. V-1 to Equ. V-4. In those equations, besides the ultimate static stress, other parameters are of importance: the rheologic parameters J and N. Since N is fixed in the literature, it is interesting to evaluate the influence of J on the slippage development. The following figures summarize this analysis with the traces of the main quantities already presented in the previous sections: the soil displacement and velocity and the rheologic stress with respect to time compared to the pile motion. J is proposed varying between 0.1 and 5 (s/m). Both damping factors (J and J_s) are used equal but they represents different behaviours. The first is linked to the soil (viscous one, J_s) and to its velocity (v_s), and the second is a failure parameter linked to the interface behaviour (J).

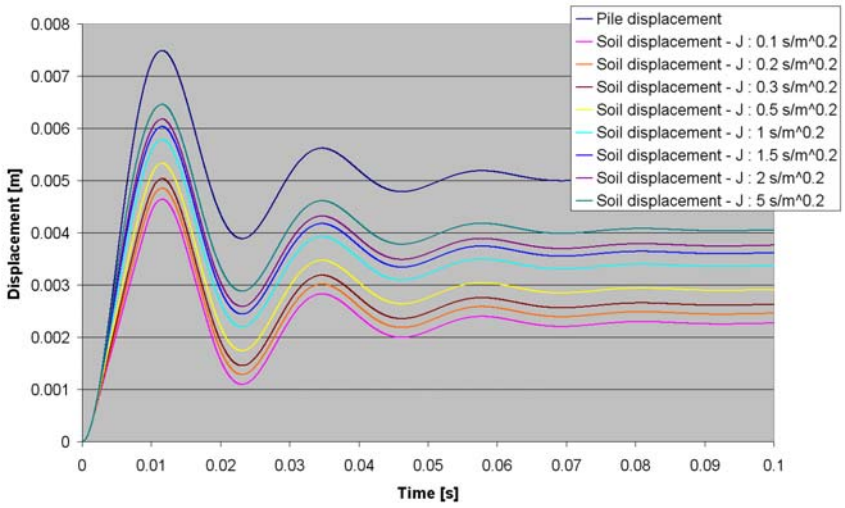

Figure V-26: Evolution of the soil displacement curves with variation of J - $\tau_{stat,\ ult}$: 0.2 MPa

Figure V-26 displays the soil displacement traces for each proposed value of J. The influence of J on the whole trace is very important. It is slightly more pronounced on the final displacement (about 2mm). The parameter J has a great influence on the soil displacement and the slippage development.

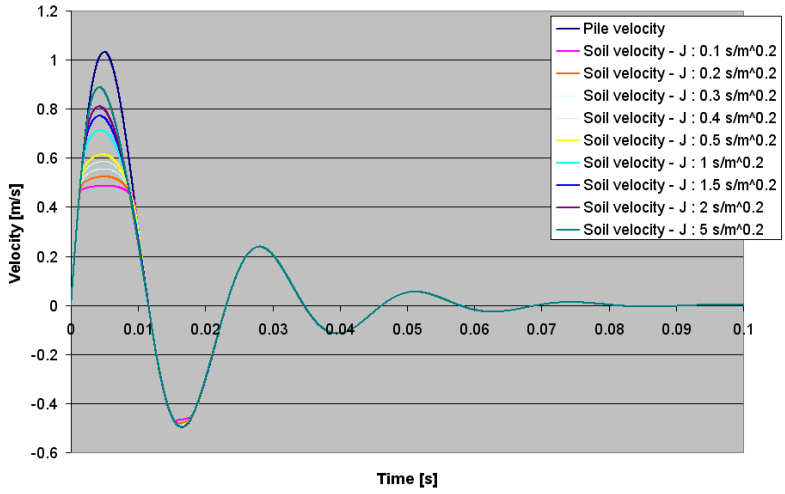

Figure V-27: Evolution of the soil velocity curves with variation of J - $\tau_{stat,\ ult}$: 0.2 MPa

Figure V-27 exhibits the evolution of the generated soil velocity for the variation of J. The influence is very important especially in the first peak of velocity. The soil velocity can vary from 0.5 m/s to more than 0.9 m/s under the selected variation of J. Moreover, the smaller the damping factor, the more sudden the starting of the slippage; the larger the parameter J, the smoother the evolution of the soil velocity during the passage from soil mobilization to failure (there is no breaking in the continuity when both curves separate and re-bond). It can be pointed out that the higher the damping factor, the smaller the penetration velocity (v_p-v_s) with a direct influence on the number of slippage occurrences. Only 5 simulations (J from 0.1 to 0.5 s/m$^{0.2}$) cause a second slip event.

The same value is used for the viscous soil parameter J_s and for the interface parameter J (Equ. V-1 and Equ. V-4). Since they represent two different behaviours, their values must be different but in order to limit the number of parameters to be variable, this research has been performed with the same value.

Figure V-28 exhibits the rheologic stress traces. The increases of the parameter J results in an increases of the soil velocity (viscous term and radiation term) and a reduction of the penetration velocity (ultimate rheologic stress). Consequently, the higher the parameter J, the more accentuated the influence of the velocity dependent terms on the rheologic stress. The viscous term is also highly influenced by the increase of J (see the trace corresponding to J= 5 s/m$^{0.2}$). When the velocity (pile or soil) becomes almost null, the effects of the variation of J tend to vanish.

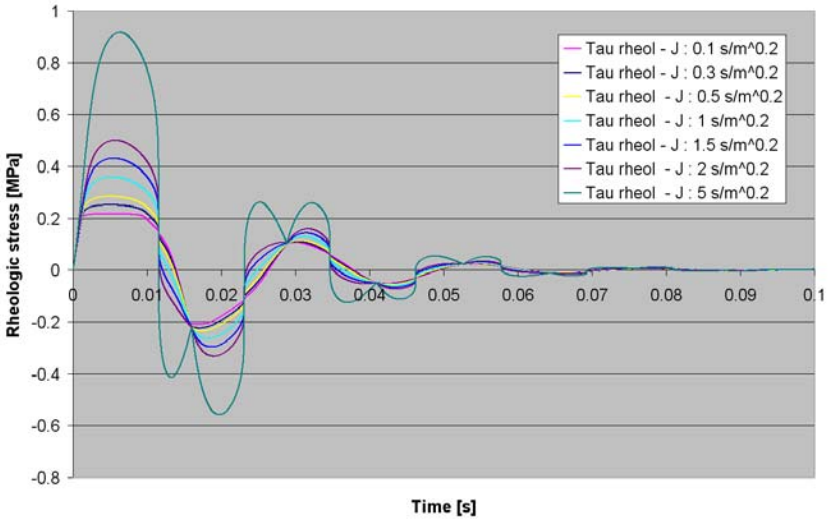

Figure V-28: Evolution of the rheologic stress curves with variation of J – $\tau_{stat, ult}$: 0.2 MPa

2.7. Influence of the differentiation of J and J_s

Equ. V-1 and Equ. V-4 illustrate the loading rate effect by the introduction of the velocity dependent terms. The first expression describes the viscous effect and the second is supposed to illustrate the evolution of the ultimate soil resistance with the soil velocity. Both expressions use a same approach with a power law of the velocity (absolute or relative) multiplied by a constant value (J and J_s). The values of J and J_s were always used equal due to a lack of information of the viscous damping factor

and due to the reduction of the number of parameters, this common value is generally fixed to $0.5 s/m^{0.2}$. However, the behaviours described are completely different: the viscous damping J_s is linked to the soil and to the absolute soil velocity v_s while the rheologic damping factor J is linked to the interface velocity only acting during slippage (v_p-v_s).

This section presents the case where the slippage is forced and where both parameters J and J_s are taken into account with a specific value.

- $J = 0.5\ s/m^{0.2}$ as usual;
- $J_s = 0.05\ s/m^{0.2}$.

The following figures (Figure V-29 to Figure V-32) present the evolutions of the displacement, velocity and stress curves of this new situation compared to the usual one with $J=J_s$.

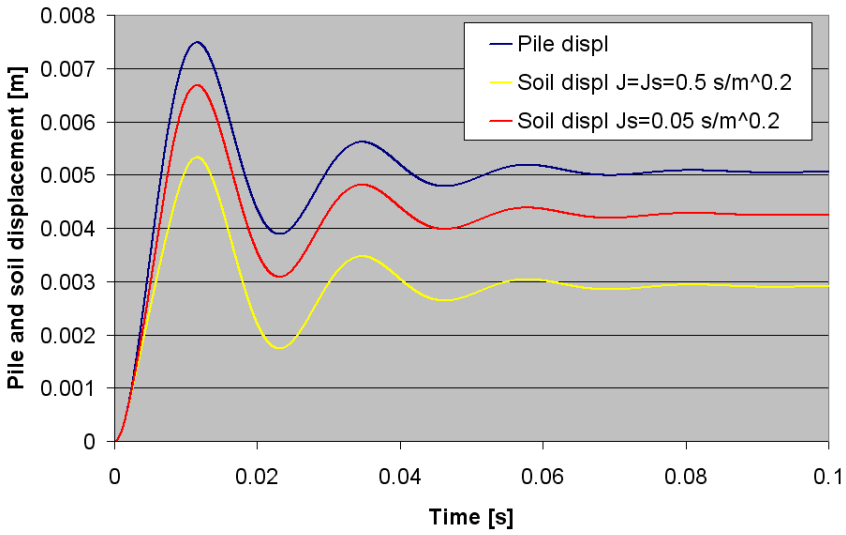

Figure V-29 : Evolution of the soil displacement curves - $\tau_{stat,\ ult}$: 0.2 MPa

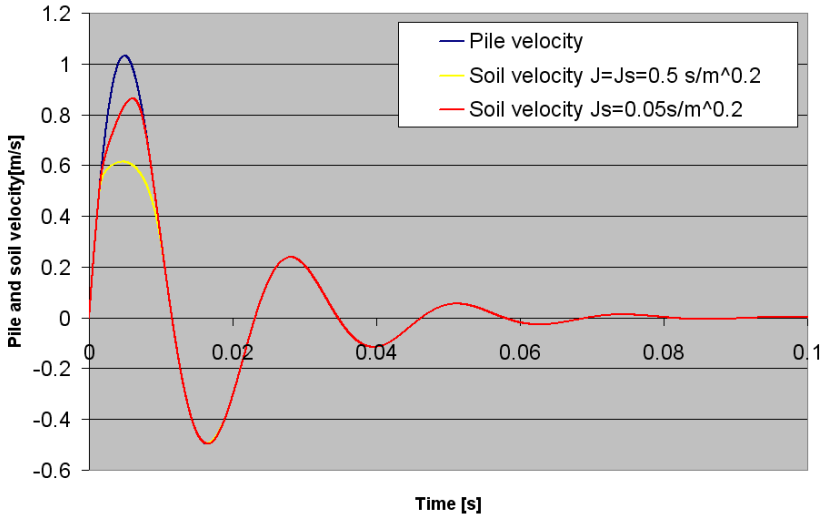

Figure V-30 : Evolution of the soil velocity curves - $\tau_{stat,\ ult}$: 0.2 MPa

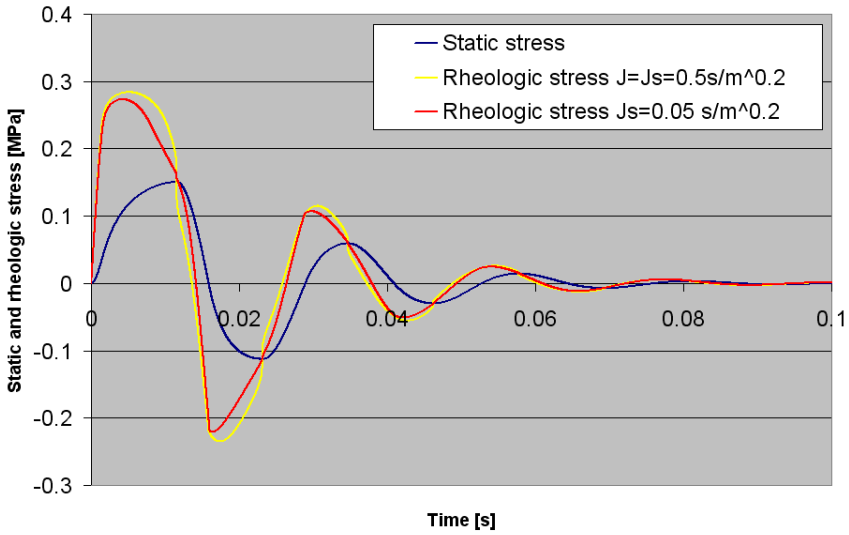

Figure V-31 : Evolution of the static and rheologic stress curves - $\tau_{stat,\ ult}$: 0.2 MPa

The slippage consequences are highly reduced with this change but not suppressed. This highlights the relative importance of the viscous term in the rheologic formulation. The soil velocity (Figure V-30) generated during the slippage in order to equilibrate the slippage condition (Equ. V-6) is larger than for the case $J=J_s$, the penetration velocity is then smaller; the soil displacement is also more developed and the pile penetration is decreased (Figure V-29). The static stress is exactly the same as expected, and the rheologic stress history does not evolve significantly (Figure V-31).

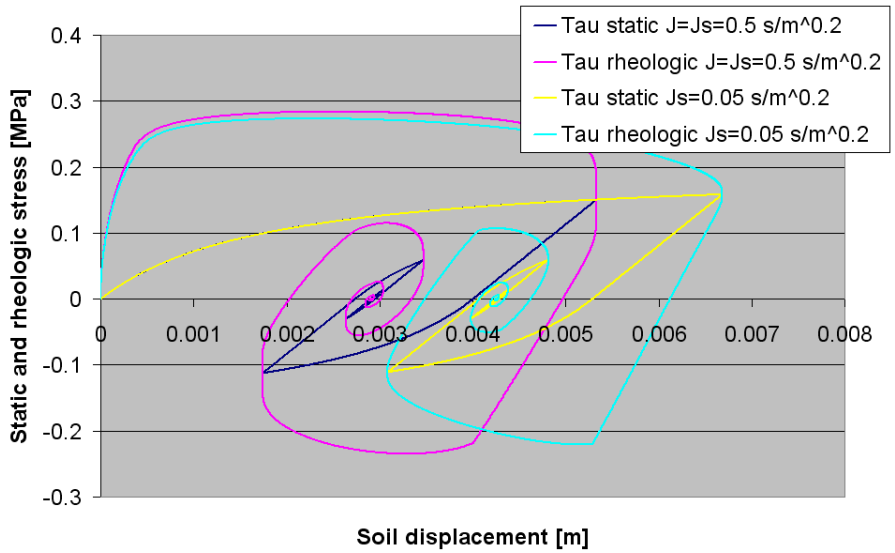

Figure V-32 : Static and rheologic stresses vs. pile & soil displacements with J & J_s different - $\tau_{stat,\ ult}$: 0.2 MPa

Since the soil motion is influenced by the differentiation of J and J_s (larger soil displacement and velocity), the stress-soil displacement relationships take these modifications of behaviour into account. The new traces (J different from J_s) are in an intermediate position between both traces related to the pile and soil motions (for $J=J_s$).

Other parameters can be studied with a particular influence on some terms of the rheologic stress. For example, the importance of the radiation term is highlighted by the influence of the variation of G_i in the generation of the slippage. Since the ultimate stress is quickly saturated if the shear modulus is increased, the slippage of both media is also influenced by the variation of this parameter.

2.8. Comparison with the SDOF model

After this description of the result of the DDOF model submitted to an imposed motion, it can be interesting to compare the responses of the DDOF model with the SDOF model under the same imposed motion and pile/soil system. The comparison is illustrated by the soil mobilization (reaction and motion). The pile and the soil are herefore described with the same parameters:

- Poisson ratio = 0.35;
- G_i = 100 Mpa;
- ρ_{sol} = 2000 kg/m³;
- Pile radius = 0.2 m;
- Pile length = 10 m;
- τ_{ult} = 2 MPa and 0.2 MPa;
- J: undifferentiated damping parameter = 0.5 s/m$^{0.2}$;
- Relative velocity exponent = 0.2.

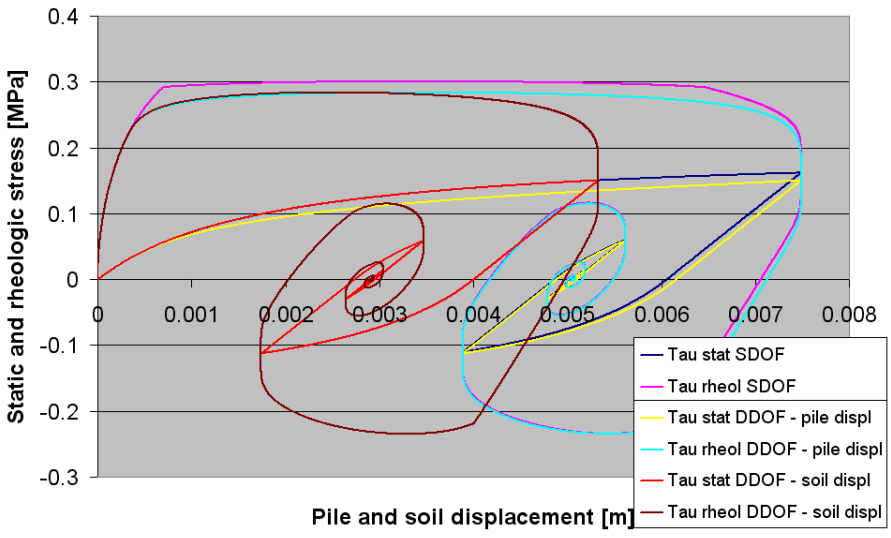

Figure V-33: Comparison of the static and rheologic stresses vs. pile and soil displacement for the models SDOF and DDOF – $\tau_{stat, ult}$: 0.2 MPa

Figure V-33 describes the stress-displacement relationships relevant for both models (SDOF and DDOF) and for the combinations soil reaction – pile and soil displacements (especially for the DDOF model). The simulations are proposed with slippage development.

Since the pile motion is imposed, the displacement histories corresponding to the pile motion (sole case for the SDOF model, one of both cases for the DDOF model) are identical. The differentiation comes from the stress evaluation.

Before the slippage happens, all the curves are superimposed (static and rheologic). After, the DDOF traces disassociate according to the pile and soil motions. The SDOF static stress history respects the DDOF soil static stress history aspect and not the pile one. This is due to the DDOF model which follows the soil motion instead of the pile motion. The development of the hyperbolic curve (stress-displacement relationship) is lead by the soil motion.

The rheologic stress histories exhibit the differentiation in the formulation of the velocity dependency. The SDOF expression is linked to the absolute pile velocity and the DDOF relationship uses the interface velocity which is activated during the slip event.

The passage from the description of the soil reaction to the failure mode is also different (marked by a discontinuity in the traces). Since the starting of the slippage is determined by the exceeding of the ultimate static shear strength in the DDOF model and of a velocity dependent formulation of this limit for the SDOF model, they cannot be similar:

$$\tau_{ult,rheol} = \tau_{ult,stat}\left(1 + J \cdot v_p^{0.2}\right) \qquad \textbf{Equ. IV-36}$$

$$\tau_{ult,rheol} = \tau_{ult,stat}\left(1 + J \cdot \left(v_p - v_s\right)^{0.2}\right) \qquad \textbf{Equ. V-4}$$

Consequently, since the pile is authorized to slip and the soil-displacement relationship allowed to be interrupted during this slippage, the final position of the displacement to be respected at the end of the unloading phase is inferior in the DDOF model. The influence on the back-analysis (see chapter 4) and in the optimisation procedure should be less significant.

The logical next step is to implement this model on a complete pile/soil model including more soil layers, a pile modelled in different elements, the base reaction represented by the equivalent soil cone and to perform the back-analysis process on real measurements of a dynamic load test. Unfortunately, this was not possible in the framework of this research by lack of time, but it remains certainly a major requirement for the future of this work.

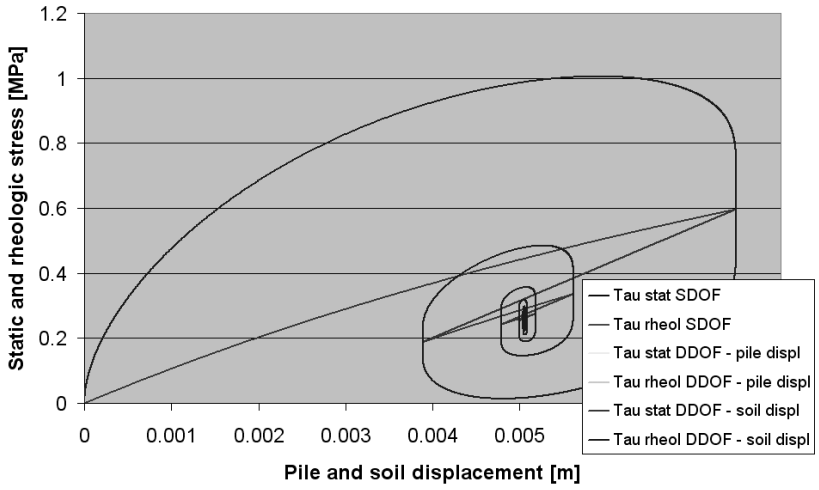

Figure V-34: Comparison of the static and rheologic stresses vs. pile and soil displacement for the models SDOF and DDOF – $\tau_{stat,\ ult}$: 2 MPa

Figure V-34 displays the same traces than in Figure V-33 but in a situation where the ultimate static stress is never exceeded. Consequently, there is no slippage. Figure V-34 confirms that in this case, both models are equivalent and all curves are superimposed (for the static and rheologic aspects).

3. The Cylindrical Model

The model described hereafter, called the Cylindrical model (Cyl model), allows one to figure the soil behaviour submitted to an excitation generated by a dynamic loaded pile. This behaviour is described in the close vicinity of the pile and farther in order to investigate the attenuation of the wave propagation into the soil. The model is firstly described, with the geometrical and algorithmic aspects. After, it is validated and the study is finally focused on the slippage between the pile and the soil and its propagation into the soil.

3.1. Description

The geometric description of this model (pile/soil system) uses a cylindrical symmetry. The soil is assumed to be a disk of which the thickness increases slightly and linearly with the distance from the centre of the pile (also the axis of the symmetry) as suggested by Holeyman (1984) (Figure V-35).

The increase of thickness is a linear function of the radius and tends to simulate the radiation damping provided by the vertical diffusion of waves around the moving pile. Equ. V-9 represents this relationship:

$$\Delta h = \alpha \cdot \Delta r \qquad \textbf{Equ. V-9}$$

where:

- Δh is the increase of thickness per unit of distance from the centre of the disk [m];
- Δr is the thickness of each cylinder [m];

- α is the coefficient of dispersion that quantifies radiation into the half-space underlying the pile base level (= 0.03 – Holeyman (2000)).

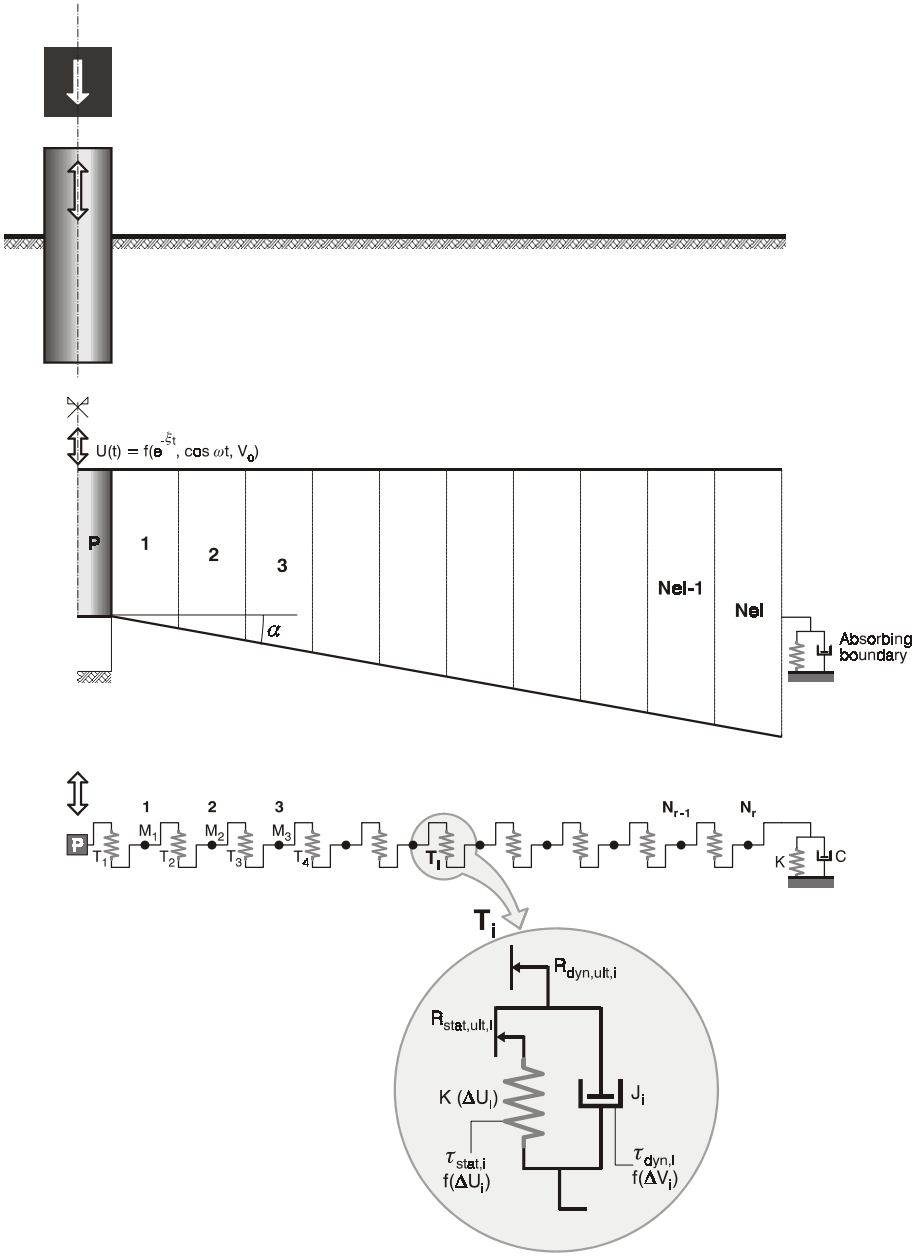

Figure V-35: Geometric model (based on Holeyman, 1984)

For the SDOF model, the radiation damping is taken into account through a linearly velocity dependent formulation called the geometric damping:

$$\tau_{geom} = \sqrt{\rho \cdot G} \cdot v \qquad \textbf{Equ. V-10}$$

where:

- ρ is the soil volumetric mass [kg/m³];
- G is the instant tangent shear modulus [MPa];
- v is the soil velocity [m/s].

The disk of soil is discretized in a set of concentric rings characterized by a mass and the same width. Each element transmits forces acting to its boundaries to the adjacent elements. The base resistance of each element is supposed to balance gravity (Vanden Berghe, 2001).

The vertical shear stress at the interface between two rings is computed based on the relative displacement of them and a corresponding stress-displacement relationship.

The loading rate effect is taken into account by a viscous term and the ultimate rheologic soil resistance. Both of them are velocity dependent. The viscous effect and the slippage condition are related to the interface velocity (or the relative velocity between two adjacent soil elements).

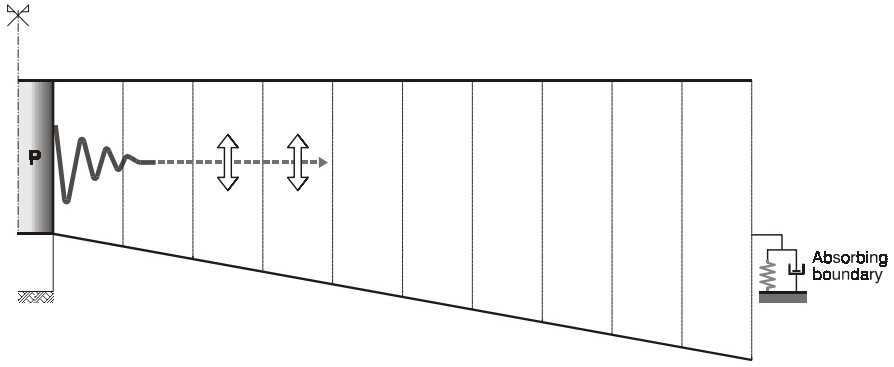

Figure V-36: Geometric propagation and interactions with the soil elements

The radial discretization is characterized by the number of rings (N_{el}), the thickness of each element (Δr) and the length of the pile (L) for the masses and surfaces (Figure V-36). The last element of the model must have a boundary condition. This border is built in a such way that the direct waves arriving from the pile are absorbed by this border (Novak et al., 1978).

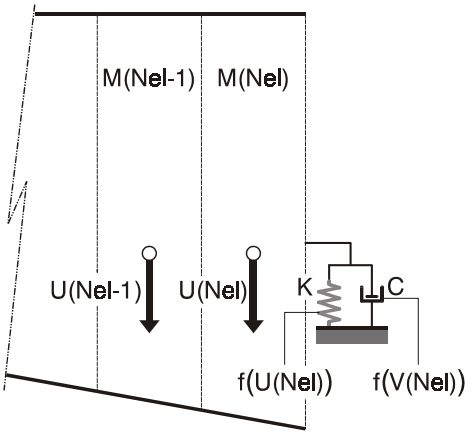

Figure V-37: Schematic description of the outer boundary of the Cyl model

This element is described in chapter 2. It is developed for a plane strain solution of soil displacement under harmonic solicitation for an infinitely long massless and rigid cylinder vibrating in an infinite elastic, homogeneous and isotropic medium (Novak et al. (1978)).

The model boundary is given by:

$$k = 2\pi G_s \frac{a_0^* K_1\left(a_0^*\right)}{K_0\left(a_0^*\right)}$$ **Equ. II-69**

- $a_0 = \frac{\omega r_0}{V_s}$ is the dimensionless frequency of the cyclic motion;
- r_0 is the pile radius;
- $a_0^* = i a_0$ with i the imaginary unit $i = \sqrt{-1}$;
- ω is the circular frequency;
- V_s is the shear wave velocity of the soil;
- $K_{0,1}$ is the modified Bessel function of the second kind of order 0 and 1 respectively.

That could be rewritten as:

$$k = G_s\left(S_{v1} + iS_{v2}\right) = K + iK'$$ **Equ. II-70**

The boundary element can be approximated by a spring and a dashpot of which the constants are frequency independent and defined by:

$$K = G_s \cdot S_{v1} \text{ [N/m/m']}$$ **Equ. II-71**

$$c = \frac{G_s r_0}{V_s} S_{v2}\left(a_0 = 1\right) \text{ [N.s/m/m']}$$ **Equ. II-72**

The units of K and c correspond to the unit of length of the vibrating cylinder (the pile in this case) Novak et al., (1978).

The model simulates the infinite medium but according to the assumptions of Novak's theory, the waves are absorbed only if the stresses generated remain in the elastic domain. To fulfil this condition, the number of soil elements and the distance of the border from the pile must be large enough to ensure that the wave is damped sufficiently at the boundary (Holeyman et al, 1994).

3.2. Algorithm

Similarly to the previous section dedicated to the DDOF model and the slippage problem, a certain motion is imposed to the pile and the pile/soil and the soil/soil responses are described and commented

with a special interest to the slippage occurrence. The descriptions of the pile and of the imposed motion are proposed in Section 2.3. of this chapter.

The forces acting on each soil element and on the pile shaft are summarized on Figure V-38 and Figure V-39 and are linked to a single cylindrical soil element (section view in Figure V-38).

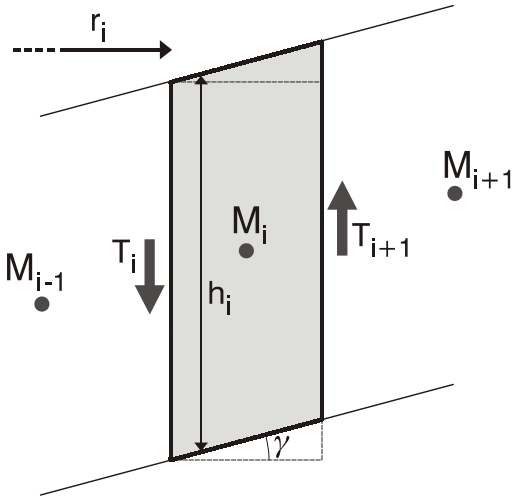

Figure V-38: Forces acting on soil elements (after Vanden Berghe, 2001)

The inter-ring reaction is calculated assuming an uniform distribution of the shear stress along the internal and external shaft of the soil element.

$$T_i = 2\pi \cdot r_i \cdot h_i \cdot \tau_i \qquad \textbf{Equ. V-11}$$

where:

- T_i is the inter-ring reaction between elements i and i-1;
- r_i is the radius of the interface between elements i and i-1;
- h_i is the average height of elements i and i-1;
- τ_i is the shear stress at the interface between elements i and i-1;
- γ is the angular distortion of the soil element caused by the resulting acting force;
- M_i is the mass of element i.

Based on the reactions acting at the interface between elements, the acceleration $acc_i(t)$ of the soil element i is calculated by:

$$acc_i(t) = \frac{(T_i - T_{i+1})}{M_i} \qquad \textbf{Equ. V-12}$$

where:

- $acc_i(t)$ is the acceleration of element i;
- T_i is the inter ring reaction between elements i and i-1;
- T_{i+1} is the inter ring reaction between elements i+1 and i.

In the same way, the stress at each interface is based on the relative displacement of the two concerned soil elements. This relative displacement is linked to the stress through the angular distortion:

$$\gamma = \frac{u_{i-1} - u_i}{\Delta r} \qquad \textbf{Equ. V-13}$$

where:

- u_i & u_{i-1} are the displacement of elements i and i-1;
- Δr is the additional radius between the positions of both soil elements.

The first interface stress, in contact with the pile, gets a shear strain influenced by the pile and the soil motions. Since the pile is rigid, the distortion is calculated only on the first soil element. The distance of reference becomes the thickness of the element reduced by half:

$$\gamma = \frac{2(u_{i-1} - u_i)}{\Delta r} \qquad \textbf{Equ. V-14}$$

The previous relation has a limited domain of validity, because the approximation agrees with the real deformation only if Δr is small enough to replace the tangent approximation by its argument ($tg(\theta) \cong \theta$ only if θ is small). Consequently, the soil element has to be small enough to ensure the algorithm precision and the numerical stability.

The resulting stress is calculated based on the distortion γ and one of the following classic stress-strain relationships:

- Pure elastic relationship;
- Elasto-plastic relationship;
- Hyperbolic relationship.

These relationships are defined in Chapter 3 in the section dedicated to the SDOF model and the shaft friction.

Classically, the loading rate effect is taken into account by a viscous stress contribution and by the definition of the ultimate rheologic shear resistance, both terms being velocity dependent. The viscous term and the ultimate rheologic shear stress are evaluated from the interface velocity (the relative velocity between elements).

The velocity of each element is obtained from the acceleration by simple time integration:

$$vel_i(t + \Delta t) = vel_i(t) + acc_i(t + \Delta t)\Delta t \qquad \textbf{Equ. V-15}$$

where:

- $vel_i(t)$ and $vel_i(t+\Delta t)$ are the velocities of element i at the time t and at the next time increment.

The loading rate effects affect the soil resistance by increasing the static term of the soil reaction by a velocity dependent term. The Gibson and Coyle (1968) proposed power law is used to account of this behaviour:

$$\tau_{rheol,ult} = \tau_{stat,ult} \cdot \left(1 + J \cdot \left(v_i - v_{i-1}\right)^{0.2}\right) \qquad \textbf{Equ. V-16}$$

$$\& \ \tau_{rheol} = \tau_{stat} \cdot \left(1 + J_s \cdot \left(v_i - v_{i-1}\right)^{0.2}\right)$$

where:

- τ_{rheol} and $\tau_{rheol,ult}$ are respectively the rheologic soil reaction and the ultimate rheologic resistance;
- τ_{stat} and $\tau_{stat,ult}$ are respectively the static soil reaction and ultimate static resistance;
- J_s and J are the damping factors defining the load rate effect for the viscous and the ultimate behaviours, respectively.

The general algorithm becomes:

- The pile is moving in function of a predetermined motion;
- This motion implies the resolution of the forces balance at the interfaces between elements (in particular between the pile and the first soil ring);
- From this equilibrium, the acceleration, the velocity and the displacement of each element are generated;
- Time is incremented to next step and process is re-iterated.

Figure V-39 summarises the different steps of the process for a full time increment.

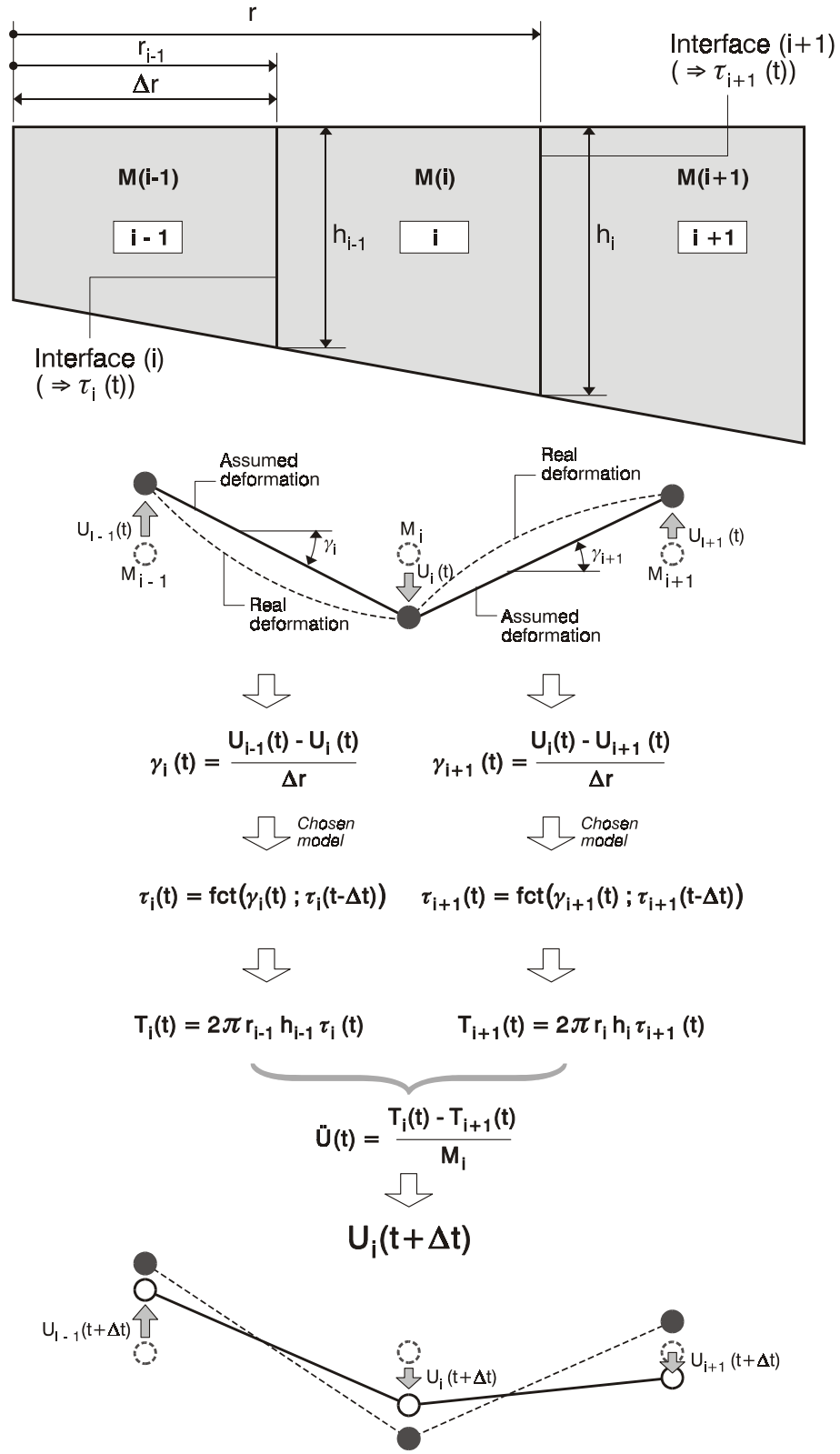

Figure V-39: Summary of the displacement of the soil element i at the time step t+Δt (after Vanden Berghe, 2001)

The axial symmetry of the model could be described with the complete stress state in a cylindrical coordinates system (r,θ,z) (Figure V-40).

In an axially symmetric distribution of stresses the non-vanishing components are σ_r, σ_θ, σ_z and τ_{rz}. The non-vanishing velocity components are u and w, respectively perpendicular and parallel to the Z axis. The velocity-component in the circumferential direction v is equal to zero since the flow is confined to meridian planes. The stresses and velocities are independent of θ and are only functions of r, z and time (i.e. $\partial(..)/\partial\theta = 0$).

The soil is assumed to be fully saturated. The dynamic event is supposed to be short enough to avoid the excess pore water dissipation during the dynamic load test. Therefore, the model considers the behaviour of the soil as undrained.

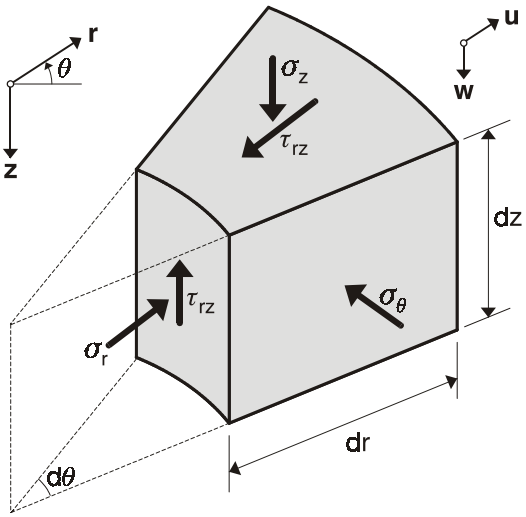

Figure V-40: Stress state in an axially symmetric distribution of stresses (after Vanden Berghe, 2001)

The model considers each soil element as simply sheared (Figure V-41). A shear displacement is imposed between the internal and external shaft of the soil element. Neither axial nor radial normal strain are permitted along these boundaries. The non-vanishing strain of the strain tensor is the shear strain γ_{rz} ($\gamma_{rz} \neq 0$; $\varepsilon_r = \varepsilon_\theta = \varepsilon_z = 0$).

It is assumed that there is no variation of stresses and strains along the z axis ($\partial(..)/\partial z = 0$). The radial normal stress and the shear stress do not change as a function of depth (Vanden Berghe, 2001).

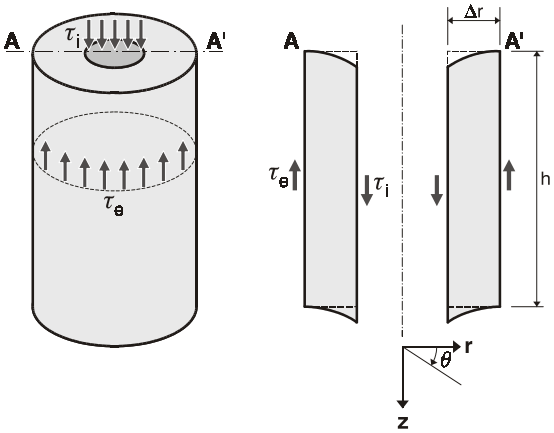

Figure V-41: Simple shearing in axisymetry (after Vanden Berghe, 2001)

Vanden Berghe (2001) showed that the assumptions concerning the stress and strain distributions in cylindrical symmetry are compatible with the equation of equilibrium. The results point out that the assumption of a constant shear strain rate between the middle points of each element was limited to thin elements. The evolution of the shear strain is naturally proportional to 1/r in an elastic and axisymetric media.

3.3. Validation of the model

3.3.1 Propagation of the wave in an elastic media

It would be interesting to check the propagation of a wave in an elastic media by confirming the wave propagation velocity, and the attenuation of the signal during its travel through the elements. The model does not take loading rate effects into account for this reference case, in order to ensure a purely elastic behaviour of the soil reaction.

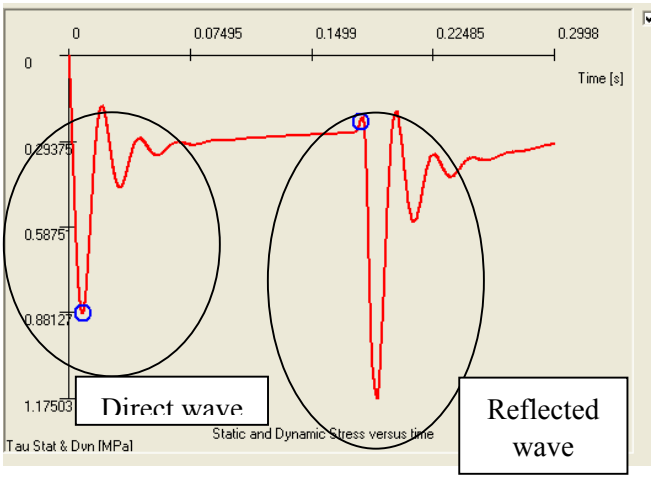

Figure V-42: direct and reflected wave

Since the model is spatially limited and the stress wave is reflected at the outer boundary, this reflection is used to evaluate the wave propagation velocity. In Figure V-42, both little circles point the same position on the wave trace but respectively on the original wave and on the reflected one after one reflection. Since the position of the element is known, the time of travel can be evaluated and compared with the theoretical one (223 m/s). A 3-D image (Figure V-43, distance from pile shaft – time – soil displacement) represents this propagation:

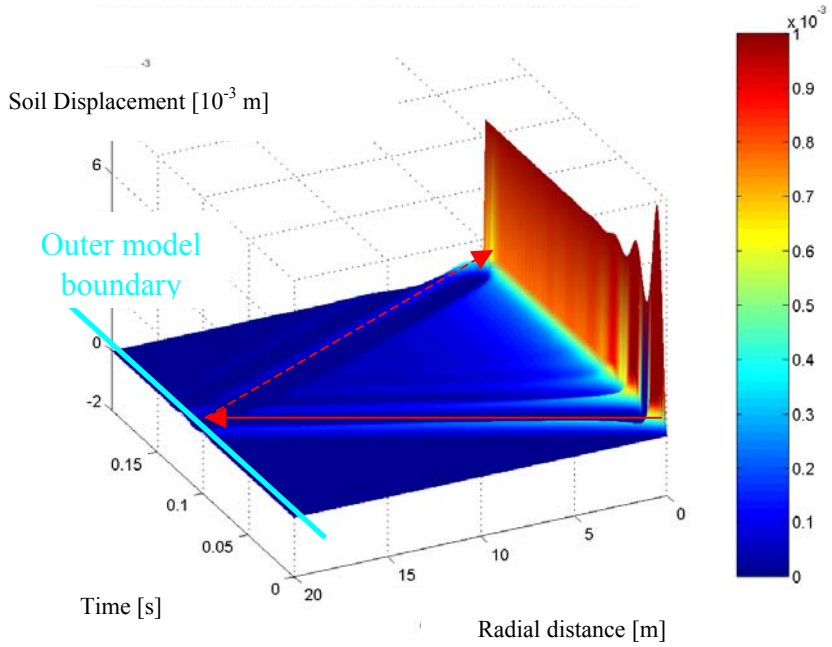

Figure V-43: 3-D representation (time, dist, Displ) of the wave propagation in an elastic soil media with reflecting boundary at r=20m.

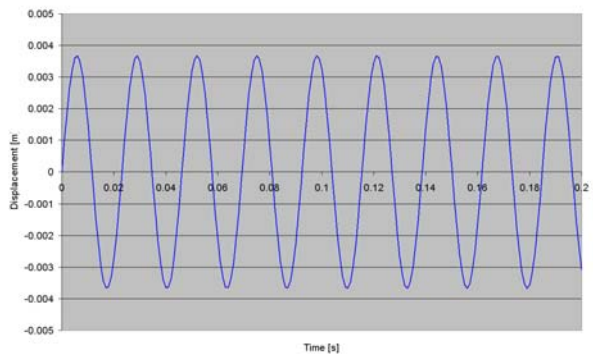

Figure V-44: Periodic displacement of the pile

The second test concerns the attenuation of the signal during its travel. The propagation of a computed wave is compared to the theoretical approach of the soil displacement (Novak et al. 1978 (Equ. II-67)).

To perform this analysis, a harmonic relationship (Figure V-44) is imposed to the pile without predefined attenuation (as the imposed motion introduced in Section 2.3. with the negative exponential function). The stress-

strain relationship of the soil is chosen linear and elastic, the ultimate resistance is chosen such as the imposed displacement never reaches it and there is no loading rate effects taken into account.

$v(t)=\cos(\omega t)$ and $u(t)=\frac{\sin(\omega t)}{\omega}$ (Figure V-44) **Equ. V-17**

The parameters of the model are:

- Number of elements (cylinders) N_{el}: 400;
- Thickness of each element: 0.1 m → 400x0.1 m = 40 m.;
- Pile radius r_0: 0.2 m;
- Pile length L: 10 m;
- Ultimate static shear resistance $\tau_{ult,stat}$: 1 MPa;
- Poisson ratio υ: 0.35;
- Initial shear modulus G_i: 100 MPa.

And $\omega = 272$ rad/s

The imposed periodic displacement is sent from the pile to the outer border through the soil elements. From element to element, the motion is eased. The attenuation is illustrated by the levels of maximum displacement reached (for each element).

Figure V-45 shows the corresponding generated stress at the interface versus time and versus displacement. It describes the expected displacement-stress relationship.

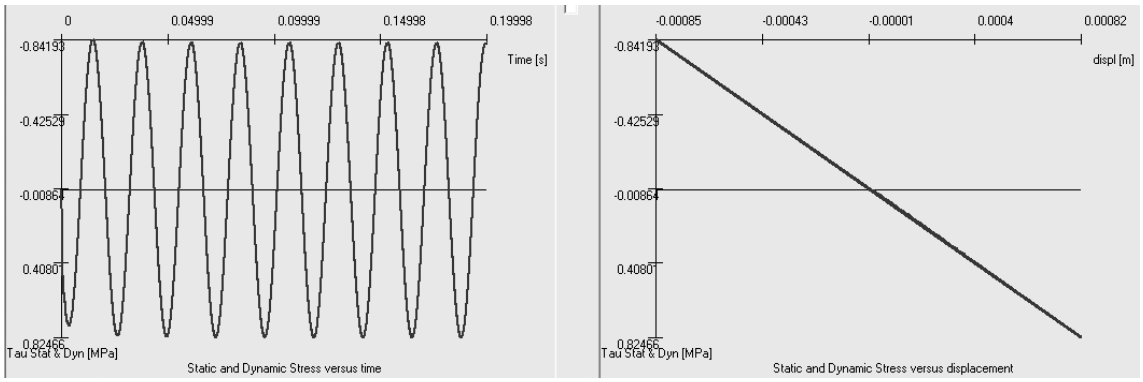

Figure V-45: Time-stress history and displacement-stress history

As expected, the soil element just next to the pile behaves elastically like all the others.

In order to compare the model response to the theoretical Novak approach, the maximum reached points of the traces crossing each element are determined and plotted on a graph vs. the distance between the pile shaft to the centre of the concerned element (Figure V-46).

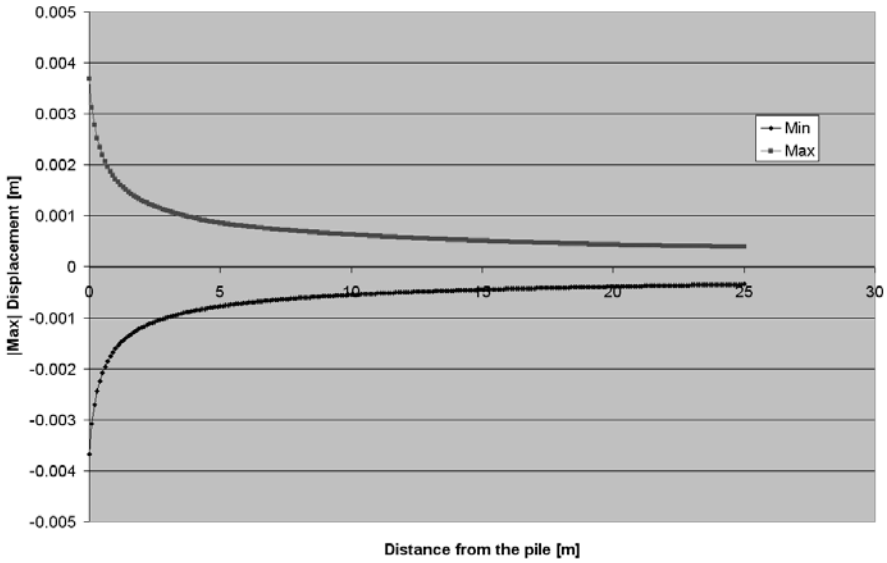

Figure V-46: Maximum and minimum displacements reached for each soil elements under harmonic solicitation around the pile

Equ. II-67 is completed by using the following parameters:

- ω: 272 rad/s;
- r_0: 0.2 m;
- G_i: 100 MPa;
- V_s: 223 m/s.

The development of this equation provides a curve very close to the computed one. Figure V-47 shows both curves. The agreement is remarkable and confirms that the model is usable and reliable.

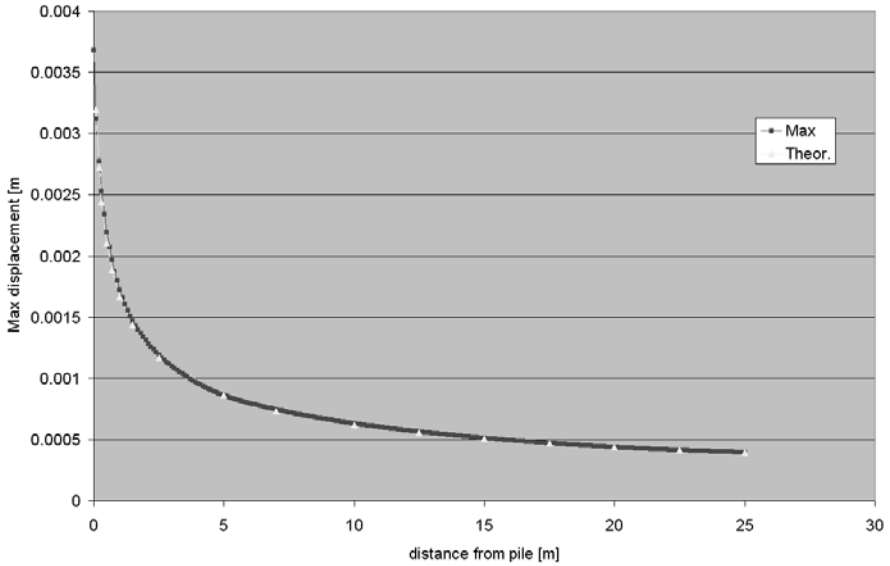

Figure V-47: Curves of attenuations after balancing

Similarly to Figure V-43, a 3D representation of the propagation of a periodic wave is shown in Figure V-48. The tangent of the angle of the yellow "lines" with the time axis represents the wave propagation velocity. The colour "dimension" represents the magnitude of the soil displacement [m].

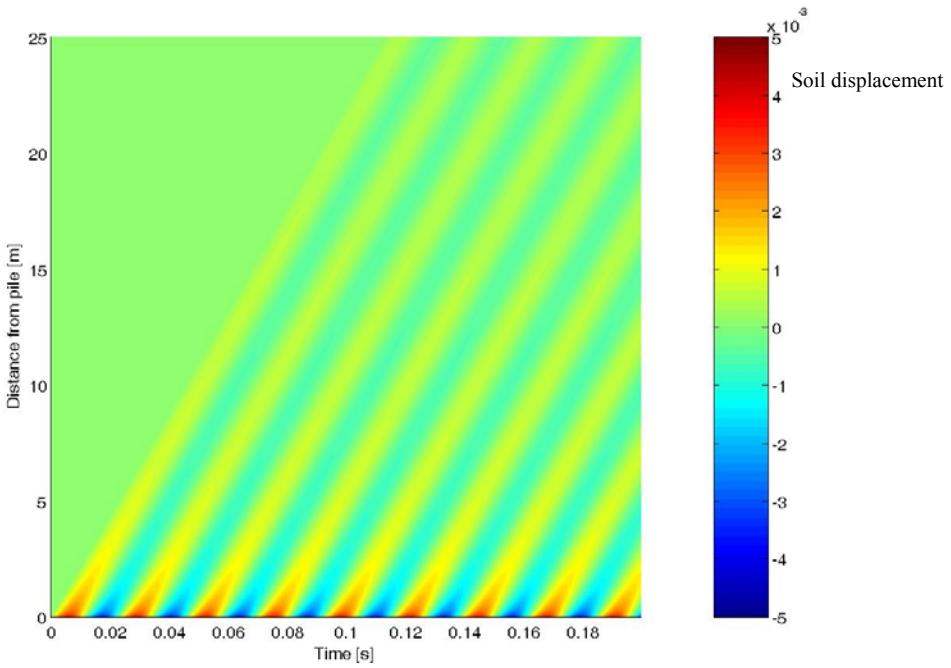

Figure V-48: 3-D representation of the propagation of a periodic wave into the soil (up to 25 m)

3.4. Results

This section presents the results of this model submitted to an imposed motion in order to highlight the slippage event, the slippage zone and the propagation of the wave into the soil.

The elasto-plastic relationship is used to describe the soil behaviour since its performances are well known and the slippage phase is also easier to discern (flat plastic stage).

3.4.1 Elasto-plastic behaviour – no loading rate effects

The parameters used are:

- N_{el} = 300 elements;
- Ring thickness Δr = 0.1 m;
- G_i = 100 MPa;
- Pile radius r_0: 0.2 m;
- Pile length L: 10 m;
- Poisson ratio = 0.35;
- τ_{ult} = 0.3 MPa and 2 MPa

The imposed motion is the harmonic and attenuated signal described in Section 2.3. of this chapter and already used in a previous analysis (Figure V-6).

When the ultimate stress is sufficiently important, the imposed motion can not generate slippage. Figure V-49 to Figure V-52 highlight this situation with the imposed pile displacement, the generated displacement of the first soil element, the generated stress into their interface and the relevant stress-displacement relationship.
As expected, the stress-displacement curve remains altogether linear according to the pure elastic relationship (Figure V-52). Figure V-49 and Figure V-50 plot the imposed pile displacement and the first soil element displacement curves. The trends and the magnitudes of both traces are similar like the permanent settlements. These observations highlight the perfect coupling between the pile and the soil confirmed by the linear stress-displacement relationship. All the information is transmitted from the pile to the soil.

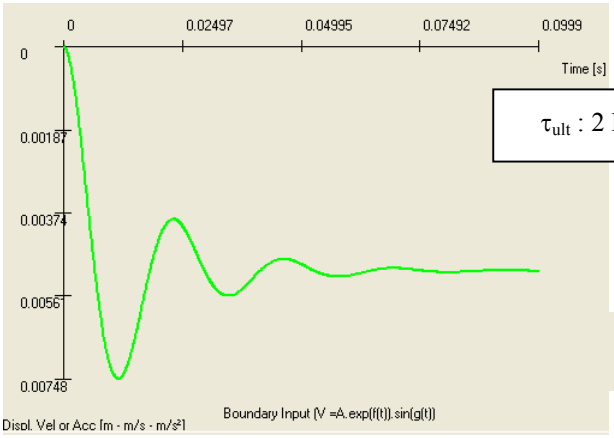

Figure V-49: Input signal imposed to the pile

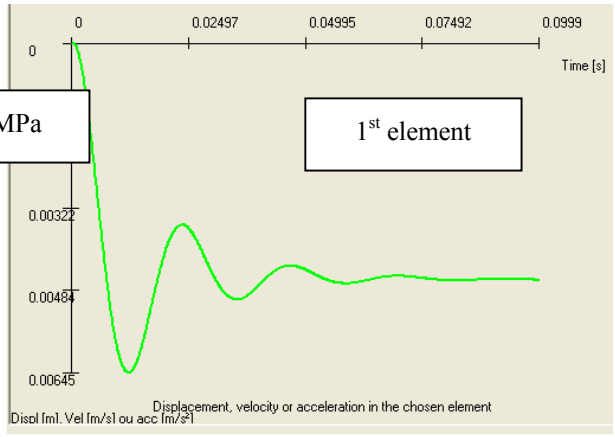

Figure V-50: Generated displacement of the first soil element

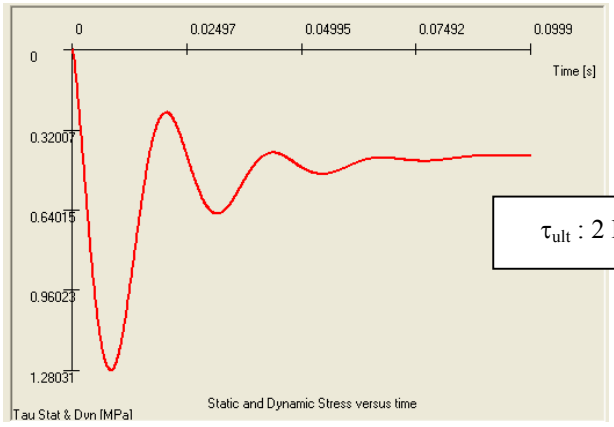

Figure V-51: Generated stress between the pile and the first soil element

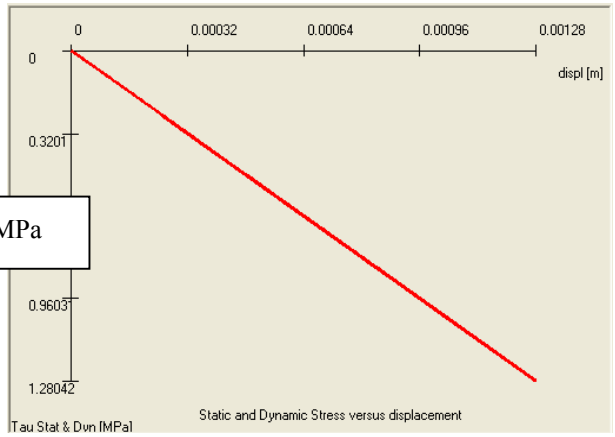

Figure V-52: Displacement-stress relationship (relative displacement)

Figure V-53 displays the displacement traces and the attenuation due to the radiation of the energy into the surrounding soil.

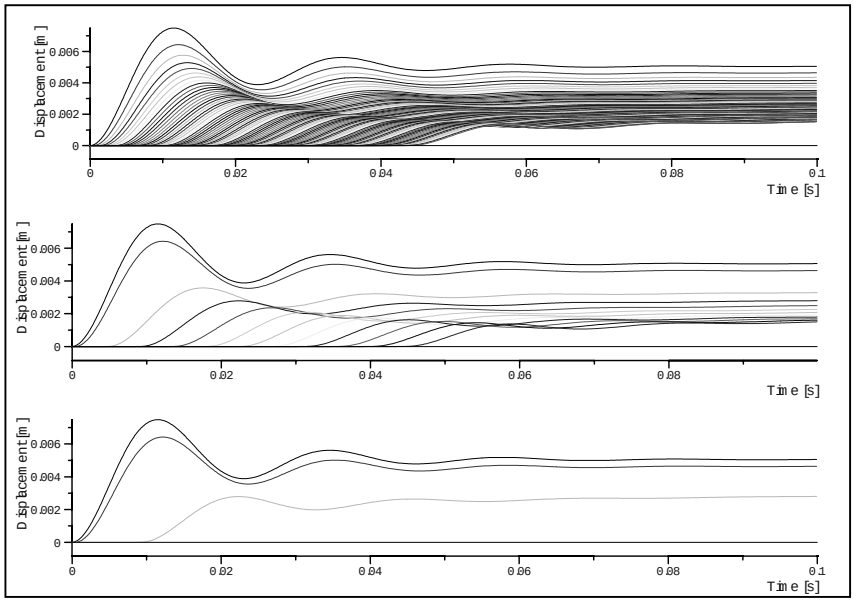

Figure V-53: Displacement traces for the first elements of the model – pile + soil (τ_{ult} = 2 MPa) (a. 100 first, b. 1/10, c. The 1st and the 20th)

The next case takes the slippage into account by reducing the ultimate static stress ($\tau_{ult,stat}$).

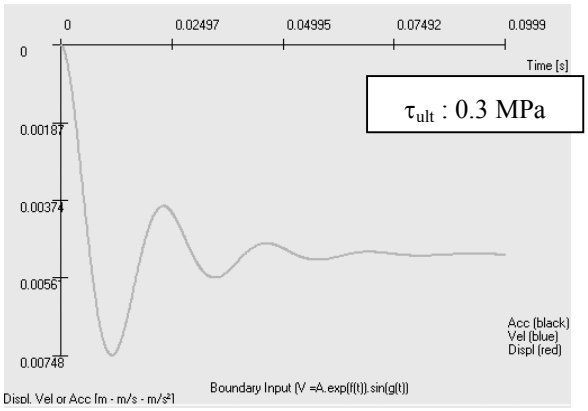

Figure V-54: Input signal imposed to the pile

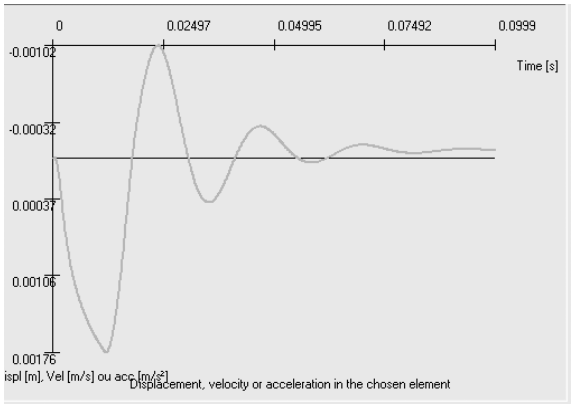

Figure V-55: Generated displacement of the first soil element

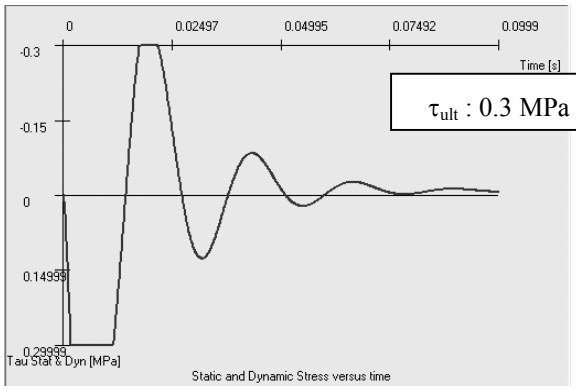

Figure V-56: Generated stress between the pile and the first soil element

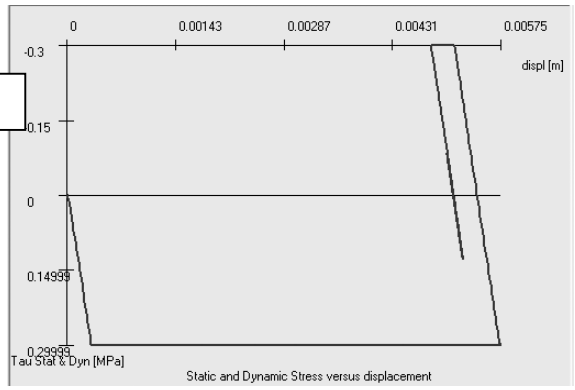

Figure V-57: Displacement-stress relationship (relative displacement)

Similarly to the Figure V-49 to Figure V-52, Figure V-54 to Figure V-57 represent the traces characterizing the pile and the first soil element of the model. The relative displacement between both elements results in a stress resisting to their movements. Due to the small value of $\tau_{ult,stat}$, the ultimate resistance is quickly exceeded and the slippage occurs (Figure V-56).

During the slippage, there is still an interaction between the pile and the first soil element limited to the ultimate shear resistance. This interaction is limited but both pile and soil are not completely uncoupled. Consequently, the motion of the soil element is not interrupted and is based on the stress balance with respect to the equations of motion. This behaviour occurs until the stress between the pile and the soil element becomes inferior to the resistance threshold. Figure V-57 shows the development of the stress vs. the relative displacement of this interface. Nevertheless, the slippage influences the form of the soil displacement. Figure V-54 and Figure V-55 represent the displacements traces of the pile and the first soil element, respectively. It can be seen that both amplitudes and permanent displacements are greatly influenced by the slippage event. The soil element displacement trace is modified. After, this "new" shaped wave is applied to the subsequent soil elements and the coupling is perfect. The slippage has been occurred only in the first interface, the "modified" signal is considered as a new imposed one.

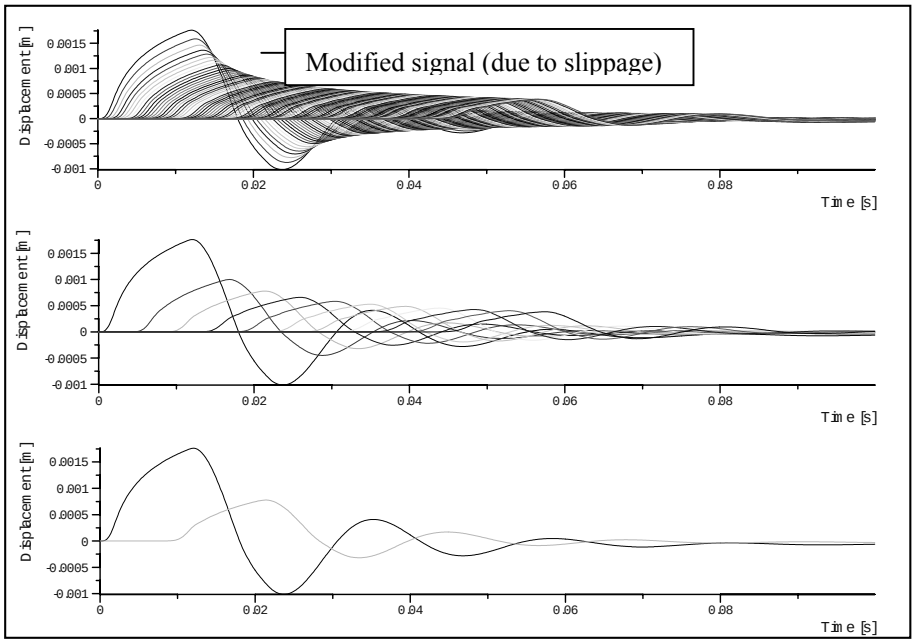

Figure V-58: Displacement traces for the first elements of the model - soil (τ_{ult} = 0.3 MPa) (a. 100 first, b. 1/10, c. The 1st and the 20th)

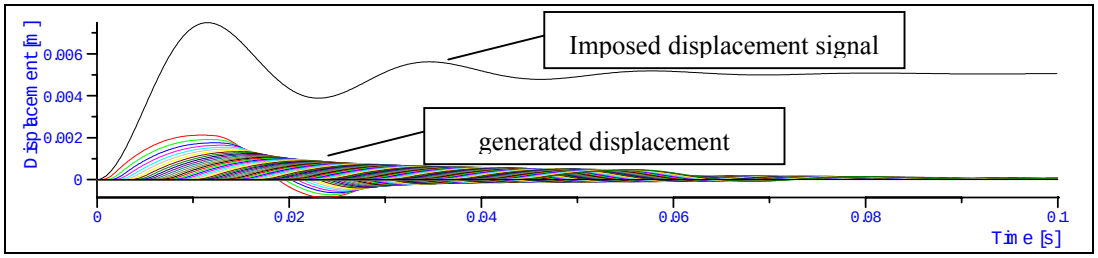

Figure V-59: Displacement traces for the first elements of the model – pile + soil (τ_{ult} = 0.3 MPa) (100 first)

The evolution through the others soil elements is also shown in Figure V-58 and Figure V-59 where all imposed and generated displacements are plotted. The difference and the consequences of the slippage are highlighted by the important gap existing between the pile and the soil displacements.

In conclusion, the slippage occurring between two elements acts like a filter to the propagation of the motion and the resultant stress and not like a barrier.

3.4.2 Elasto-plastic behaviour – Viscous influence

The loading rate influence is located in one stress term called the viscous stress, velocity dependent term and in the ultimate shear stress also a velocity dependent term. The formulations used to quantify these effect are based on the Coyle and Gibson power law (Equ. V-16) with:

- The damping factor of the viscous term (J_s [$s/m^{0.2}$]);
- The damping factor of the ultimate term (J [$s/m^{0.2}$]);

Their values are in this case fixed to $J = J_s = 0.5\ s/m^{0.2}$.

The effects and the probability of slippage are amplified in the first soil elements in the direct vicinity of the pile shaft due to the addition of the viscous contribution to the soil reaction. And the relative velocities are dependent of the slippage state. In case of non-slippage, the difference of velocities between adjacent elements is small. But, on the other hand, during the slippage, the difference becomes higher and influences the threshold of resistance (increase). Figure V-60 shows the amplitude of the absolute velocities of the first elements of the model (pile + soil elements). The maximum magnitude decreases due to the geometric attenuation from the value of approximately 1 m/s (pile velocity) to 0.25 m/s (100th element – 10 m).

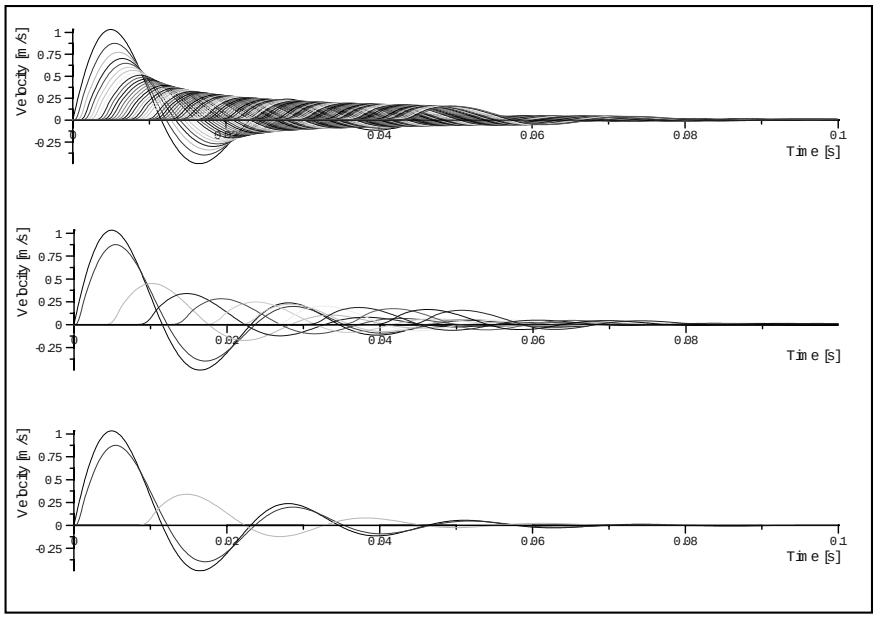

Figure V-60: Velocity traces for the first elements of the model – pile + soil ($\tau_{ult,stat}$ = 2 MPa) (a. 100 first, b. 1/10, c. The 1st and the 20th)

Figure V-61 shows the same simulation results, but expressed in the relative form or the interface velocity (v_{i-1}-v_i). The effects on the rheologic ultimate soil resistance and on the viscous term is an increase of about 10 % of the ultimate static resistance for the elements close to the pile and at 10 m, the increase is only 3% of the ultimate static resistance[1].

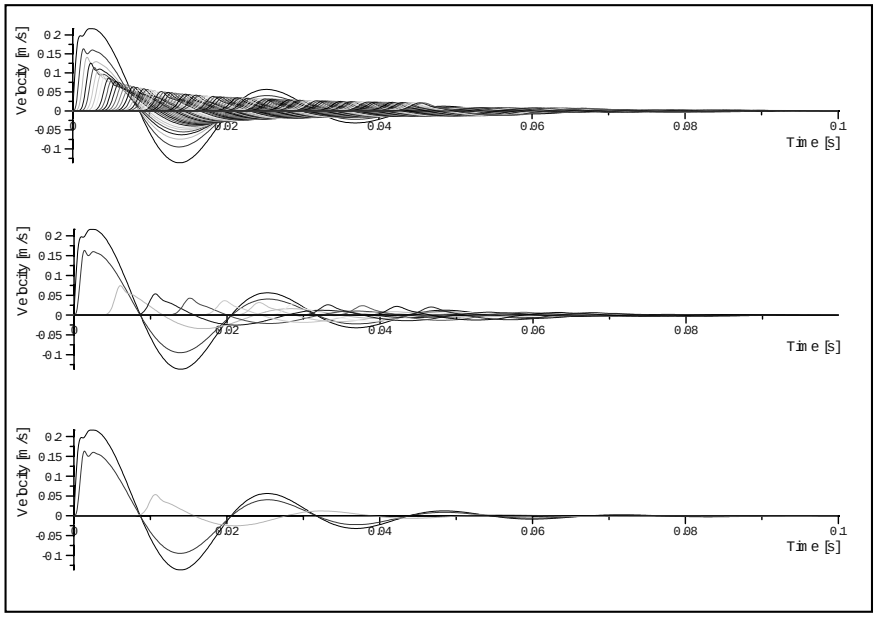

Figure V-61: Relative velocity traces for the first elements of the model ($\tau_{ult,stat}$ = 2 MPa) (a. 100 first, b. 1/10, c. The 1st and the 20th)

Moreover, Figure V-60 and Figure V-61 correspond to a situation of no slippage ($\tau_{ult,stat}$ = 2 MPa). The reduction of the velocity between soil elements follows the geometric attenuation due to the radiation around the pile. If the slippage is provoked by fixing the ultimate shear stress to a small value: 0.3MPa, the influences on the relative velocities are significant. Figure V-62 and Figure V-63 display the velocity curves in the same model configuration than the previous figures and it can be pointed out that the net velocities drop directly through the first interface. Consequently, the relative velocities are also influenced. The first interface velocity is quite large and the following rather small.

[1] With $J = J_s = 0.5$ s/m$^{0.2}$

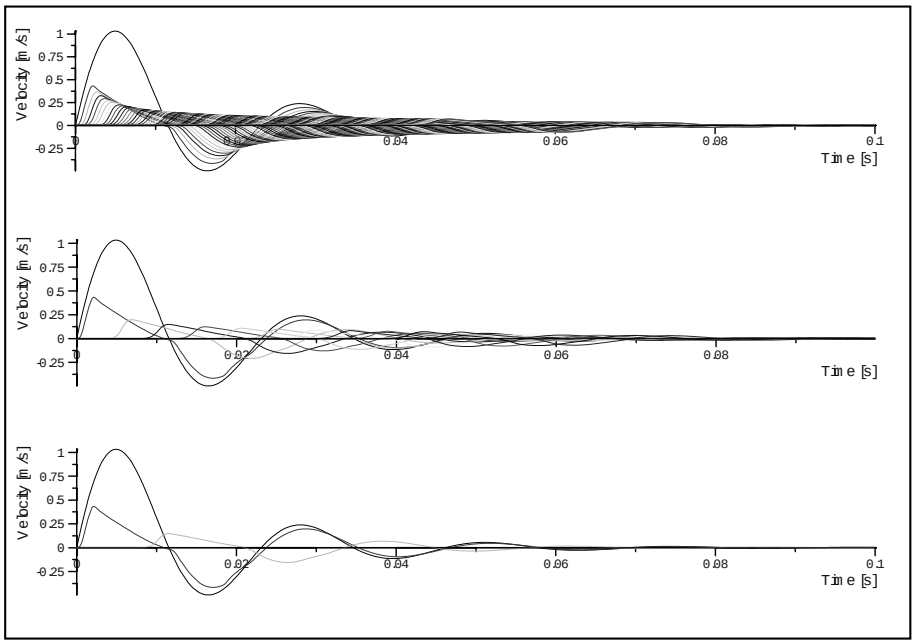

Figure V-62: Velocity traces for the first elements of the model – pile + soil (τ_{ult} = 0.3 MPa) (a. 100 first, b. 1/10, c. The 1st and the 20th)

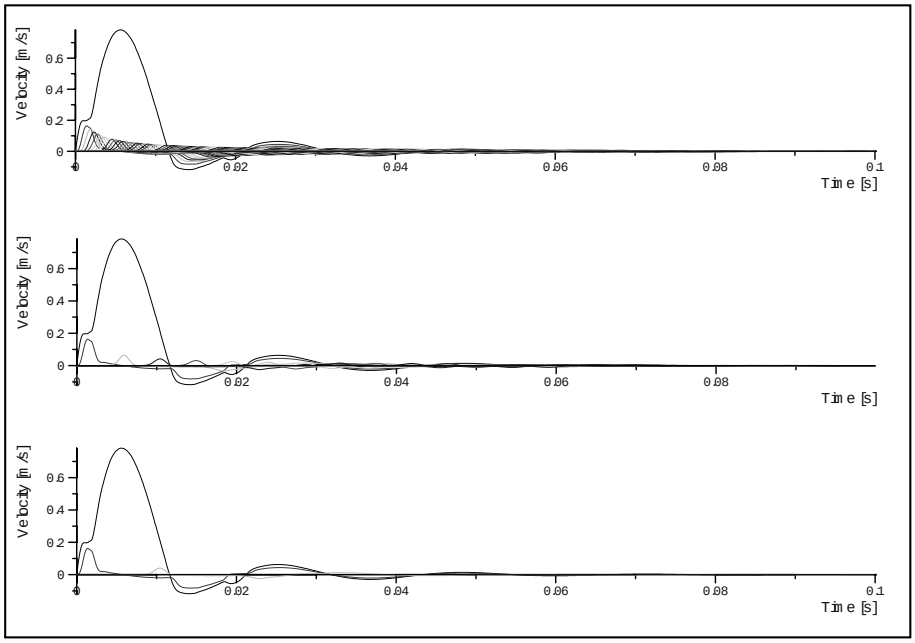

Figure V-63: Relative traces for the first elements of the model (τ_{ult} = 0.3 MPa) (a. 100 first, b. 1/10, c. The 1st and the 20th)

In others words, when the slippage occurs between two elements, the interface velocity increases as the rheologic ultimate soil reaction and the viscous term.

3.5. Depth of the slippage zone

In order to discern if a certain depth of soil or only the interface between the pile and the soil is disturbed by the slippage, a sequence of simulations has been performed in the Cyl model set up to

have a sufficient precision in the quantities calculated (small thickness of soil elements) and to avoid reflections at the outer border of the model (N_{el} sufficiently high).

The ultimate static shear stress is fixed in order to ensure the slip ($\tau_{ult,stat}$ = 0.2 MPa).

The others parameters are given by:

- G_i = 100 MPa ;
- Poisson ratio = 0.35 ;
- Pile length = 10 m;
- Pile radius = 0.2 m.

The stress-displacement relationships of the 7 first interfaces are presented in order to check the propagation of the slippage front. Moreover, to have a better chance to distinguish the slippage occurrence, the fundamental relationship remains the elasto-plastic law.

3.5.1 Static aspect

The first simulation concerns the static term without any loading rate effects.

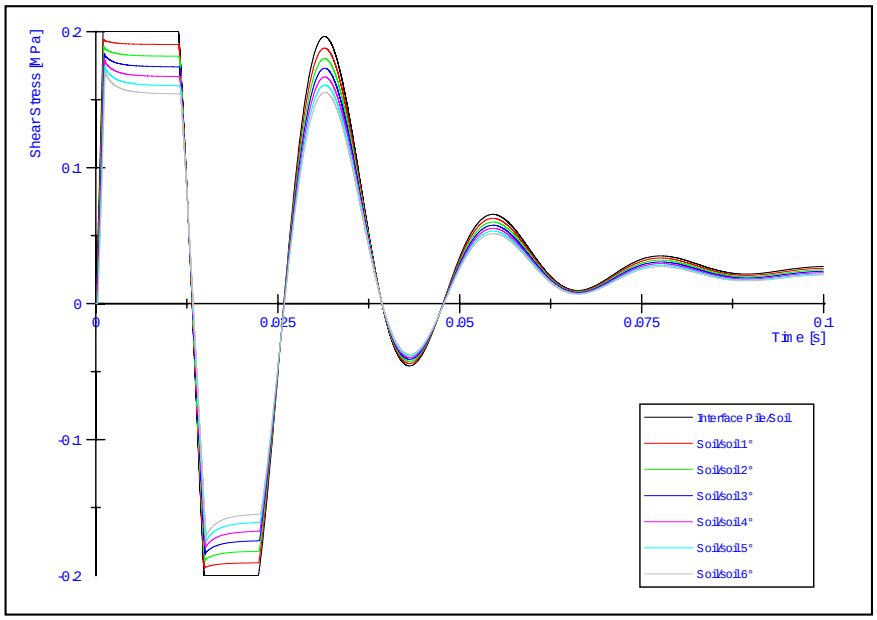

Figure V-64: Static stress behaviour of the 7 first interfaces between pile and soil elements. (τ_{ult} = 0.2 MPa)

Figure V-64 displays that the slippage occurs only at the first interface between the pile and the soil. It was pointed out in section 3.4.1. that the first interface has the role of a moderator or a filter of the transmitted motion. The slippage occurring in this surface reduces the magnitude of the soil motion according to the ultimate soil resistance. The coupled displacement of the soil is maximum equal to the displacement generated by a static stress equal to the ultimate soil resistance. For the following interfaces and soil elements, the attenuation due to the radiation reduces this value with the distance

from the pile. Consequently, it is not possible to exceed anew the soil resistance and to generate the slippage in another interface. If the model remains in the static domain, the slippage will remain only at the pile/soil interface. The same event (only one surface of slippage) happens if the ultimate static resistance is reduced by half (0.2 MPa → 0.1 MPa) or doubled.

In conclusion, when only the static part of the soil reaction is taking into account and when the stress follows an elasto-plastic relationship, the ultimate static resistance does not influence the depth of the slip zone but influences the slip duration and the final conditions (pile penetration and residual stresses). Finally, the ultimate stress influences also the shape from stress and displacement traces transmitted to the soil.

3.5.2 Viscous aspect

If a term is added to the static soil reaction which is not related to the stress-displacement relationship, as the viscous term, the slippage front spreading behaviour could be different of the static case.

The viscous influence, velocity dependent, is added to the static soil reaction to generate the rheologic soil reaction limited by the ultimate rheologic resistance of the soil (Equ. V-16). But, as assessed in the model description (Section 3.2) and reminded in Equ. V-16, the same formulation and the same parameter value rules the calculation of both ultimate rheologic resistance and the processing viscous term: $J=J_s$, the damping parameters. For the convenience, these values are equal even if they represents different behaviours. An analysis could be performed focused on the differentiation of those two values and the consequences on the slippage event.

$$\tau_{rheol,ult} = \tau_{stat,ult} \cdot \left(1 + J \cdot \left(v_i - v_{i-1}\right)^{0.2}\right) \qquad \textbf{Equ. V-16}$$

$$\& \ \tau_{rheol} = \tau_{stat} \cdot \left(1 + J_s \cdot \left(v_i - v_{i-1}\right)^{0.2}\right)$$

Since the same formulation and the same parameter rules the ultimate and the viscous contribution of stress, and since this value of $J=J_s$ remains the same for both formulations, both expressions between bracket ("$\left(1 + J_s \cdot \left(v_i - v_{i-1}\right)^{0.2}\right)$") give the same result for any values of the velocities, the slippage occurs only in case of exceeding the static ultimate resistance. If the static threshold is reached, the ultimate rheologic resistance is exceeded and inversely. A consequence of this observation is the possibility to visualize the effect of the rheologic slippage on the static curves. It is easier and more comfortable to analyse because the rheologic slippage is variable with respect to the time, on the other hand, the elasto-plastic zone of failure is easily identified by the flat portion of the stress-displacement relationship (Figure V-65).

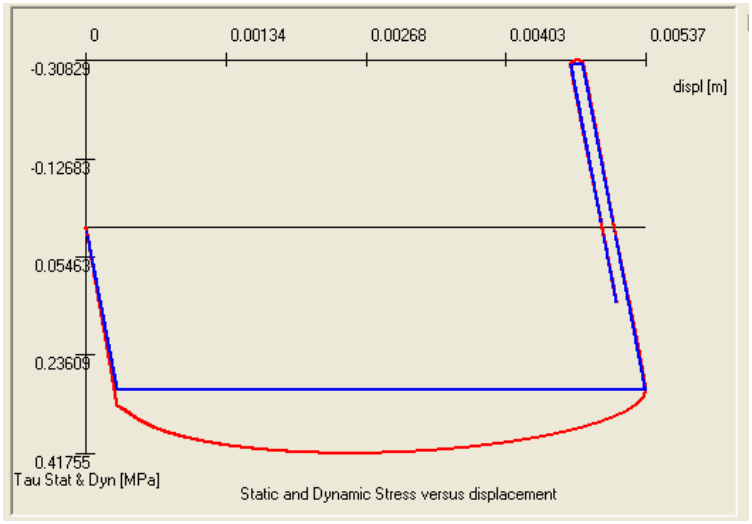

Figure V-65: Generated static (blue) and rheologic (red) stresses-displacement relationships

The rheologic curves are plotted on Figure V-66 (time-static shear stress histories but including to the loading rate effect) and correspond to the pile/soil system of the previous simulation (Figure V-64). The only change is the use of the viscous influence. The sliding occurs, as expected, inside of the first interface but also into the 4 next interfaces between the elements. The slippage is not hold on the first sliding surface along the pile, but can be evaluated in term of number of rings, depth of the slippage zone, parameter values, …The last curve that achieves the slippage is the 4th interface between soil elements. The sliding acts on 5 interfaces (4 between soil elements and one between the pile and the soil), namely on 4 cm.

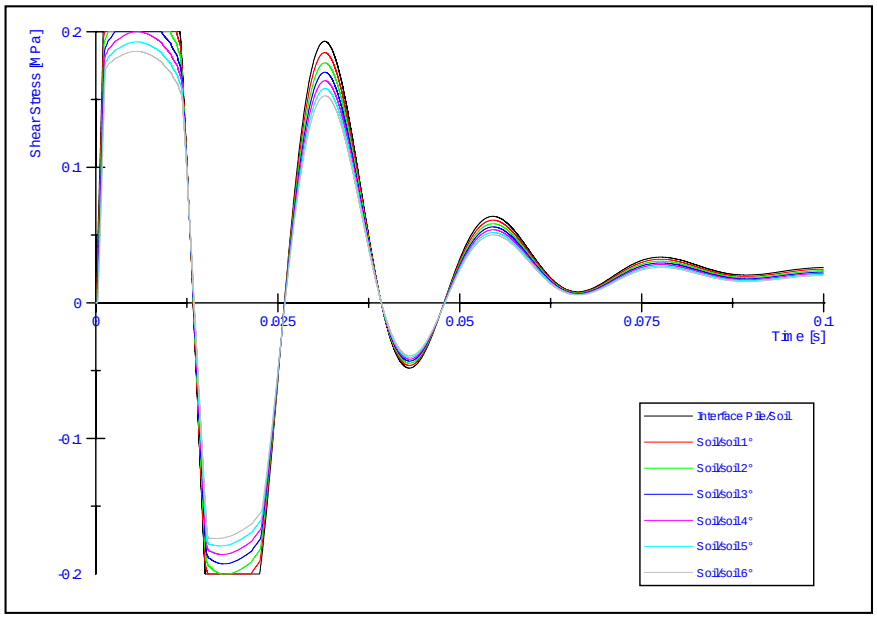

Figure V-66: Static shear stress behaviour of the 7 first interfaces between pile and soil elements - (τ_{ult} = 0.2 MPa, J = 0.5 s/m, e = 0.01 m) – viscous field

If the ultimate resistance is reduced, the sliding depth increases but not in the same proportion than the reduction of resistance. Figure V-67 displays the evolution of the sliding depth for a variation of the ultimate static shear stress (from 0.01 MPa to 2 MPa.). This figure gathers the envelope curves of the

maximum reached shear stresses vs. the distance from the pile shaft. A dashed straight line separates the zone where the threshold is reached and where it is not.

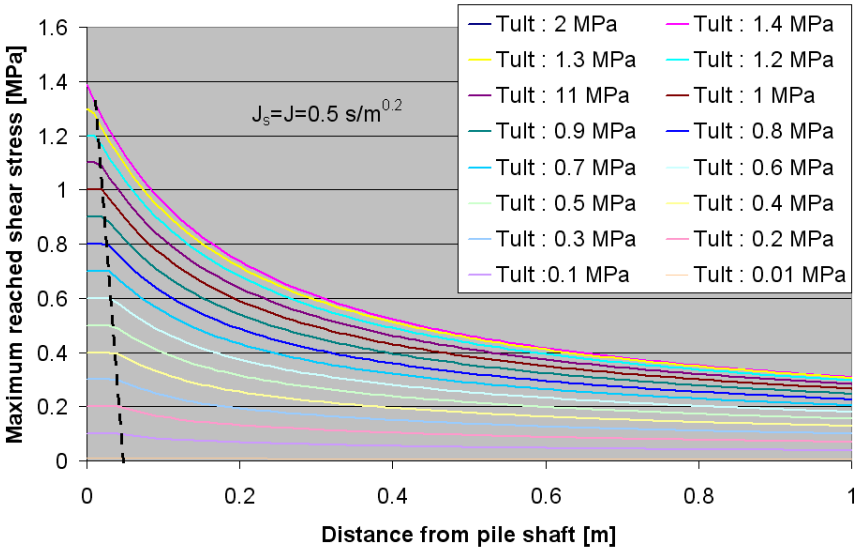

Figure V-67: Curve envelopes of the maximum reached shear stress for τ_{ult} varying from 2 MPa to 0.01 MPa. ($J = J_s = 0.5$ s/m$^{0.2}$)

Besides the ultimate resistance $\tau_{ult,stat}$, others parameters have a significant influence on the slippage event. Particularly the value of J (=J_s), the damping parameter: the higher this value, the more spread out the slip zone. Another parameter could influence the slippage area like the damping factor and the ultimate resistance: the initial shear modulus G_i. Since G_i increases the rate of mobilization of the soil, the slip event happens faster and influences the depth of the perturbed zone (increase). The Poisson ratio does not seem to have a significant influence on the depth of the slip zone.

The chosen discretization of the model is still too coarse, and thinner elements could be used to have a more precise description of the perturbed area progression. But the main goal was not to find the exact dimensions of the slip zone, but to evaluate the existence, the progression and the limits of this specific and important failure zone in the vicinity of the pile, by using a simple law (elasto-plastic) without using the particular behaviours probably interacting in this phenomena (increase of pore water pressure, liquefaction, …). Another goal was to find some influential parameters on this perturbation. These parameters are, for the chosen model and the utilized laws, the ultimate resistance τ_{ult} and the damping factor J (for both viscous and ultimate formulations).

It would be very interesting to validate these model observations by a set of laboratory tests on soil samples. Tests like simple shear tests could be easily performed in order to check the real depth and/or the real existence of this zone in the vicinity of the concrete (or steel) contact with the soil. Different shear rates and transducers placed at different distance from the contact into the soil could highlight this important mechanism.

3.6. Detail of the slippage process: about the spreading of the slip zone

This section is dedicated to a detailed explanation of the spreading or not of the slip zone when only the static aspect is taken into account or enhanced with the loading rate influence.

This analysis presents the details of the main quantities involved in the pile/soil and soil/soil responses evaluation. Both cases are detailed separately (specific static point of view and rheologic analysis). the pile/soil system is characterized by the following parameters:

- N_{el} = 2000 elements;
- Ring thickness = 0.01 m;
- G_i = 100 MPa;
- Poisson ratio = 0.35;
- τ_{ult} = 0.2 MPa.
- Pile length = 10 m;
- Pile radius = 0.2 m.

3.6.1 Static field

If the loading rate effects are not taken into account, only the algorithm in Figure V-68-a is followed.

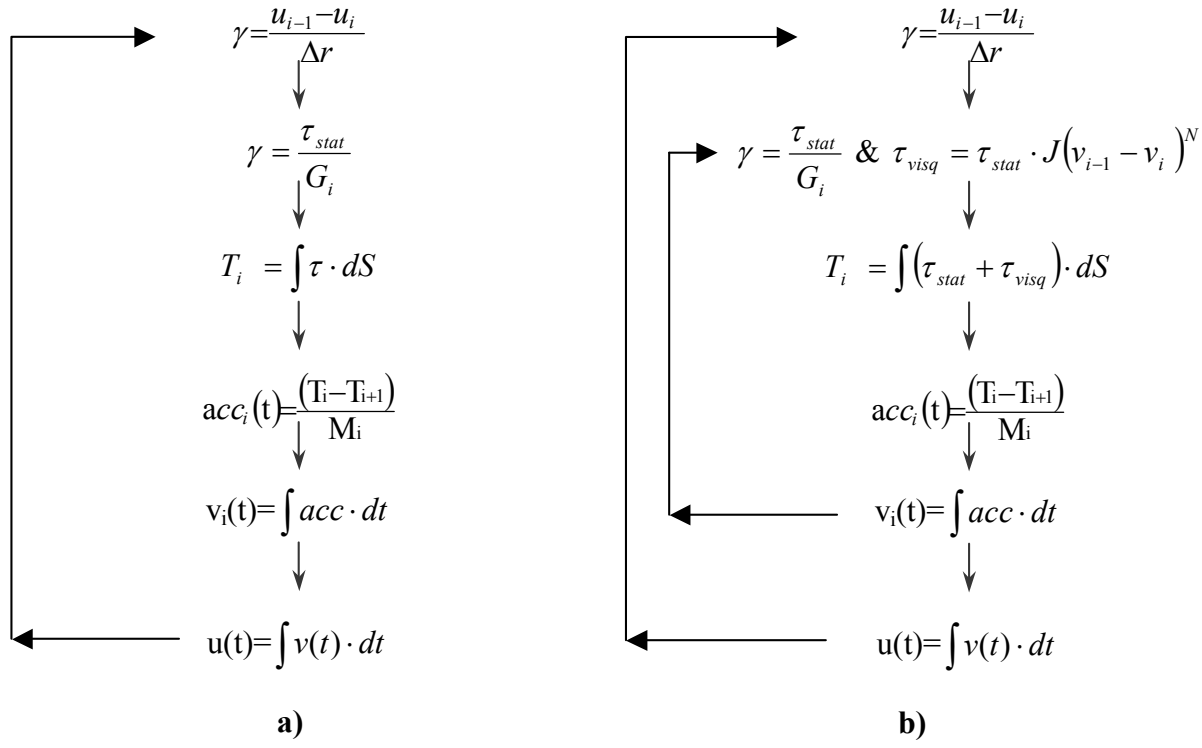

Figure V-68 : Explicit algorithm (static and rheologic aspects)

The used stress strain relationship is the elasto-plastic law:

$$\text{if } \tau_{stat} < \tau_{stat,ult} \rightarrow \gamma = \frac{\tau_{stat}}{G_i}$$

$$\text{if } \tau_{stat} > \tau_{stat,ult} \rightarrow \tau_{stat} = \tau_{stat,ult}$$

The displacement curve (Figure V-69) of the first soil element is highly influenced by the slippage and all the next elements follow this new curve only influenced by the geometric attenuation.

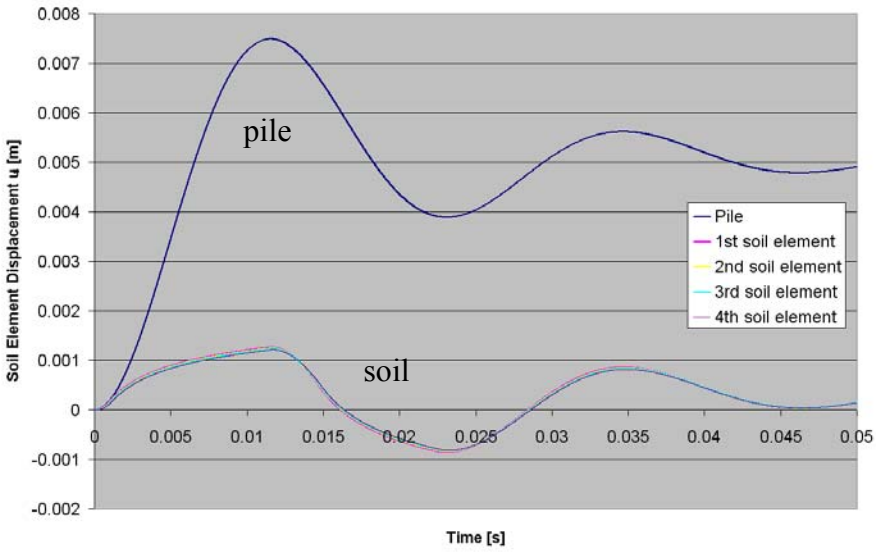

Figure V-69 : Displacement traces of the pile and of the 4 first soil elements - static aspect

If the static threshold is reached, the shear stress into the first interface remains constant (Figure V-70 and Figure V-71). Consequently, it is the same for the corresponding force $T_1 = \int \tau \cdot dS$ Figure V-72 and Figure V-73 for the 1st interface.

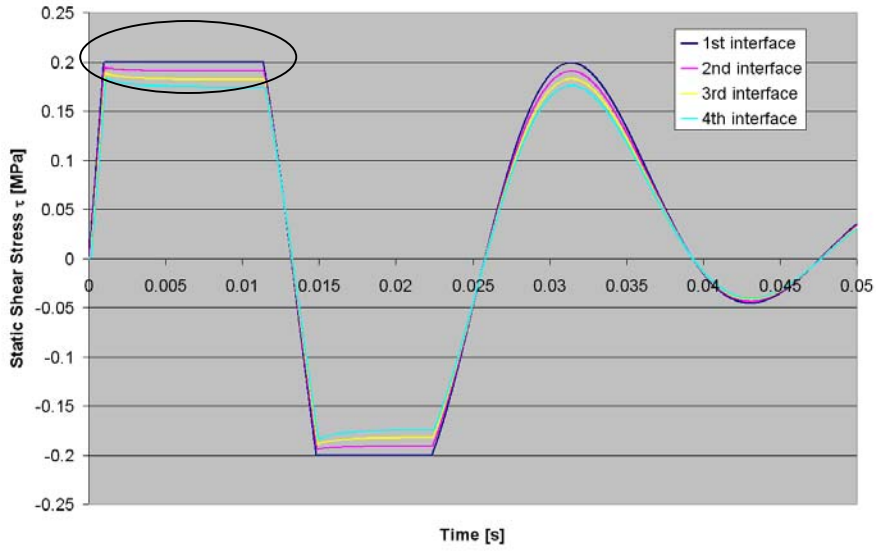

Figure V-70 : Static shear stress traces of the 4 first interfaces - Static aspect

However, during the slippage, the static shear stress curves seem to reach a peak value directly followed by a damped behaviour to an asymptotic value (Figure V-70 & Figure V-71).

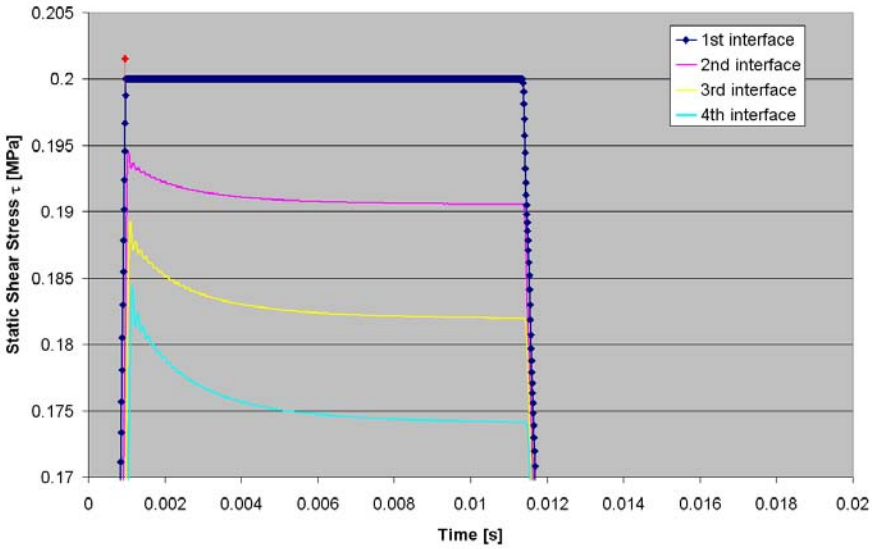

Figure V-71 : Static shear stress traces of the 4 first interfaces - Static aspect – Zoom

In the cylindrical model, all the interfaces forces must be equal (Figure V-72). Since the surfaces of each rings on which the stresses are integrated increases with the distance from the pile, the corresponding stresses must decrease. In these conditions, the ultimate stress can not be exceeded in the farther interfaces and the slippage can not be initiated. This is the main reason of the only slippage in the first interface in a static situation.

When the first interface reaches the ultimate resistance threshold, the natural evolution of the stress should be the red point on Figure V-71. That means that the explicit algorithm stage of the static stress calculation would give this point if the ultimate resistance test of exceeding has not been achieved. Since the numerical test was successful, the stress was limited to the threshold and the blue limit. However, the others interfaces do not reach the ultimate limit at this same time, because they are not in the same position in their own evolution (the transmission of information respects the shear wave propagation velocity in the soil) and because of the geometric attenuation that reduces the corresponding stress with distance. They follow they own behaviour, lead by the imposed pile motion transmitted through the prior soil element until the effect of the first interface slippage event arrives. Since the first interface force is fixed to the ultimate value (T_1 constant) and since the next interface forces are higher, the resulting acceleration becomes of sign opposite to the prior one ($\mathbf{a}cc_1(\mathbf{t}) = \frac{(\mathbf{T_1} - \mathbf{T_2})}{\mathbf{M_1}}$), and tends to zero in an oscillating equilibrium. The non sliding interface forces tend to reach the natural position expected with the geometrical attenuation (stress value such the interfaces forces are constant on the model, Figure V-72 and Figure V-73).

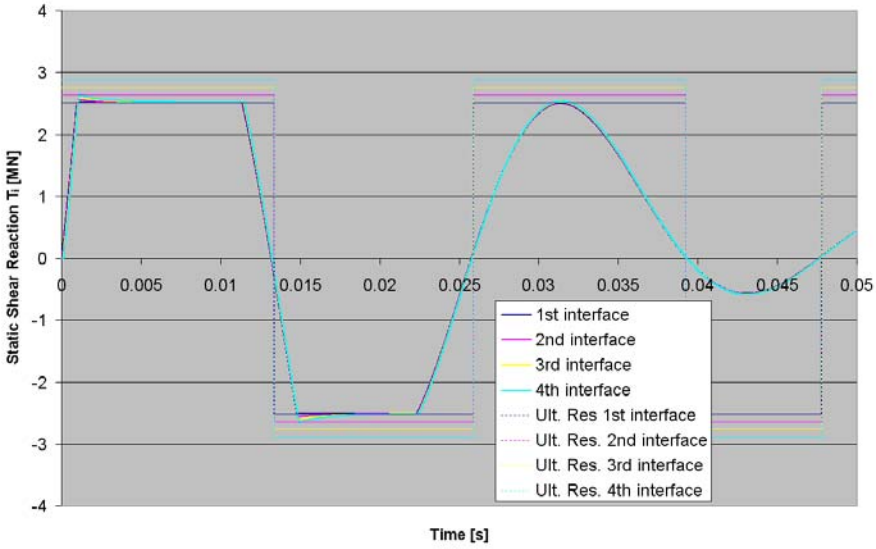

Figure V-72 : Static shear soil reaction of the 4 first interfaces (+ corresponding ultimate resistance) - Static aspect

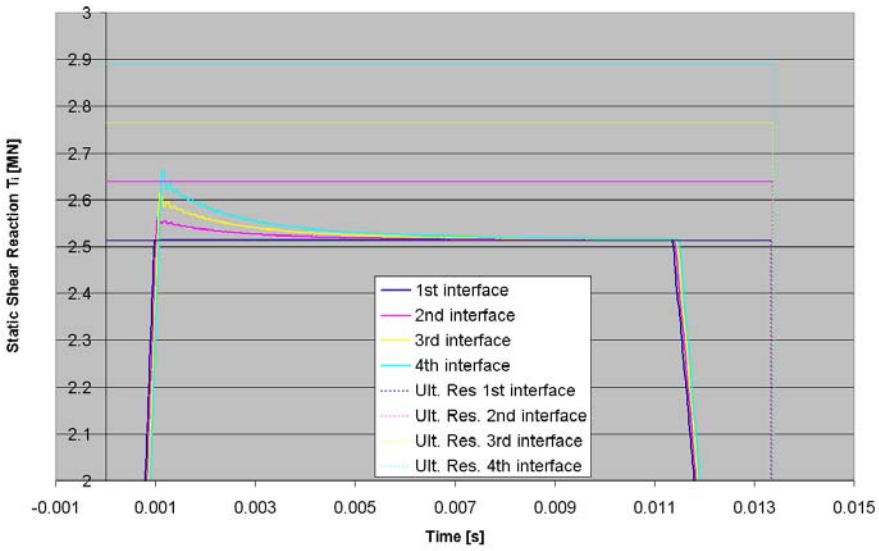

Figure V-73 : Static shear soil reaction of the 4 first interfaces (+ corresponding ultimate resistance) - Static aspect - Zoom

Figure V-73 highlights that the forces tend to the same value which is the static ultimate resistance of the soil into the first interface. The oscillations disturbing the stress and force displays find their origin in the mechanical behaviour of the spring supposed to model the static behaviour of the soil. The spring associated to the mass of the soil cylinder acts like the static response of the soil but also like a damped Single Degree of Freedom System submitted to an imposed motion. The spring has its own frequency, also called damped frequency, function of its stiffness, of the mass of the element and of the critical damping of the system.

Figure V-74 and Figure V-75 show the velocity results: the soil element velocities and the interfaces velocities. The velocity of the 1st soil element is directly reduced due to the slippage into the 1st interface and the next soil elements velocity traces remain quasi identical to this one.

The interface velocity shows only a significant value for the first interface, during the two periods of slippage. According to Paquet (1988), it could be called the penetration velocity.

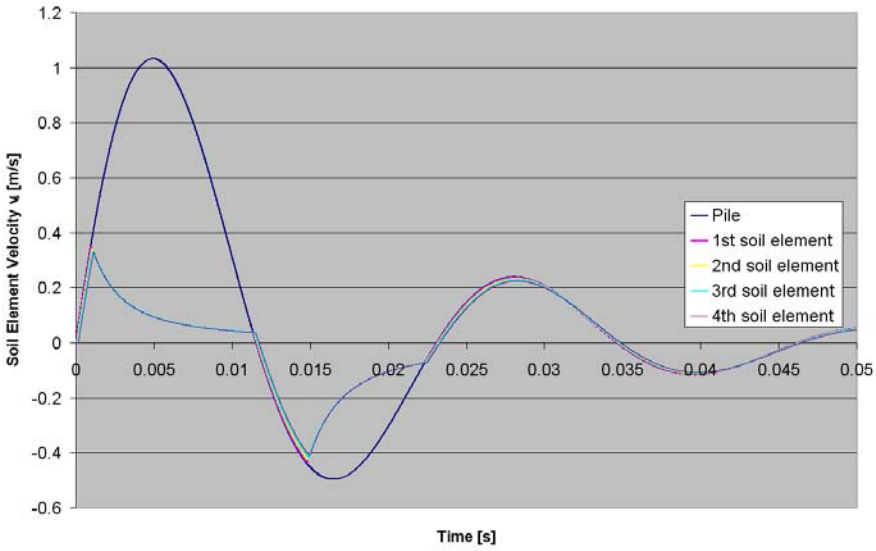

Figure V-74 : Velocity traces of the pile and of the 4 first soil elements - Static aspect

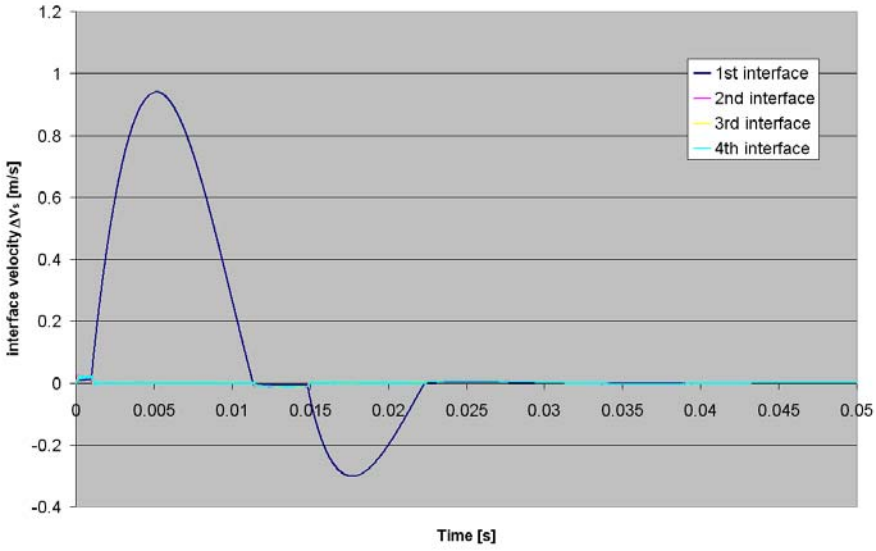

Figure V-75: Interface velocity traces of the 4 first interfaces - Static aspect

3.6.2 Rheologic field

When the use of the viscous contribution to the soil reaction is included, the model response is totally different because a viscous contribution is added to the static term calculated at each time increment.

In the algorithm presented in Figure V-68-b, the eventual exceeding of the ultimate threshold is checked twice per time step: a first time after the calculation of the static shear stress (at each interface) and the second time after addition of the viscous term to generate the rheologic shear stress. After, this stress is integrated and the equations of motion are solved. But, in fine, only the rheologic interface forces are used for the forces balance and the evaluation of the acceleration.

Since the interface forces T_i are larger than for the only static aspect (due to the viscous contribution), the acceleration history is likewise different and so the velocity and displacement histories. Consequently, the static stresses are also influenced. The evolution of the stresses into each interfaces can possibly result in a slippage event not only at the pile/soil interface but also into the next ones depending of the relative weight of the velocity dependent terms. The T_i remain constant along the model, but these forces correspond to the rheologic forces and not the only static ones and includes the displacement and velocity dependent components.

The displacement curves display a progression between the pile displacement and the "static" corresponding curves. Indeed, the curve of the 4th soil element displacement of Figure V-76 presents a similar trend compared to the displacement curves observed for the soil elements in Figure V-69. It is as if the static behaviour was the final state reached after slippage.

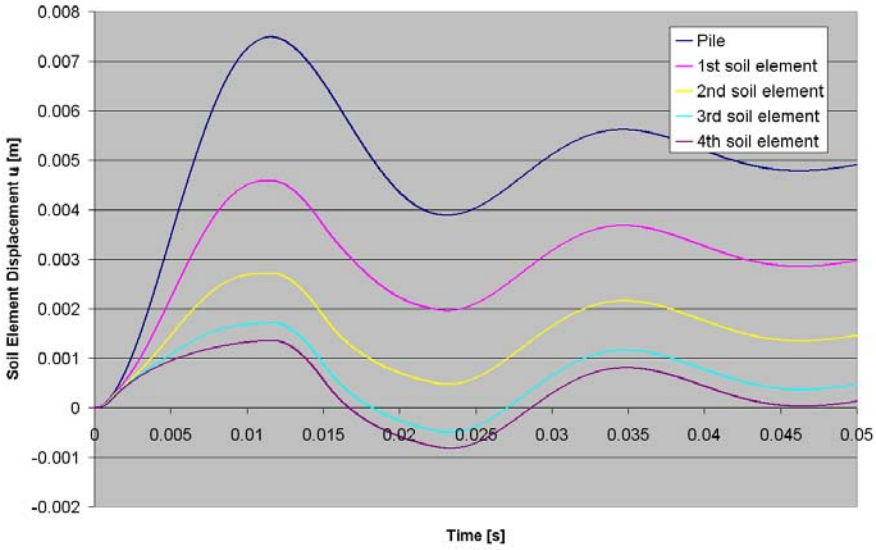

Figure V-76 : Displacement traces of the pile and the 4 first soil elements - Rheologic aspect

Figure V-77 shows that more than one interface reaches the static limit of soil resistance. The figure exhibits also that the consecutive interfaces reach the slippage state with not a constant velocity. The slippage propagation velocities are respectively el#1 → el#2: 45 m/s, el#2 → el#3: 20 m/s and el#3 → el#4: 10 m/s (pronounced marks on Figure V-78). The decrease of velocity points out that the slippage behaviour tends to vanish with the distance from the pile shaft.

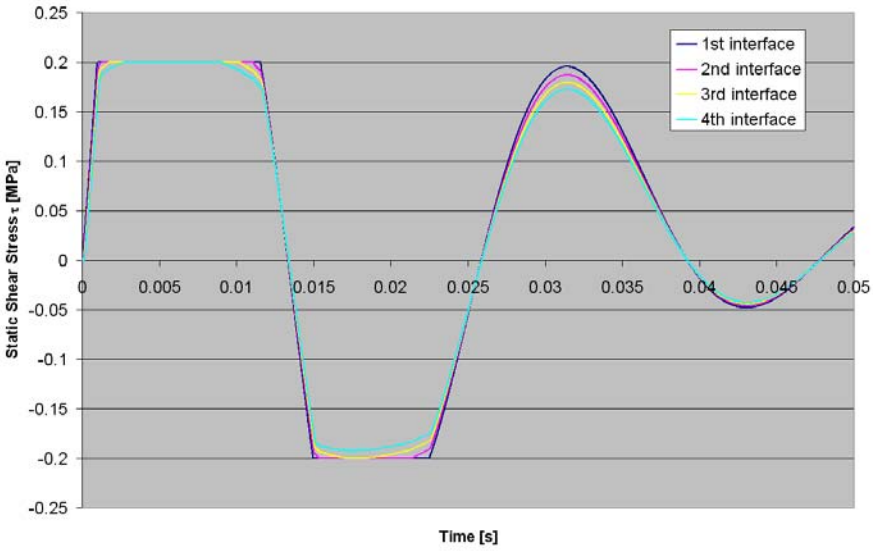

Figure V-77 : Static shear stress traces of the 4 first interfaces - Rheologic aspect

Figure V-78 shows that the static term of the rheologic shear stress reaches four times the ultimate threshold. This is due to the interface displacement which is bigger than in the static aspect due to the addition of the viscous term in the acceleration calculation. All the break points seen on each curves correspond to a direct influence of the prior interfaces when they reached the slip behaviour.

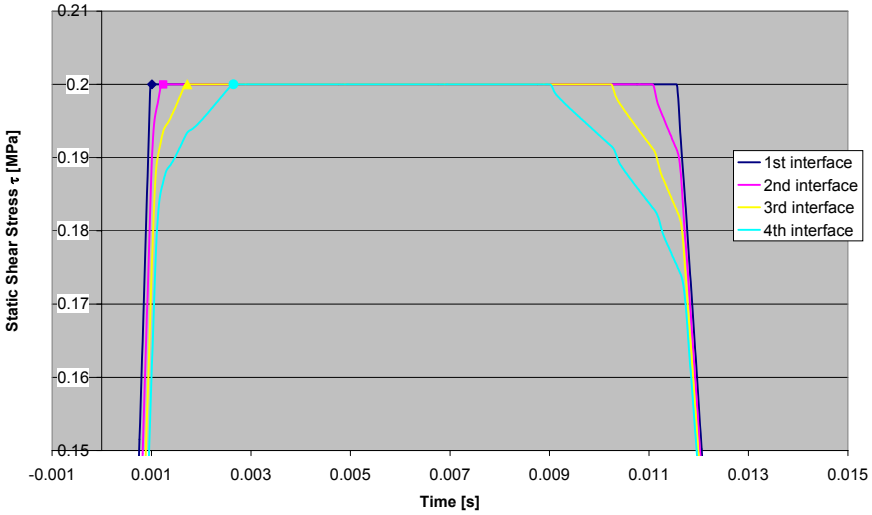

Figure V-78 : Static shear stress traces of the 4 first interfaces - Rheologic aspect – Zoom

Figure V-79 displays the rheologic shear stress influenced by the interface velocity:

$$\tau_{rheol} = \tau_{stat} \cdot \left(1 + J_s \left(v_{i-1} - v_i\right)^{0.2}\right)$$

Since the rheologic parameters J and J_s are identical for the evaluation of the ultimate rheologic shear stress and the rheologic soil reaction, if the static ultimate resistance is reached, it is certain that the rheologic ultimate threshold is also reached

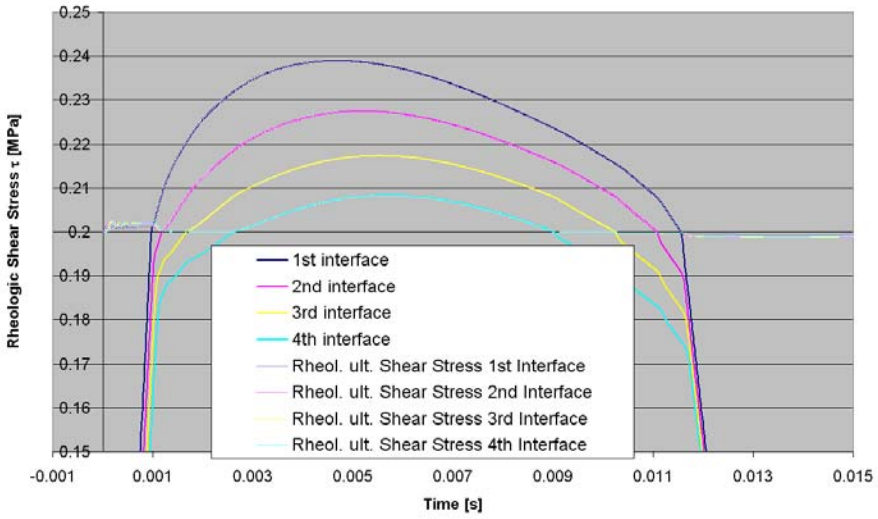

Figure V-79 : Rheologic shear stress traces of the 4 first interfaces (+ Ult. rheol. shear stress) - Rheologic aspect - Zoom

Figure V-80 displays the rheologic interface forces that have to remain constant (after time shifting due to the shear wave propagation).

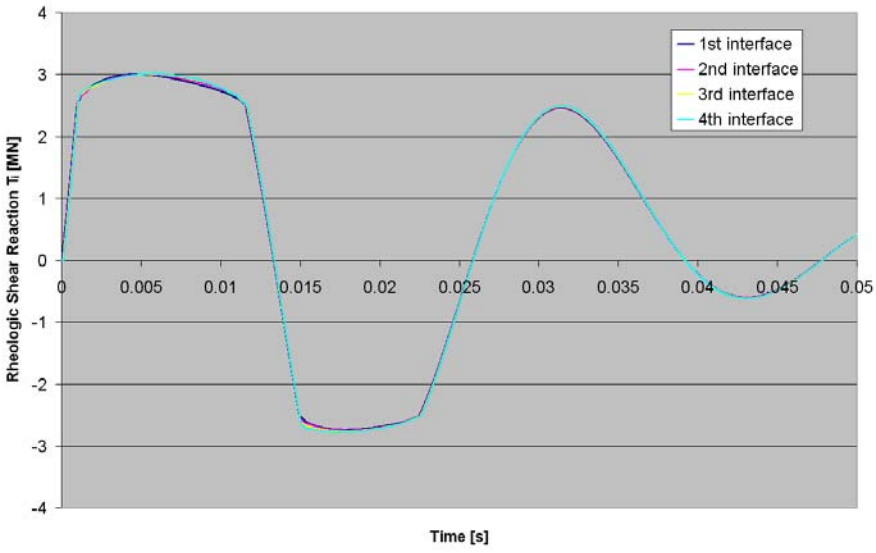

Figure V-80 : Rheologic shear soil reaction traces of the 4 first interfaces - Rheologic aspect

Figure V-81 and Figure V-82 show the velocity results: the soil element velocities and the interface velocities. The soil element velocities acts like the displacement curves. They are in an intermediate situation between the pile velocity and the equivalent velocity of the 1st element in the static analysis. The interface velocities evolves to zero with the slippage condition.

It must be pointed out that the oscillating problems shown in the first part of this section are less present under the rheologic aspect. This is expected because of the use of a dashpot in parallel of the static spring. This mechanical device eases the oscillations.

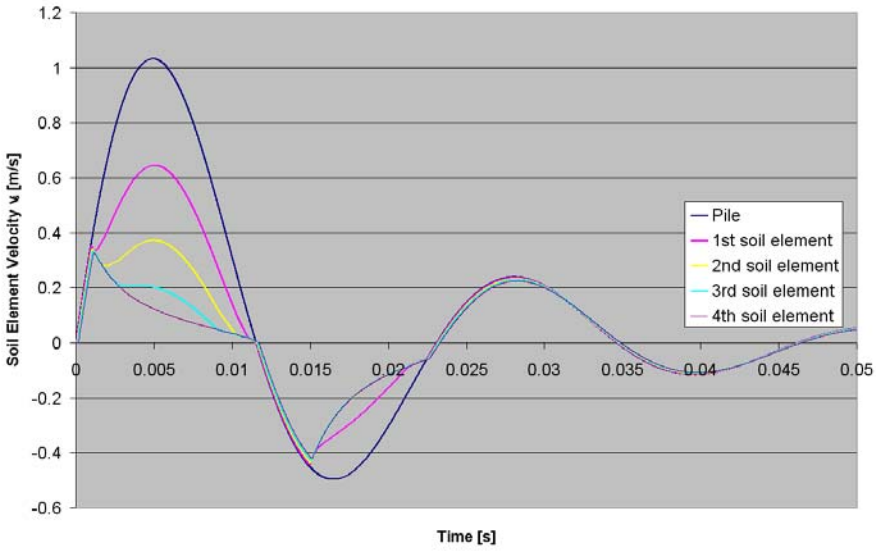

Figure V-81 : Velocity traces of the pile and the 4 first soil elements - Rheologic aspect

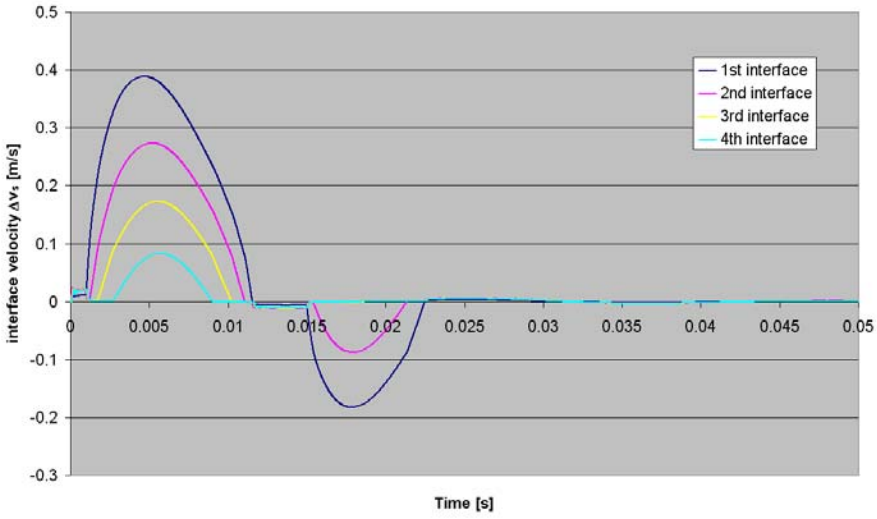

Figure V-82 : Interfaces velocity traces of the 4 first interfaces- Rheologic aspect

4. Conclusions

This chapter is dedicated to the slippage event required by the analysis performed on chapter 4. When the soil reaction exceeds a certain limit, the pile must be authorized to slip into the soil. Consequently, both pile and soil motions are differentiated. This requirement needs a modification of the pile/soil model presented in chapter 3 of this thesis. Only the shaft friction modelling is concerned. Two methods were proposed, described and commented to dissociate the pile and the soil motions:

- The DDOF model;
- The Cylindrical model.

The DDOF[2] model only considers the soil reaction in the direct vicinity of the pile shaft. The soil reaction is represented by a static term (≡ a non linear spring and a soil displacement dependent term), a viscous term for the internal dissipation of energy into the soil (≡ a non linear dashpot and a soil velocity dependent term) and a radiation term (≡ a non linear dashpot, function of the mobilization of the static term and of the soil velocity). The ultimate rheologic resistance of the soil beyond of which the slippage occurs, is function of the ultimate static shear stress and of the interface velocity (difference between pile & soil velocities). Since the pile and the soil are perfectly coupled before the soil reaction reaches the limit of resistance, this interface velocity is nil; when slippage occurs, the two media decouple and the resulting interface velocity influences the value of the ultimate rheologic resistance of the soil. During the slippage event, the soil motion is evaluated so that the soil reaction perfectly balances the ultimate rheologic resistance.

This method was developed and implemented in an explicit method. In order to analyse the results, a simplified pile/soil model was created in which a defined motion is imposed to a rigid pile installed in a single soil layer. The curves of soil displacement and velocity were compared to the pile displacement and velocity traces. The corresponding difference is defined as the pile penetration and the penetration velocity. The same approach was found in the model of Paquet (1988) who defined similarly the pile penetration and the penetration velocity.

This model keeps the advantages of the SDOF model (size, simplicity, time computing) and allows to distinguish the pile and soil displacement histories. The pile settlement, governed by the loading, is often longer than the settlement to be followed by the stress-displacement fundamental relationship. Since this information was of importance in the back-analysis and especially in the optimisation of the unloading parameters, the next step required is to validate this approach by implementing the complete pile/soil model (shaft + base) and back-analysing some real dynamic measurements with the algorithm developed in chapter 4. Unfortunately, it was not possible to perform it within this research due to a lack of time.

For a same imposed pile motion, the soil motion, and consequently, the pile penetration are strongly influenced by the choice of the ultimate static resistance and by the value of the damping parameter

[2] Double Degree Of Freedom Model

$J_{(s)}$. This parameter, used in both expressions of the ultimate rheologic resistance (J) and in the viscous term formulation (J_s) with the same value must be differentiated (two different values) what seems to be more logical because both formulations represent different behaviours.

Unfortunately, these observations are only the result of simulations and can not be confirmed by real measurements. There is a need of data allowing to discern the static, viscous and rheologic behaviours along the pile shaft under large strains.

The Cylindrical (Cyl) model describes the soil reaction by mean of concentric cylinders surrounding the pile. The cylinders are a set of rings with the same thickness and an increasing height. The last ring closes the model by an absorbing boundary respecting the theory of Novak et al, 1978. The Cyl model allows the computing of the displacements and the stresses induced in the soil due to a dynamic pile solicitation. The static soil reaction is completed by a viscous term function of the relative velocity between soil elements and the geometry of the model is supposed to represent the radiation term usually modelled in the 1D pile/soil system. This model was developed to highlight the slippage event and its major parameters. The loading rate influence is also marked in the ultimate rheologic resistance of the soil which is also function of the interface velocity.

The model is firstly validated by comparison of results obtained from a simulation with the theoretical approach of Novak et al., 1978. Afterward, the slippage occurring at the interface between pile and soil is described in function of the soil reaction terms authorized to be mobilized.

If only the static terms are used, the slippage is confined to the sole interface between the pile and the soil. On the other hand, if the velocity dependent terms are added to the static soil reaction, it appears that the slippage can spread out in a certain depth around the pile (between soil elements). This depth is function of the ultimate static resistance, of the rheologic parameters (like the ultimate and the viscous damping factors J and J_s) and of the initial shear modulus of the soil. The development of the slippage beyond the pile/soil interface is due to the velocity dependent terms and especially to the viscous term.

Another observation of importance is the fact that despite the slippage, a certain information (a certain motion or energy) goes through the slip surface and propagates into the soil. The slippage is not modelled as an insurmountable barrier but acts as a filter defined by the ultimate soil resistance and stiffness and the rheologic parameters: the smallest the ultimate soil resistance and the faster the mobilization of the soil, the less the transmitted information. A zone of slippage develops around the pile and is determined by the loading rate.

According to its relative weight in the definition of the slippage event and consequently in the development of the shaft friction failure, there is a need to complete the knowledge of the velocity dependent viscous stress. As corollary, a better knowledge of the velocity of which this term is relevant is also required because the choice of the pile, the soil or the interface velocity has a strong influence upon the viscous stress influence on the pile/soil response.

CHAPTER 6

Conclusions and Perspectives

1. Outline of the research

The main purpose of this research was to study the influence of the loading rate on the load-settlement relationship through the results of two testing procedures loading piles with variable durations (Static Load Test (SLT) → Dynamic Load Test (DLT)). Pile load test results belong to two national research programs organised by the BBRI and shortly described in chapter 3 of this thesis. The possibility to compare these measurements obtained on identical piles installed in the same well documented geotechnical environment could result in a better understanding of the loading rate effect within the range of high and low velocities covered by the testing procedures.

The objective was to refine the rheological parameters in relation to the sites investigated and with respect to the loading tests. The goal was also to find a characterisation of the pile/soil interaction system allowing to predict the load-settlement curves of each loading procedure by introducing the corresponding velocity history at the pile head.

This thesis includes a description of the load testing procedures and their main methods of interpretation plus a short description of the wave equation applied to pile dynamic analysis (chapter 1). The loading rate effects through the literature are investigated and approached according to the behaviour evaluation, to the description of this behaviour in simple and general formulations used in the dynamic piling practice and to the lumped models describing the rheologic soil response in terms of rational and fundamental geotechnical parameters (chapter 2).

Moreover, a complete analysis of the dynamic measurements of which the main results are summarized hereafter is presented in chapter 3.

The pile/soil interaction system is modelled by a non-linear mass/spring/dashpot system supposed to represent the pile, the soil and the constitutive relationships existing between them. These relationships account for the static and the so-called dynamic behaviour (chapter3). A back-analysis process based on a matching procedure between measured and computed curves (force/velocity) allows one to describe the pile/soil interaction in terms of constitutive and rheologic parameters based on the dynamic measurements. After optimisation of the matching procedure, the parameters obtained are used to simulate the "static" load-settlement curve to be compared with the measured one.

However, there is a large amount of parameters to be optimised. Since the original procedure performed the matching "manually" by modifying some parameters one by one, it was wished to refine the optimisation phase and to transform it into an automatic process. This will was supported by the requirement to have an impartial, objective and rapid method to optimise all the parameters in the same time. This method was developed and its satisfactory performance was assessed as described in chapter 4. A hierarchy of the parameters based on their relative weight in the optimisation process was highlighted allowing a powerful optimisation by sorting and optimising the parameters by level of influence.

But the strict results of these optimisations resulted in the need of the modification of the basic pile/soil interaction modelling: the pile and the soil have to be differentiated using two degrees of freedom to allow an independent motion of each in case of slippage at their interface. Indeed, the classical model behaved as a moving pile embedded in a motionless soil. Consequently, the pile/soil interaction links the generated stress to the pile motion without considering any slippage at their interface. It has been shown that this constraint results in a questionable optimisation of the initial stiffness and of the unloading parameters (chapter 4) and influences the ultimate soil resistance optimisation.

Chapter 4 provides also a complete back-analysis of the dynamic tests performed on prefabricated piles in both sites of Sint-Katelijne Waver and Limelette. The results are commented and the simulations compared to the static load settlement curves. These analysis are carried out with the model where the soil is motionless and the motion lead by the pile. So these conclusions are still influenced by the unloading phase.

Since the loading stiffness and the ultimate resistance are directly involved in the simulation of the static load settlement curve, it was required to develop a pile/soil model authorizing the slippage at the interface between the pile and the soil (DDOF model – chapter 5). Moreover, a general study of this slippage event was also undertaken in a simplified but complete model (the Cylindrical model – chapter 5) with the aim to describe the spreading of this behaviour in the close vicinity of the pile. Unfortunately, a lack of time prevented the implementation of these models into the general pile/soil system impeding a complete analysis of real dynamic measurements.

The main conclusions of this research are listed by chapter followed by the main practical contributions and the prospective, summarized and described.

2. Conclusions

2.1. The literature review

The literature review presents mainly the loading rate effects occurring during the failure. This affect is described according to a power law of the velocity of the moving body. The exponent of the power law is generally fixed to 0.2 and the rheologic parameter varies with the author, the procedure or the type of soil and testing.

A small analysis has highlighted the danger to reference the relationships describing the loading rate effect to a given velocity considered as the static test reference velocity. This implies a negative influence in the case where the studied velocity is lower than the reference one. A complete loading history where the velocity starts from 0, reaches its maximum value and goes back to zero provides such a case.

The literature presents very little information about the influence of the loading rate during the loading and the unloading stages. The main results concern the failure, namely under large strains and stresses.

The observed trend of the loading rate effect is commonly described by a generic parameter: the rheologic parameter J (Smith, Coyle & Gibson, Case method, …). Despites the fact that many authors tried to correlate this parameter with soil type or other quantities, no satisfactory conclusions can be drawn and one often imposes to confirm the proposed values of J by a field verification under the same loading conditions and by testing a similar foundation.

The models describing the terms of the rheologic soil reaction with rational parameters (primarily of the friction modeling) give a strong importance to the geometric damping. This term is directly influenced by the rate of static soil mobilization and the underlying degradation of the tangent modulus. This term leads quickly the soil to failure in the range of high velocities (like the DLT). Theoretically, the radiation term vanishes when the slippage occurs but since the static soil mobilization is not complete, and the tangent modulus not completely degraded yet, the radiation term does not disappear and still influences the rheologic stress evaluation. That implies the addition of a term assuming to generate an additional stress due to the loading rate in the range of large strain to compensate the vanishing of the radiation term (namely the velocity dependent stress).

2.2. The model and the dynamic measurements analysis

The analysis is mainly focused in the friction modeling. The terms of the rheologic stress include a static, a radiation and a viscous component. These elements are summed and limited by a value (the ultimate rheologic stress) dependent of the velocity and the ultimate static stress. A study showed the influence of the radiation term in the range of the dynamic velocities especially for the stiffness of the stress-displacement curve. At the beginning of the loading, this term is the main component of the rheologic stress due to the rapid increase of velocity and the small mobilized displacement. The failure occurs quickly and the passage to the failure mode is marked by an angular break that might be interpreted as a quake but that is strictly determined by the dynamic behavior. When the static

mobilization increases, the importance of the radiation term decreases the degradation while the viscous term (proportional to the velocity and the static mobilization) becomes more important.

The analysis of the measurements of the dynamic load tests showed that there is a link between the maximum settlements, the permanent settlements of the pile head and the drop heights. A critical drop height is defined. If the drop height is smaller than this limit, no permanent settlements occur, if it is higher, the pile significantly settles down. The maximum settlements measured are also influenced because the difference between both settlements is almost constant (= rebound) for a drop height beyond the critical one. The analysis of the maximum quantities (force measured, pile head velocity, energy transmitted to the pile) shows a similar result. There are critical quantities defining the permanent settlement of the pile. For a same pile of similar length, both sites present similar trends and different values. The summary of these quantities is given in Table VI-1. There is a pronounced difference between the clay and the sand.

	Sint Katelijne Waver	Limelette
Critical Drop Height [m]	0.5 – 0.7	1.3 – 1.4
Critical Maximum Velocity [m/s]	1.2 – 1.4	1.5 – 1.6
Critical Maximum Force [MN]	1.9 – 2.0	1.75 – 1.8
Critical Energy [MNm]	0.007	0.012 – 0.03

Table VI-1: Summary of the critical quantities to get significant permanent settlement (prefabricated pile 11 & 13 m long)

The analysis of the Boom clay site measurements including two DLT campaigns separated by one year does not show any marked differences. The analysis of the Bruxellian sand site measurements including the results of two different piles does not show any marked differences.

The relationships between the drop height & the settlements and the enthru & the settlements follow a similar trend: a concave-convex relationship for the permanent and maximum settlements, respectively (Figure VI-1). The relationships between the velocity and the settlements and the force measured and the settlements follow also a similar trend: the superposition of two straight lines with their crossing corresponding to the start of the permanent settlement generation (Figure VI-1).

The expected relationships between maximum quantities (force-velocity related to the nominal pile impedance; and transmitted energy-drop height related to the efficiency of the dropping system) are confirmed and allow one to characterize the quality of the signals (eccentricity).

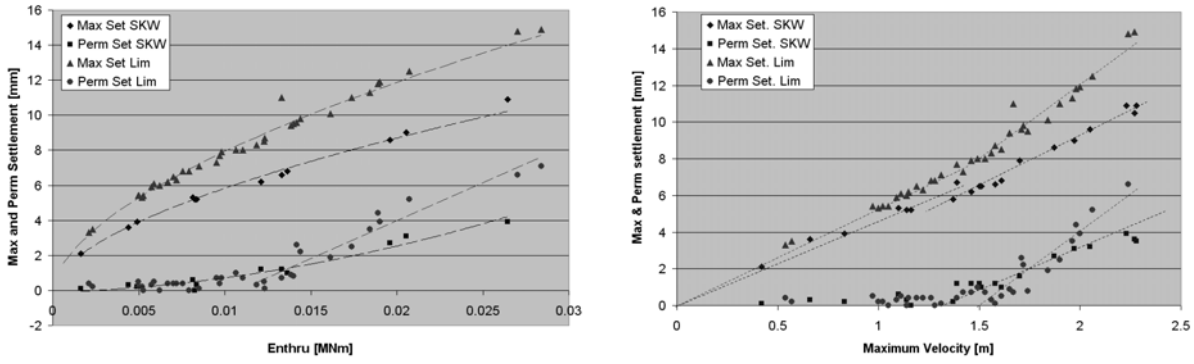

Figure VI-1 : Relationships between quantities based on the dynamic measurements

2.3. The back analysis and the optimisation procedure

This part of the research aims to automate the main step of the analysis process of the dynamic measurements: the back analysis and the optimisation procedure of the matching between measured and modelled dynamic curves (force and pile head velocity). The dynamic data are dealt with by extracting the pile/soil interaction parameters and by sorting them according to their static or dynamic influence. This treatment is called the back-analysis and the procedure followed to achieve it is an optimisation between the measured and the modelled pile/soil response. After that, the static load-settlement curve is simulated based on the interaction modelling assessed.

The principles of the matching procedure, the details and the requirements to have an objective and rapid method to perform the back analysis are presented. The method developed is based on the multi dimensional parameter perturbation sensitivity analysis (Berzi, 1999). It consist in exploring the close vicinity of a point (defining a combination of n parameters in their R^n space) in order to obtain a new combination improving the matching quality. This process is followed until a stop criterion is achieved (success or end of process). The final combination is considered as the solution of the back-analysis.

The implemented method allows to obtain a solution that minimizes the gap between measured and calculated pile/soil responses (force or pile head velocity) and authorizes a sensitivity analysis of this solution around it. Consequently, the parameters can be classified according to their relative weight in the matching procedure. Figure VI-2 presents two sensitivity analysis of parameters and the influence of their variation ($\Delta p/p$) on the matching quality factor D(p). A sorting is performed into the set of parameters allowing a sequential optimisation. All the parameters are firstly used to give a first step to the process. Aftewards, the most influential are successively retrieved to allow the optimisation of the less influential parameters. The parameters leading the process are the static soil reaction ones (ultimate resistance, thickness of the layers), the rheologic ones are less influential.

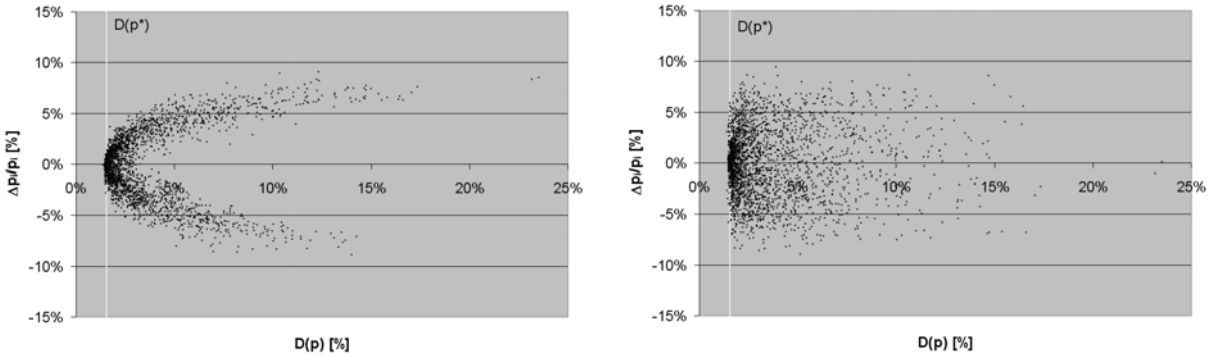

Figure VI-2 : Influential parameter and non influential parameter

The back-analysis has been carried out on the dynamic measurements performed in Sint Katelijne Waver and Limelette. The matching procedure succeeds in all cases but the back-analysis results are less reliable. The systematic analysis has shown that profiles of the soil resistance were respected in comparison with the CPT ones used as reference. But the net values are wrongly influenced by a bad modelling of the loading and unloading initial shear modulus. The reason of that is found to be the motion coupling of pile and soil enforcing the follow-up of the settlement path by the constitutive

stress-displacement relationships without any possibility of slippage between pile and soil. The main consequence is that the initial shear modulus G_i and the ratio of modulus G_2/G_i get small and unrealistic values. Unfortunately, the stiffness parameters influence greatly the simulation of the static load-settlement curve. So, a modification of the pile/soil system modelling is required. The slippage between pile and shaft must be authorized and both motions have to be independent during its occurrence.

However, the systematic back-analysis brings results of interest:

- The highlighting of the prior mobilization of the shaft friction before the base resistance and the confirmation of the settlement of this mobilization as about 1 to 1.5 % diameter of the pile;
- The ratio of the base/shaft friction capacities for both sites (Boom clay and Bruxellian sand) as observed with the static load tests;
- The respect of the expected profile given by the CPT;
- A first indication of the rheologic parameters values for both types of soil:

J value	Sint Katelijne Waver	Limelette
Shaft damping factor	0.6 $s/m^{0.2}$	0.1 to 0.75 $s/m^{0.2}$
Base damping factor	1.75 s/m	0.9 s/m

Table VI-2 : First estimation of the rheologic parameters

- The simulations of the static load settlement curves agree with the measured ones but are probably influenced by the pile/soil motion coupling.

Finally, one can points out that the load rate effects are more developed in clay compared to the sand environment. It can be observed that a good matching is not a sufficient condition to have a good back-analysis result. Guides must orientate the matching. The first and the most important one is the comparison with a relevant geotechnical information about the soil environment. Automatic guides can be implemented, but the most reliable is the human control of a seasoned engineer.

2.4. The slippage event at the pile shaft

In order to authorize the pile to slip into the soil when a certain resistance is exceeded along the pile shaft as required by the conclusions of chapter 4, two new pile/soil systems are proposed to dissociate the pile and the soil referentials:

- The DDOF[1] model;
- The Cylindrical model.

[1] Double Degree Of Freedom Model

The DDOF model only considers the soil reaction in the direct vicinity of the pile shaft and is modelled by a non linear static term, a velocity dependent term for the internal dissipation of energy into the soil (the viscous term) and a radiation term. The three terms are function of the soil motion. The ultimate rheologic resistance of the soil is function of the ultimate static shear stress and of the interface velocity (difference between pile & soil velocities) which is nil when pile and soil are coupled and variable when the slippage occurs. During the slippage, the soil motion is evaluated so that the soil reaction perfectly balances the ultimate rheologic resistance of the soil. The results allow to discern the pile penetration and the penetration velocity defined as the difference of settlements and velocities between pile and soil, similarly to a model described by Paquet in 1988.

The DDOF model keeps the advantages of the SDOF model (size, simplicity, time computing) and allows to distinguish the pile and soil displacement histories in order to fulfil the requirements of the chapter 4. The soil motion (shape, maximum and permanent values), and consequently, the pile penetration are strongly influenced by the choice of the ultimate static resistance of the soil and by the value of the damping parameters $J_{(s)}$.

The Cylindrical model describes the soil reaction by mean of concentric cylinders surrounding the pile. The last ring closes the model by an absorbing boundary respecting the theory of Novak et al, 1978. The Cylindrical model allows the computing of the displacements and the stresses induced in the soil due to a dynamic pile sollicitation. The static soil reaction is completed by a viscous term function of the relative velocity between soil elements and the geometry of the model is supposed to represent the radiation term usually modelled in the 1D pile/soil system. The loading rate influence is also marked in the ultimate rheologic resistance of the soil which is also function of the interface velocity.

Firstly validated with the theoretical approach of Novak et al., 1978. the model is used to study the slippage occurring at the interface between pile and soil. If only the static terms of the soil reaction are used, the slippage is confined to the sole interface between the pile and the soil. On the other hand, if the velocity dependent terms are added to the static soil reaction, it appears that the slippage can spread out to a certain range around the pile (between soil elements). This thickness is function of the ultimate static resistance of the soil, of the rheologic parameters and of the initial shear modulus of the soil. The development of the slippage beyond the pile/soil interface is due to the velocity dependent terms and especially to the viscous term.

Moreover, the slippage is not modelled as an insurmountable barrier but acts as a filter defined by the ultimate soil resistance and stiffness and the rheologic parameters: the smallest the ultimate soil resistance and the faster the mobilization of the soil, the less the transmitted information to the soil.

3. Contributions of the research

The definition of the different terms intervening in the loading rate effect are defined and described. The strict overview of the loading rate influence was investigated through literature. The importance of the radiation term is highlighted and the need of better knowledge of its evolution with the static and dynamic soil resistance degradation is pointed out. The traditional attempt to classify the rheologic

parameter J (from Smith, Case method, or Coyle-Gibson approaches) with the type of soil must be avoided.

A systematic analysis of the dynamic measurements provides informations about the pile/soil response in function of the maximum force, energy and velocity needed to significantly settle down the pile. The type of soil differentiates also the observed results. This can be applied directly to the driving analysis. The energy and the settlements can be used to compare the different loading procedures.

The back-analysis and optimisation modules allow to automate and accelerate an objective analysis of the dynamic measurements. The proposed method authorizes to check the given solution by a sensitivity inspection of its close vicinity. Statistics become conceivable. The sorting of parameters give the opportunity to refine the less influential of them.

The matching procedure is successful in all cases but the analysis of the optimised parameters brings out the requirement of the slippage in the pile/soil modelling. This improvement could result in a better knowledge of the pile/soil interaction and also of the behaviour of the soil reaction at the end of each blow (with a special attention to the residual stresses along and beneath the pile).

The models developed or improved in order to authorize the slippage between the pile and the soil show results of interest:

- The distinction of both soil and pile motions with a light and reliable model;
- The relationships between the soil parameters (resistance, rheologic) and the generated soil motion;
- The possible spreading of the slippage zone under dynamic conditions;
- The transmission of movement through the failure surface.

All these results must be confirmed and refined with real measurements or specific tests.

4. Perspectives

Since almost all the results available in the overview of the loading rate effect in literature concern the ultimate rheologic resistance of the soil and a relatively high level of velocity, it is required to investigate the intermediate ranges of velocity and strain. The path is of the same importance than the failure mode. It is needed to investigate the low range of velocity and the low level of static mobilization. The type of soil must be also widened. Major part of the studies concerns a clayey soil or a mix of sand and clay. The other types of soil are concerned by the influence of the loading rate and must be investigated.

Finally, it was observed that the influence of the loading rate is composed of different terms. However, generally, the tests undertaken give a global coefficient, dependent of the velocity, including all the influences. It is required to perform tests allowing to point out each term independently, with the minimum of interference. The viscous term is often neglected or set to a low contribution. However,

its importance is highlighted by the increase of soil resistance with the velocity in the vicinity of the failure where the radiation is theoretically vanished. A proposition would be to study this component by performing the same test on the same sample of soil saturated with many fluids of gradual viscosity. It is also of importance to carry out tests where the inertial effects are removed or evaluated with precision.

The synthetic analysis on the loading rate effect performed in chapter 3 pointed out the existence of a marked threshold between the description of the soil reaction and the failure mode in the friction modelling. Laboratory tests allowing the highlighting of this threshold and its characterization with regard to the soil parameters and without influence of inertial effects are wished. The comparison of tests performed with a constant level of energy transmitted but a variable velocity is another way of investigation of the loading rate effect.

The results obtained after analysis of the dynamic measurements must be confirmed with a larger sample of data coming from another piles (diameter and length) in different sites. The critical quantities and the beginning of a significant permanent settlement must be related to the quake analysis for both pile resistance components: the base resistance and the shaft friction. There is an equilibrium between the base and the integrated shaft quakes. The understanding of this behaviour must take into account the slippage at the interface between pile and soil, the residual stresses, the initial and the unloading stiffness of the different stress-displacement relationships.

The implementation of the back-analysis module highlights the need of the slippage possibility. This must to be implemented in the general pile/soil system. The sensitivity analysis authorizes the development of statistic tools on the back-analysis results beside the geotechnical sources of information (correlation of profiles, link $\Delta p/p - D(p)$ and static load settlement simulation). All these tools could better the process toward the best geotechnical solution.

The complete set of dynamic measurements of a complete sequence of DLT tests could also be used as one sole signal to be studied and optimised in order to describe the pile/soil interaction system accounting for all the tests carried out.

Concerning the slippage event, the first action of importance to be continued is to complete the pile/soil model by implementing the DDOF model into the system described in chapter 3 and to perform back-analysis of real dynamic measurements with the algorithm developed in chapter 5.

A more complete model could be also put together by merging both models presented in chapter 5. The pile/soil model is described by the DDOF model, and the soil description is described by the Cylindrical model connected to the preceding (Figure VI-3). The results could differentiate the pile and the soil motions and evaluate the soil behaviour in the direct vicinity of the pile and in the far field allowing the comparison with measurements obtained from transducers installed on the field (geophones, …).

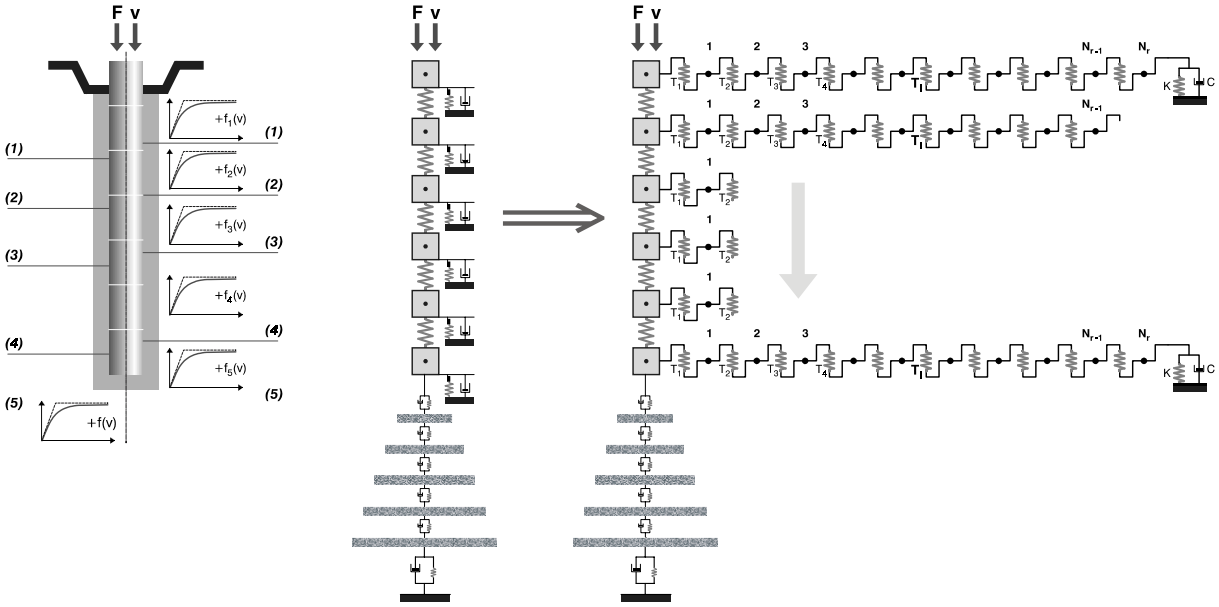

Figure VI-3 : Complete model to be implemented

The analysis of the slippage allowed one to highlight the requirement to differentiate the rheologic terms with respect to the relevant velocity (pile, soil, interface). Since there is too little information available in literature about this differentiation, it could be interesting to confirm the simulation observations by real measurements. In corollary, both damping factors, J & Js, used in the ultimate rheologic soil resistance and in the viscous term must be differentiated due to the difference in the behaviours described. If the first damping factor (J) is easier to estimate by measuring the failure under dynamic solicitation, the second parameter (J_s) requires more refinements.

List of Symbols

1.1. Symbols

A is the normal section of the pile [m²]

Acc_i is the acceleration of the node i [m/s²]

c is the wave propagation velocity [m/s]

C_H is the damping factor of the Lysmer analogue [Ns/m]

C_p is the internal damping factor of the pile (0.5) [-]

c_u is the undrained cohesion [MPa]

$\Delta displ_i$ is the increment of displacement of the node i [m]

$displ_i$ is the displacement of the node i [m]

D is the embedded pile length or the soil layer thickness [m]

D(p) is the normalized average gap between the measured and calculated quantities [-]

dz is an infinitesimal thickness of pile [m]

E_p is the elastic modulus of the pile material [MPa]

E_2/E_1 is the ratio of elastic soil moduli during loading and unloading [-]

E' is the modulus of viscosity of the soil [$Pa.s^{-1}$]

E_i is the initial modulus of elasticity of the soil [MPa]

F_1 and F_2 are the rheologic parameters of the Bea's theory [-]

$F_{result,\,i}$ is the resulting force at the node i [MN]

$F_{int,\,i}$ is the internal forces applied at the node i [MN]

$F_{ext,\,i}$ is the external forces applied at the node i [MN]

f_s is the local shear strength measured with the CPT [MPa]

g is the local tangent shear modulus of the soil[MPa]

G_i is the initial shear modulus of the soil [MPa]

G is the gravity acceleration [9,81 m/s²]

G_2/G_1 is the ratio of shear moduli during loading and unloading [-]

h is the dropping height [m]

h_i is the height of the pile element [m]

Δh is the increase of cylinder's thickness per unit of distance in the Cyl model [m]

I the nominal impedance of the pile [MN.s/m]

J is the damping factor expressing the loading rate influence [s/m^N]

J_c is the CASE damping constant [-]

J_b is the base damping factor [s/m]

J_s is the viscous or soil damping factor [$s/m^{0.2}$]

J is the rheologic damping factor [$s/m^{0.2}$]

J_R is the Rausche damping factor [s/m^N]

J_S is the Smith standard damping [s/m]

K_l is the coefficient of soil viscosity of the Dayal & Allen's theory [-]

K_H is the spring stiffness of the Lysmer analogue[N/m]

$k_{el,i}$ is the elementary stiffness of two consecutive pile elements [MN/m]

$K_{0,1}$ is the modified Bessel function of the second kind of order 0 and 1 respectively. [-]

L is the pile length [m]

$Mass_i$ is the mass of the pile element i [kg]

M_m is the ram mass [kg]

n is the viscous exponent of the Briaud's theory [-]

N is the exponent expressing the non-linear dependency of the loading rate influence [-]

N_{el} is the radial discretization (the number of rings in the Cyl model) [-]

P_v is the vertical exciting force [MN]

p is the vector of parameters to be optimised

$\mathbf{p}^0$ is the initial set of values for **p**

Δp_i is the variation of the parameter p_i [unit of p_i]

q is the soil quake [m]

q_c the cone resistance measured with the CPT [MPa]

Q_u is the static ultimate pile capacity [MN]

Q_b and Q_s are the base and shaft capacities [MN]

Q_c is the creep Resistance [MN]

Q_{stat} is the static soil reaction [MN]

Q_{rheol} is the rheologic soil reaction [MN]

R_a is the maximum static reacxtion mobilized prior the time under consideration [MN]

R_s is the static soil reaction mobilized at the time of consideration [N]

R_f is the ratio of friction and cone resistance from the CPT [-]

R_p the pile radius [m]

R_{rheol} is the rheologic soil reaction [MN]

$R_{rheol,,ult}$ is the ultimate rheologic soil resistance [MN]

$R_{stat,ult}$ is the ultimate static soil resistance [MN]

R_m is the radius of influence from Randolph and Wroth' theory [m]

r_b is the pile base radius [m]

Δr is the thickness of each cylinder in the Cyl model [m]

s is the pile settlement [m]

ΔS is the settlement of the cone of soil [m]

S_H is the settlement of the half-space medium beneath the base [m]

S_{ui} is the undrained shear strength [MPa]

$t = \frac{L}{c}$ is the travel time of the wave into the pile [s]

T_i is the inter-ring reaction between elements i and i-1 in the Cyl model [MN]

u_p, v_p are the pile displacement and velocity [m, m/s]

u_s, v_s are the soil displacement and velocity [m, m/s]

v is the pile velocity [m/s]

Vel_i is the velocity of the node i [m/s]

V_o initial velocity of the harmonic loading [m/s]

v_i is the impact velocity [m/s]

v_p is the pile material wave velocity [m/s]

v_x is the maximum velocity achieved up prior the time under consideration [m/s]

V_p and V_s are the compressive and shear wave velocities [m/s]

V_0 is the initial velocity [m/s]

z_i is the depth of the bottom of the i° soil layer [m]

1.2. Greek symbols

α is the coefficient of dispersion of Holeyman (2000) [-].

α and β are the rheologic parameters of the Randolph approach [MPa; -]

β is the rate of increase in shearing resistance per log cycle of increase in strain [-];

β is the soil material damping ratio.

γ is the angular distortion or shear strain [-].

γ_r is the reference shear strain [-];

Δt is the time increment [s];

ε is the axial strain [-];

$\dot{\varepsilon}$ is the strain rate [s^{-1}];

η is the mobilization ratio [-];

η_c : falling efficiency [-];

η_i : impact efficiency [-];

η_p is the mobilization ratio at pile shaft [-];

λ is the loading rate in the Bea's theory [$\%.h^{-1}$];

υ is the Poisson's ratio [-].

ξ is the attenuation coefficient [rad^{-1}]

ρ is the volumetric mass of the soil [kg/m]

ρ_p the volumetric mass of the pile material [kg/m^3];

σ the normal stress [MPa];

σ_{stat} is the static axial strength of the soil [MPa];

σ_{rheol} is the rheologic axial strength of the soil [MPa];

σ_{max} is the maximum static axial static stress reached during the test [MPa]

$\sigma_{stat,ult}$ is the ultimate static axial strength of the soil [MPa];

$\sigma_{rheol,ult}$ is the ultimate rheologic axial strength of the soil [MPa];

τ the shear stress [MPa];

τ_{stat} is the static shear stress [MPa];

τ_{visq} the viscous shear stress [MPa];

τ_{rheol} is the rheologic shear stress [MPa];

τ_p the shear stress mobilized at the pile shaft [MPa].

τ_{max} is the maximum static shear stress reached during the test [MPa]

$\tau_{stat,ult}$ is the ultimate static shear strength of the soil [MPa];

$\tau_{rheol,ult}$ is the ultimate rheologic shear strength of the soil [MPa];

$w(a_0,r)$ is the displacement amplitude at a distance r and of dimensionless frequency a_0;

ω is the circular frequency [rad/s];

References

Author's references:

HOLEYMAN A., COUVREUR J.M. & CHARUE N. 2001. Results of the Dynamic and Statnamic Pile Load Tests and presentation of the Prediction Event. Proceedings of the Symposium on screw piles – installation and design in stiff clay. Brussels, Belgium, pp 247-273.

CHARUE N., HUYBRECHTS N. & HOLEYMAN A., 2001. Prediction and verification of a precast concrete pile driven in boom clay. Proceedings of the 15th ICSMGE, Istanbul, Turkey, pp 863-866.

CHARUE N. & HOLEYMAN A., 2001. Comparison and correlations between electrical and mechanical CPT tests in Boom Clay with reference to the Belgian practice design of axially loaded piles. Proceedings of the YGEC, Sofia, Bulgaria, in Additional Papers Proceedings, pp 36-44.

CHARUE N., HOLEYMAN A., HUYBRECHTS N., LEGRAND Ch. & MAERTENS J., 2002. Results of an international pile load testing prediction event, Proceedings of the 27th Deep Foundation Institute Conference, San Diego, USA.

HOLEYMAN A., VANDEN BERGHE J-F. & CHARUE N. editors, 2002. Proceedings of the International Conference in Vibratory Pile Driving and Deep Soil Compaction – Transvib 2002. Swets & Zeitlinger B.V., Lisse, The Netherlands. 233 p.

HOLEYMAN A. & CHARUE N. 2003. International pile capacity prediction event at Limelette. Proceedings of the Symposium on screw piles in sand – design & recent developments. Brussels, Belgium, pp 215-234.

Research references:

ABEBE A. & SMITH I., 1999. Pile Foundation Design: A Student Guide. School of the Built Environment, Napier University, Edinburgh – WEB SITE : http://sbe.napier.ac.uk/projects/piledesign/guide/index.htm

ABOU-MATAR H., RAUSCHE F., THENDEAN G., LIKINS G. & GOBLE G., 1996. Wave equation soil constants from dynamic measurements on SPT. Proceedings of the 5th international Conference on the application of the stress-wave theory to piles, Orlando, USA. pp 163-175.

AL-SHAMRANI M.A., 2001. Loading rate effects on the bearing capacity of shallow footings in clay. Journal of the Southeast asian geotechnical society. December 2001, pp 191-203.

ANDERSON W.F., BROWN M.J., HYDE A.F.L. & BALDERAS MECA J., 2003. A laboratory study of Statnamic testing of piles in clays. Proceedings of the International Conference on Advances in Soft Soil Engineering and Technology, 2nd, Putrajaya, Malaysia, pp 117-127.

AOKI N. & DE MELLO V.F.B.1992. Dynamic loading tests curves. Proceedings of the 4th international Conference on the application of the stress-wave theory to piles. The Hague, The Netherlands, pp 525-530.

ASTM D1143-81, 1994. Standard test method for piles under static axial compressive load.

ASTM D4945-89, 1994. Standard test for high-strain dynamic testing of piles.

AXELSSON G. & HINTZE S., 2000. Evaluation of pile set-up from penetration per blow. Proceedings of the 6th International Conference on the application of the stress-wave theory to piles, Sao Paulo, Brazil, pp 665-672.

BALDERAS-MECA J., 2003. Rate Effects in Rapid Loading of Clay Soils, PhD Thesis, University of Sheffield.

BARANOV V.A., 1967. Sur le calcul des foundations enterrées soumises à vibrations. in Russian, N°14, Institut Polytechnique de Riga.

BBRI (1998-2000). Soil displacement screw piles – calibration of calculation methods and automatisation of the static load test procedure : stage 1 - friction piles. Research program subsidised by the Belgian Federal Ministry of Economical Affairs, convention number CC-CIF-562.

BBRI (2000-2002). Soil displacement screw piles – calibration of calculation methods and automatisation of the static load test procedure : stage 2 – end-bearing piles. Research program subsidised by the Belgian Federal Ministry of Economical Affairs, convention number CC-CI-756.

BEA R.G., 1982. Soil strain rate effects on axial pile capacity. Proceedings of the 2nd International Conference on Numerical Methods in Offshore Piling, Austin, USA, pp 107-132.

BERRE T. & BJERRUM L., 1973. Shear strength of normally consolidated clays. Proceedings of the 8th International Conference on Soils Mechanics and Foundation Engineering. Vol 1, pp 39-49.

BERZI P., 1994. Pile soil interaction due to static and dynamic load. In the Proceedings of the XIII ICSMFE, New Delhi, India, pp 609-612.

BERZI P., 1996. Conditions of reliable predictions from dynamic pile load tests Proceedings of the 5th international Conference on the application of the stress-wave theory to piles, Orlando, USA, pp 495-505.

BERZI P., 1999. Paramater identification by a generalized secant method. In the Proceedings of the 3rd International Conference on Inverse Problems in Engineering: Theory and Practice. Washington, USA, pp 1-8.

BRIARD M., 1970. Contrôle des pieux par la méthode des vibrations. Annales de l'institut Technique du Bâtiment et des Travaux Publics, N° 270, pp 105-107.

BRIAUD J.L. & GARLAND E., 1985. Loading rate method for pile response in clay. In Journal of Geotechnical Engineering. Vol 111, N°3, pp 319-335.

BRIAUD J.L., BALLOUZ M. & NASR G., 2000. Static capacity prediction by dynamic methods for three bored piles. Journal of Geotechnical and Geoenvironmental Engineering. Vol 126, N°7, pp 640-649.

BROMS B. B., Foundation Engineering, collection of figures (http://www.geoforum.com/knowledge/texts/broms/)

BROWN M.J., 2003. Research developments- progress report. Ground Engineering Journal, Vol 36, No. 4, April 2003. pp. 31-32.

BROWN, M.J., HYDE, A.F.L & ANDERSON, W.F., 2002. Kinematic load tests on a model pile in clay. Proceedings of the 9th International Conference on Piling and Deep Foundations, Nice, France, pp. 617-623.

BSI, 1986. British Standard code of practice BS 8004– Foundations; section 7 pile foundations.

BURLAND J. B. & TWINE, D. 1988. The shaft friction of Bored Piles in terms of Effective Strength, Proceedings of the Seminar on Deep Foundations on Bored and Augered Piles, Ghent, Belgium, pp. 411 - 420.

CAPWAP© Manual 2000, Goble Rausche Likins and Associates, Inc. Cleverland, USA.

CHARUE N., HOLEYMAN A., HUYBRECHTS N., LEGRAND Ch. & MAERTENS J., 2002. Results of an international pile load testing prediction event, Proceedings of the Deep Foundation Institute Conference, San Diego, USA.

CHIN F.K. 1970. Estimation of the ultimate load of piles from tests not carried to failure. Proceedings of the 2nd Southeast Asian Conference on Soil Engineering, p. 91-90.

CHO C.W., LEE M.W. & RANDOLPH M.F., 2000. Set-up considerations in wave equation analysis of pile driving. Proceedings of the 6th international Conference on the application of the stress-wave theory to piles, Sao Paulo, Brazil, pp 41-46.

CHOW Y.K., WONG K.Y., KARUNARATHNE G.P. & LEE, SL., 1988. Wave equation analysis of piles - a rational theoritical approach. Proceedings of the 3rd international Conference on the application of the stress-wave theory to piles, Ottawa, Canada, pp 208-214.

CORTE J-F & LEPERT P., 1986. Résistance latérale pendant le battage et l'essai dynamique des pieux, In C.R. 3° Colloque International sur les méthodes numériques de calcul des pieux pour les ouvrages en mer, Nantes, éd. Technip, Paris, pp. 19-33.

COURAGE W.M.G. & VAN FOEKEN R.J., 1992. TNOWAVE automatic signal matching for dynamic load testing. Proceedings of the 4th international Conference on the application of the stress-wave theory to piles, The Hague, The Netherlands, pp 241-246.

COURAGE W.M.G., SCHREURS P.J.G. & JANSSEN J.D., 1990. Estimation of mechanical parameters values of composites with the use of finite element and system identification technique. Computers & Structures, Vol 34, N°2, pp 231-237.

COUVREUR J-M, 2000. Mode d'emploi du programme d'interprétation des essais dynamiques – EssaiDyn, in french, internal report of the Unité of Génie Civil, UCL, 19p.

COX W., KRAFT L.M. & VERMER, 1979. Axial load tests on 14-inch pipe piles in clay. 11th Offshore technology Conference, Huston, USA, Vol 2, pp 1147-1158.

COYLE H.M. & GIBSON G.C., 1970. Empirical damping constants for sands and clays, Journal of Soil Mechanics and Foundations. ASCE, Vol 96, N° SM3, pp 949-965.

DALI B. & HERITIER B., 1992. A new way for the dynamic static equivalence load. Proceedings of the 4th international Conference on the application of the stress-wave theory to piles, The Hague, The Netherlands, pp 551-556.

DAYAL U. & ALLEN J.H., 1973. Instrumented impact cone penetrometer. Canadian Geotechnical Journal, Vol 10, N°3, pp 397-409.

DAYAL U. & ALLEN J.H., 1975. The effect of penetration rate on the strength of remoulded clay and sand sample. Canadian Geotechnical Journal, Vol 12, pp 336-348.

DE BEER E. 1971-1972. Méthodes de déduction de la capacité portante d'un pieu à partir des résultats des essais de pénétration. Annales des Travaux Publiques de Belgique, No 4 (p.191-268), 5 (p321-353) & 6 (p 351-405), Brussels, Belgium.

DE BEER E., LOUSBERG E, WALLAYS M., CARPENTIER R., DE JAEGHER J. & PAQUAY J, 1977. Bearing capacity of displacement piles in stiff fissured clays. Belgian Governmental institute for scientific research in industry and agriculture, IRSIA-IWONL Research report n° 39, Brussels, Belgium.

DE COCK F., LEGRAND C. & HUYBRECTHS N. 2003. Axial Static Pile Load Test (ASPLT) in compression or in tension – Recommendations from ERTC3-Piles, ISSMGE Subcommittee. In Proceedings of the XIIth European Conference on Soil Mechanics and Geotechnical Engineering. Prague, Tcheck Republic, pp 717-741.

DE VOS M, BAUDUIN C., MAERTENS J. 2003. Current draft of the application rules of EC7 in Belgium for the design of pile foundations, Proceedings of the Symposium on screw piles in sand – design & recent developments, Brussels, Belgium, pp 303-322.

EIKSUND G. & NORDAL, 1996. Dynamic model pile testing with pore pressure measurements. Proceedings of the 5th International Conference on the application of the stress-wave theory to piles, Olrlando, USA. pp 1-11.

EL NAGGAR M.H. & NOVAK M., 1992. Analytical model for an innovative pile test. Canadian Geotechnical Journal, Vol 29, pp. 569-579

EL NAGGAR M.H. & NOVAK M., 1994. Non-linear Axial Interaction in Pile Dynamics. Journal of Geotechnical Engineeering, Vol 120, N° 4, pp 678-697.

EL NAGGAR M.H. & NOVAK M., 1994. Non-linear Model for Dynamic Axial Pile Response. Journal of Geotechnical Engineeering, Vol 120, N° 2, pp 308-329.

EL NAGGAR M.H. & BALDINELLI M., 1998. Stress wave analysis of Statnamic load test for bearing capacity prediction. In the Proceedings of the 2nd International Statnamic Seminar, Tokyo, Japan, pp 327-336.

ENGLAND M., 1999. A pile behaviour model. PhD Thesis, Imperial College.

FLEMMING W. G. K., 1958. The Bearing Capacity of Pile Groups. PhD Thesis, Queen's University of Belfast.

FLEMMING W.G.K., WELTMAN A.J., RADOLPH M.F. & ELSON W.K., 1985. Piling Engineering. Halsted Press, New York. 380 p.

FOREHAND P.W. & REESE J.L., 1964. Prediction of pile capacity by the wave equation. Journal of Soil Mechanics and Foundations. ASCE, march 1964, N° SM2, pp 1-25.

GIBSON G.C. & COYLE H.M. 1968. Soil damping constants related to common soil properties in sands and clays (Bearing capacity for axially loaded piles). Texas A&M University, Research Report Number 125-1, Sept 1968.

GOBLE G.G. 2000. Some wave mechanics applications. Proceedings of the 6th International Conference on the Application of the Stress-Wave Theory to Piles, Sao-Paulo, Brazil, pp 3-9.

GOBLE G.G., LIKINS G.L. & RAUSCHE F., 1975. Bearing capacity of piles from dynamic measurements – Final report. OHIO-DOT-05-75, Department of Solid Mechanics, Structures and Mechanical Design, Case Western Reserve University, Clerverland, Ohio, USA. 76p.

GOBLE G.G. & ABOU-MATAR H., 1992. Determination of wave equation soil constants from the standard penetration test. Proceedings of the 4th International Conference on the Application of the Stress-Wave Theory to Piles, The Hague, The Netherlands, pp 99-103.

GOBLE G.G. & LIKINS G., 1996. On the application of PDA dynamic pile testing. Proceedings of the 5th International Conference on the Application of the Stress-Wave Theory to Piles, Orlando, 1996. pp 263 – 273.

GOSSUIN B., 2001. Contribution à l'étude de l'influence du frottement lateral sur le comportment des pieux lors du battage. In French, under-graduate thesis, Université catholique de Louvain, Belgium.

GRAHAM J., CROOKS J.H. & BELL A.L., 1983. Time effects on the stress strain behaviour of soft natural clays. Geotechnique, Vol 33, N°3, pp 327-340.

GRL and associates, Inc, 1992. Determination of pile driveability and capacity from penetration tests, Interim report submitted to the FHWA, Washington DC, USA.

HARDIN B.O. & DRNEVICH V.P., 1972. Shear modulus and damping in soils: design equations and curves. Journal of Soil Mech. and Found. Eng., ASCE, Vol 98, SM7, pp. 667-692.

HEEREMA E.P. 1979. Relationships between wall friction, displacement, velocity and horizontal stress in clay and in sand for pile driveability analysis. Ground Engineering, 12, N°1, pp 55-61.

HENDRIKS M.A.N., OOMENS C.W.J., JANS H.W.J., JANSSEN J.D. & KOK J.J., 1990. A numerical experimental approach for the mechanical characterization of Composites. Proceedings of the 9th International Conference on Experimental Mechanics, Copenhagen, Denmark.

HERITIER B. & PAQUET J., 1984. Battage d'un pieu en milieu pulvérulent: acquistion des données et simulation. Annales de l'institut Technique du Bâtiment et des Travaux Publics, N° 450, décembre 1986, Série : Sols et Fondations 198, 19p.

HOLEYMAN A., 1984. Contribution à l'étude du comportement transitoire non-linéaire des pieux pendant leur battage. Thèse présentée en vue de l'obtention du grade légal de Docteur en Sciences Appliquées, Université Libre de Bruxelles, 584p.

HOLEYMAN A. 1985. Dynamic-non linear skin friction of piles. Proceedings of the International Symposium on Penetrability and Driveability of piles, San Francisco, USA, Vol 1, pp. 173-176.

HOLEYMAN A., 1988. Modelling of dynamic behaviour at the pile base. Proceedings of the 3rd International Conference on the Application of Stress-Wave Theory to Piles, Ottawa, Canada, pp. 174-185.

HOLEYMAN A., 1992. Keynote lecture: Technology of pile dynamic testing. . Proceedings of the 4th International Conference on the Application of Stress-Wave Theory to Piles, The Hague, The Nederlands. pp 195 – 215.

HOLEYMAN A., 1993. HYPERVIB IIa, a detailed numerical model proposed for future computer implementation to evaluate the penetration speed of vibratory driven sheet-piles. Research report prepared for BBRI. September 1993, 54 p.

HOLEYMAN A., 2000. *Vibratory Driving Analysis – Keynote Lecture*. Proceedings of the 6th International Conference on the Application of Stress-Wave Theory to Piles, Sao Paulo, Brazil, pp 479-494.

HOLEYMAN A., 2001. Screw Piles – Installation and design in stiff clay. Swets & Zeitlinger B.V., Lisse, The Netherlands.323 p.

HOLEYMAN A., BAUDUIN C., BOTTIAU M., DEBACKER P., DE COCK F., DUPONT E., HILDE J. -L., LEGRAND C., HUYBRECHTS N., MENGE P., MILLER J. -P., and SIMON G., Design of axially loaded piles - Belgian practice in Design of axially loaded piles - European Practice, edited by De Cock and Legrand, Balkema, Rotterdam, 1997, pp.57-82.

HOLEYMAN A. & CHARUE N. 2003. International pile capacity prediction event at Limelette. Proceedings of the Symposium on screw piles in sand – design & recent developments. Brussels, Belgium, pp 215-234.

HOLEYMAN A., COUVREUR J.M. & CHARUE N. 2001. Results of the Dynamic and Statnamic Pile Load Tests and presentation of the Prediction Event. Proceedings of the Symposium on screw piles – installation and design in stiff clay. Brussels, Belgium, pp 247-273.

HOLEYMAN A. & LEGRAND C., 1994. Soil Modelling for Pile Vibratory Driving, U.S. FHWA "International Conference on Design and Construction of Deep Foundations", December 1994, Orlando, Florida, USA, pp. 1165-1178.

HOLEYMAN A. & LEGRAND C., 1996. A Method to Predict the Drivability of Vibratory Driven Piles. Proceedings of the 5th International Conference on the Application of Stress-Wave Theory to Piles, Orlando, Florida, USA, pp. 1101-1112.

HOLEYMAN A., MAERTENS J., HUYBRECHTS N. & LEGRAND C., 2000, Preparation of an International Pile Dynamic Testing Prediction Event. Proceedings of the 6th International Conference on the Application of Stress-Wave Theory to Piles, Sao Paulo, Brazil. pp. 733-739.

HOLEYMAN A., MAERTENS J., HUYBRECHTS N. & LEGRAND C., 2000, Results of an International Pile Dynamic Testing Prediction Event. Proceedings of the 6th International Conference on the Application of Stress-Wave Theory to Piles, Sao Paulo, Brazil. pp. 725-733.

HORVATH, R.G., 1995. Influence of loading rate on the capacity of a model pile in clay. Canadian Geotechnical Journal, Vol 32, pp 364-368.

HORVATH R.G., BERMINGHAM P. & MIDDENDORP P., 1993. The equilibrium point method of analysis for the Statnamic loading test with supporting case histories. In the Proceedings of the 18th Annual Conference of the Deep Foundation Institute, Pittsburgh, USA.

HUYBRECHTS N. 1998. Static and dynamic pile loading tests on different types of driven piles in Limelette (B). Proceedings of the Deep Foundation Institute Conference, Vienna, Austria.

HUYBRECHTS N. 2001. Grondverdringen schroefpalen (RE 480) – 2° biennale eindverslag 2000-2002, BBRI, Belgium.

HUYBRECHTS N., 2001. Test campaign at Sint-Katelijne-Waver and installation techniques of screw piles. Proceedings of the Symposium Screw Piles – Installation and Design in Stiff Clay, Brussels, Belgium, pp 151-204.

HUYBRECHTS N. 2003. Screw piles in sand – Design and recent developments, Swets & Zeitlinger B.V., Lisse, The Netherlands. 349p.

HUYBRECHTS N., LEGRAND C., DE COCK F., 1997. Paalbelastingsproeven te Limelette. Deel 1: Statische proeven. WTCB Tijdschrift, 4de trimester 1997.

HUYBRECHTS N., MAERTENS J. 2003. Excavation of the test piles on the Limelette site: observations and measurements, Proceedings of the Symposium on screw piles in sand – design & recent developments, Brussels, Belgium, pp 131-166.

HUYBRECHTS N, WHENHAM V., 2003. Pile testing program on the Limelette test site – Survey. Proceedings of the Symposium on screw piles in sand – design & recent developments, Brussels, Belgium, pp 71-130.

HYDE A.F.L., ANDERSON W.F. & ROBINSON S.A., 1998. Rate effects in clay soils and their relevance to Statnamic pile testing. In the Proceedings of the 2nd International Statnamic Seminar, Tokyo, Japan, pp 303-309.

ISSMFE Subcommittee on Field and Laboratory testing. 1985. Axial Pile Loading Test-Part 1: Static Loading. ASTM Geotechnical Testing Journal , p.79-90.

KALMAN R.E., 1960. A new approach to linear filtering and prediction, Trans ASME. Ser. D. J. Basic Engineering, Vol 82, pp 95-109.

KONDNER R.L.. 1963. Hypebolic stress strain response: chesive soils. Journal of Soil Mechanics and Foundations. ASCE, Vol 89, N° SM1, pp 115-143.

KRAFT L., COX W.R. & VERNER, E.A., 1981. Pile load tests: Cyclic loads and varying load rates. Journal of the Geotechnical Engineering Division, ASCE, Vol 107, pp 1-19.

KULHAWY F.H. & MAYNE P.W., 1990. Manual of estimating soil properties for foundation design. Geotechnical Engineering group, Cornell University, Ithaca, New York, USA.

LEE, S.L., CHOW Y.K., KARUNARATHNE G.P. & WONG K.Y., 1988. Rational wave equation model for pile driving analysis. Journal of Geotechnical Engineering ASCE, Vol 114, N°3.

LEGRAND C., 2001. Deep foundations and the need for research on screw piles in Belgium. Proceedings of the Symposium Screw Piles – Installation and Design in Stiff Clay. Brussels, Belgium, pp 3-9.

LEGRAND C. & POORTEMAN F. 2003. Deep Foundation and the need for research on screw piles in Belgium, Proceedings of the Symposium on screw piles in sand – design & recent developments, Brussels, Belgium, p 3-10.

LEPERT Ph., 1986. Un exemple d'analyse de measures effectuées lors du battage de pieux. Bull. Liaison Labo. Ponts et Chaussées, 145, sept-oct 1986, pp. 21-30.

LIANG R.Y., 2000. Correlative study of Smith damping coefficient and SPT blow count Proceedings of the 6th International Conference on the Application of Stress-Wave Theory to Piles, Sao-Paulo, Brazil, pp 461-467.

LIANG R.Y., 2003. New wave equation technique for high strain impact testing of driven piles. In journal of Geotechnical Testing, Vol 26, N°1. pp 111-117.

LIKINS G., DIMAGGIO J., RAUSCHE F. & TEFERRA W., 1992. A solution for high damping constants in sands. Proceedings of the 4th International Conference on the Application of Stress-Wave Theory to Piles, The Hague, The Netherlands, pp 117-120.

LIKINS G., RAUSCHE F., THENDEAN G. & SVINKIN M.R. 1996. CAPWAP correlations studies. Proceedings of the 5th International Conference on the Application of Stress-Wave Theory to Piles, Orlando, USA, pp 447-464.

LITKOUHI S. & POSKITT T.J., 1980. Damping Constant for pile driveability calculations. Geotechnique, 30(1): 77-86.

LYNDON A., WEI M. J., PRICE G. & STANSFIELD L., 1993. Strain measurements in CFA bored piles in soft clay, International seminar, Deep Foundations on Bored and Auger Piles, Ghent, Belgium, pp. 413-416.

LYSMER J. & RICHART F.E., 1966. Dynamic response of foting to vertical loading Journal of Soil Mechanics and Foundations. ASCE, Vol 92; SM1, pp. 65-91.

MAEKAWA H.; MIYAKITA K. & SEKIGUCHI H., 1991. Elasto-viscoplastic consolidation of a diatomaceous mudstone. Soil and Foundations, JSSMFE, Vol 31, pp 93-107.

MAERTENS J., HUYBRECHTS N. 2001. Results of the Static Pile Load Tests. Proceedings of the Symposium on screw piles – installation and design in stiff clay. Brussels, Belgium, pp 205-246.

MAERTENS J., HUYBRECHTS N. 2003. Results of the static pile load tests at the Limelette test site. Proceedings of the Symposium on screw piles in sands - design and recent developments. Brussels, Belgium, pp 167-214.

MATSUMOTO T. & NISHIMURA S., 1996. Wave propagation phenomena in statnamic tests of a steel pipe pile. Proceedings of the 5th International Conference on the Application of Stress-Wave Theory to Piles, Orlando, USA. pp 1015-1030.

MATSUMOTO T. & TAKEI M., 1991. Effect of Soil plug on behavior of driven pipe pile. Soils and Foundations, JSSMFE, 31(2), pp 14-34.

MATSUMOTO T., ASAI Y. & HAYASHI T., 1998. Two successive Statnamic tests on a cast in situ concrete pile. In the Proceedings of the 2nd International Statnamic Seminar, Tokyo, Japan, pp 159-168.

MENGE P., 2001. Soil investigation at Sint-Katelijne-Waver (Belgium). Proceedings of the Symposium Screw Piles – Installation and Design in Stiff Clay. Brussels, Belgium, pp 19-62.

MIDDENDORP P. & VAN BREDERODE, 1984. Skin friction models for sand from static and dynamic laboratory tests. Proceedings of the 2nd International Conference on the Application of Stress-Wave Theory to Piles, Stockholm, Sweden, pp 210-220.

MIDDENDORP P., BERMINGHAM P. & KUIPER B., 1992. Statnamic load testing of oundation piles. Proceedings of the 4th International Conference on the Application of Stress-Wave Theory to Piles, The Hague, The Netherlands. Pp 581-588.

MITCHELL J.K., 1976. Fundamental of soil behavior. New York, USA. John Wiley & Sons.

MITWALLY N. & NOVAK M., 1988. Pile driving analysis using shaft models and FEM. Proceedings of the 3rd International Conference on the Application of Stress-Wave Theory to Piles, Ottawa, Canada, pp. 455-466.

MORTELMANS F. 1988. Berekening van constructies deel 3 – gewapend beton. In dutch, Acco, Leuven.

NBN B 15-001, 1992. Beton – performances, production, mise en oeuvre et critères de conformité, 206p.

NGUYEN T. T., BERGGREN, B. & HANSBO, S., 1988. A new soil model for pile driving and drivability analysis. Proceedings of the 3rd international Conference on the application of the stress-wave theory to piles, Ottawa, Canada, pp 353-367.

NOVAK M., 1974. Dynamic Stiffness and Damping of Piles. Canadian Geotechnical Journal, Vol 11, N°4, pp. 574-598.

NOVAK M., NOGAMI T. & ABOUL-ELLA, F., 1978. Dynamic soil reactions for plane strain case. Journal of Mechanical Engineering Div., ASCE, 104(EM4): 953-959.

PAIKOWSKY S.G. & CHERNAUSKAS L.R., 1996. Soil inertia and the use of pseudo visco damping parameters. Proceedings of the 5th International Conference on the Application of Stress-Wave Theory to Piles. Orlando, USA, pp 203-216.

PAIKOWSKY S.G., REGAN J. & McDONNEL J., 1994. A simplified field method for capacity valuation of driven piles. FHWA Report N° FHWA-RD-94-042.

PAIKOWSKY S.G. & STENERSON K.L.. 2000. The performance of the dynamic methods, their controlling parameters and deep foundation specification. Proceedings of the 6th International Conference on the Application of Stress-Wave Theory to Piles, Sao-Paulo, Brazil, pp 281-304.

PAQUET J. 1988. Checking Bearing capacity of dynamic loading – choice of methodology. Proceedings of the 3rd International Conference on the Application of Stress-Wave Theory to Piles, Ottawa, May, pp 383-398.

PECK G.M., 1962. Bearing theories related to model tests on a remoulded clay. M. Eng. Thesis, Mc Gill University, Montreal, Canada.

RANDOLPH M.F., 1983. Settlement considerations in the design of axially loaded piles. Ground Engineering. 16(4), 28-32.

RANDOLPH M.F. & DEEKS A.J., 1992. Dynamic and static soil models for axial pile response. Proceedings of the 4th International Conference on the Application of Stress-Wave Theory to Piles, The Hague, The Netherlands, pp 3-14.

RANDOLPH M.F. & PENNINGTON D.S., 1988. A numerical study of dynamic cavity expansion. Proceedings of the 6th International Conference on Numerical Methods in Geomechanics, Innsbruck, Austria, Vol 3, pp 1713-1721.

RANDOLPH M.F. & SIMON H.A. , 1986. An improved soil model for one-dimensional pile driving analysis. In the Proc. of the 3rd International Conference of Numerical methods in Offshore piling, Nantes, France, pp 3-17.

RANDOLPH M.F. & WROTH C.P., 1978. Analysis of deformation of vertically loaded piles. Journal of Geotechnical Engineering Div., ASCE, 104(GT12), pp 1-17.

RAUSCHE F., GOBLE G.G. & LIKINS G.E., 1985. Dynamic determination of pile capacity. ASCE Journal of Geotechnical Engineering, Vol 111, N°3, pp 367-383.

RAUSCHE F., GOBLE G. & LIKINS G., 1992. Investigation of dynamic soil resistance on piles using GRLWEAP. Proceedings of the 4th International Conference on the Application of Stress-Wave Theory to Piles, The Hague, The Netherlands, pp 137-142.

RAUSCHE F., LIKINS G. & GOBLE G., 2000. Appendix B: A rational and usable wave equation soil model based on field test correlation. In the GRLWEAP help manual. 9p.

RAUSCHE F., MOSES F. and GOBLE G.G., 1972. Soil resistance predictions from pile dynamics, ASCE Journal of Soil Mechanics and Foundations, Vol 98, SM9, pp 917-937.

RAUSCHE F., ROBINSON B. & LIANG L., 2000. Automatic signal matching with CAPWAP. Proceedings of the 6th International Conference on the Application of Stress-Wave Theory to Piles, Sao-Paulo, Brazil, pp 53-58.

REISSNER E., 1936. Stationare, axialsymmetrische durch eine Schuttelnde Masse erregte Schwingungen eines homogen elastischen Halbraumes. Ingenieur, Archiv, Vol7, part 6, dec., pp 381-396.

RICHARDSON A.M. & WHITMAN R.V., 1963. Effect of strain rate upon undrained shear resistance of a saturated remolded fat clay. Géotechnique, Vol 13, N03, pp 310-324.

ROBERTSON. 1998. An application guide for the CPT, ConeTec Investigations Ltd & Gregg In-situ Inc.

SCHITTEKAT J., 2001. Engineering geology of The Boom clay in the Antwerp area. Proceeding of the Symposium on screw piles – installation and design in stiff clay. Brussels, Belgium, pp 11-17.

SCHITTEKAT J., HENRIET J. & VANDENBERGHE N., 1983 – Geology and geotechnic of the Schelde surge barrier. Characteristics of an overconsolidated clay. Proceedings of the 8th International Harbour Congress Antwerp, Belgium, pp121-135.

SEIDEL J.P. & KALINOWSKI M., 2000. Pile Set-up in sands. Proceedings of the 6th International Conference on the Application of Stress-Wave Theory to Piles, Sao Paulo, Brazil, pp 267-274.

SEKIGUCHI H., NISHIDA Y., MATSUMOTO T. & UESAWA M., 1985. Characterization of a diatomaceous mudstone by elasto-viscoplasticity. Proceedings of the 5th International Conference in Numerical Methods in Geomechanics, Nagoya, Japan, Vol 1, pp 437-444.

SIMON H.A. & RANDOLPH M.F., 1985. A new approach to one-dimensional pile driving analysis. Proceendingds of the 5th International Conference on Numerical Methods in Geomechanics, Nagoya, Japan, Vol 3, pp 1457-1464.

SKOV, R. & DENVER H., 1988. Time dependency of bearing capacity of piles. Proceedings of the 3rd international Conference on the application of the stress-wave theory to piles, Ottawa, Canada, pp 879-888.

SMITH E.A.L. 1960. Pile driving analysis by the wave equation. Journal of Soil Mechanics and Foundations. ASCE, Vol 86, NO, SM4, pp 35-61.

SMITH I.M. & CHOW Y.K., 1982. Three-dimensional analysis of pile driveability. Proceedings of the 2nd International Conference on Numerical Methods in Offshore Piling, Austin, USA, pp 1-20.

STAIN D. 1992. SIMBAT – a dynamic load test for bored piles. In Piling: European practice and worldwide trends. Tomas Telford, London, 1992, pp 198-205.

SVINKIN M.R., 1996. Velocity-impedance-energy relationships for driven piles. Proceedings of the 5th International Conference on the Application of Stress-Wave Theory to Piles, 1996, Orlando, USA, pp870-890.

SVINKIN M.R., 1996. Soil damping in wave equation analysis of pile capacity. In the Proceedings of the 5th international Conference on the application of the stress-wave theory to piles, Orlando, USA. pp 128-143.

SVINKIN M.R., 1997. Time-Dependent Capacity of Piles in Clayey Soils by Dynamic Methods. Proceedings of the XIVth International Conference on Soil Mechanics and Foundation Engineering, Hamburg, Germany, Vol. 2, pp 1045-1048.

SVINKIN M.R., 2000. Time effect in determining pile capacity by dynamic methods. Proceedings of the 6th international Conference on the application of the stress-wave theory to piles, Sao Paulo, Brazil, pp.35-40.

SVINKIN M.R. & ABE S. 1992. Relationship between case and hysteretic damping. Proceedings of the 4th international Conference on the application of the stress-wave theory to piles, The Hague, The Nederlands, pp 175-182.

SVINKIN M.R. & SKOV, R. 2000. Set-up effect in cohesive soils in pile capacity. Proceedings of the 6th international Conference on the application of the stress-wave theory to piles, Sao Paulo, Brazil. pp 107-112.

THENDEAN G., RAUSCHE F., SVINKIN M.R. & LIKINS G.. 1996. Wave equation correlation studies. Proceedings of the 5th international Conference on the application of the stress-wave theory to piles, Orlando, USA, pp 144-162.

TNOWAVE Manual, 2000.

VAID Y., ROBERTSON P.K. & CAMPANELLA R.G., 1979. Strain rate behaviour of Saint-Jean Vianney lay. Canadian geotechnical Journal, Vol 16, N°1, pp. 34-42.

VAN ALBOOM G., WHENHAM V. 2003. Soil investigation campaign at Limelette (Belgium): Results. Proceedings of the Symposium on screw piles in sand – Design & recent developments, Brussels, Belgium, pp 21-70.

VAN FOEKEN R.J., MIDDENDORP P. & COURAGE W.M.G., 1998. Application of stress wave method for automatic signal matching and Statnamic predictions. Proceedings of the 2nd International Statnamic Seminar, Tokyo, Japan, pp 345-354.

VANDEN BERGHE J-F., 2001. Sand Strength degradation within the framework of pile vibratory driving. Doctoral Thesis, Université catholique de Louvain, Belgium, 360p.

VOITUS VAN HAMME G.E.J.S.L., JANSZ J.W., BOMER H. & ARENTSEN D., 1974. Hydroblok an improved pile driving analysis. Der Ingenieur, Vol 86, N°8, pp 344-352.

WARRINGTON D.C., 1988. A new type of wave equation analysis program. Proceedings of the 3rd international Conference on the application of the stress-wave theory to piles, Ottawa, Canada, pp 142-151.

WHITAKER T., 1963. The constant Rate of Penetration Test for the determination of the ultimate bearing capacity of a pile. Proceedings of the Instrumentation. Civil. Engineering, pp 119-123.

WHITAKER T. & COOKE R. W., 1966. An investigation of the shaft and base resistances of large bored piles in London Clay, Large Bored Piles, Inst. Civ. Engrs, London.

WOLF J.P., 1988. Soil-structure interaction analysis in time domain. Prentice Hall. 464p.

WOLFE P., 1959. The secant method for simultaneous nonlinear equations. Communication of ACM, Vol 2, pp 12-13.